Dissertation

Improvement of Fragmentation by Blasting

Investigation of the influence of delay-times on the crack development in the surrounding rock, the characteristics of the blasted bench face and the fragmentation of the further rows

Dipl.-Ing. Peter Schimek

09/10/2015

Chair of Mining Engineering and Mineral Economics
Department Mineral Resources Engineering
Motanuniversitaet Leoben

A-8700 LEOBEN, Franz Josef Straße 18
Phone: +43/(0)3842-402-2001
bergbau@unileoben.ac.at

Improvement of Fragmentation by Blasting

Investigation of the influence of delay-times on the crack development in the surrounding rock, the characteristics of the blasted bench face and the fragmentation of the further rows

Dissertation

by Peter Schimek

Submitted to the Chair of Mining Engineering and Mineral Economics

in fulfilment of the requirements of the degree of

Doktor der montanistischen Wissenschaften

at the

Montanuniversitaet Leoben

Supervisors:

Ouchterlony, Finn, Dr.mont. h.c. Dr.tekn.

Moser, Peter, Univ.-Prof. Dipl.-Ing. Dr.mont.

Declaration of Authorship

„I declare in lieu of oath that this thesis is entirely my own work except where otherwise indicated. The presence of quoted or paraphrased material has been clearly signalled and all sources have been referred. The thesis has not been submitted for a degree at any other institution and has not been published yet.”

Acknowledgement

My first words of gratitude have to go to my supervisor Finn Ouchterlony, who supported me from the beginning of this thesis on through extensive discussions and valuable comments.

The second major contributor to the completion of this thesis was Peter Moser, who accepted the expensive and time consuming testing methodology.

The work at Swebrec (Swedish Blasting Research Centre at Luleå University of Technology), where the testing with the present set up started, has to be acknowledged. Here Daniel Johansson has to be mentioned.

Prof. Kräuter from the Chair of Mathematics and Statistics is acknowledged for the contributions to the statistical analyses of the data.

I want to express my gratitude to all the persons who have been involved in the preliminary work for the investigations, the blasting tests themselves and the follow-up analyses. Special thanks go to Gerold Wölfler and Georg Glatz for their enthusiasm during the blasting tests and to Thomas Seidl and Juan Navarro for the development of the analysis methods. Additionally Radoslava Ivanova, Erhard Maierhofer, Arno Hofmann, Enrico Dal Farra, Markus Beschliesser, Martin Wrienz, Heath Milton, Stefanie Streit and Tobias Ladinig are acknowledged.

I also want to say thank you to my colleagues at the Chair of Mining Engineering at the Montanuniversitaet Leoben for our fruitful discussions. Here Christian Heiss, my vis-à-vis colleague in the office, is especially mentioned.

Finally I would like to thank my family, my friends and Erika. Without their support it would never have been possible to finish my studies.

Abstract

This thesis summarises the findings of 27 model-scale bench blasts in magnetic mortar, which were done from 2011 to 2014 at the blasting site of the Montanuniversitaet Leoben.

The aim of the study was the investigation of the influence of blasthole delay-time in small scale bench blasts on the face characteristics and the cracking damage created in the surrounding rock, which affects the fragmentation in subsequent rows.

The test specimens or blocks, which were made of magnetite-mortar, were roughly 1:100 in scale to normal bench blasts. The confinement of the testing blocks at the sides and at the back ensured the similarity to normal bench blasts with regard to the wave transmission into the surrounding rock. The specimen contained three or four rows with 5 blastholes each and were shot row by row, with virgin (undamaged) material in row 1 and increasingly damaged or preconditioned material in the following rows.

The tested in-row delay-combinations varied between 0, 28, 73 and 140 µs which corresponds to 0, 0.4, 1.0 and 2.0 ms/m of burden.

The measured material properties showed that the magnetite-mortar used modelled the inhomogeneous behaviour of rock but some unexpected differences of the different production cycles were still detected.

The characteristics of the bench after each blast was evaluated along three horizontal lines out of a 3D-model of the bench face. The tested delay-time sequences of the virgin (1st row) and single pre-conditioned blasts (2nd row) produced more overbreak for longer delay-times while the 3rd row shots resulted in a flatter surface independent of the chosen delay.

The visible cracks at the top of the testing blocks were documented and divided into several crack families according to their angle, length and origin. The remaining block was broken out of the blasting site after blasting and cut into several horizontal and vertical slices and dye-penetrant spray was used to visualize the cracks created. Some of the detected crack families showed an

influence of the delay-time. The calculated mean crack density (MCD) showed that longer delays resulted in a higher degree of damage.

The fragmentation results were well reproduced by the basic three parameter Swebrec function. The blasts showed coarser fragmentation for the shortest delays while the longest delays generated the finest material. The observed improvement of fragmentation in the 2nd and 3rd row blasts was linked to the pre-conditioning of the burden for the following row while blasting the actual row.

Zusammenfassung

Die vorliegende Dissertation fasst die Ergebnisse von 27 Sprengversuchen im Kleinmaßstab zusammen, welche zwischen 2011 und 2014 in der sprengtechnischen Versuchsanlage der Montanuniversität Leoben durchgeführt wurden.

Ziel der Dissertation war die Untersuchung des Einflusses der Verzögerung von einzelnen Bohrlöchern einer Reihe auf die Rauigkeit der neu geschaffenen Bruchwandoberfläche sowie auf die ins anstehende Gebirge eingetragenen Risse, da diese die Zerkleinerung der weiteren Reihen maßgeblich beeinflussen.

Die Betonblöcke für die Sprengversuche wurden aus Beton mit Magnetit-Partikeln hergestellt. Diese hatten in etwa den Maßstab von 1:100 zu normalen Tagebausprengungen und waren in einem Auflagerblock seitlich sowie hinten eingespannt. Daher war die Wellenausbreitung ins anstehende Gebirge vergleichbar mit normalen Tagebausprengungen. Die Betonblöcke wurden mit drei bzw. vier Reihen mit jeweils 5 Bohrlöchern hergestellt, wobei die erste Reihe in ungeschädigtem Material sowie die weiteren Reihen in bereits vorgeschädigtem Material aufgrund der vorangehenden Sprengungen gezündet wurden.

Die untersuchten Kombinationen der Verzögerung waren 0, 28, 73 und 140 µs und entsprachen somit 0, 0.4, 1.0 und 2.0 ms/m Vorgabe.

Die Auswertung der Materialeigenschaften ergab, dass der verwendete Magnetit-Beton die Inhomogenität von Gestein weitestgehend ausschließt. Allerdings wurden unerwartete Unterschiede in den Materialeigenschaften der verschiedenen Produktionszyklen festgestellt.

Die Rauigkeit der gesprengten Bruchwand wurde nach jeder Sprengung anhand des Verlaufs von drei horizontalen Konturlinien aus dem 3D-Modell der Bruchwand bewertet. Die untersuchten Verzögerungskombinationen der ungeschädigten ersten sowie bereits vorgeschädigten zweiten Reihen erzeugten mehr unregelmäßigen Rückriss für längere Verzögerungen zwischen den Bohrlöchern. Die Sprengversuche in der dritten Reihe resultierten in homogener ausgebildeten Oberflächen, unabhängig von der gewählten Verzögerung.

Die sichtbaren Risse an der Oberfläche der Testblöcke wurden dokumentiert und in verschiedene Rissfamilien gemäß deren Winkel, Länge sowie Ursprung eingeteilt. Der verbleibende Testblock wurde nach der letzten gesprengten Reihe aus dem Auflagerblock herausgebrochen und in mehrere verschiedene horizontale sowie vertikale Scheiben geschnitten. Auf den Schnittoberflächen wurden die erzeugten Risse mittels Farbeindringmittel visualisiert und ebenfalls in Rissfamilien klassifiziert. Einige der detektierten Rissfamilien zeigten Abhängigkeiten von den gewählten Zeitverzögerungen wobei längere Verzögerungen mehr Schädigung hervorriefen.

Die Ergebnisse der Zerkleinerung wurden mit der 3-parametrigen Swebrec-Funktion sehr gut beschrieben. Die Zerkleinerung zeigte sich abhängig von der Vorschädigung wobei Sprengungen in der zweiten sowie dritten Reihe jeweils feineres Material als in den vorangegangenen Sprengungen produzierten. Mit Ausnahme der simultan initiierten Sprengung (0 µs Verzögerung) zeigte die kürzeste Verzögerung die gröbste Zerkleinerung während das feinste Material durch die längste Verzögerung erzeugt wurde.

Table of Contents

1 Introduction

Blasting is by far the most effective way for the excavation of raw materials in hard rock mines and quarries. Although the procedure seems to be well known and is carried out all over the world several aspects of the process are still not fully understood.

During the detonation process the explosives generate high pressures and a large amount of gases. The compressive pressure pulse exceeds the compressive strength of the blasted material and the first cracks are generated. At the free face the compressive waves are reflected and these "*reflected waves play a major role in determining which fractures develop from the region of the borehole and in which directions they propagate*" (Field & Ladegaard-Pedersen, 1971). The produced gases flow into these cracks, open them further and are also responsible for the throw of the material. The combination of the two processes (generated waves and gas expansion) is the reason for the success of the excavation process and the rock breakage.

In normal bench blasting in mines and quarries the individual blastholes have a specific delay. The possible delays are dependent on the type of detonator used. The available delay-times of electric and NONEL-detonators are fixed by the manufacturers due to the inaccuracy of the pyrotechnic delay-timing element. Their available delays are normally in the range of 17 to 25 ms or longer and accordingly the possibility of overlapping of individual delay-times is minimized. By using electronic detonators the possible interval for delay-times is 1 ms (or even less) due to the high accuracy of the micro-chips used.

Although Blair (2010) states that "*delay accuracy and timing are typically not the major variables that govern blast vibration and fragmentation*" there are several papers available, which investigate the reasons for choosing different delay-time arrangements. Cardu & Giraudi (2013) summarized a collection of published cases, which showed that on one hand the blast-vibrations are influenced by the delay-time arrangement (e.g. Sharma, 2009) and on the other hand the fragmentation is improved by choosing the correct delay-time for the present rock conditions (e.g. Winzer et al., 1983).

The delay-time of the individual blastholes is also influencing the surrounding rock. Anyhow the phenomenon of crack introduction is not that well investigated, although the cracks created might have a severe influence on the stability of the bench face (Cunningham, 2003). They might be responsible for safety issues due to rock fall risk or for extensive support to guarantee the needed stability of the bench face. This is especially important in the case of final pit walls, which should be stable over a long time. In this case the wall control is of highest priority. From the procedure of smooth blasting (e.g. Rustan, 1998) it is known that simultaneously blasted holes (zero delay between blastholes) in combination with a special type of explosive and smaller side-spacing are generating fewer cracks in the surrounding rock.

1.1 Objectives and Summary of Work

The objective of this doctoral thesis is the investigation of the influence of blasthole delay-times on the characteristics of the fresh blasted bench face and the cracking damage created in the surrounding rock. While the characteristics of the surface may have an effect on the reflection of compressive waves and may consequently influence the orientation of the generated tensile wave, the cracks created are responsible for the pre-conditioning of the further rows and may consequently affect their fragmentation.

The following research questions are the basis for this doctoral thesis:

- RQ 1: Is the delay-time influencing the fragmentation and backbreak in specimens with given pre-conditioning?
- RQ 2: How far does the pre-conditioning of the 1st row blasts reach?
- RQ 3: How many rows have to be blasted before the pre-conditioning becomes constant?
- RQ 4: How is the delay-time influencing the cracks created?
- RQ 5: Is there an effect of a staggered pattern?

Before these research questions can be answered the following methodological questions have to be answered:

- Are the results from the different mortar production cycles comparable?

- Are the results within the mortar production cycles comparable?
- Are neighbouring holes influencing the backbreak or the cracks created?
- Is a detachment of the testing block influencing the results?
- Which method is best suitable to quantify the damage created?

Due to the possibility of a larger number of tests the investigations were done in small scale. The properties of the test set-up had to be comparable to normal bench blasts. Especially the transmission of the blasting waves to the surrounding rock should be guaranteed because a reflected tensile wave will influence the cracking and the fragmentation (Field & Ladegaard-Pedersen, 1971; Blair, 2010). The Chair of Mining Engineering at the Montanuniversitaet Leoben developed for this purpose a blasting site at the Styrian Erzberg where bench blasts in small scale could be done (Maierhofer, 2011).

Due to better repeatability and to avoid the large influence of geological conditions to the crack development and the fragmentation, the material for the blasting tests should be homogeneous. A magnetite-mortar mixture, which was already used at the Luleå University of Technology (Johansson, 2008) was chosen to be an acceptable testing material.

The blastholes, which were drilled in the laboratory, had a diameter of 10 mm and were going through the entire height of the testing blocks. They were charged with a 20 g/m PETN-cord and initiated from the top of the blasthole.

With the geometry used in the experiments the analysis of the crack development and fragmentation in virgin (first row) and in already damaged material (further rows of the testing blocks) was possible.

The blasted bench surface behind each row was evaluated along three horizontal lines of a 3D-model of the bench face and processed with AutoCAD® (by Autodesk, Inc.) and MATLAB® (by MathWorks, Inc.). The surface was described by statistical parameters (min, max, mean and std dev) of the deviation from the as-drilled line connecting the blasthole centres plus under- and overbreak areas. The mean distance of the individual data points to the reference line (D_{Mean}) was used as a comparative figure for the broken out volume. The normalized slope

inclination of the individual sections of the contour lines (S_{Norm}) was used as a comparative figure for the micro-roughness of the fresh blasted surface.

The visible cracks at the top of the testing blocks were traced and crack families based on angles, lengths and origin identified. The damage cracks in the block remnants behind the last row were quantified on vertical and horizontal slices which were cut out of the broken-out block. The visualized cracks were used to create a digital 3D-model with AutoCAD® and out of this model a categorization of different crack families, the crack density and a study of crack intersections was carried out (Navarro, 2015). Several thin sections as well as a computer tomography were done at interesting parts to investigate the cracks created.

After blasting a sieving analysis was done and the fragmentation was quantified by the determination of sieving parameters and sieving curves. The Swebrec distribution (Ouchterlony, 2005, 2010) was used as a fitting function because it gives better fits than most other functions (Sanchidrián et al., 2010, 2012, 2014).

The investigations were finalized by a statistical evaluation of the data sets and correlations between the cracks created, the surface characteristics and the fragmentation were established.

A summary of the methods used and the results obtained can be found in Schimek et al. (2015).

2 Literature Review

2.1 Basics of Crack Generation

The following literature review summarizes the basics of crack generation because the aim of this thesis was to investigate the influence of delay-time on the fractures created in the surrounding rock which effect the fragmentation of the following rows. The review starts with theoretical observations of the mechanism of crack development followed by the investigations of blasted specimen and benches and their numerical simulations.

There are many papers available which distinguish in terms of rock fragmentation between the two main mechanisms of breakage related to stress waves and breakage related to the gas pressure. Saharan et al. (2006) made a summary of the literature available and came to the conclusion that "*controversies exist for the respective roles of gas pressure and shock wave energy in dynamic fracture initiation and propagation.*" The following review is mainly based on the breakage mechanism related to stress waves.

The detonation of a point charge or small spherical charge generates a longitudinal compressive wave propagating radially in all directions (see Figure 1).

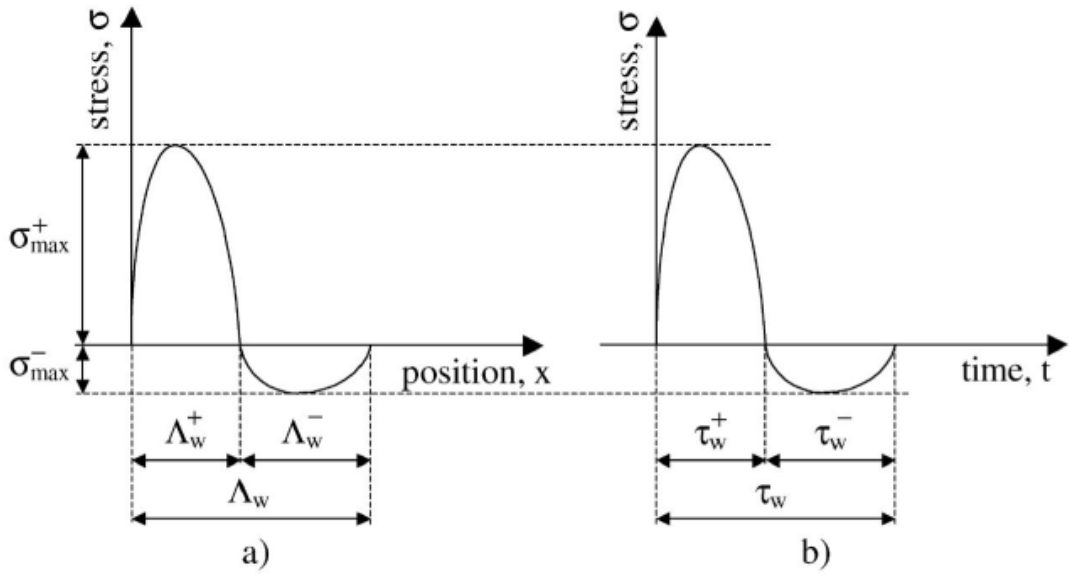

Figure 1: Representation of a one-dimensional stress wave / pulse in the space domain (a) and time domain (b) (Rossmanith, 2002)

Zhu et al. (2007) explains that the generated "*high pressure on the borehole wall sets off a shock wave in the adjacent rock mass, but it soon decays to a high amplitude stress wave propagating at the velocity of longitudinal wave in the rock mass.*"

According to Rossmanith (2002) this stress wave, which travels with the P-wave-velocity of the unblasted material, can be divided in a leading compressive part (index "+") and a tailing tensile part (index "-").

When the compressive wave hits a free surface it is reflected as a tensile wave. In the case of a 90° incidence the generated tensile wave is heading directly back to the blasthole (see Figure 2).

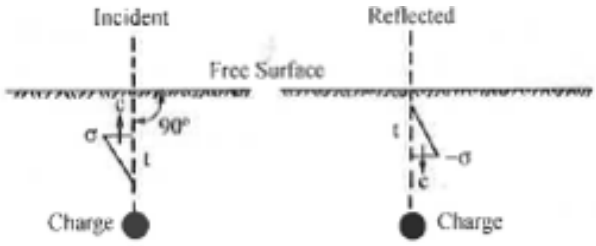

Figure 2: Wave interaction at the free surface (Hustrulid, 1999)

The generated waves which hit the free surface at an oblique angle are reflected in a slightly different way (see Figure 3).

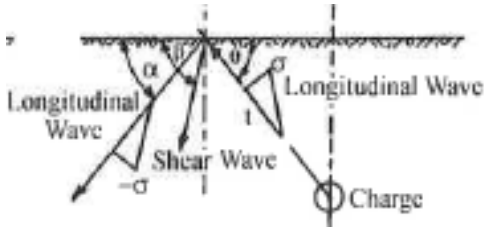

Figure 3: Reflection of angled waves (Hustrulid, 1999)

The outgoing radial longitudinal compressive wave generates a reflected longitudinal tensile wave. The angle of reflection is the same as the angle of the incidence ($\alpha = \theta$). Additionally a reflected shear wave is generated at the free surface.

Radial cracks, which are oriented in all directions, start growing shortly after the stress wave is generated. The cracks perpendicular to the free surface will be slowed down due to the reflected tangential compressive wave (see Figure 4).

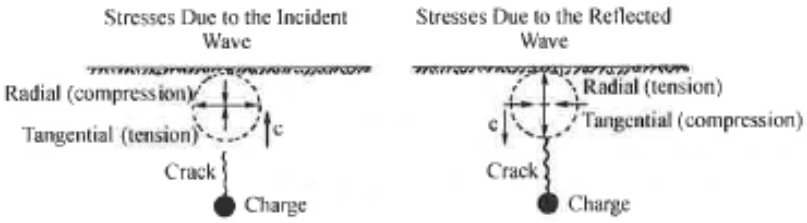

Figure 4: Crack extension in relation to the incident and reflected waves (Hustrulid, 1999)

The inclined cracks are influenced by the reflected waves in the way that there is a reflection geometry which favours the crack growing. The reflected longitudinal tensile wave (see Figure 3) is perpendicular to one specific inclined radial crack (see Figure 5) and acts as a tensile radial component which is increasing the growth of this crack (see Figure 6).

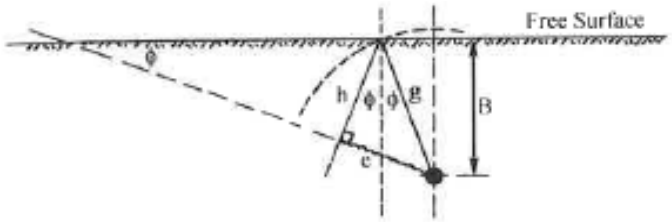

Figure 5: Inclined reflection geometry influencing crack growing (Hustrulid, 1999)

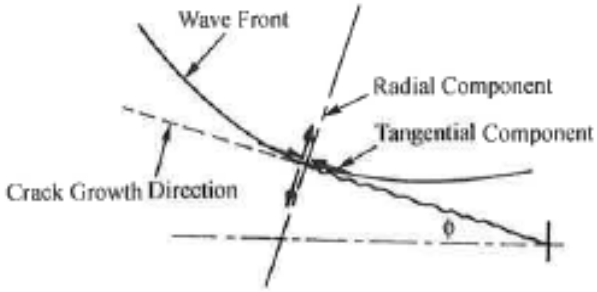

Figure 6: Reflected waves favouring the crack growth (Hustrulid, 1999)

To investigate the influence of the reflected tensile wave on the crack-growing in a practical experiment Field & Ladegaard-Pedersen (1971) did several single-hole small scale blasting tests in Perspex models. The borehole had a diameter of 1.5 mm and a length of 30 mm. The lower 4 mm were filled with explosives. The setup used can be seen in Figure 7.

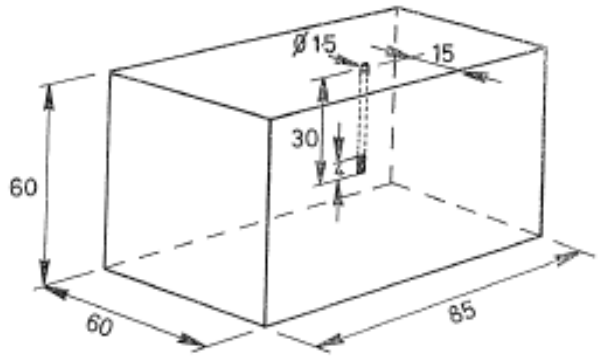

Figure 7: Schematic drawing of the test-setup of Field & Ladegaard-Pedersen (1971); Units in [mm]

The tests were split up into parts where different conditions of wave reflection were investigated. The result of a blasting test without adding any specific conditions to the above mentioned geometry is presented in Figure 8.

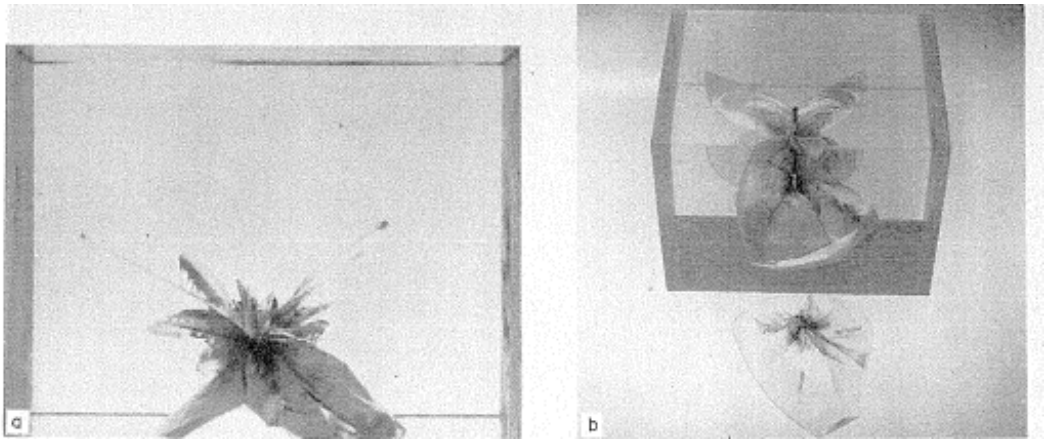

Figure 8: Top (a) and angled (b) view after blasting test (Field & Ladegaard-Pedersen, 1971)

The blasting waves were reflected at the free surface and favoured the crack growing in the forward direction. The model shown in Figure 6 seems to be confirmed by this test.

In a further test the Perspex block was put into a liquid. In that arrangement all surfaces were acoustically matched which means that the distance to the free surface seems to be almost infinite for compressive waves. These blasting waves were not reflected at a free surface but transmitted away from the blasted hole. Figure 9 shows the result of this blasting test.

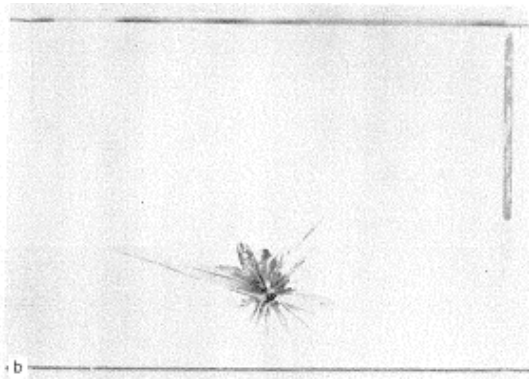

Figure 9: Top view of blasting test with acoustically matched surfaces (Field & Ladegaard-Pedersen, 1971)

Many radial cracks were created, but there is no detectable trend for the radial cracks to grow to the direction of the nearest surface.

Further tests with regard to the reflection of the longitudinal compressive wave at the free surface were done with saw-toothed, concave and convex surfaces in front of the blasted holes (see Figure 10).

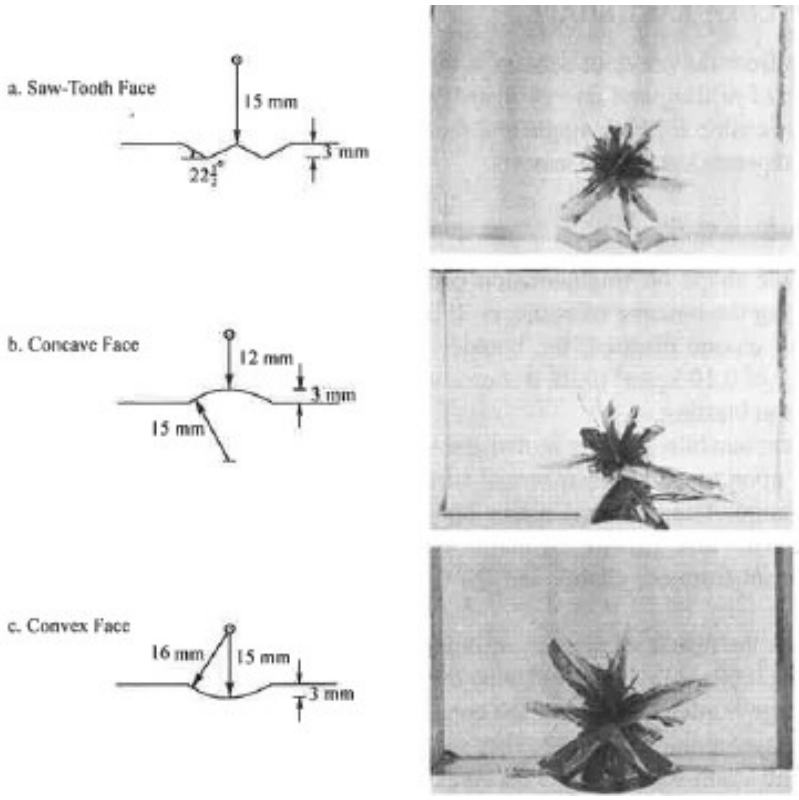

Figure 10: Effect of face-shape on crack development (Field & Ladegaard-Pedersen, 1971)

The saw-tooth shaped surface resulted in a dispersion of the blasting waves which hit the surface directly in front of the blasthole. The outer angled surfaces reflected

the waves directly back to the blasthole. This resulted in no boulder formation, but relatively more radial cracks compared to a flat surface were created (see Figure 8). With a concave face all of the reflected waves were dispersed and no detached boulder was observed. Due to the smaller distance of 12 mm to the free surface the cracks reached the front face though. In the case of the convex face the blasting waves were reflected and concentrated back to the blasthole and a detached boulder was formed.

This concentration of blasting waves can be explained by the investigation of a detonating point charge in a circular model. The generated longitudinal compressive waves are reflected at the free surface and concentrated back to the blasthole. Rossmanith & Uenishi (2006) explained this phenomenon, where the longitudinal compressive wave is reflected at the free surface and exhibits circumferential tension. When the induced circumferential tensile stress is larger than the tensile strength of the material, then radial boundary cracks are created (see Figure 11).

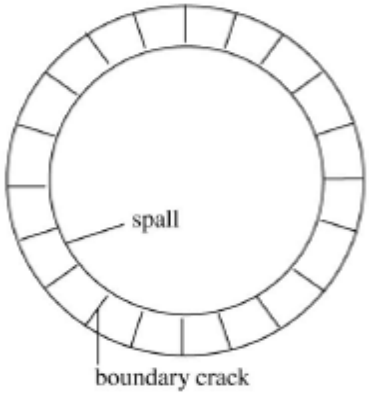

Figure 11: Boundary cracking and spalling after a detonated point charge (Rossmanith & Uenishi, 2006)

Additionally to the boundary cracks circumferential cracks may be created during the blast. These circumferential cracks are explained by Rossmanith & Uenishi (2006) as a spalling phenomenon where a plane wave acts normally on a plane free surface. At a specific distance from the free surface the tensile stress from the reflected waves is higher than the tensile strength of the material and the circumferential P-spall is formed.

Recent numerical investigations (Zhu et al., 2007 & 2008) simulated these single centrally loaded circular rock model blasts using the AUTODYN 2D code (see

Figure 12). The simulations had the aim to investigate the dynamic fracture process in the first stages of rock blasting during which the induced stress waves dominate. A coupling medium was used between the explosive (PETN) and the borehole wall. The simulation stops before the generated gases penetrates into the cracks and results in further fragmentation.

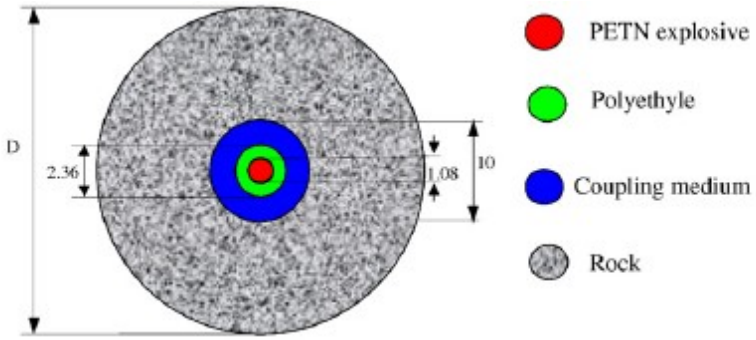

Figure 12: Properties of the circular simulation model. Units in [mm] (Zhu et al., 2007)

The rock fracturing process was analyzed at six target points which can be seen in Figure 13 where the fractures for different time-periods are shown.

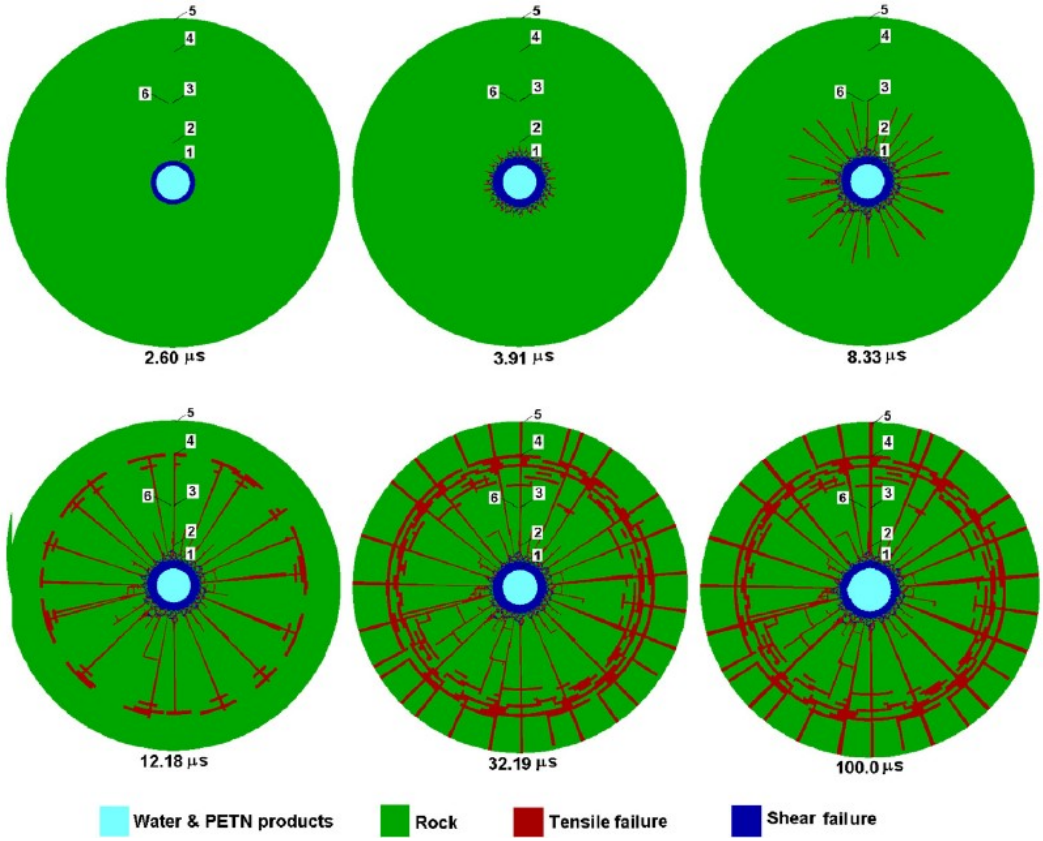

Figure 13: Material status of a rock sample (diameter = 100 mm) as a function of time after initiation of the explosive in the borehole (Zhu et al., 2007)

Around the blasthole a shear failure zone is developed where the rock is completely pulverized. Outside this shear failure zone lies a region which is heavily fractured with small radial cracks followed by a region with a lower crack density. The above mentioned circumferential cracks developed also at a specific distance from the outer surface. The simulated boundary cracks are not symmetrical due to the applied interaction logic between two contact materials and the failure criterion used.

An additional simulation was done for the case of an outer boundary which transmits the blasting waves away from the blasthole and doesn't reflect them back. This is comparable to the investigations done by Field & Ladegaard-Pedersen (1971) where they did tests with acoustically matched surfaces (see Figure 9). The results of this simulation are shown in Figure 14.

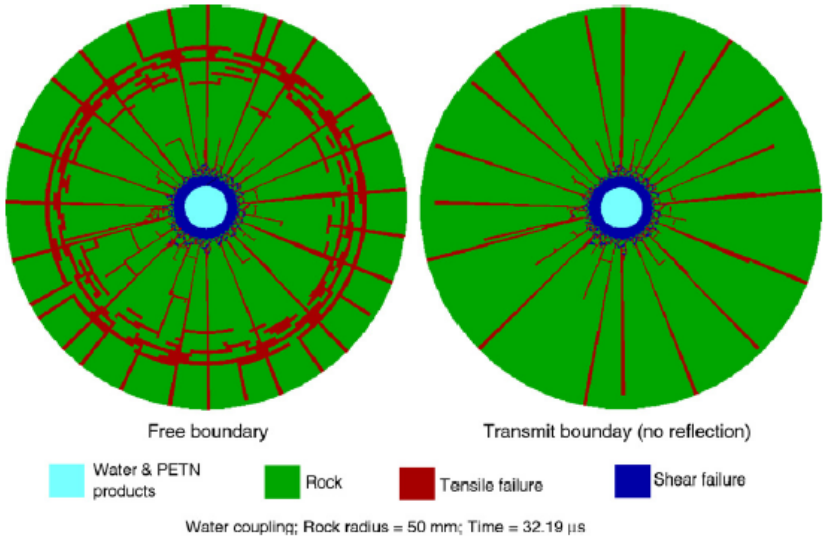

Figure 14: Comparison of material status for the rock sample with free (left) and transmit boundary (right); the rock sample outer diameter = 100 mm (Zhu et al., 2007)

The pulverized shear failure zone and the following heavily fractured region are quite similar for both cases. The outer regions of the cylinder are different. In the case of transmitting boundaries the longitudinal compressive wave is not reflected back. The tensile stress doesn't exceed the tensile strength of the material and no circumferential cracks are generated.

In a 3-dimensional model a linear charge detonating with supersonic speed generates a set of two P- and S-wave Mach cones (see Figure 15).

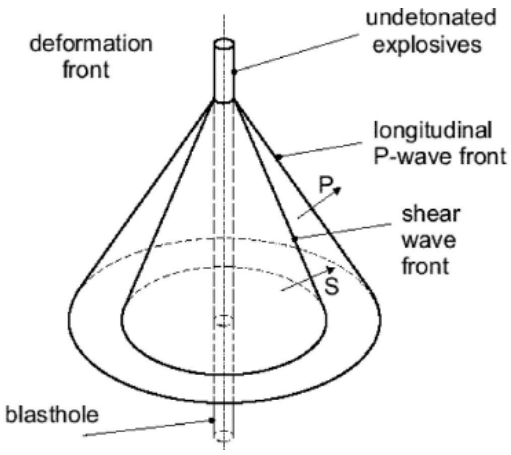

Figure 15: Wave fields of a linear charge detonation (Rossmanith et al., 2005)

The Mach cones are reflected at the free surface and generate boundary cracks along the outer surface of the blasted cylinders (see Figure 16).

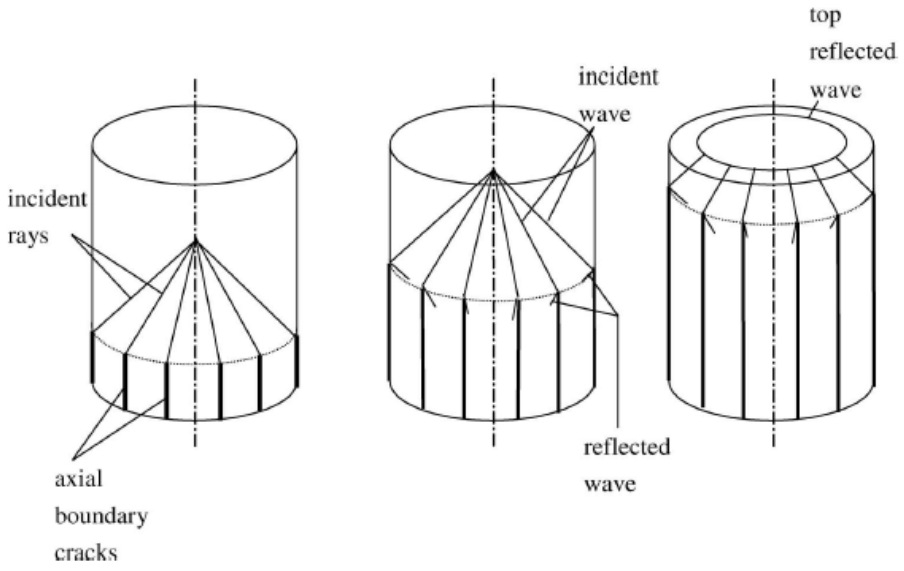

Figure 16: Generation of boundary cracks on the free surface (Rossmanith & Uenishi, 2006)

If there are imperfections of the specimen then the critical circumferential strain is reduced and unloading waves are generated at the imperfections (see Figure 17).

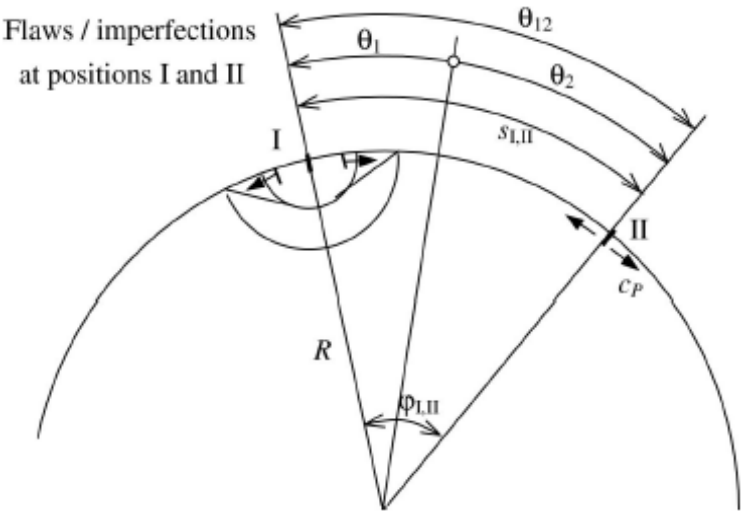

Figure 17: Imperfections at boundary of cylindrical specimen (Rossmanith & Uenishi, 2006)

These imperfections are finally the drivers for the distribution of the cracks at the outer surface of the cylinders (see Figure 18).

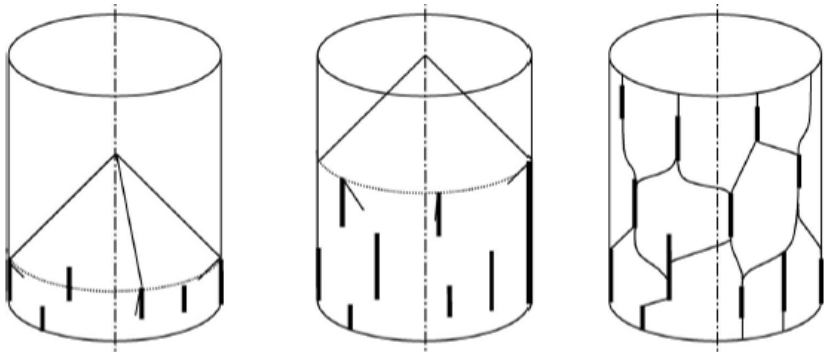

Figure 18: Vertical longitudinal cracks generated on the free surface in specimen with randomly distributed imperfections (Rossmanith & Uenishi, 2006)

The above mentioned circumferential cracks are also formed in the 3-dimensional model due to the wave reflections at the outer boundary and the tensile stress which is exceeding the tensile strength of the material. The circumferential cracks are formed in a cylindrical way (see Figure 19).

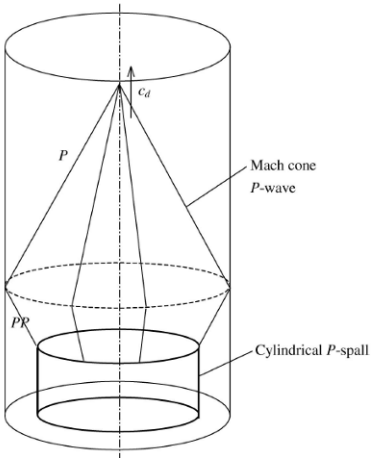

Figure 19: Cylindrical spall fracture during reflection of Mach type conical P-wave (Rossmanith & Uenishi, 2006)

The above mentioned crack formation mechanisms were observed at the Montanuniversitaet Leoben (Wagner, 2002) where free-standing mortar cylinders were blasted. The samples were centre-line loaded with a detonating cord. After blasting the samples were rebuilt (see Figure 20).

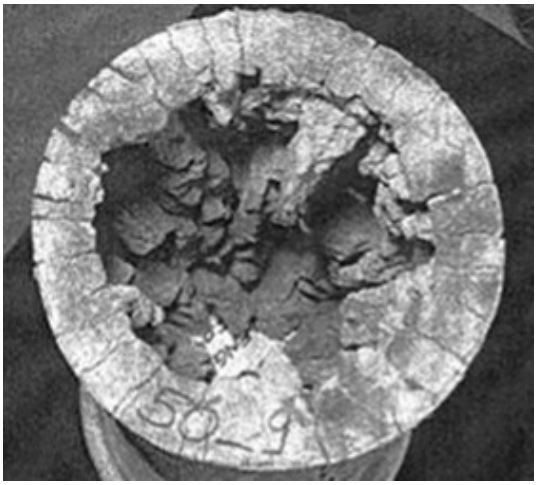

Figure 20: Crack pattern of blasted and rebuilt cylinder (Wagner, 2002)

The boundary cracks and the cylindrical P-spall are detectable and the picture is comparable to Figure 11. Such results inspired the work of Rossmanith & Uenishi (2006).

The vertical longitudinal cracks on the free surface (as seen in Figure 18) were also detected during these blasting tests (see Figure 21).

Figure 21: Vertical longitudinal cracks on the free surface of a rebuilt cylinder (Moser, 2003)

Zhu et al. (2008) simulated the crack initiation and propagation in an axial cross section of a cylindrical rock specimen. The 2D-axial symmetric model was the base for the 2D simulation calculation. A single centrally located line of PETN detonating cord was used as explosive (see Figure 22). The properties of the simulation model (coupling medium, type of rock) were similar to the model used in the above mentioned simulations by Zhu et al. (2007).

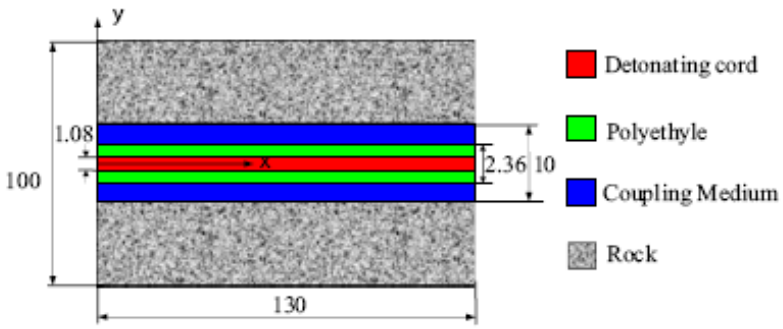

Figure 22: Properties of the simulation model. Units in [mm] (Zhu et al., 2008)

The initiation of the detonating cord started on the left side of the model and the detonation travels along the x-axis. Due to the finite length of the model there were reflecting surfaces at both ends of the cylinder. Along the y-axis the model and the crack initiation and propagation was still symmetric.

The fracturing process was analyzed at eight target points which can be seen in Figure 23 where the fractures for different time-periods are shown.

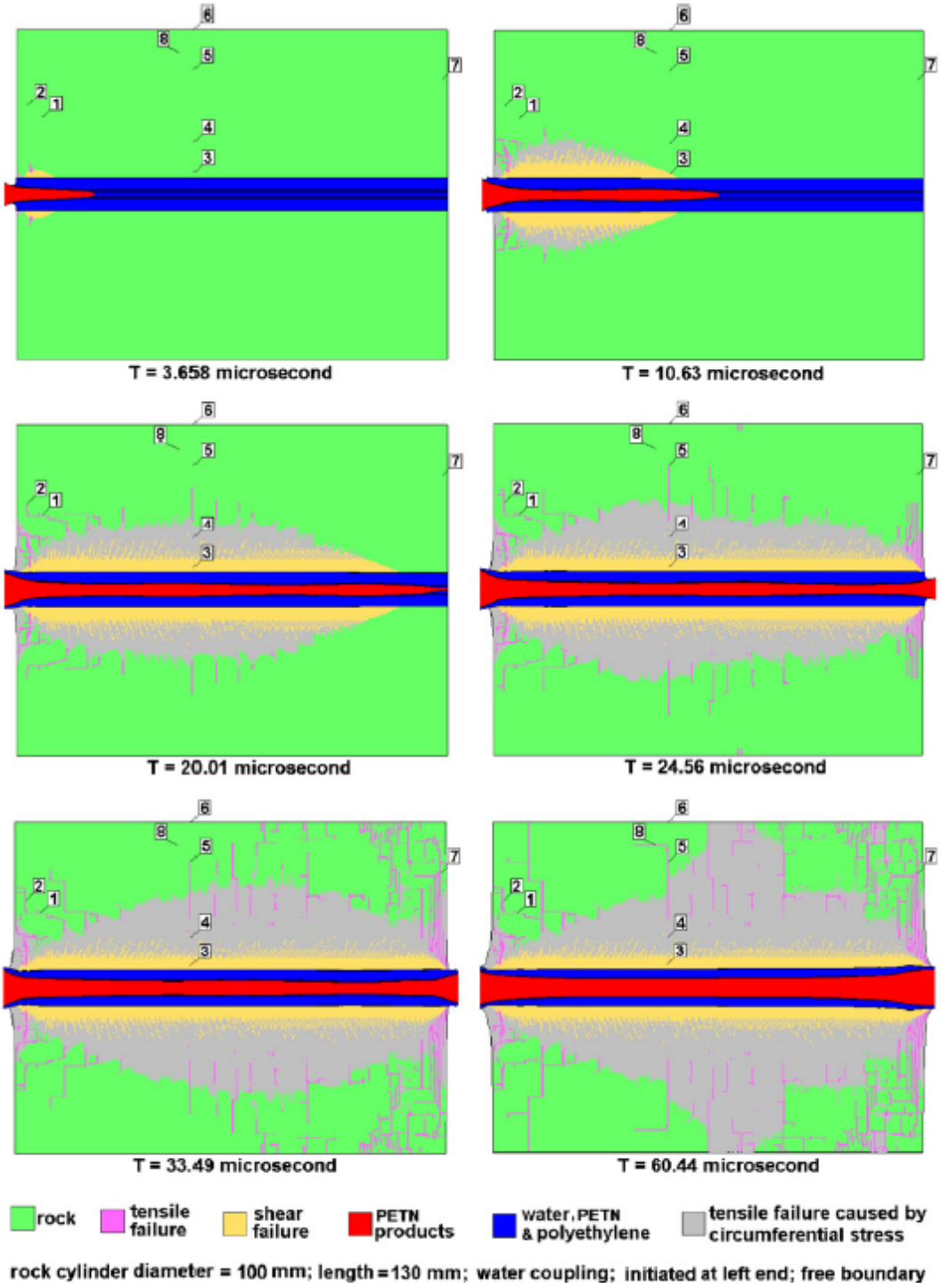

Figure 23: Material status of a cylindrical rock as a function of time after initiation of the explosive (Zhu et al., 2008)

Around the blasthole a shear failure zone was developed due to the compressive pressures which were generated during the detonation. The fracture pattern developed until the explosive had detonated through the complete length of the specimen. The density of cracks was, due to the larger borehole pressure, at the right side higher than at the left side of the simulation model.

Zhu et al. (2008) divided the failure zones into three types:

- Type I: These cracks were perpendicular to the axis of the cylindrical rock specimen and caused by the tensile stress σ_x.
- Type II: Cracks which were parallel to the axis of the cylindrical rock specimen and caused by the reflected stress σ_y.
- Type III: This type of crack occured in any axial cross section plane in a 3D-model and was caused by the circumferential stress σ_θ.

In the case of cube-shots the longitudinal compressive waves are also reflected at the free surface as tensile waves. They are distributed and not concentrated back to the blasthole. The dominant circumferential cracks are not that obvious and the boundary cracks are also formed in a different way than described in Figure 11. The corners of the cubes are more or less untouched (see Figure 24).

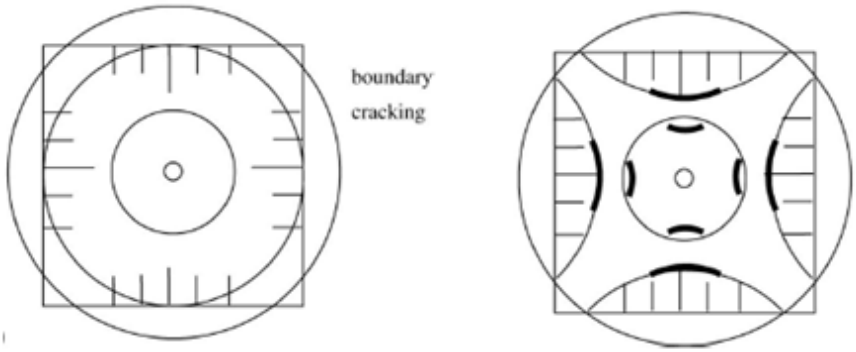

Figure 24: Boundary cracking and spalling of cube-shots (Rossmanith & Uenishi, 2006)

Similar to the free standing cylinders of Figure 20 free standing cubes were also blasted at the Montanuniversitaet Leoben (see Figure 25).

Figure 25: Crack pattern of blasted and rebuilt cube (Wagner, 2002)

At the cube test specimen the cylindrical P-spall was not detected. The rest of the observed crack pattern looked similar to the expectations of Figure 24.

Wimmer (2007) repeated some cube-shots at the Montanuniversitaet Leoben with the aim to rebuild the specimen after blasting to be able to investigate the crack development.

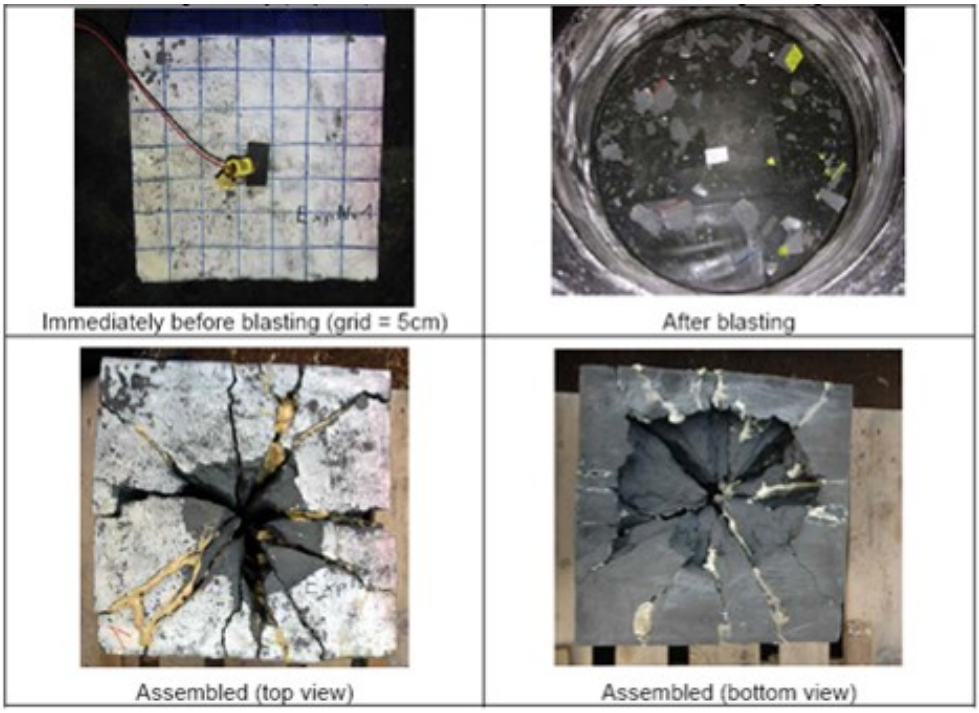

Figure 26: Blasting test in a cubic specimen (Wimmer, 2007)

The result of this blasting test was comparable to the results seen before.

Furthermore Wimmer (2007) did several shots with asymmetrically placed blastholes in specimens elongated towards the back and the sides (see following figures). The burden and the type of explosives used were the same. He found that "*the asymmetric position of boreholes resulted generally in a reduced number of cracks propagating backwards into the block, whereas the radius of effects (seen from the midpoint of the hole) is slightly larger in the direction of the solid block. This suggests that the main stress wave reflection occurred at the nearest free face.*" (Wimmer, 2007)

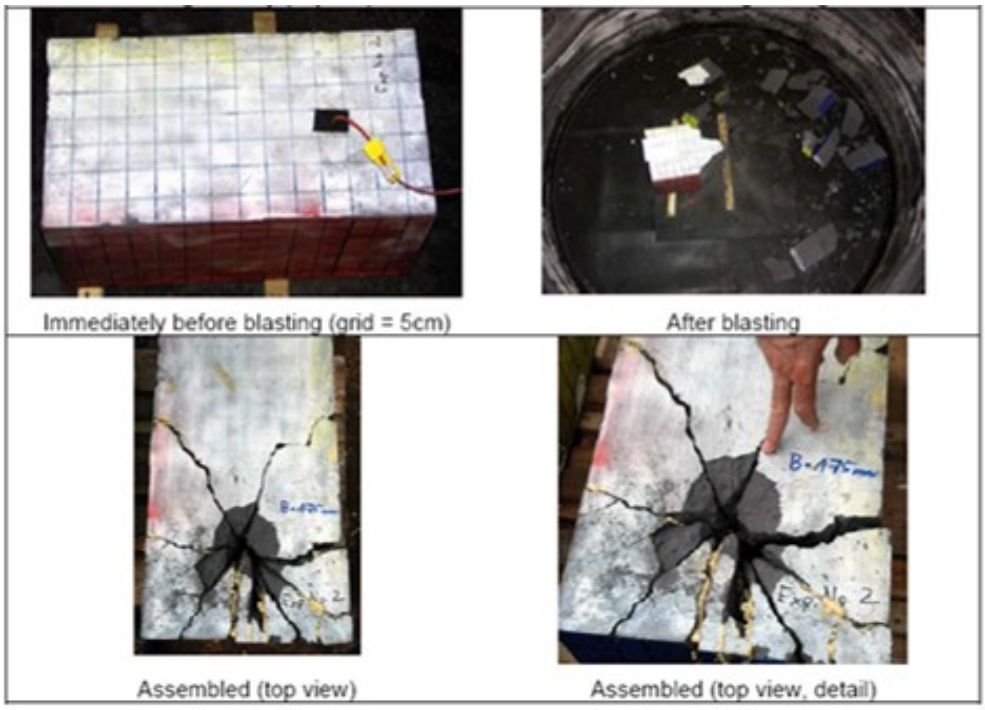

Figure 27: Blasting test in an elongated specimen (Wimmer, 2007)

Figure 28: Blasting test with eccentric charge in a specimen (Wimmer, 2007)

Investigations in “half-scale” were also done in recent years (Maierhofer, 2011). The size of the test-specimen was one tenth of normal bench blasts.

Maierhofer (2011) investigated the fragmentation and breakout angle in a 2 m³ mortar block half-scale experiment with varying burden for single-hole shots. The test arrangement was comparable to normal bench blasts (see Figure 29).

Figure 29: Half-scale experiment of Maierhofer (2011)

The resulting breakout angle was similar to that described by Hustrulid (1999) and in the range of 140 – 150° (see also Ouchterlony & Moser, 2013).

Ma & An (2008) simulated the crack initiation and propagation in bench-like models using the software LS-DYNA (see Figure 30). Three surfaces were transmitting, i.e. non-reflecting (acoustically matched). The longitudinal compressive waves, which were generated during the detonation, were not reflected at these surfaces. The nearest surface to the borehole was a free surface where compressive waves were reflected as tensile waves.

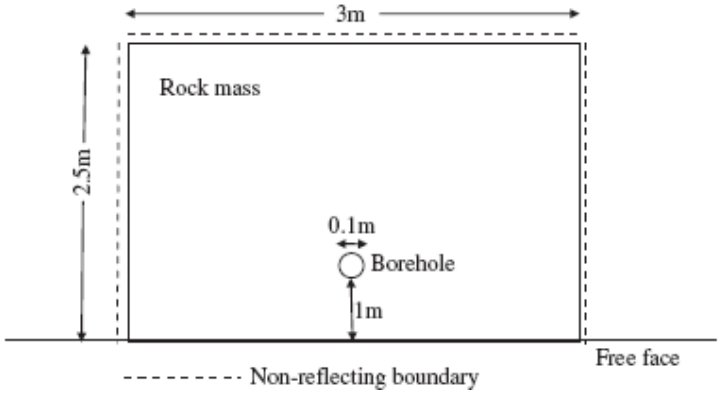

Figure 30: Analytical model with one free face (Ma & An, 2008)

The modelled rock fracturing process can be seen in Figure 31 where the fractures for different time-instances are shown.

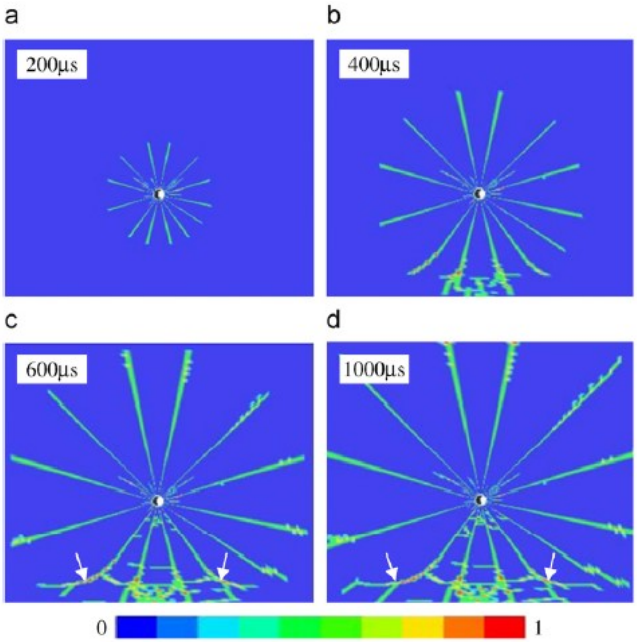

Figure 31: Crack propagation process in a one-free-face model (Ma & An, 2008)

The radially initiated cracks were in the early stages growing equally in all directions. After the longitudinal compressive wave hit the free (reflecting) surface, this wave was reflected back as a tensile wave. When the reflected tensile stress exceeded the tensile strength of the material further cracks were generated. The cracks marked with white arrows in Figure 31 were called spalling cracks and can extend to a considerable length (Ma & An, 2008).

Wilson & Holloway (1987) described the crack development for bottom-initiated bench blasts as follows: "*It is believed that the radial fractures which form around a borehole in the top surface and the crack network patterns which form in the bench face in front of the boreholes are caused by tangential stresses in the P-wave which become tensile and are intensified as the wave reflects at near-normal incidence from the free surfaces. These fractures open at the free surface and propagate back into the interior, and are initiated before any spall-type fracture surfaces are created. If the reflected wave is intense enough, then spall fractures will occur below the surface in planes roughly orthogonal to the radial fractures…*"

2.2 Superposition of Blasting Waves

The delays between the individual blastholes in normal bench blasts are nominally in the range of 17 – 25 ms or longer. One reason for this delay is the low accuracy of the pyrotechnic delay-timing element of the electric or NONEL-type detonators used. With the delay steps used the manufacturers of the detonators guarantee that there is virtually no overlap of the individual delay-sequences. When using the newest electronic detonators, the delay between the individual blastholes can be chosen in steps of 1 ms (or even less) due to the high accuracy of the built-in micro-chip. With this short delay it is possible that the generated blasting waves of the individual detonated blastholes (see chapter 2.1) interact with the waves generated from the next hole in a shots-in-a-row arrangement.

Rossmanith (2002) postulated that an overlap of the negative (tensile) tailing part of the compressive wave (see Figure 1) as well as of the shear waves results in a much more effective fragmentation. This is the case due to the achieved tensional states of the overlapped tensile tails which are higher than those obtained by the reflection of the compressive waves. Rossmanith (2002) explained the generated P- and S-waves in Lagrange diagrams in only one geometrical dimension (Figure 32).

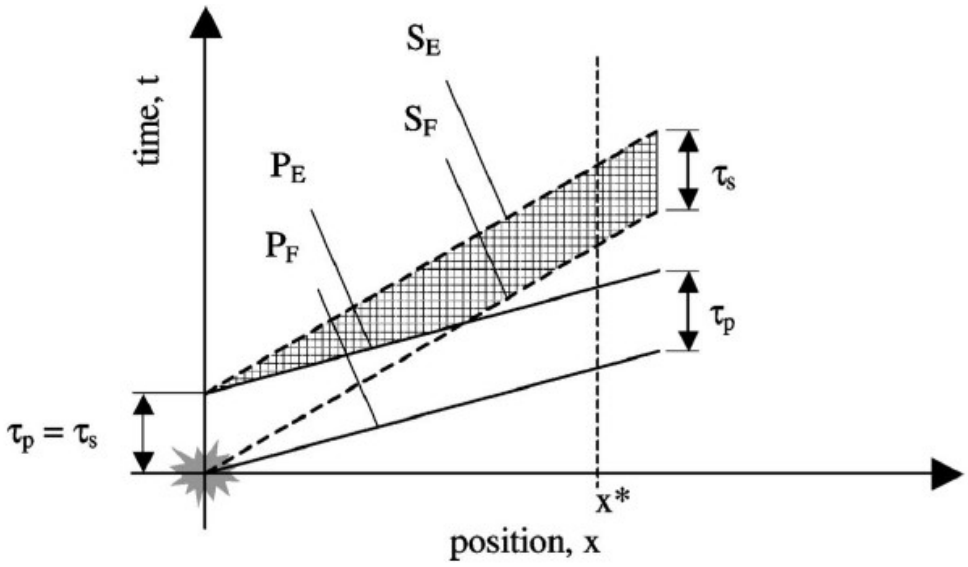

Figure 32: Definition of fronts and tails of a P-wave (P_F, P_E) and an S-wave (S_F, S_E) for a short pulse (Petropoulos et al., 2013)

Petropoulos et al. (2013) explained that "*the tangents of the associated lines are the inverse of the speeds of the waves. Since the propagation speed of P-waves is larger than that of S-waves, its associated line is of smaller slope.* T_S *and* T_P *represent the duration of compressive and shear waves, of which a part is the positive leading followed by a negative tailing."*

Vanbrabant & Espinosa (2006) did a large scale investigation in the Chuquicamata mine in Chile where the fragmentation of blasts with conventional pyrotechnic detonators to that of blasts with electronic detonators was compared. The aim was to improve the fragmentation by the interaction of the negative tailing parts of the compression waves (see Figure 1 above) with the use of very short delays.

It is mentioned that the tests showed an average improvement of the fragmentation parameter x_{50} of 45.6 %.

Another large-scale investigation in the Aitik open pit mine (Petropoulos et al., 2013) had the aim to reduce the crushing energy needed within the concept of "Mine-to-Mill". Several blasting tests with a delay between 1 and 42 ms were done and the crushing energy was measured for all tests. Due to a limited amount of data, some errors in the data acquisition and variations in geology and confinement conditions the authors came to the conclusion, that "*the differences in fragmentation and crushing energies of benches were not as discernible as experienced by for example Vanbrabant & Espinosa (2006)*."

Blair (2010) analysed 72 full-scale blasts with regard to the shovel dig rates as an indicator for the fragmentation. 36 of the blasts were fired with pyrotechnic delayed detonators while the other 36 used electronic detonators. The findings were that the "*stress wave collision certainly plays no predictable role in rock fragmentation by blasting, and most likely plays no significant role either.*" The explanation for finding no significant change in the fragmentation was on one hand, that even if all the blastholes are charged in an identical way, the produced waveforms can differ although the geology seems to be uniform. Also the dynamic ground behaviour during the progressing blast will largely influence the waveforms. Blair (2010) also states that the interaction of the generated waves at precise locations is not possible due to the inaccuracy of electronic detonators, even if this is small.

Additionally Blair (2010) states that "*even if the regions of wave collision could be predicted, they would be highly localized and so comprise only a small fraction of the total volume of rock to be fragmented.*"

Finally he states that "*the results from a new analytical model of wave propagation do not support the assumption that stress-wave superposition promotes fragmentation.*"

Based on these observations Johansson (2011) did several small scale tests where he investigated this influence of delay-time to the fragmentation with super positioned blasting waves (see also Johansson & Ouchterlony, 2013).

The blasted specimens were produced of a mortar with well-known physical properties and prepared with two rows of five blastholes with 10 mm in diameter. The arrangement (see Figure 33) guaranteed that the blasting waves had just one reflecting free surface at the front which made the tests comparable to normal bench blasts.

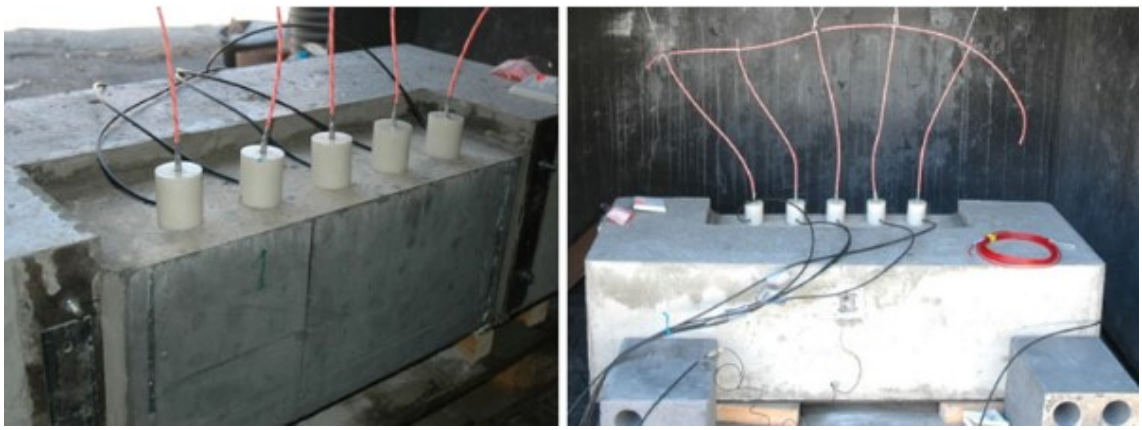

Figure 33: Test-Set-up for superposition of blasting waves (Johansson & Ouchterlony, 2013)

The delay-time was based on accelerometer measurements where the particle wave velocity was determined. The ideal delay-time, where the next blasthole is initiated exactly at the time when the tensile tail of the shock wave from the previous blasthole arrives, is shown in Figure 34.

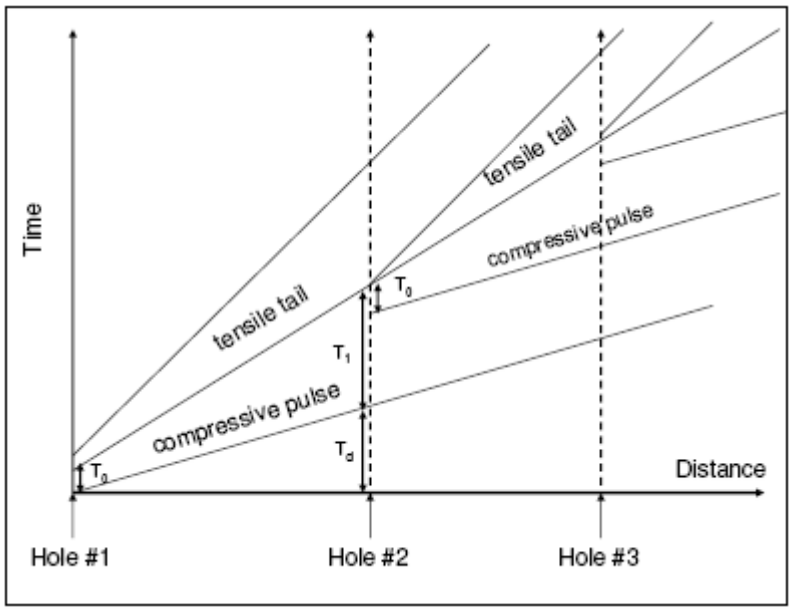

Figure 34: Superposition of tensile tail of blasted holes (Johansson & Ouchterlony, 2013)

Johansson & Ouchterlony (2013) calculated this ideal delay-time between the individual blastholes with the following formula based on the work of Vanbrabant & Espinosa (2006):

$$T_{ideal} = T_d + T_1 - T_0$$

with

T_d Time which the compressive wave needs to reach the next blasthole

T_1 Duration of the first (negative) half-wave at the neighbouring hole

T_0 Duration of the first half-wave at the blasted hole when the charge detonates

The tested delays reached from 0 µs (simultaneous initiation) to 146 µs with variations in between where different wave interactions were investigated.

"*The results showed no distinct differences or high improvements of the fragmentation when the delays were in the time range of interactions compared with no shock wave interactions. The decrease of x_{50} (mean size) was around 20 % at a delay-time ~1.1 ms/m burden compared with longer delays like 2 ms/m. A statistical analysis of the results has been made to evaluate the minimum at short delays and it is not significant.*" (Johansson & Ouchterlony, 2013)

Due to these observations and also regarding Blair's (2010) statements the conclusions that wave interactions have no clear influence on the fragmentation are clearly supported although Stagg & Nutting (1987) found in their small-scale tests in 1.14 m high dolomite benches that "*delay time did influence the distribution of fragment sizes*" and that the "*fragmentation was coarsest for shots fired simultaneously and at delay times of 80 ms/m of burden or greater. Better fragmentation was observed for delay times from 3 to 56 ms/m, with the tests at 37 and 56 ms/m resulting in the best fragmentation".* Their explanation for this result was that *"strains induced by stress waves constructively interact with strains induced by gas pressure from an earlier detonated hole".*

Stagg & Roll (1987) conducted similar full-scale tests in 6.7 m high benches with the result that "*optimum fragmentation occurred with delays of 3.3 to 26 ms/m*". Their conclusion was "*that the fragmentation process should be complete before the next hole fires*". Katsabanis & Omidi (2015) concluded that "*the fragmentation is optimized when a hole fires prior to the radial cracks, produced by the previous hole, reach the free face of the blast*". Further Katsabanis & Omidi (2015) state "*that the larger sizes of the blast, such as the x_{80}, show a clear optimum at a delay time, while the smaller sizes do not show a clear relationship with delay*".

Lownds & Seligman (1976) brought the fragmentation also in context with the cracks created and stated that "*each hole must be allowed to develop its entire crack system without interference from the others*". Further they (Lownds & Seligman, 1976) stated that "*the minimum inter-hole delay will increase with quality of stemming and hole depth, since both will tend to maintain the pressure in the hole, and therefore the stress in the surrounding rock, for a longer time.*" The fragment sizes are according to Lownds (1983) influenced by "*a wedge of rock bounded by two radial cracks*" which "*will break up during secondary fracture processes into a fragment of about the dimension of the wedge thickness*."

Wilson & Holloway (1987) found in instrumented concrete models up to 1 m³ with high speed photography that "*very early in the event, radial cracks were formed around the borehole at the top surface, and a radial crack network pattern was formed at the bench face in front of the loaded borehole*". Further Wilson & Holloway (1987) stated that the "*early cracks were important in determining subsequent fracture growth and fragmentation. The smaller fragments from the*

bench were formed by the early network cracks and any spall fractures which occurred … Larger fragments from the bench subsequently were formed as radial fractures were driven out from the boreholes".

For the case of pre-split blasting, where the creation of a crack along the line of the blastholes is the aim while the surrounding rock should remain undamaged, wave interactions may play a critical role. The holes of the pre-split line are drilled with a smaller side-spacing (see Figure 35) and charged with a special type of explosives.

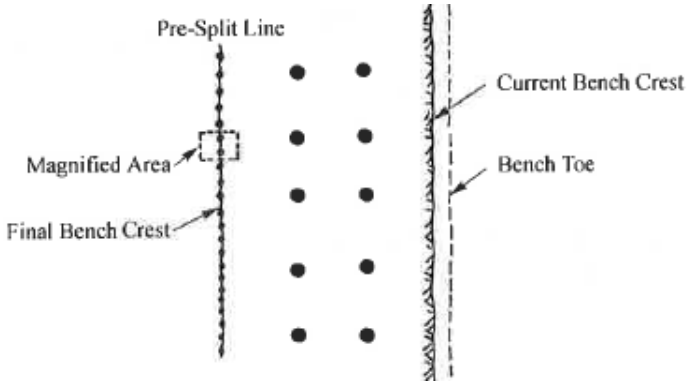

Figure 35: Pre-split line along a final bench crest (Hustrulid, 1999)

The final result of these special blasting techniques should be cracks which are linking the blastholes. The remaining rock shouldn't be much disturbed (see Figure 36).

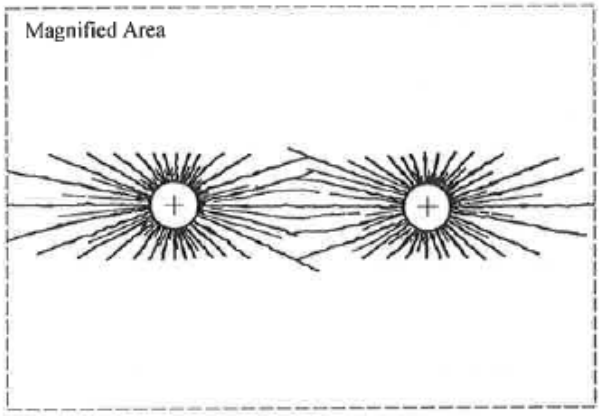

Figure 36: Idealized pre-split fracture pattern (AECI, 1978; Hustrulid, 1999)

Hustrulid (1999) explained that the method of simultaneous initiation results, in combination with the lower spacing, in a regime where crack growing perpendicular to the line of blastholes is inhibited (see Figure 37).

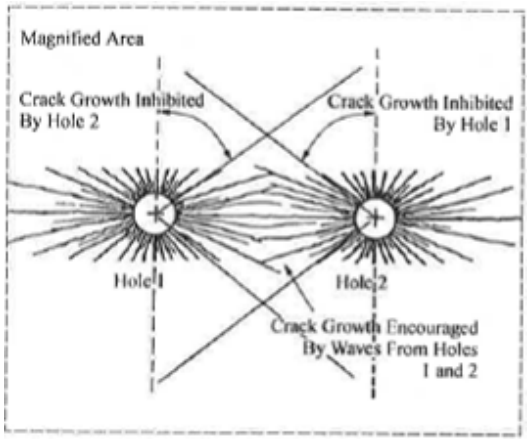

Figure 37: Crack growth inhibited zones (AECI, 1978; Hustrulid, 1999)

Lownds (1983) explained that "*when adjacent holes fire simultaneously, cracks within + or - 30° of the line joining the holes are lengthened by 50%. Those travelling away from the free face at an angle > 30° are truncated at a length equal to half the spacing*."

According to Hustrulid (1999) this is the case due to the two components of the generated blasting waves which are radial compressive pulses and tangential tensile ones (see Figure 4). "*The radial (compressive) wave component from hole 1 will tend to close cracks trying to grow in the direction normal to the borehole line away from hole 2. The tangential (tensile) wave component from hole 1 will encourage the growth of cracks from hole 2 along the borehole line. The wave from hole 2 has the same effect on the cracks radiating from hole 1.*" (Hustrulid, 1999)

Hustrulid (1999) explained further, that finally the explosive gases will flow into the cracks created and extend those cracks (see Figure 38).

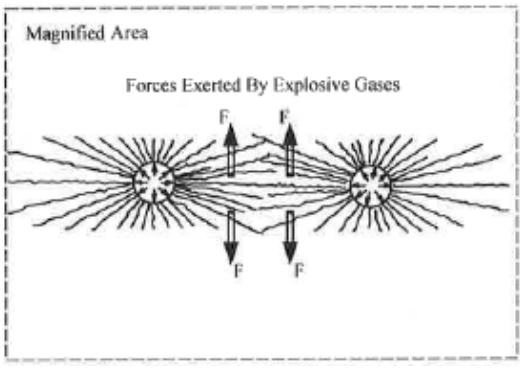

Figure 38: Crack extension by gas pressure (AECI, 1978; Hustrulid, 1999)

Rossmanith (2002) analysed this case of smooth or pre-split blasting where the individual blastholes were initiated simultaneously. For this case the generated compressive waves, their tensile tail as well as the shear waves overlap and hence provide an interaction (see Figure 39).

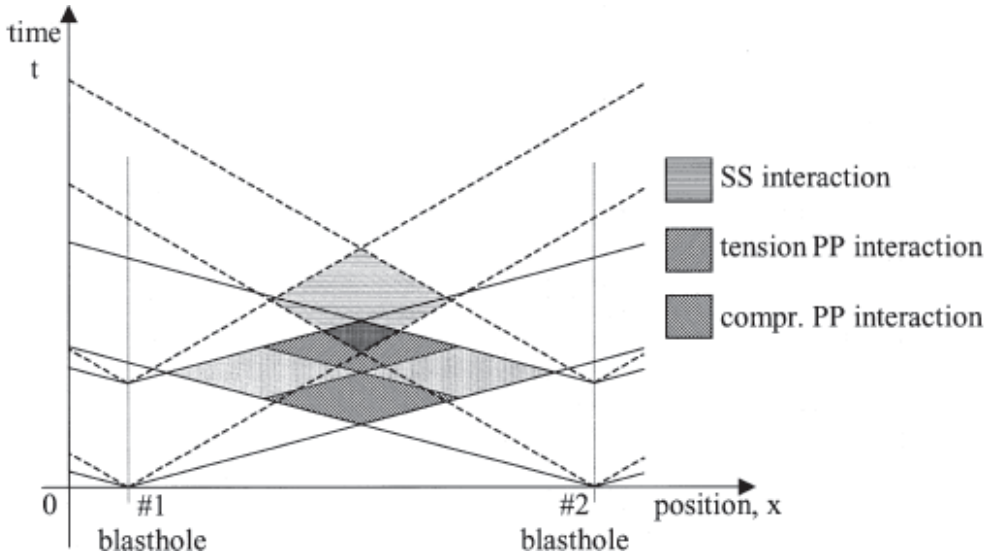

Figure 39: Overlapping interaction of two simultaneously initiated blastholes (Rossmanith, 2002)

In the case of pre-splitting one critical point of Blair (2010), which dealt with the inaccuracy of electronic detonators, could be excluded because pre-splitting is done prior to normal bench blasts. Ouchterlony et al. (2010) called this "*the crack suppression effect of simultaneous initiation.*" The delays used are either 0 (when using electric detonators without any built-in delay element) or in a low range where the inaccuracy of electronic detonators used is negligibly low. Olsson & Bergqvist (1996) draw the conclusions that "*instantaneous firing reduces the crack length. Even small deviations (1 ms) in delay-time between neighbour holes may ruin the result.*"

In the case of underground drift blasting the smooth blasting technique is used for the contour holes, which are initiated at the last stage of the blast. These blastholes might have a delay which is in the range of a few seconds. The accuracy of electronic detonators, which is around 0.05 % of the delay-time used, is not enough to guarantee an exact overlapping interaction of the blasting waves generated.

3 Test-Methodology

3.1 Magnetite Mortar Test Specimen

The following description is taken from Schimek et al. (2013, 2015).

The testing blocks for the model-scale bench blasts with the dimensions of 660×210×280 (350) mm (L×H×W) were produced in three cycles. The basic ingredients (see Table 1) had the same proportions as used for small-scale tests at the Luleå Univ. Techn. (Johansson, 2008) but used magnetite powder from Ferroxon instead of Minelco.

Table 1: Ingredients of the magnetite mortar testing blocks

Ingredient	[%]
Portlandcement CEM II / A-M 42.5 N	25.60
Water	12.65
Plasticizer	0.256
Defoamer	0.129
Magnetite powder (Ferroxon 618)	29.65
Quartz sand 0.1 – 0.5 mm	31.70

Additional to the testing blocks several cubes were produced for a comparison of the physical material properties. Several cylinders with a diameter of 138.5 mm and a length of 280.0 mm were produced for a comparison of the fragmentation characteristics and the blastability.

The first two production cycles were carried out by a plant for precast concrete with large batches of about 680 kg. The third cycle was carried out in the laboratory of the Chair of Mining Engineering at the Montanuniversitaet Leoben in small batches of about 100 kg. The curing time of all testing blocks was at least 28 days.

Due to delivery problems of the quartz sand a slightly different product had to be used during production cycle #03. While the production cycles #01 and #02 used the quartz sand “ME 31” production cycle #03 used the quartz sand “ME 0,1 – 0,4 mm”. Table 2 shows the types of quartz sand used. The data-sheets of the ingredients can be found in Appendix 1.

Table 2: Sieving parameters for the types of quartz sand used

Mesh size [mm]	ME 31 Sieving residue [%] Reference	ME 31 Sieving residue [%] Tolerance	ME 31 Passing [%] Reference	ME 0.1 - 0.4 mm Sieving residue [%] Reference	ME 0.1 - 0.4 mm Sieving residue [%] Tolerance	ME 0.1 - 0.4 mm Passing [%] Reference
0.71		max. 0.5	100	0	0	100
0.5	1.5	max. 3	98.5	1	max. 2	99
0.355	26	20 - 35	72.5	10	5 - 15	89
0.25	49	40 - 60	23.5	36	30 - 55	53
0.125	23	18 - 28	0.5	50	40 - 60	3
0.063	0.5	max. 2		3	1 - 6	
< 0.063		max. 0.5			max. 1	

While the maximum grain size was similar for both types of quartz sand the passing of the medium grain sizes (0.125 – 0.355 mm) was different. The passing of the finest particles (0.063 mm) was comparable for both types. These different grain sizes were the reason for additional water which was needed during production cycle #03.

3.2 Blasting Site Erzberg

The following description is taken from Schimek et al. (2013, 2015).

The blasting tests were done at the blasting site of the Chair of Mining Engineering at the Styrian Erzberg (see also Maierhofer, 2011). This blasting site, which is a heavily reinforced concrete arrangement, is directly connected to the surrounding rock mass. Inside the walls of the blasting site a yoke, which was surrounded by compacted sand, was installed (Figure 40).

Figure 40: Yoke within the walls of the blasting site (Schimek et al., 2013). The cut-in portion in the yoke will contain the testing block

This arrangement makes sure that the waves, which were produced by blasting, were transmitted away from the blastholes into the surrounding rock mass. The blocks for the blasting tests were finally placed inside the space of the yoke on a mat cut out of a used conveyor belt. At the sides and at the back the testing block was grouted into the yoke by using fast hardening cement, which had similar material properties as the block.

3.3 Blasting Tests

While the 1st small scale preliminary blasting tests of this thesis were used to find the correct test arrangement, the other stages were used for answering the research questions (see chapter 1.1).

- Preliminary Tests: Comparison of shots in a sequence to shots with infinite delay with regard to the collective breakage effect (Schimek et al., 2013)
- Stage 1: Defined pre-conditioning of the testing blocks with similar 1st row shots in all testing blocks
- Stage 2: Changed delay-times of the 1st row shots introducing different pre-conditioning into the testing blocks
- Stage 3: Investigation of the influence of geometrical properties and the staggered pattern

The blasting geometry during stages 1-3 was constant, single rows with a burden of 70 mm and a side-spacing of 110 mm. This resulted in an S/B-ratio of 1.57. The blastholes of 10 mm diameter were blasted with a 20 g/m detonating cord. The delayed initiations were achieved by using a 5 g/m detonating cord with different lengths according to the velocity of detonation. The delay-times used were 0 (simultaneous initiation), 28, 73 and 140 µs (2 ms/m of burden). The 0 and 28 µs delay, where the shock wave of the first detonating blasthole arrives when the second hole detonates, generated a superposition effect of the shock waves. The 73 µs delay was chosen guided by the work of Vanbrabant & Espinoza (2006). The chosen delay-times of 140 µs excluded an interaction of the shock waves from the individual blastholes (see Johansson & Ouchterlony, 2013).

All test series were done first in virgin material (first row of the testing blocks) and then in already damaged material (further rows).

Table 3 shows the origin of the testing blocks and the numbering of the blasting tests (#xxyy) which had the following meaning:

xx…sequential number of the blasting test

yy…year of the test (20yy)

Table 3: Overview of blasting tests

Production Cycle	Test-Numbers	Preliminary Tests	Stage 1	Stage 2	Stage 3
#01	#0111 - #0711	x			
	#0212 - #0912		x		
#02	#0113 - #0713			x	
#03	#0114 - #0414				x

Figure 41 gives an overview of the blasting tests and the assignment of delay-times to the research questions (see chapter 1.1).

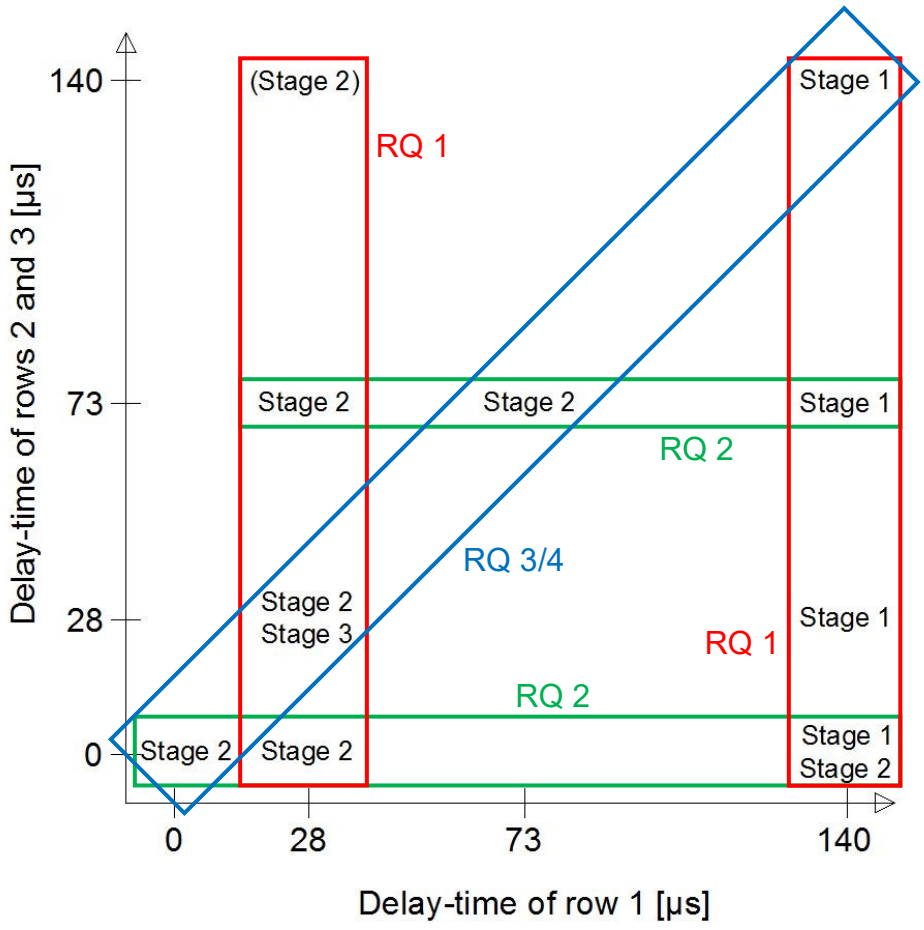

Figure 41: Blasting tests used for answering the research questions (RQ)

3.3.1 Preliminary Tests

The preliminary test-series was used to find the correct test set-up for the following blasting tests. Therefore shots in a sequence (shots in a row with finite delay) were compared to shots with infinite delay (single-hole shots in one row) with regard to the collective breakage effect (Schimek et al., 2013).

The shots with finite delay were carried out as single-row-shots (2 rows per testing block) with 5 respectively 7 holes in a row. The arrangement for the 5 holes per row setup can be seen in Figure 42.

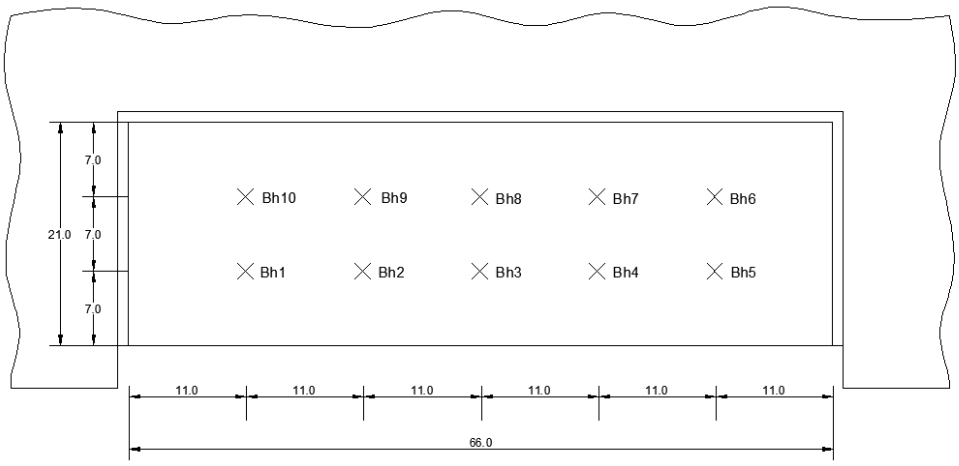

Figure 42: Arrangement for 5 holes per row (units in cm)

The side-spacing (S) of 110 mm and the burden (B) of 70 mm gave a ratio of S/B of 1.57. The arrangement with 7 holes per row had a side-spacing of 95 mm and a burden of 70 mm which gave a ratio of S/B of 1.36.

The delay-times of the blastholes were decided to be 2 ms per meter of burden. Due to the burden of 70 mm this delay had to be 140 µs. This delay-time means that there is very little or no interaction of the shock waves from the individual blastholes (Johansson & Ouchterlony, 2013). A 5 g/m detonating cord with a specific length (according to the velocity of detonation) was used to achieve this delay-time. The actual initiation times were measured using short-circuiting cables connected to the 20 g/m detonating cord at the collaring points of the blastholes. The arrangement of the 5 blastholes per row can be seen in Figure 43.

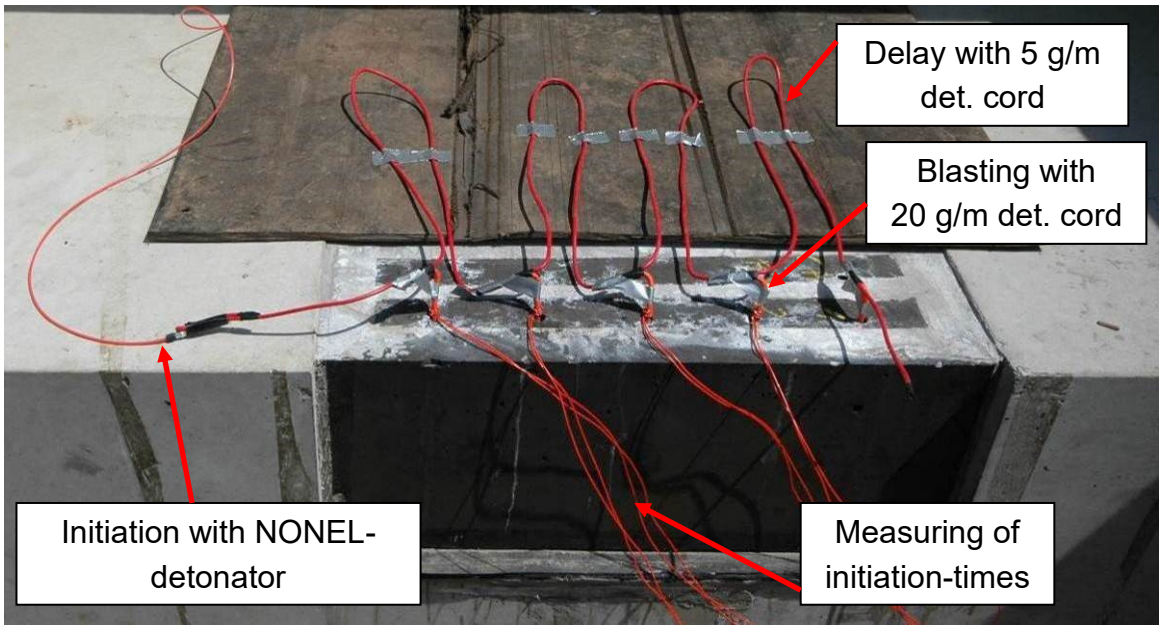

Figure 43: Arrangement for blasting of 5-holes-in-a-row in block #0111

The testing block with 7 holes per row was initiated in the middle of the row. Table 4 shows the arrangements of the shots in a row.

Table 4: Overview of the shots-in-a-row

Test Nr.	Type of blast		Comment
#0111	Shots in a row with 5 holes per row	Row 1 Row 2	Initiation from left to right Initiation from right to left
#0211	Shots in a row with 7 holes per row	Row 1 Row 2	Initiation in the middle of the row Initiation in the middle of the row
#0711	Shots in a row with 5 holes per row	Row 1	Initiation from left to right

Testing block #0711 with 5 blasted holes was used for testing of a new initiation system and for a test of possible crack detection scenarios (see chapter 3.4.2.2). This block is missing in the following chapters because no sieving analysis was done after blasting.

For the shots with infinite delay (single-hole shots) it was decided that the 5 holes per row arrangement is useful. The tests were carried out as shots in the 1st and in the 2nd row where in both cases the first shots were made in the middle of the row (see Figure 44).

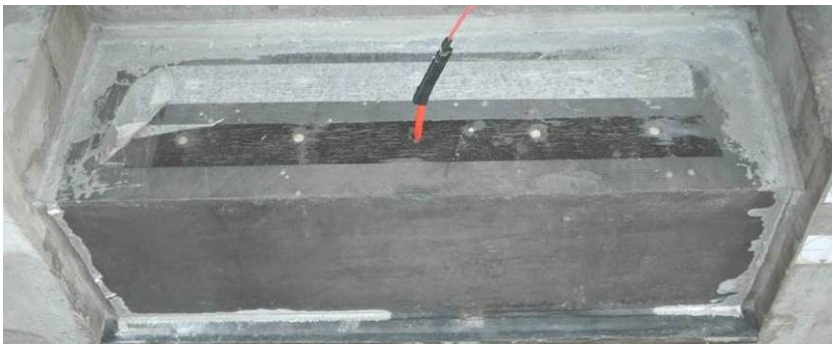

Figure 44: Single-hole-shot in the middle of the 1st row

During these single-hole-shots the influence of different filling materials of the neighbouring holes of the row on the breakout and the cracks created was investigated. One test was carried out with unfilled holes, one with wooden sticks in the holes, one with fast hardening cement in the holes and the last one with undrilled neighbouring holes.

Additionally to these tests two testing blocks were blasted with single-hole-shots, which started from one side of the block. This ensures the same geometrical properties for the following holes of the rows. To simplify the throw of the burden of the first single-hole-shot one corner of the block was cut away. This would guarantee a smaller burden for the first blasthole. The following Figure 45 shows the geometrical properties of this “cut-away-corner” arrangement.

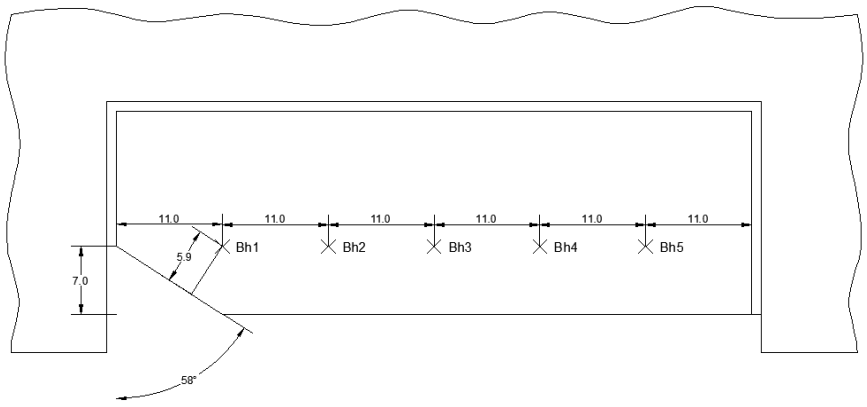

Figure 45: Arrangement for single hole shot with cut-away corner (units in cm)

The first testing block with this arrangement (#0511) was prepared with 5 blastholes in the first row and 1 blasthole in the middle of the second row. The holes were filled with fast hardening cement and drilled just before blasting. Due to the problems which occurred during drilling of the holes right before blasting the

holes of the next block with the cut-away corner and the 5 holes per row arrangement (#0611) weren't filled with any material (see Figure 46).

Figure 46: Test block with cut-away corner

Table 5 summarizes the arrangements of the single-hole shots.

Table 5: Overview of the single-hole shots

Test Nr.	Type of blast		Comment
#0311	Single hole shots in the middle of the rows	Row 1	Wooden sticks in the neighbouring holes
		Row 2	No filling material in neighbouring holes
#0411		Row 1 Row 2	Fast hardening cement in the right side, no filling material on the left side
#0511	Single hole shots with "cut away corner"	Row 1	Fast hardening cement in the neighbouring holes
		Row 2	No filling material in neighbouring holes
#0611		Row 1 Row 2	No filling material in neighbouring holes

3.3.2 Stage 1

For the blasting tests of the 1st stage the testing blocks were turned 90 degrees so that the smallest dimension of 21 cm became the height. With this arrangement 3 rows per testing block could be blasted while the geometrical properties (burden and side spacing) were the same as in the preliminary tests (see Figure 47).

Figure 47: Testing block lying in the space of the yoke

The 28 cm depth of the lying block was now deeper than the space in the yoke. Just half of the burden of the 1st row was confined at the sides.

The first rows of all testing blocks were blasted with the same nominal delay of 140 µs. This specific delay of 2 ms per meter of burden was, as mentioned in chapter 3.3, too long to give an interaction of the shock waves from the individual blastholes (see also Johansson & Ouchterlony, 2013).

The same delay-times for the 1st row blasts created a comparable pre-conditioning in the testing blocks. For the investigation of the influence of different delay-times on the crack development and the fragmentation the 2nd and 3rd row shots were used. The delay-time of these two rows was chosen according to possible superposition of the generated shock waves (see chapter 2.2). The tested delay-combinations were 0, 28, 73 and 140 µs which corresponds to 0, 0.4, 1.0 and 2.0 ms/m of burden (see Table 6).

Table 6: Overview of the testing blocks and the delay-time of stage 1

Row-Nr.	Delay		Nr. of tests
	[µs]	[ms/m]	
1	140	2.00	8
2	0	0.00	3
	28	0.40	1
	73	1.04	1
	140	2.00	3
3	0	0.00	1
	28	0.40	1
	73	1.04	1
	140	2.00	3

The length of the delay-timing cord used was calculated according to the velocity of detonation of the 5 g/m detonating cord which was 7220 ± 100 m/s. The arrangements can be seen in the following figures.

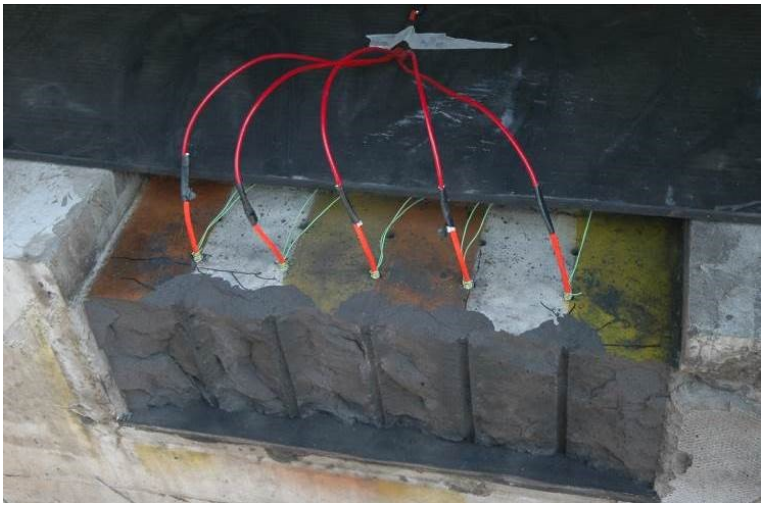

Figure 48: Arrangement for 0 µs delay

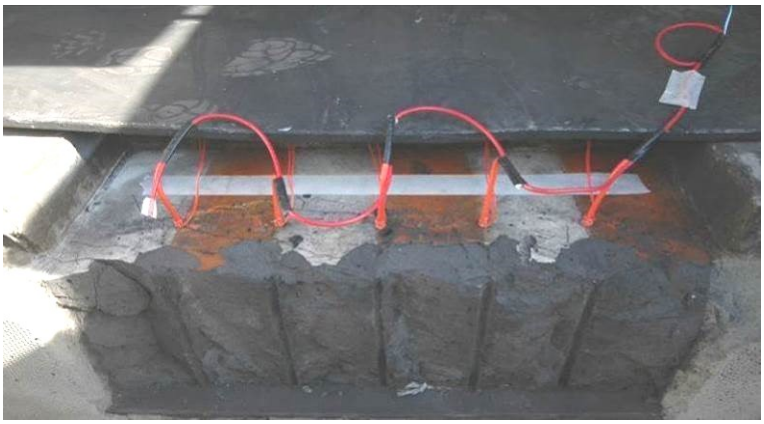

Figure 49: Arrangement for 28 µs delay

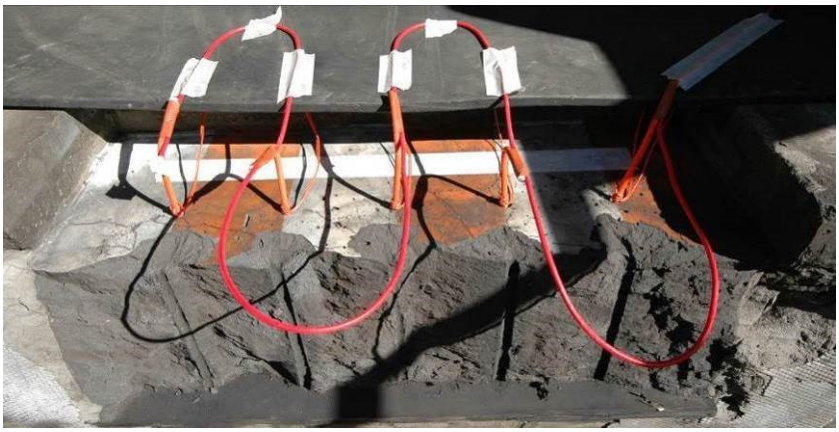

Figure 50: Arrangement for 73 µs delay

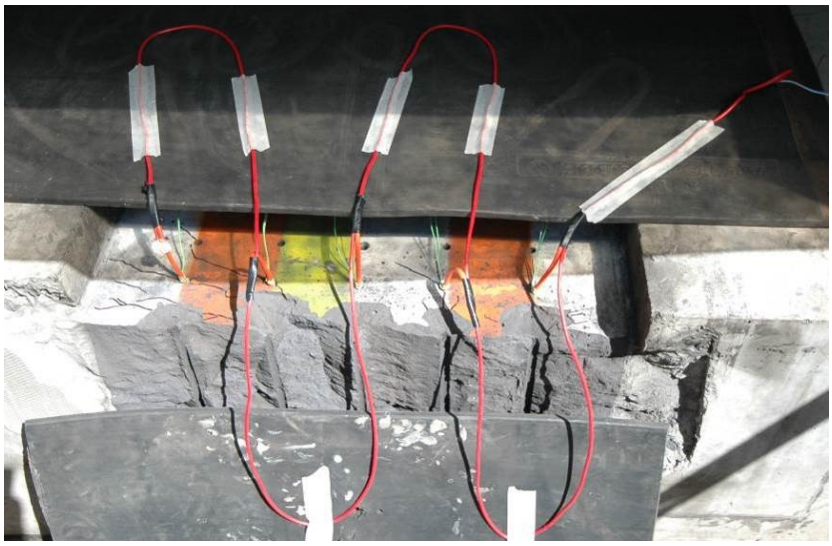

Figure 51: Arrangement for 140 µs delay

The delay-timing arrangement with the use of the 5 g/m detonating cord was critical due to several observed cut-offs. Especially in the case of longer delay-times the limited place above the testing blocks competed with the needed length of the delay-timing cord.

3.3.3 Stage 2

The blasting tests of the 2nd stage investigated the crack development and the fragmentation in differently pre-conditioned mortar-blocks. The shots of the first rows of the blocks created different pre-conditionings in the way that either 0, 28, 73 or 140 µs delay-times were used. The second and the third row of the testing blocks were used for the investigations. They were blasted with varying delay-times which can be seen in Table 7.

Table 7: Overview of the testing blocks and the delay-times of stage 2

Row-Nr.	Delay		Nr. of tests
	[µs]	[ms/m]	
1	0	0.00	1
	28	0.40	4
	73	1.04	1
	140	2.00	1
2	0	0.00	3
	28	0.40	1
	73	1.04	2
	140	2.00	1
3	0	0.00	3
	28	0.40	1
	73	1.04	2

3.3.4 Stage 3

The blasting tests of the 3rd stage investigated the influence of the geometrical properties of the confinement to the crack development and the fragmentation. Two testing blocks (#0114 and #0314) were prepared with 4 rows and 5 blastholes per row (see Figure 52). The burden of 70 mm and the side-spacing of 110 mm were the same as in the previous tests.

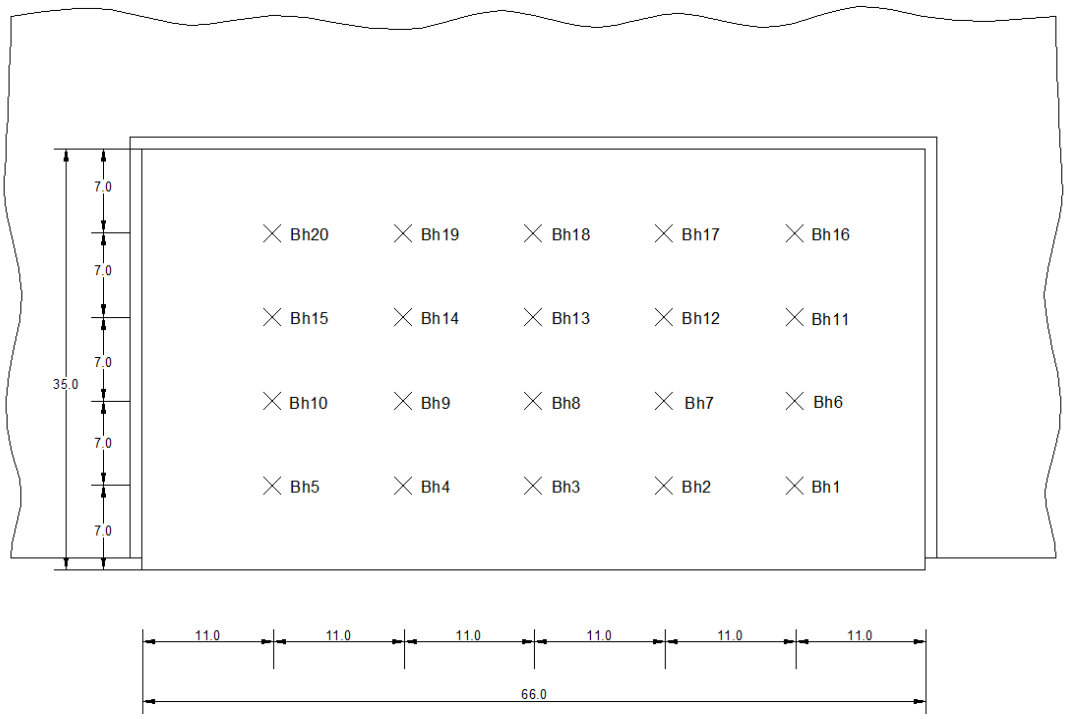

Figure 52: Geometrical properties for 4 rows per testing block (units in cm)

During the first two tests of this arrangement, a joint between the testing block and the yoke was detected after three blasted rows. This joint of about 1 mm might have been influenced by the gases which were generated during the detonation. They could have been trapped at the bottom of the block and activated a movement of the block. The use of silicone at the bottom of the block in the further stage #03 tests probably prevented the produced gases to be trapped at the bottom of the block because not joint separations were observed.

Additionally the hypothesis of Hustrulid (1999) that a staggered layout will give finer fragmentation than a normal layout was investigated.

Cunningham (2005) explained this phenomenon with a more uniform distribution of the explosives in case of the staggered pattern (Figure 53).

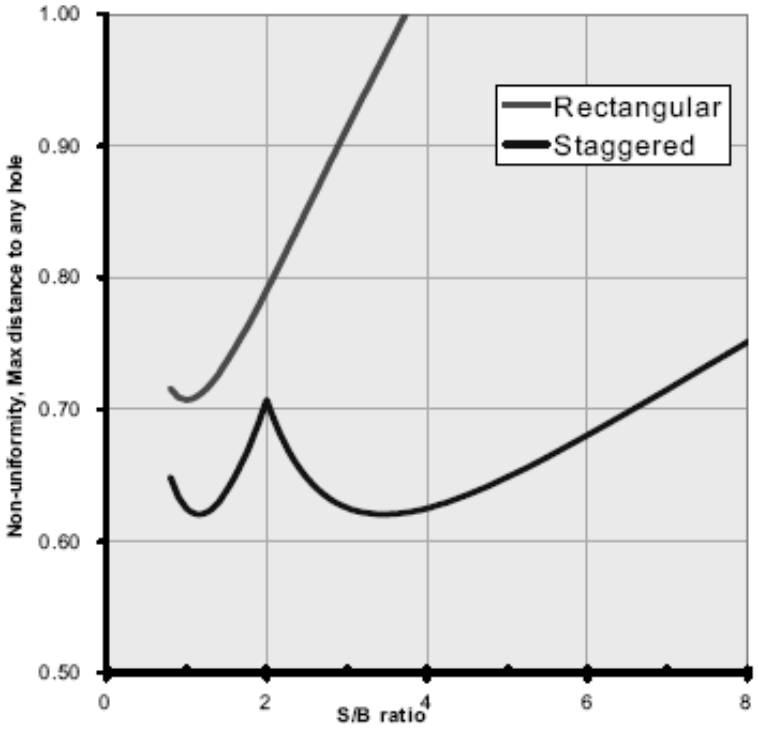

Figure 53: Effect of S/B ratio and layout on the maximum distance of any point from any hole and on the explosive distribution (Cunningham, 2005)

Hustrulid (1999) explains that a cylindrical plug around a borehole represents in a useful way the influenced region around a blasthole and "*though the percent energy coverage has not changed with this staggered design, the un-touched area has been redistributed into two smaller pieces and the maximum distance from any charge has been reduced…*" (Figure 54).

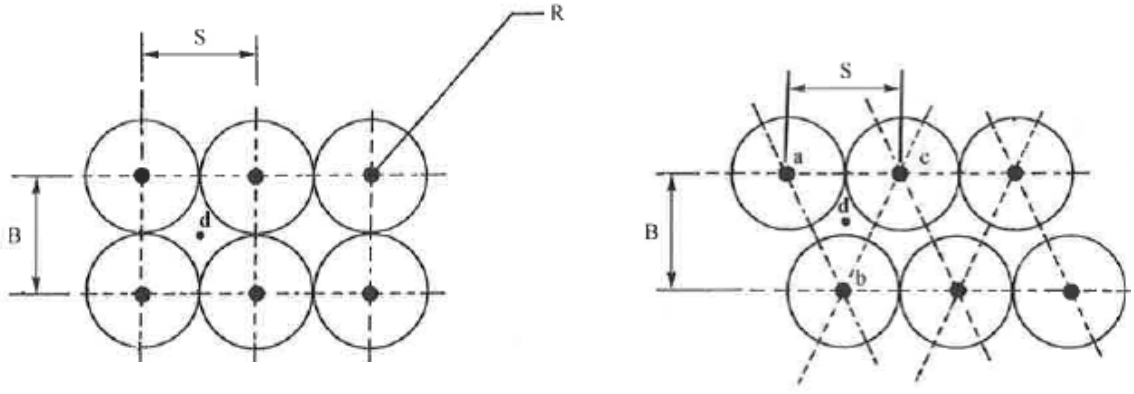

Figure 54: Square (left) and staggered layout (right) with influenced regions around the blastholes (Hustrulid, 1999)

Lownds & Seligmann (1976) explained that "*the firing sequence and delays between shots can be arranged to allow each hole to develop its cracks fully. This*

is equivalent to firing holes independently." Further they (Lownds & Seligmann, 1976) stated that "*when holes are fired independently, there will effectively be a cylinder of broken ground round each hole after firing*" and "*that every point in the plan must be within at least one of these circles*" (see Figure 55).

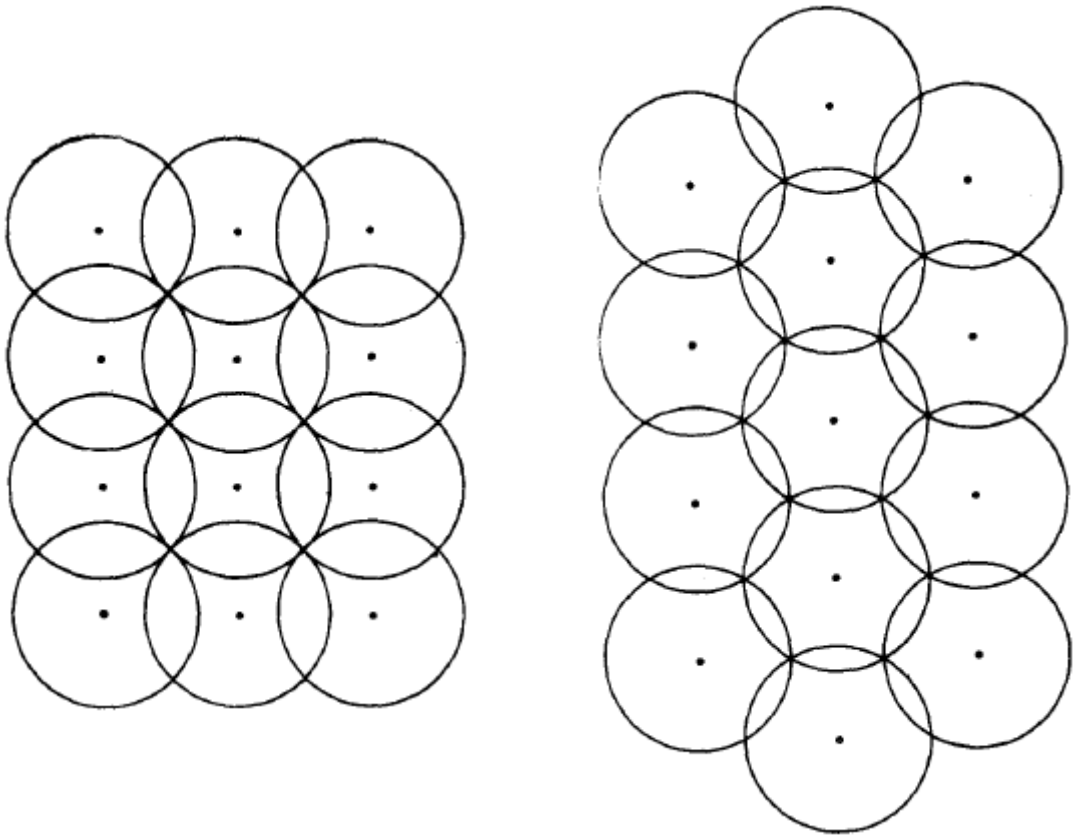

Figure 55: Effective circles in a square drilling pattern (left) and an equilateral-triangular drilling pattern (right) (Lownds & Seligmann, 1976)

According to the findings of Lownds & Seligmann (1976) "*a saving of 30 per cent in drilling and in the consumption of explosives is theoretically possible by a change from square to equilateral-triangular hole placing…*".

Two testing blocks (#0214 and #0414) were blasted with the staggered pattern (see Figure 56).

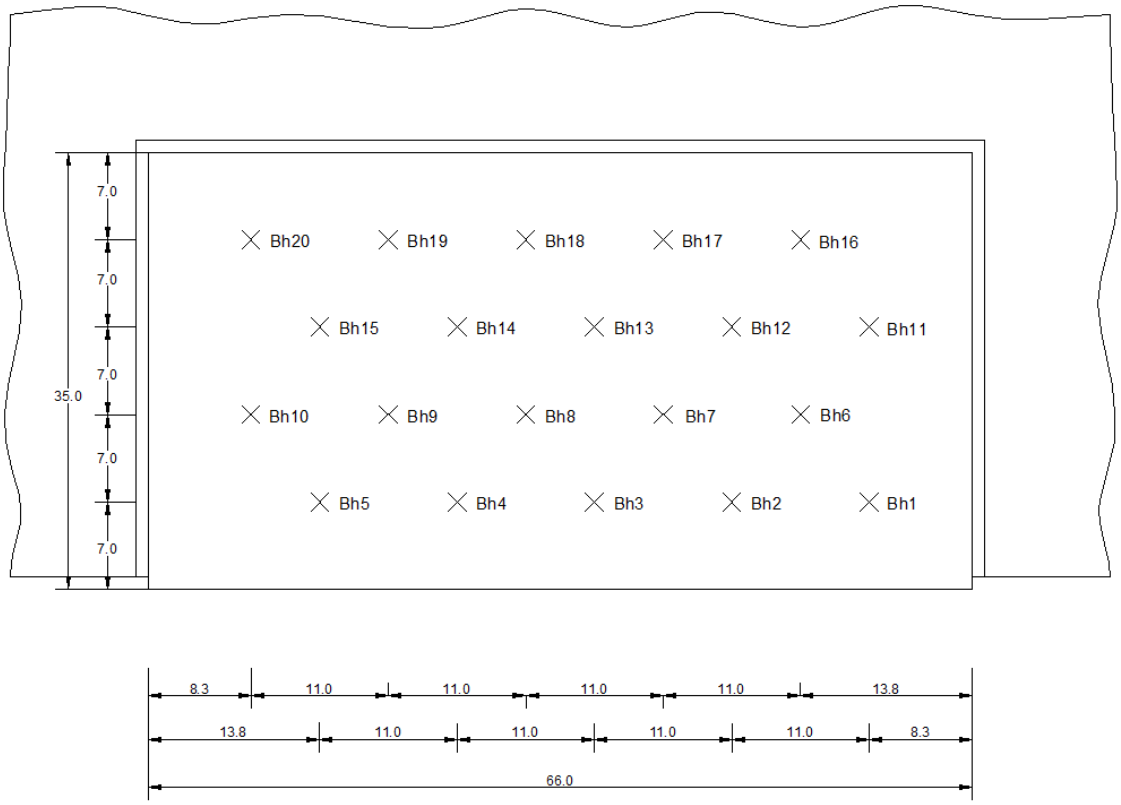

Figure 56: Geometrical properties for the staggered pattern (units in cm)

The delay-time used for all rows of stage 3 was 28 µs which corresponds to 0.4 ms/m of burden (see Table 8).

Table 8: Overview of the testing blocks and the delay-time of stage 3

Row-Nr.	Delay		Nr. of tests
	[µs]	[ms/m]	
1	28	0.40	4
2	28	0.40	4
3	28	0.40	4
4	28	0.40	2

3.4 Measurement of Crack Development

One of the aims of this thesis was the investigation of the influence of different delay-times on the crack development. Therefore the cracks created in the remaining testing block had to be quantified somehow. Gertsch (1995) described a method for investigating the crack network in laboratory scale rock samples via grinding or cutting small slices from the test specimen. After each grind / cut the surface was documented and finally all pictures were compiled in a CAD- software package. With this method the test specimen were destroyed and no further test could be done.

The investigation of the crack development was improved during the individual stages of our blasting tests and done in several steps:

- Analysis of the surface characteristics of the bench face using BlastMetrix^{3D} (by 3GSM, GmbH)
- Crack detection
    - Use of dye-penetrant spray
        - Surface crack detection at the top of the testing blocks after every blast (stage 3)
        - Surface crack detection at slices which were cut out of the rest of the block after blasting (stages 2-3)
    - Crack detection at thin sections out of drill cores (stage 1)
    - Computer tomography of cut slices (stage 1)

3.4.1 Surface Characteristics of the Bench Face

To get an idea of the characteristics of the bench face after blasting, the BlastMetrix^{3D} software package (by 3GSM, GmbH) was used for modelling of the bench face. This photogrammetric system needs two delimiters (at the top of the bench) and one or two range-poles (at the bottom), which were placed close to the fresh blasted face (see Figure 57).

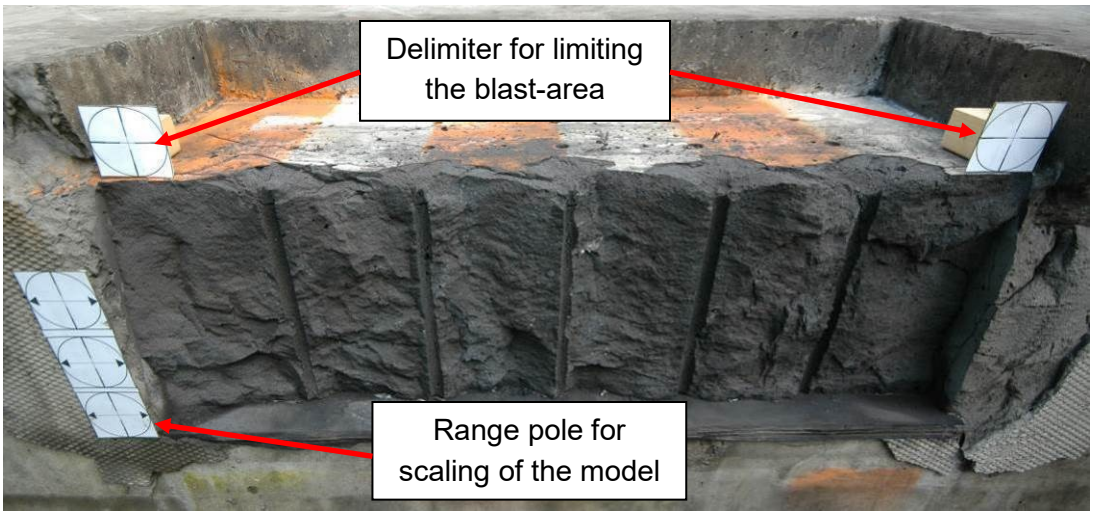

Figure 57: Arrangement of markers for BlastMetrix^{3D}

Due to the known geometry of the range-poles a 3D-model was produced out of the taken pictures (see Figure 58).

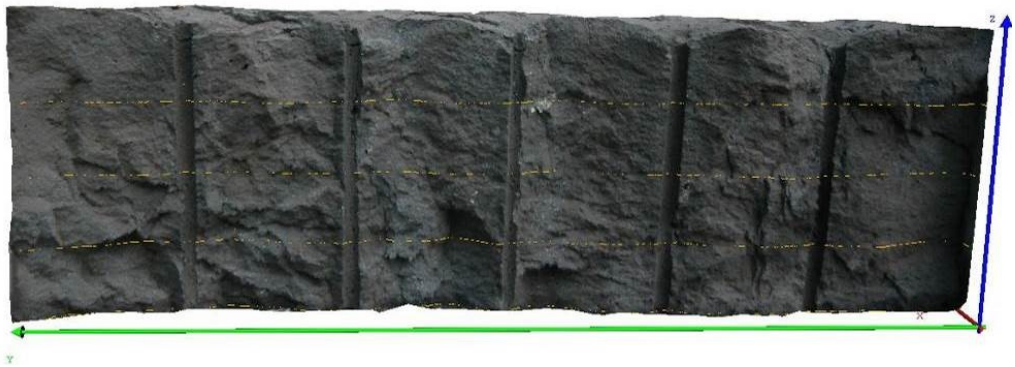

Figure 58: 3D-model of the blasted bench face

By using the BlastMetrix^{3D} software a triangular mesh of the bench face was generated (see Figure 59). The coordinates of all triangular-points could be extracted as a *.csv-file and used for detailed analysis.

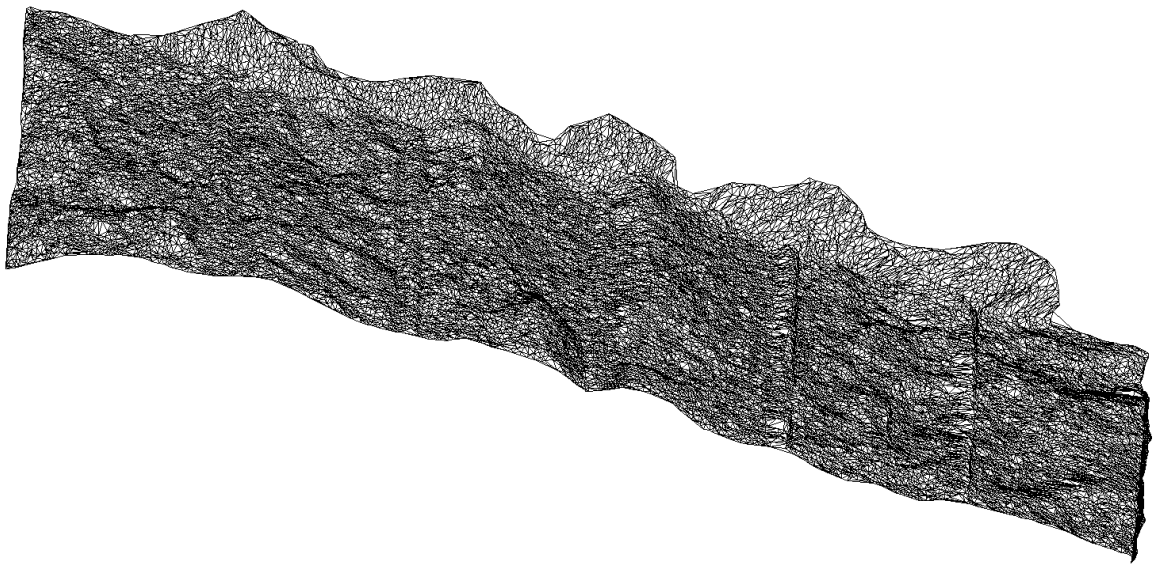

Figure 59: Triangular mesh of the bench face

For an analysis of the bench surface the 3D-model was, similar as done by Johansson & Ouchterlony (2013), divided into three horizontal contour lines at 5, 10 and 15 cm height (see yellow lines in Figure 58). The coordinates of the individual points at the contour-lines were extracted as a *.dxf-file for further analysis in AutoCAD® (Figure 60).

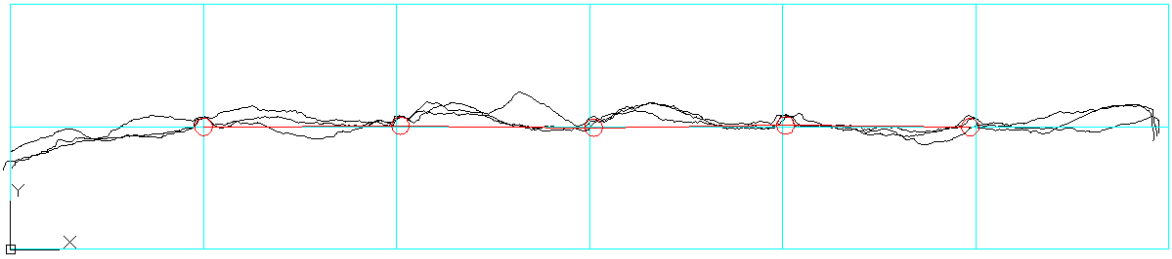

Figure 60: Horizontal contour lines implemented into AutoCAD®; Scale x:y = 1:1

These extracted data points were coordinated with the line connecting the as-drilled blasthole-centres where drilling inaccuracies were taken into account (see Figure 61).

When using the software-package MATLAB®, where the CAD-file was the input, the following diagrams were the output.

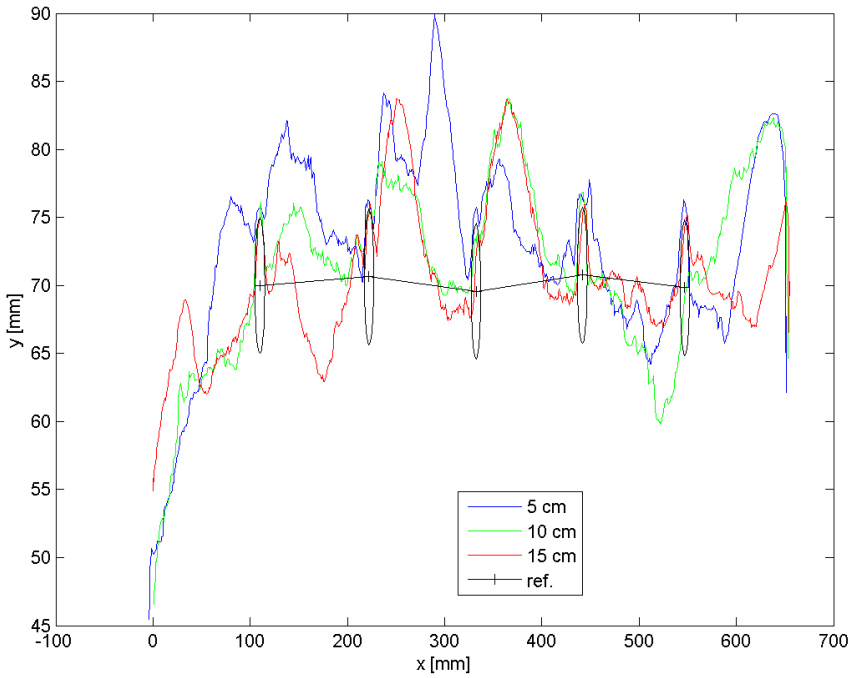

Figure 61: Blasted contour and as-drilled (reference) centre-line of blastholes (black ellipses); Scale x:y = 1:13.8

As a measure of the backbreak the perpendicular distance of the contour lines to the reference line was taken. The contour line parts at both sides of the block were excluded from the analysis and only the surface between the 1st and the last (5th) blasthole was analysed (see Figure 62).

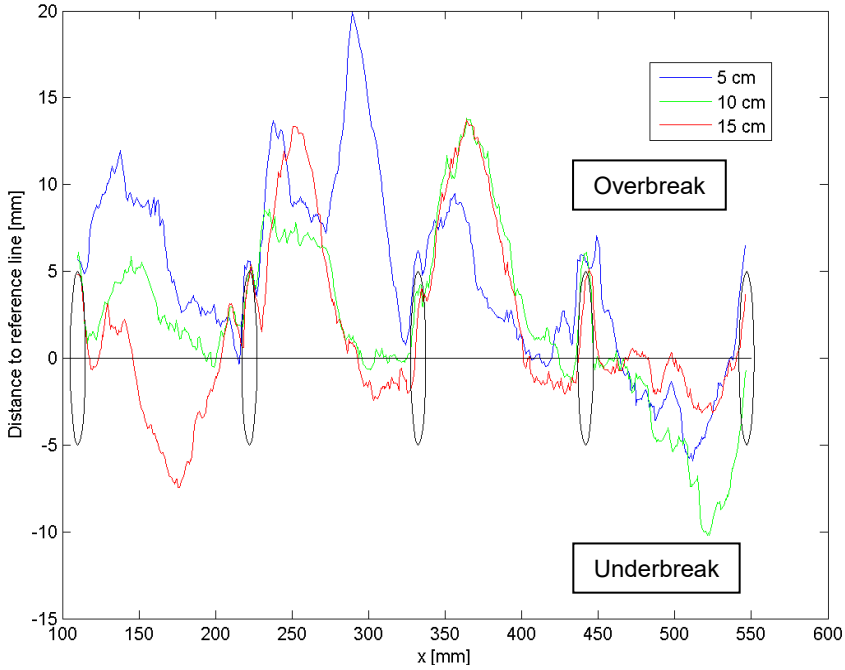

Figure 62: Perpendicular distance of contour-lines to reference line; black ellipses mark blastholes; Scale x:y = 1:11.5

The distances of the individual data points to the reference line was displayed as boxplots (Figure 63) for all points along the contour lines of the 3D-model and as histograms (Figure 64) for the individual contour lines as well as for the combination of the 3 contour lines. With these measures a conclusion about over- or underbreak can be drawn.

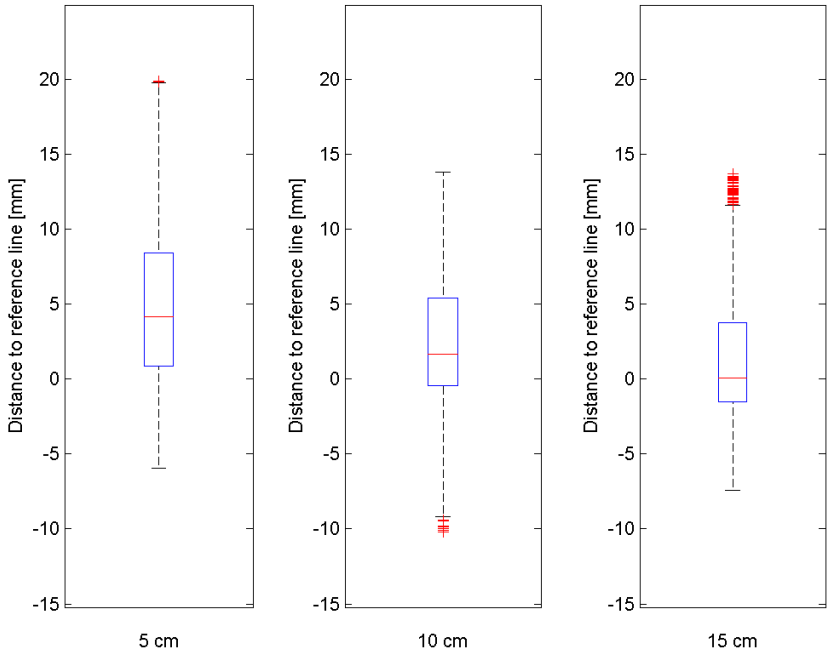

Figure 63: Boxplots of distance of the contour lines to the reference line

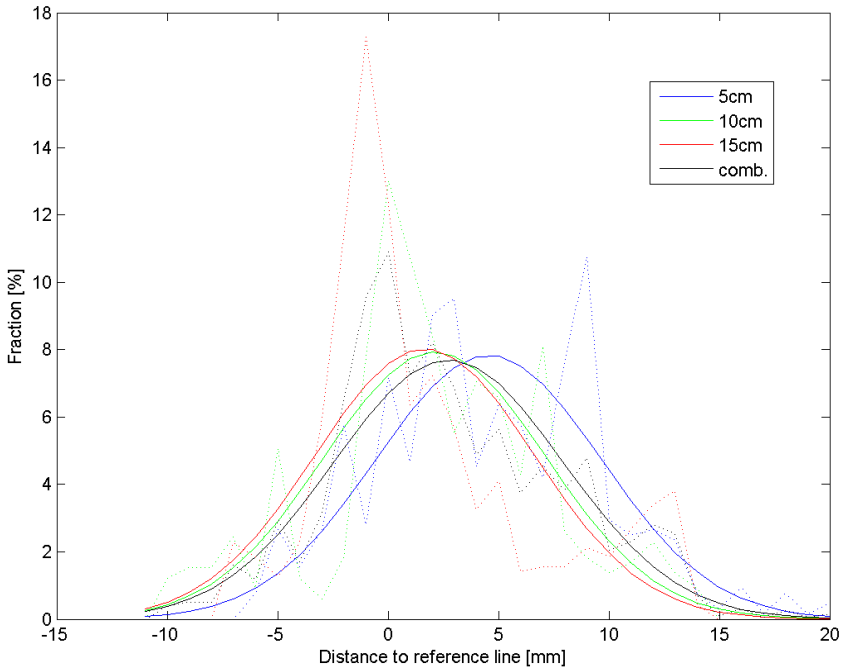

Figure 64: Histogram of the distance of the contour lines to the reference line with superposed calculated normal distributions; Bin width ~ 1.5 mm

Additionally to the diagrams the following parameters for further analysis were calculated with a MATLAB®-code:

- D_{Mean} [mm]
  The mean distance of the individual data points to the reference line is a comparative figure for the evaluation of the broken out volume (Holloway et al., 1987). If D_{Mean} was positive (sign "+") then overbreak occurred and if D_{Mean} was negative ("-") then underbreak was dominant. It is calculated as follows:

$$D_{Mean} = \bar{d} = \frac{\sum d}{n} = \frac{\sum_{i=2}^{n} d_i}{n}$$

- S_{Norm} [-]
  The normalized slope inclination of the individual sections of the contour line is a comparison figure for the micro-roughness of the contour-line and is calculated as follows:

$$S_{Norm} = \frac{\sum s_i \cdot \Delta x}{l} = \frac{\sum \frac{\Delta d_i}{\Delta x_i} \cdot \Delta x_i}{l} = \frac{\sum_{i=2}^{n} | d_i - d_{i-1} |}{x_{\max} - x_{\min}}$$

with

d_i Distance from the individual data points to the reference line

n Number of data points

s_i Inclination of connection line between two data points

x_{max} Maximum x-value along contour line

x_{min} Minimum x-value along contour line

l Length of contour between the 1st and last blasthole

These parameters were calculated for the 3 contour-lines (at a height of 5, 10 and 15 cm) individually and as the sum of these 3 contour-lines to 1 combined average parameter. The description for the procedure of the bench surface analysis can be found in Appendix 9.

3.4.2 Crack Detection

During the individual stages of the blasting tests several different possibilities for crack detection were tested to find the most suitable method.

3.4.2.1 Dye-Penetrant Spray

1. *Tracing the cracks created at the top of the testing block after every blast*

The dye penetrant spray was applied to the top surface of the testing blocks and the cracks were documented with a camera. Figure 65 shows the cracks created after blasting of the 1st row.

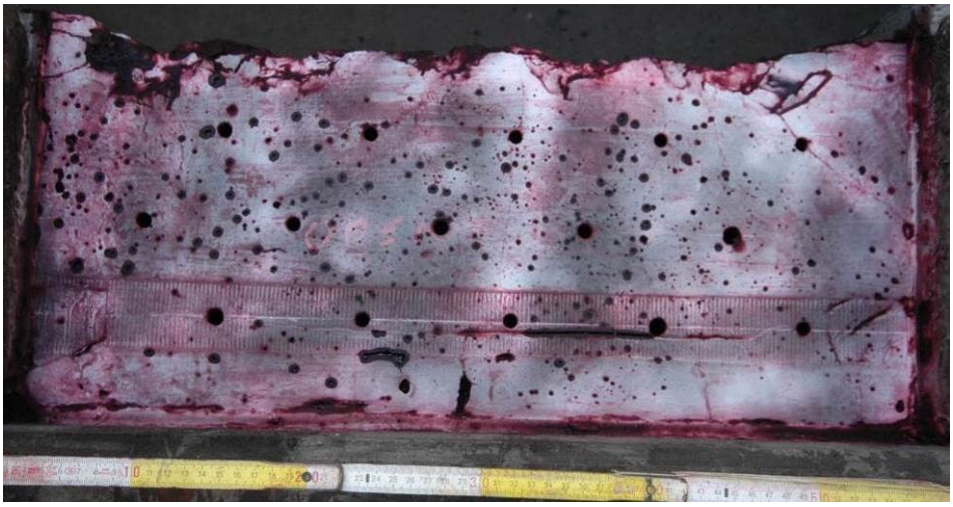

Figure 65: Cracks created after blasting of the 1st row of block #0414

These pictures were imported into the software-package AutoCAD® and the cracks were manually drawn (see Figure 66).

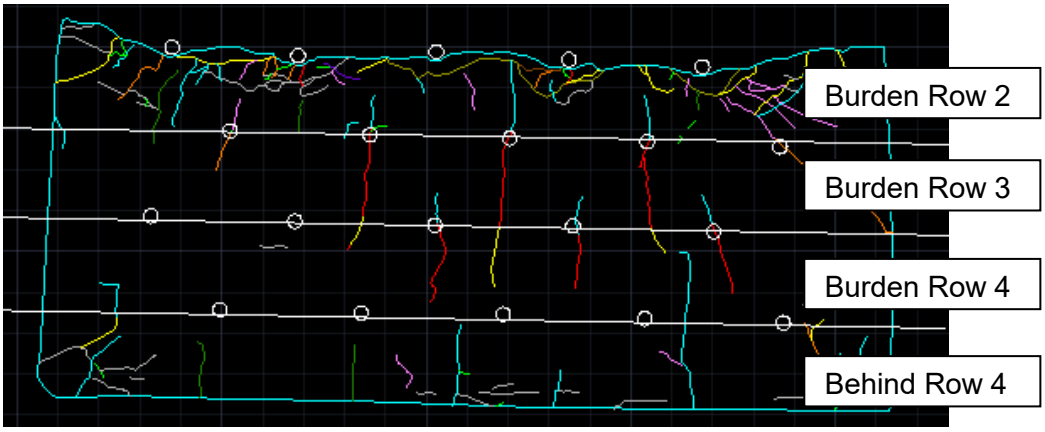

Figure 66: Manually drawn cracks from blasting the 1st row of block #0414

The cracks were subdivided into the different rows (with their associated burdens). In the case that a crack crossed two burden sections it was counted in both sections.

2. *Tracing the cracks created in the remaining test specimen*

After the last row of the block had been blasted the space in the yoke was sealed off and filled with fast hardening cement (see Figure 67). With this procedure it was possible to break out the remaining block without the danger that the block will break apart at the cracks created.

Figure 67: Space after blasting filled with fast hardening cement

In the laboratory the block was cut into several horizontal and vertical slices (see Figure 68) to see internal cracks created by blasting.

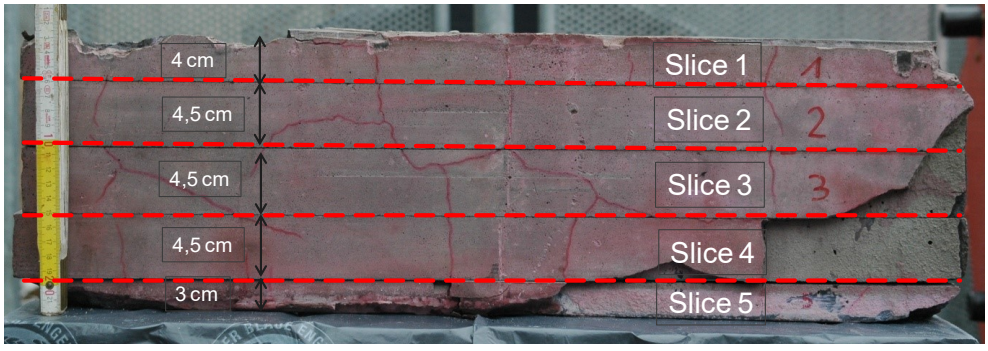

Figure 68: Block cut into several horizontal slices (Navarro, 2015)

At the cut surfaces a dye-penetrant spray was used to make the cracks created in the magnetite mortar visible (see Figure 69).

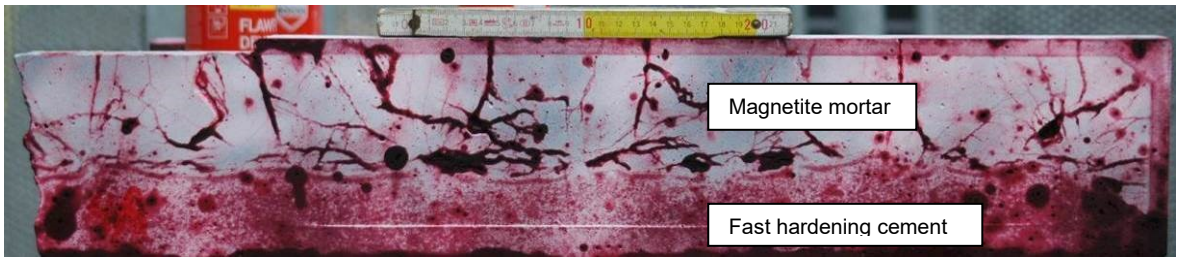

Figure 69: Cracks made visible by using dye-penetrant spray

This picture was finally imported into the software-package AutoCAD® and the visible cracks were traced as seen in Figure 70.

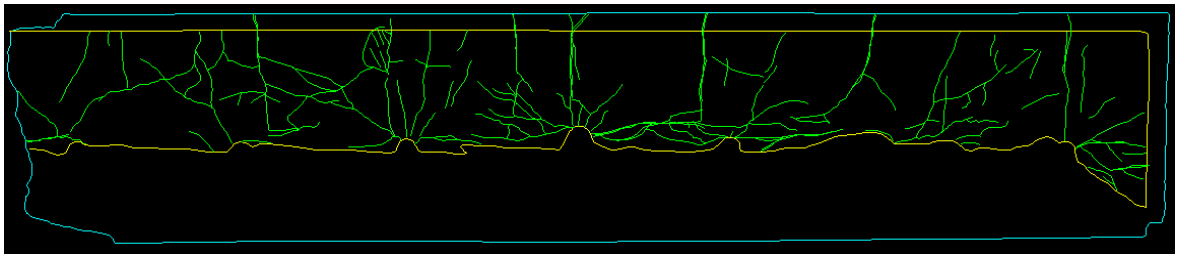

Figure 70: Traced cracks in AutoCAD® (Navarro, 2015)

The sections at both sides of the block were excluded from the analysis due to possible influences of the break-out procedure. Only the detected cracks between the 1st and the last (5th) blasthole were counted for the further analysis. This procedure was done for all individual slices of the blocks and therefore it was possible to analyse the cracks created at different heights of the block.

3. Analysis of the cracks

The cracks were counted manually and divided into the following crack families (Figure 71) according to their angle, length and origin (Navarro, 2015).

- CB 90 – 80 [1]; first family
  Cracks originating from the borehole with an angle between 90° and 80° to the bench face
- CB 80 – 30 [2]
  Cracks originating from the borehole with an angle between 80° and 30°
- CB 30 – 0 [3]
  Cracks originating from the borehole with an angle between 30° and 0°

- CD 90 – 80 [4]

  Cracks with no direct link to a blasthole but with a radial direction to a blasthole and an angle between 90° and 80°

- CD 80 – 30 [5]

  Cracks with no direct link to a blasthole but with direction to a blasthole and an angle between 80° and 30°

- CD 30 – 0 [6]

  Cracks with no direct link to a blasthole but with direction to a blasthole and an angle between 30° and 0°

- Parallel [7]

  Cracks parallel to the bench face with no link to a blasthole

- Connection [8]

  Cracks which form connections between neighbouring blastholes

- SCB [9]

  Straight cracks between blastholes (from the back or front side of the block)

- Short [10]

  Short (< 1 cm) radial cracks around the blastholes

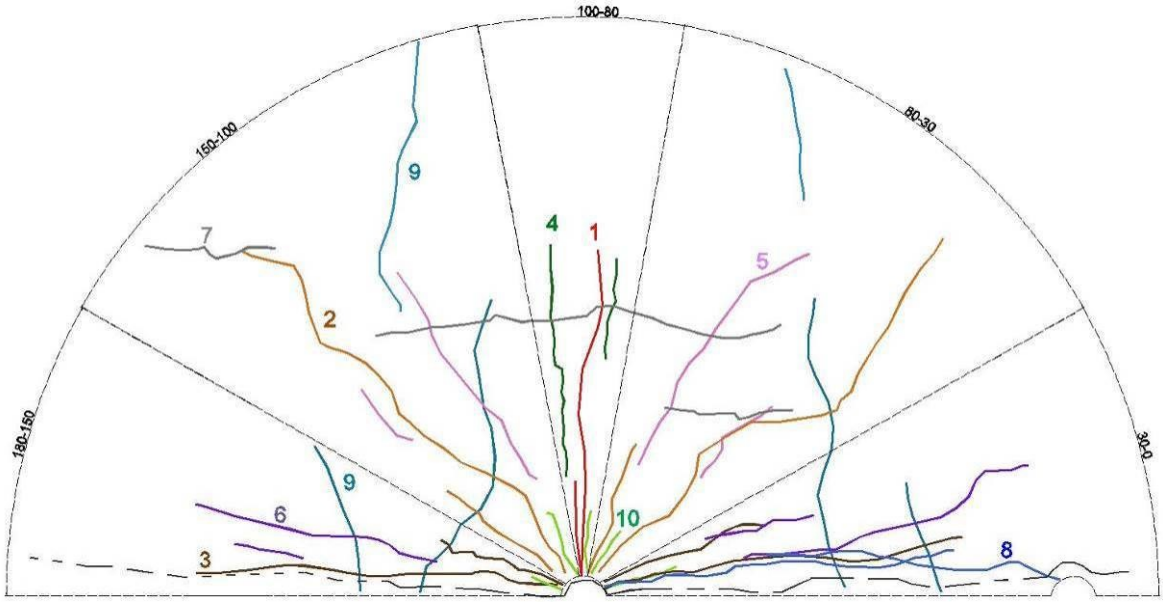

Figure 71: Crack families 1 to 10

After the crack pattern was divided into a 2 x 2 cm grid the number of cracks created in different areas of the slice was determined (see Figure 72).

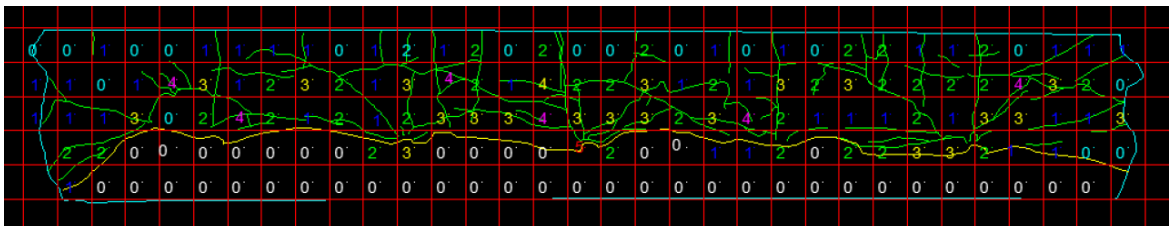

Figure 72: Grid of 2 x 2 cm over the traced cracks (Navarro, 2015)

Out of this data the damage map (see Figure 73) for an overview of heavily damaged regions of the remaining block was generated.

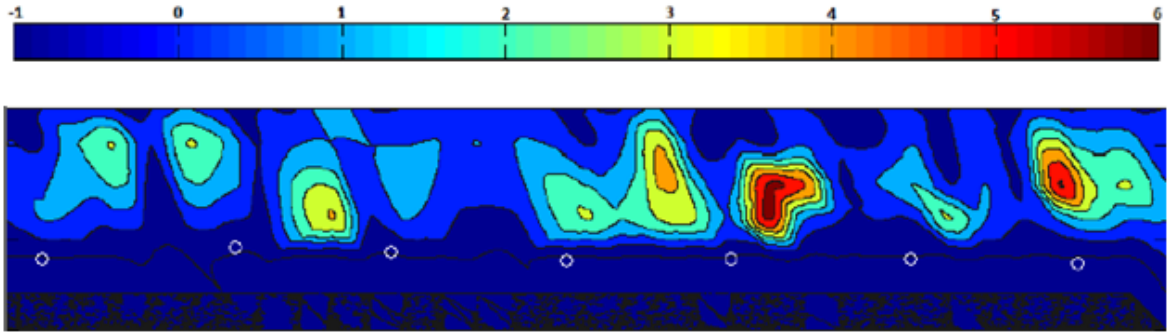

Figure 73: Damage map (Navarro, 2015)

For a comparison of the damage of individual slices two measures were introduced.

- Mean crack density (MCD)

  Sum of all cracks in the individual cells of the grid divided by the total number of 2 x 2 cm cells

- Mean crack intersection density (MCID)

  Sum of the intersections of the cracks in the individual cells of the grid divided by the total number of cells

A detailed description of the procedure can be found in Navarro (2015).

3.4.2.2 Thin Sections

After blasting the space in the yoke was sealed off and filled with fast hardening cement. To quantify the cracks created on the micro-scale several drill-cores were taken at selected places around, behind or near blasted holes (Figure 74).

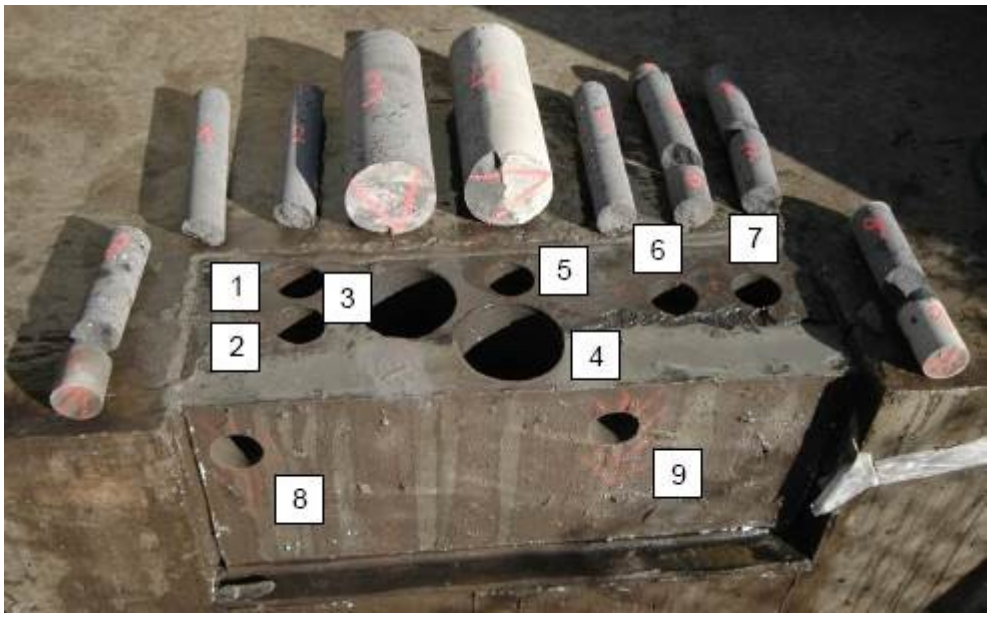

Figure 74: Taken drill-cores around / behind / between blasted holes

The drill-cores were cut into several slices and thin sections with an area of 2.0 cm x 4.0 cm were made (see Figure 75).

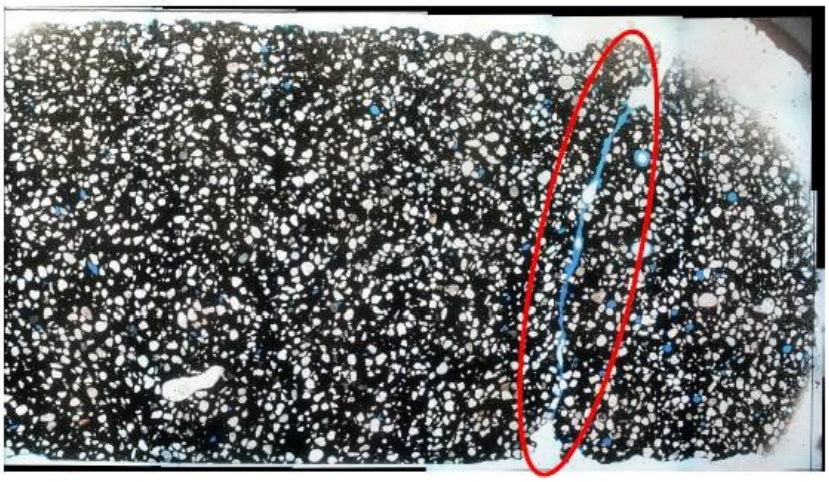

Figure 75: Example of a thin section; red ellipse marks a crack (Wrienz, 2013)

Although the procedure of taking drill-cores worked well during the preliminary stage of the blasting tests, it was decided to skip this procedure for the further stages. The reason for this was that with the existing equipment only small

sections with an area of 2.0 cm x 4.0 cm could be produced as a thin section. The handling of these small sections was difficult due to the already existing cracks. They were activated during the preparation process of the thin sections and the sections broke apart. Afterwards it was difficult to distinguish between cracks which were created by blasting and cracks which were activated during the post-blast processing. The crack (red ellipse) in the above figure was clearly detected, but in the related thin sections this crack could not be followed.

Details can be found in Wrienz (2013).

3.4.2.3 Computer Tomography

Due to the availability of a computer-tomography system at the ÖGI (Österreichisches Gießerei Institut) a test-scan was done on an already cut slice (see Figure 76).

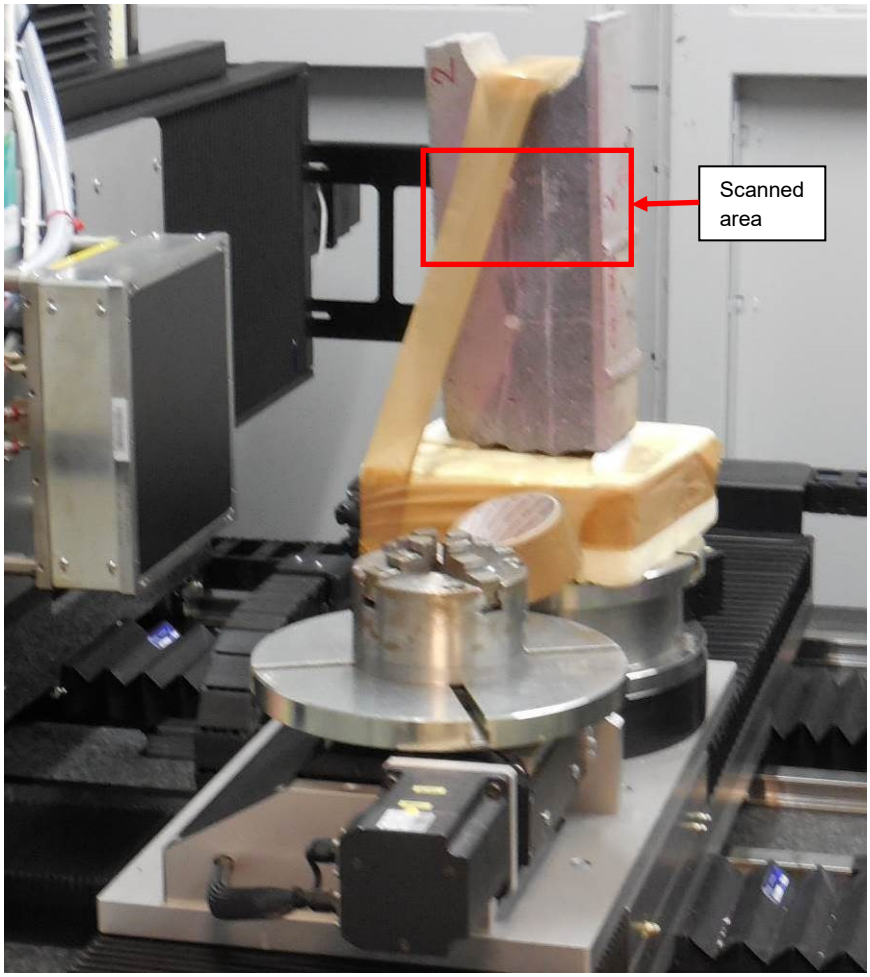

Figure 76: Computer Tomography at a cut slice

The resolution (by means of the size of the voxels) of the equipment used was 0.1075 x 0.1075 mm.

Figure 77 shows the result of a test computer tomography at an already cut slice with the dye-penetrant-procedure as a reference. The visible vertical line in the right picture (using dye-penetrant) is a result from the cutting process.

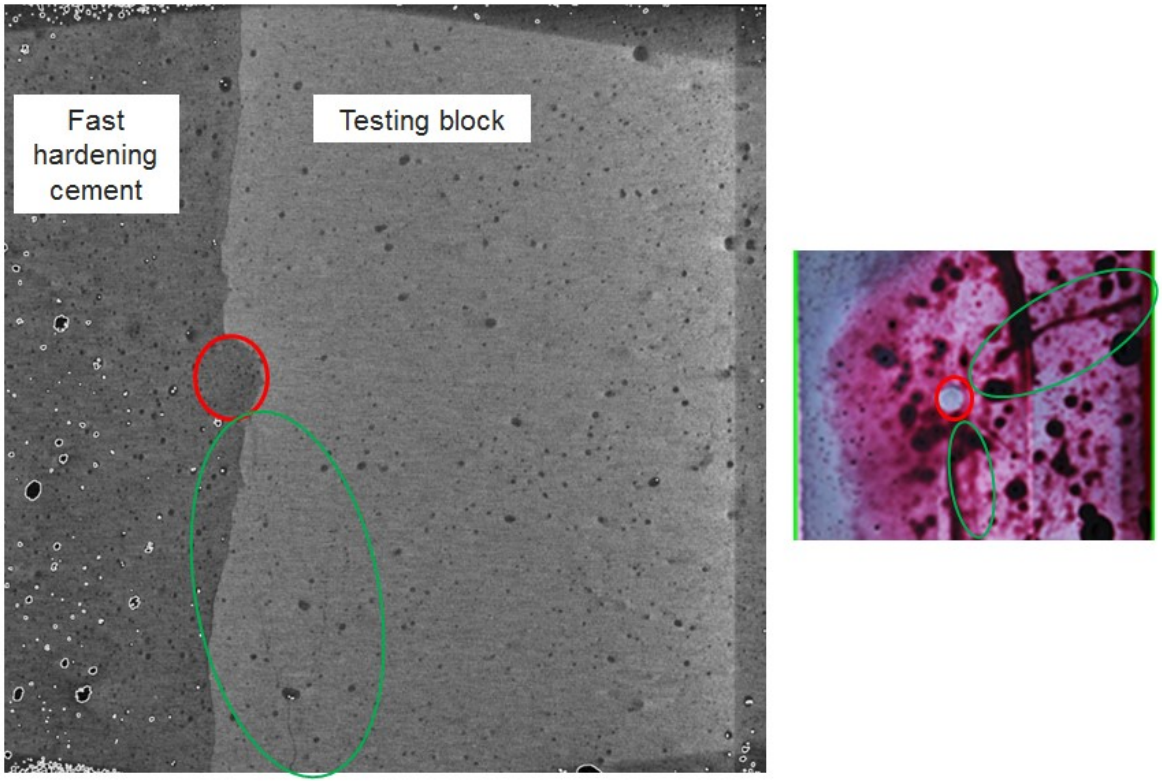

Figure 77: Computer tomography (left) and dye-penetrant test (right) of the same specimen

The half-cast of the blasted hole as well as the crack, which seemed to be a connection crack to the next blasthole, was detected with both procedures.

The dye-penetrant procedure detected an additional crack to the right side which was not visible with the computer tomography. The reason might be that the resolution of the computer tomography equipment used was not able to detect closed fractures. Therefore (and due to the high costs) it was decided not to proceed with computer tomography as a method for the quantification of the cracks created.

A detailed description of the procedure can be found in Navarro (2015).

3.5 Quantification of Fragmentation

The following description is taken from Schimek et al. (2013).

The blasted material was collected after each blast and a sieving analysis was done. As a result of the sieving analysis the particle size distribution and several k-values (percentile fragment sizes) were calculated.

The sieving analysis was done according to the sieving standard of the Chair of Mining Engineering, see Grasedieck (2006).

The blasted material was sieved in two steps. The grain sizes of the coarser material were obtained by pushing every single piece through the mesh of the sieves. The following sieves were used for that procedure: 125; 100; 80; 63; 50; 40; 31.5; 25; 20; 14; 12.5; 10 mm.

The blasted material was split at a grain size of 14 mm if there were more than 3.0 kg which passed through.

The finer material was sieved by hand using the following screen sizes: 6.3; 4; 2; 1; 0.5 mm. It was decided not to use a sieving machine because secondary breakage while sieving should be avoided. The screening stopped at a grain size of 0.5 mm due to the fact that the quartz sand used for the magnetic mortar had grain sizes up to 0.5 mm. The sieving result in this finest region would be influenced by the separation of the large quartz sand particles and not representative for the fragmentation.

During each sieving step an optical sorting process was carried out. This was done because a number of unwanted lighter pieces came from the fast hardening cement or the yoke and the dark pieces were the desired particles from the testing block (magnetic mortar).

Additionally for the finest fragments (< 4 mm) a hand-magnet was used during the 2^{nd} and 3^{rd} stage to separate the magnetic material of the testing block from the non-magnetic material of the yoke and from the grouting material or other origin.

3.5.1 Particle Size Distribution

The result of the sieving analysis was plotted in a Gates-Gaudin-Schuhmann (GGS) diagram (Schuhmann, 1940). This diagram is a log-log-plot where the x-axis shows the screen size and the y-axis shows the accumulated mass passing. The Swebrec distribution (Ouchterlony, 2005, 2010) was used as a fitting function because it gives better fits than most other functions (Sanchidrián et al., 2010, 2012, 2014).

3.5.2 Determination of k-values

In addition to the particle size distribution the k-values at the cumulative mass passing at 30 %, 50 % and 80 % were calculated with linear interpolation:

$$k_{50} = k_L + \frac{k_U - k_L}{P_U - P_L} \cdot (P_{50} - P_L)$$

with

k_{50} calculated grain size at cumulative mass passing of 50 %

k_L lower screen size next to cumulative mass passing of 50 %

k_U upper screen size next to cumulative mass passing of 50 %

P_L cumulative mass passing at k_L

P_U cumulative mass passing at k_U

P_{50} cumulative mass passing at k_{50} (= 50 %)

The calculation of the specific k-values k_{30} and k_{80} is similar to that shown for k_{50}.

3.5.3 Coefficient of Uniformity k_{80}/k_{30}

"*The coefficient of uniformity is a method to describe the particle size distribution of 50 % of the passing material. Therefore the specific particle size at 80 % passing (k_{80}) is divided by the specific particle size at 30 % passing (k_{30}). As the k_{80} of a fragmentation process is always larger than the k_{30} the minimum value of the coefficient of uniformity is always larger than 1."* (Reichholf, 2003)

3.6 Statistical Evaluation

Some statistical methods have the restrictions that the populations have to be normally distributed. Due to the small amount of data which were compared, the distribution of the population couldn't be determined. Therefore the following non-parametric methods were used for testing whether samples originate from the same distribution or not.

Since the two methods chosen have the requirements of independence within each sample (Conover, 1999) they can be used for a comparison of the D_{Mean} and S_{Norm} values (see chapter 3.4.1), the cracks detected (see chapter 3.4.2.1) and the fragmentation parameters k_{30}, k_{50}, k_{80} and k_{80}/k_{30} of different rows (see chapter 3.5). However they can't be used for a comparison of whole sieving curves (sets of k_{30}, k_{50} and k_{80} values).

3.6.1 Mann-Whitney-U-Test (MWU-Test)

This method can be used for comparing two samples that are independent. The following assumptions are made (Conover, 1999):

- *Both samples are random samples from their respective populations.*
- *In addition to independence within each sample, there is mutual independence between two samples.*
- *The measurement scale is at least ordinal.*

The null hypothesis is that there are no differences between the means of the samples. The calculation is done as follows:

- All data from the two groups have to be ranked together.
- The sum of the ranks for each group has to be calculated (T_1 and T_2)
- The lower quantile (Q_L) is taken from Table 9 with α/2
- The upper quantile (Q_U) is calculated as follows:

$$Q_U = n(n+m+1) - Q_L$$

Table 9: Quantiles of the MWU-Test (Conover, 1999)

n	p	m = 2	3	4	5
2	0.001	3	3	3	3
	0.005	3	3	3	3
	0.01	3	3	3	3
	0.025	3	3	3	3
	0.05	3	3	3	4
	0.10	3	4	4	5
3	0.001	6	6	6	6
	0.005	6	6	6	6
	0.01	6	6	6	6
	0.025	6	6	6	7
	0.05	6	7	7	8
	0.10	7	8	8	9
4	0.001	10	10	10	10
	0.005	10	10	10	10
	0.01	10	10	10	11
	0.025	10	10	11	12
	0.05	10	11	12	13
	0.10	11	12	14	15
5	0.001	15	15	15	15
	0.005	15	15	15	16
	0.01	15	15	16	17
	0.025	15	16	17	18
	0.05	16	17	18	20
	0.10	17	18	20	21

The null hypothesis of equal population means would be rejected, if

$$Q_L > T_{1or2}$$

or

$$T_{1or2} > Q_U$$

with

T_1 Sum of the ranks of group 1

T_2 Sum of the ranks of group 2

n Number of observations in group 1

m Number of observations in group 2

α Significance level (= 5 % = 0.05)

Too few data points in the groups compared may lead to a sum of the ranks of the individual groups which can't fall below the lower quantiles of Table 9. This fact may lead to inconsistent results of the MWU-Test.

3.6.2 Kruskal-Wallis One-Way Analysis of Variance (KW-ANOVA)

This method can be used for comparing more than two samples that are independent. The following assumptions are made (Conover, 1999):

- *All samples are random from their respective populations.*
- *In addition to independence within each sample, there is mutual independence among the various samples.*
- *The measurement scale is at least ordinal.*
- *Either the k population distribution functions are identical, or else some of the populations tend to yield larger values than other populations do.*

The null hypothesis is that there are no differences between the means of the samples. The calculation is done as follows:

- All data from all groups have to be ranked together.
- The test statistic "H" is chi-squared distributed and has to be calculated as follows:

$$H = \frac{12}{n(n+1)} \cdot \sum_{i=1}^{k} \frac{{R_i}^2}{n_i} - 3(n+1)$$

The null hypothesis of equal population means would be rejected, if

$$H \geq {\chi^2}_{1-\alpha,k-1}$$

with

H	Test statistic for the KW-ANOVA
k	Number of groups
n	Number of observations
n_i	Number of observations in group i

R_i^2	Sum of the ranks of group i squared
α	Significance level (= 5 % = 0.05)
k-1	Degrees of freedom
χ^2	Critical value of the test statistic for the KW-ANOVA where χ^2 is the chi-squared distribution

Conover (1999) states that "*if k = 3, all of the sample sizes are 5 or less, and there are no ties, the exact quantile may be obtained from*" Table 10.

Table 10: Quantiles of the KW-ANOVA (Conover, 1999)

Sample Sizes	$w_{0.95}$
2, 2, 2	4.5714
3, 2, 1	4.2857
3, 2, 2	4.5000
3, 3, 1	4.5714
3, 3, 2	5.1389
3, 3, 3	5.0667
4, 2, 1	4.8214
4, 2, 2	5.1250
4, 3, 1	5.0000
4, 3, 2	5.4000
4, 3, 3	5.7273
4, 4, 1	4.8667
4, 4, 2	5.2364
4, 4, 3	5.5758
4, 4, 4	5.6538
5, 2, 1	4.4500
5, 2, 2	5.0400
5, 3, 1	4.8711
5, 3, 2	5.1055
5, 3, 3	5.5152
5, 4, 1	4.8600
5, 4, 2	5.2682
5, 4, 3	5.6308
5, 4, 4	5.6176
5, 5, 1	4.9091
5, 5, 2	5.2462
5, 5, 3	5.6264
5, 5, 4	5.6429
5, 5, 5	5.6600

4 Results and Analysis

4.1 Methodological Questions

4.1.1 Are the Results from the Different Production Cycles Comparable?

Since the testing blocks were produced in three production cycles (see chapter 3.1) the results of these different cycles have to be compared to see if they are comparable by means of similar.

4.1.1.1 Material Properties

The statistical evaluation of the material properties from the different production cycles can be seen in Table 11.

Table 11: Statistical evaluation of the material properties with the KW-ANOVA (α = 0.05)

Material Property	H	X^2	Significant Difference
Density	17.22	5.99	Yes
Young's modulus	15.19	5.99	Yes
UCS	15.37	5.99	Yes
Brazilian tensile strength	12.35	5.99	Yes
P-wave velocity	22.28	5.99	Yes

The material properties of the mortar from the different production cycles were significantly different. The complete set of data of the material property measurements can be found in Appendix 2.

4.1.1.2 Cylinder Shots

Several cylinders (chapter 3.1) from each production cycle were blasted to check the fragmentation characteristics and the blastability (Table 12 and Appendix 3).

Table 12: Fragmentation characteristics of the different production cycles

Production Cycle		Sieving parameters [mm]		
		k_{30}	k_{50}	k_{80}
#01	**Average**	**6.3**	**11.5**	**19.3**
	Std. dev.	0.3	0.5	0.8
#02	**Average**	**8.4**	**15.1**	**24.6**
	Std. dev.	0.4	0.8	1.8
#03	**Average**	**8.0**	**13.4**	**23.0**
	Std. dev.	0.3	0.2	1.0

The statistical evaluation of the sieving parameters showed significant differences in the mean values of the different production cycles (see Table 13).

Table 13: Statistical evaluation of the sieving parameters of all 3 production cycles with the KW-ANOVA (α = 0.05; 4 + 4 + 3 data)

	H	X^2	Significant Difference
k_{30}	7.33	5.58	Yes
k_{50}	8.91	5.58	Yes
k_{80}	7.85	5.58	Yes

4.1.1.3 Testing Blocks from Production Cycles #01 and #02

The identically blasted, here called similar testing blocks from production cycle #01 (#0312) and #02 (#0313) with delay-time sequences of 140 µs in their 1st rows and 0 µs in their 2nd and 3rd rows showed the results seen in Figure 78. The benches of both testing blocks were similar after the 1st row shots, which created larger overbreak on the left side than on the right side. The 2nd row blast created in contrast to the 1st row blast less overbreak in both cases. The results of testing block #0312 showed less overbreak than testing block #0313. The results of the 3rd row blast were in both cases again similar. In all cases a thin slab at the top of the blastholes was broken off.

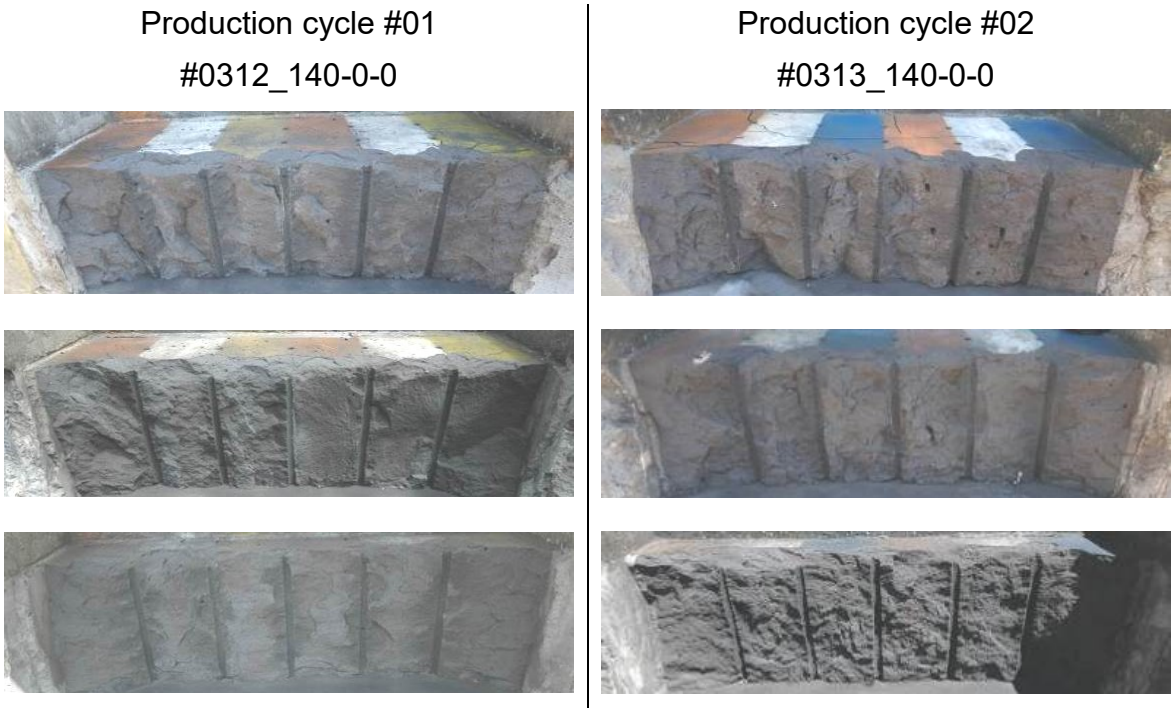

Figure 78: Bench face after blasting the 1st (top), 2nd (middle) and 3rd (bottom) row from production cycle #01 (left) and #02 (right)

The evaluation of the bench surface by using D_{Mean} (see chapter 3.4.1) confirmed the observations. Figure 79 shows the D_{Mean} values for the three contour lines at the heights of 5, 10 and 15 cm. The complete set of data can be found in Appendix 10.

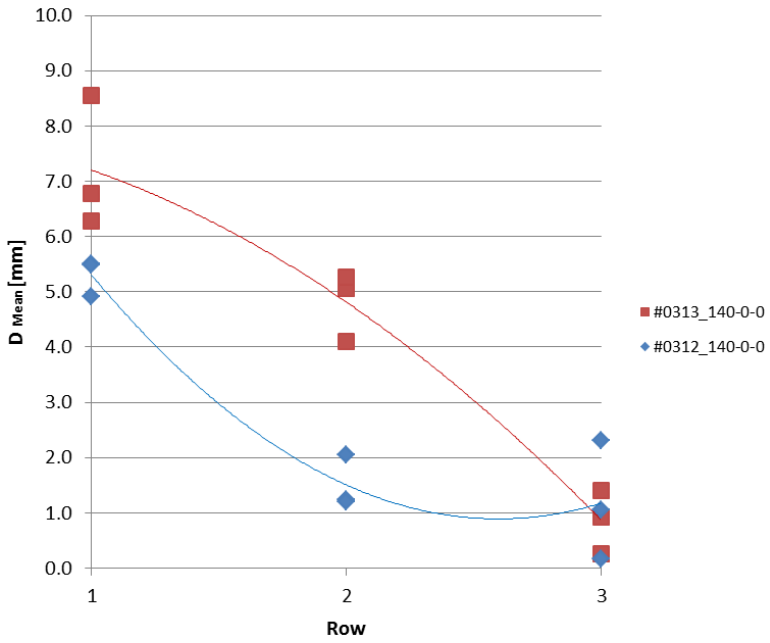

Figure 79: D_{Mean} of similar testing blocks from production cycle #01 (#0312) and #02 (#0313)

The statistical evaluation of the D_{Mean} values from the individual rows gave the following results (Table 14).

Table 14: Statistical evaluation of D_{Mean} of the individual rows with the MWU-Test ($\alpha = 0.05$; $Q_L = 6$; $Q_U = 15$; 2 x 3 data)

	T_1	T_2	Significant Difference
1st rows	6.0	15.0	No
2nd rows	6.0	15.0	No
3rd rows	11.0	10.0	No

No significant differences of the means were detected although the comparisons of the 1st and 2nd rows were on the verge of being significant. This is related to the small number of data points in the groups which is problematic for the MWU-Test (see chapter 3.6.1). Therefore the obviously different results from the 1st and 2nd rows are interpreted as different.

The sieving parameters (Table 15) showed that the blasted material of production cycle #02 (#0313) had a somewhat coarser fragmentation for the first two rows than the material from production cycle #01 (#0312). This result was consistent with the results for the cylinder shots (see Table 12). The fragmentation of the 3rd row with this arrangement (140 µs – 0 µs – 0 µs) was almost the same for both testing blocks. The coefficient of uniformity values for the production cycles #01 and #02 showed a similar trend with increasing row number. The values for testing block #0313 (production cycle #02) were smaller than those for testing block #0312. The complete set of data can be found in Appendix 15 and 16.

Table 15: Fragmentation of similar testing blocks from production cycle #01 (#0312) and #02 (#0313)

		k_{30} [mm]	k_{50} [mm]	k_{80} [mm]	Uniformity Coefficient	Planned delay [µs]
Production cycle #01	Row 1	18.0	36.3	78.8	4.37	140
	Row 2	15.5	30.2	72.6	4.69	0
	Row 3	17.1	35.1	66.1	3.86	0
Production cycle #02	Row 1	20.6	40.3	79.8	3.87	140
	Row 2	15.9	36.7	70.2	4.41	0
	Row 3	18.2	36.1	65.7	3.61	0

A comparison of cracks created was not possible as the dye-penetration method was developed just after the blasts of the 1st stage.

4.1.1.4 Testing Blocks from Production Cycles #02 and #03

Another set of identically blasted or similar testing blocks of different production cycles are #0213 from production cycle #02 and #0314 from production cycle #03. The delay-time sequences of 28 µs for all three rows gave the following results.

While the first and third row in both cases resulted in a comparable bench face, the second row shot of testing block #0213 resulted in more backbreak. The broken off thin slab at the top of the blastholes was larger and the half-casts were broadened for testing block #0314 of production cycle #03.

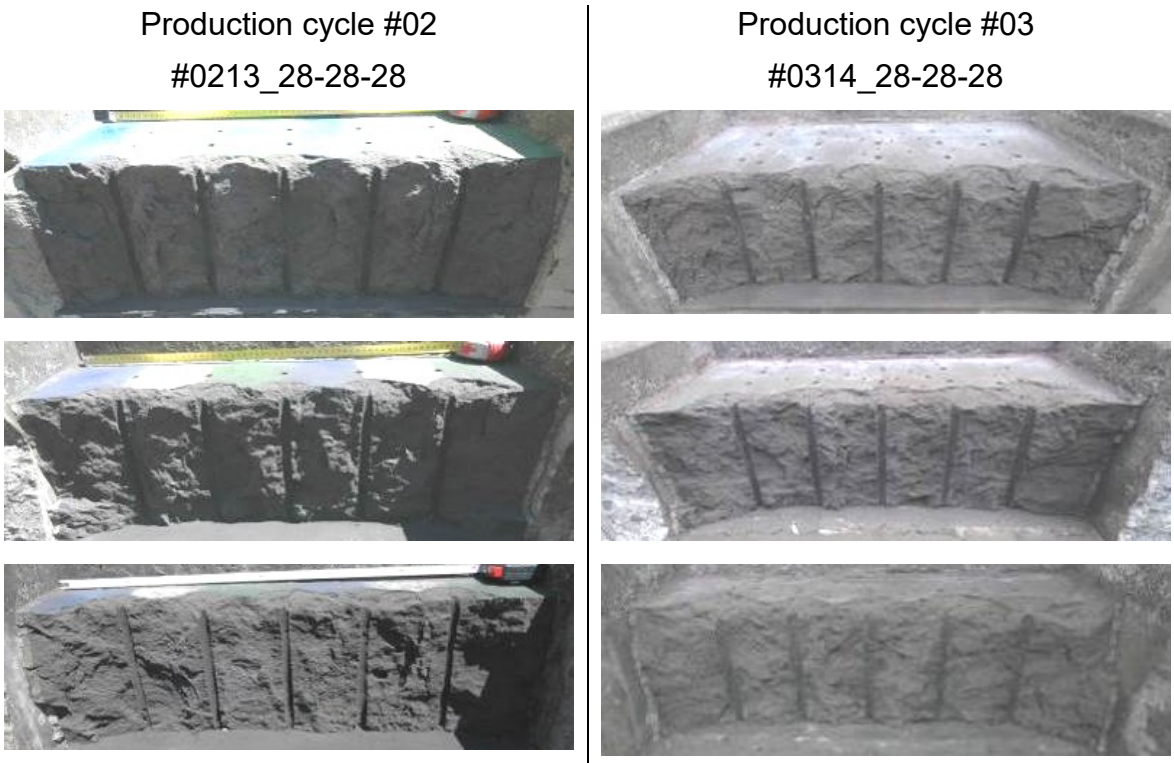

Figure 80: Bench face after blasting the 1st (top), 2nd (middle) and 3rd (bottom) row from production cycle #02 (left) and #03 (right)

The evaluation of the bench surface by using D_{Mean} (see chapter 3.4.1) confirmed these results (see Figure 81) although a larger variation in the measured values of the first and second row of block #0314 was observed. The complete set of data can be found in Appendix 10.

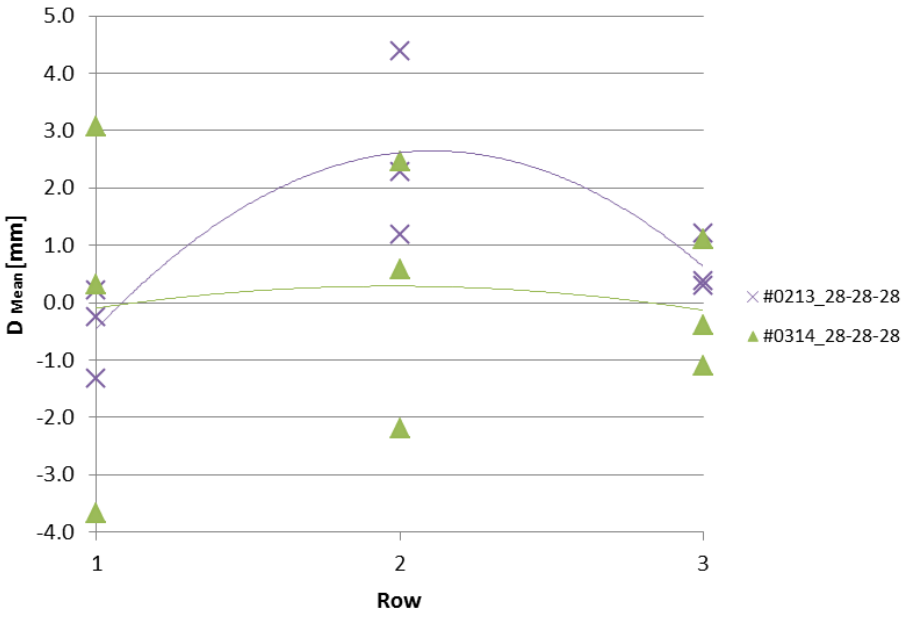

Figure 81: D_{Mean} of similar testing blocks from production cycle #02 (#0213) and #03 (#0314)

The statistical evaluation of the D_{Mean} values from the individual rows showed no significant differences of the means (see Table 16).

Table 16: Statistical evaluation of D_{Mean} of the individual rows with the MWU-Test (α = 0.05; Q_L = 6; Q_U = 15; 2 x 3 data)

	T_1	T_2	Significant Difference
1st rows	9.0	12.0	No
2nd rows	13.0	8.0	No
3rd rows	13.0	8.0	No

The sieving parameters k_{30}, k_{50} and k_{80} as well as the ratio of k_{80}/k_{30} of the different rows are given in Table 17.

Table 17: Fragmentation of similar testing blocks from production cycle #02 (#0213) and #03 (#0314)

		k_{30} [mm]	k_{50} [mm]	k_{80} [mm]	Uniformity Coefficient	Planned delay [µs]
#0213	Row 1	40.2	67.0	94.4	2.35	28
	Row 2	24.4	63.2	101.6	4.17	28
	Row 3	19.9	43.5	74.1	3.72	28
#0314	Row 1	38.0	71.0	112.3*	2.96*	28
	Row 2	18.5	43.9	92.7	5.02	28
	Row 3	16.7	36.6	61.5	3.68	28

*…extrapolated value

While the k_{30} and k_{50} of the first rows were nearly the same for both testing blocks the extrapolated k_{80} of testing block #0314 (production cycle #03) was much coarser. The blasted second and third rows of production cycle #02 (#0213) had a somewhat coarser fragmentation than those of production cycle #03 (#0314). This result was consistent with the results of the cylinder shots (see Table 12).

The coefficient of uniformity values for the production cycles #02 and #03 showed a similar trend with increasing row number. The values for testing block #0213 (production cycle #02) were smaller than those for testing block #0314.

A comparison of the cracks created in the remaining part was not possible since in testing block #0314 four rows were blasted instead of three rows from testing block #0213.

4.1.1.5 Findings

The findings of chapter 4.1.1 showed significantly different results in the material properties and in the fragmentation of the cylinder shots of the different production cycles. In the testing blocks of production cycle #03 the half-casts were broadened and the thin slab, which was thrown off at the top of each blasthole, seemed to be larger.

The fragmentation and backbreak of identically blasted testing blocks from different production cycles showed in contrast to the material properties and the cylinder shots no significant differences. This result might be influenced by the small number of data points in the groups which is a problem when using the MWU-Test (see chapter 3.6.1). Due to the observed differences in the D_{Mean} values of the 1^{st} and 2^{nd} row blasts of the identically blasted blocks from production cycle #01 and #02 the conclusion can be drawn, that an absolute comparison of the results from different production cycles is not meaningful. On the other hand a relative comparison of results from different production cycles might be meaningful.

4.1.2 Are the Results within the Production Cycles Comparable?

Due to the detected significant differences of the results from the different production cycles (see chapter 4.1.1), the comparability of the test-results from the same production cycle is investigated.

4.1.2.1 Production Cycle #01

The cylinder blasts from production cycle #01 (Table 18) gave nearly the same fragmentation with only small variations (see also Appendix 3).

Table 18: Sieving parameters for cylinder-blasts of production cycle #01

Cylinder Number	Sieving parameters [mm] k_{30}	k_{50}	k_{80}	Uniformity Coefficient
#0101	6.1	11.4	19.3	3.17
#0201	6.7	12.2	20.6	3.06
#0301	6.0	11.0	18.3	3.04
#0401	6.2	11.2	19.1	3.08
Average	**6.3**	**11.5**	**19.3**	**3.09**
Std. dev.	0.3	0.5	0.8	0.06

Additionally a number of identically blasted testing blocks can be compared. As mentioned in chapter 3.3.2 all 1st rows of the eight testing blocks of the first stage (#0212 - #0912), were blasted with the same nominal delay of 140 µs. The initiation started from the right side. The following two figures are examples for the bench faces.

Figure 82: Front view of block #0212 after blasting of the 1st row with 140 µs delay

Figure 83: Front view of block #0912 after blasting of the 1st row with 140 µs delay

In both cases the bench surface showed less backbreak on the right side than on the left side where deep trenches were visible. Similar surface characteristics were seen on the other testing blocks (see Appendix 6). The measured D_{Mean} values for the 1st rows lay between +1.7 and +7.5 mm with an average of +4.5 mm. The statistical evaluation of the D_{Mean} values from the first rows showed no significant differences between the specimens (Table 19). The complete data set can be found in Appendix 10.

Table 19: Statistical evaluation of D_{Mean} of the first rows of stage 1 with the KW-ANOVA (α = 0.05; 8 x 3 data)

	H	X^2	Significant Difference
1st rows	11.27	14.07	No

In contrast to that the statistical evaluation of the calculated S_{Norm} values (see Appendix 10) showed significant differences (Table 20) which leads to the conclusion that this parameter is not valuable for a comparison of the bench face characteristics.

Table 20: Statistical evaluation of S_{Norm} of the first rows of stage 1 with the KW-ANOVA (α = 0.05; 8 x 3 data)

	H	X^2	Significant Difference
1st rows	16.64	14.07	Yes

The sieving parameters of the first row shots of all eight testing blocks of stage 1 (Table 21) showed that there are two testing blocks (#0612 and #0812) with a fragmentation which was finer than those of the others (see also Appendix 15).

Table 21: Fragmentation of the 1st rows of stage 1 with a delay of 140 µs

	k_{30} [mm]	k_{50} [mm]	k_{80} [mm]	Uniformity Coefficient
#0212	19.6	37.8	84.2	4.30
#0312	18.0	36.3	78.8	4.37
#0412	16.9	35.8	77.2	4.58
#0512	18.5	33.9	79.2	4.29
#0612	14.3	28.0	66.6	4.66
#0712	18.8	36.4	80.6	4.29
#0812	12.5	26.7	66.2	5.32
#0912	16.5	36.5	75.6	4.58
Average	**16.9**	**33.9**	**76.1**	**4.55**
Std. dev.	2.3	4.0	6.0	0.32

Additional to the identically blasted 1st rows several 2nd rows were blasted in the same way. While the second rows of three testing blocks (#0312, #0512 and #0812) were blasted simultaneously the second rows of three other blocks (#0212, #0412 and #0912) had a nominal delay of 140 µs. The results of the D_{Mean} measurements can be seen in Figure 84.

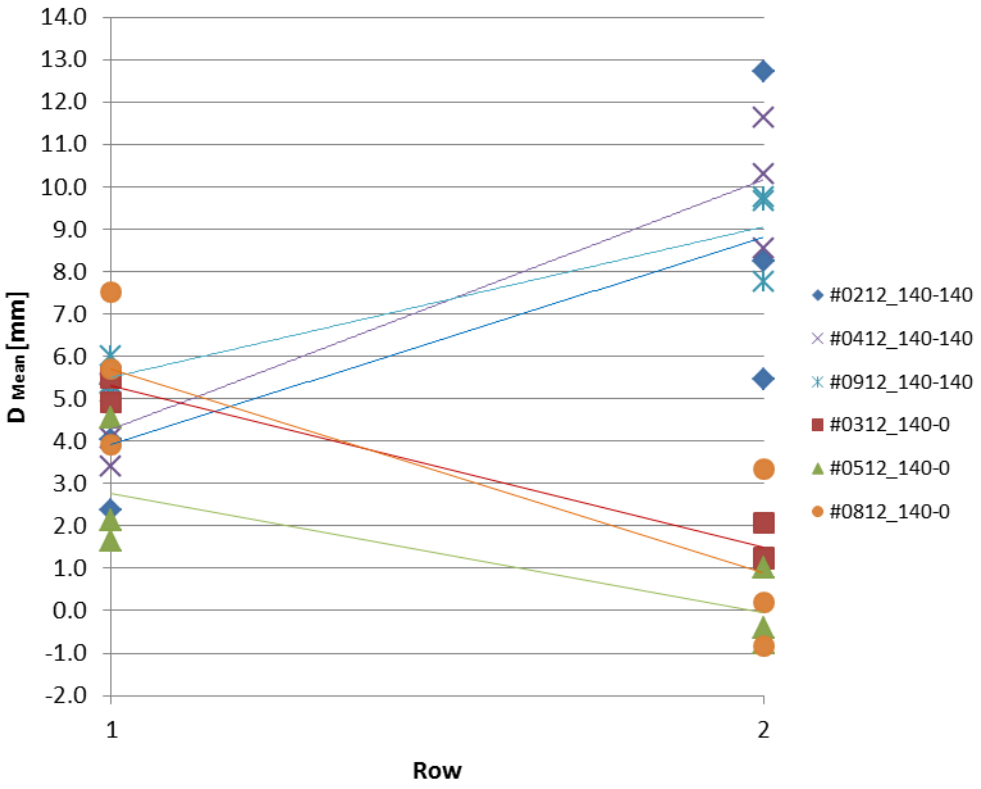

Figure 84: Development of D_{Mean} from 1st to 2nd row in stage 1

While the backbreak from the first to the second row decreased in case of simultaneously blasted 2nd rows it increased for the 2nd row blasts with 140 µs delay. The statistical evaluation of the D_{Mean} values (Table 22) showed that there were no significant differences between the data from the identically blasted rows. The complete data set can be found in Appendix 10.

Table 22: Statistical evaluation of D_{Mean} with the KW-ANOVA (α = 0.05; 3 x 3 data)

		H	X^2	Sign. Diff.		H	X^2	Sign. Diff.
1st rows	#0212, #0412 and #0912	3.29	5.07	No	#0312, #0512 and #0812	4.36	5.07	No
2nd rows		1.07	5.07	No		2.76	5.07	No

The influence of the delay-time on the D_{Mean} values will be investigated in chapter 4.2.1.2.

The statistical evaluation of the S_{Norm} values (Table 23) showed significant differences in the first row values of the testing blocks #0212, #0412 and #0912. The other values were not significantly different. These inconsistent results confirmed the conclusion that this parameter is not valuable for a comparison of the bench face characteristics.

Table 23: Statistical evaluation of S_{Norm} with the KW-ANOVA (α = 0.05; 3 x 3 data)

		H	X^2	Sign. Diff.		H	X^2	Sign. Diff.
1st rows	#0212, #0412 and #0912	7.20	5.07	Yes	#0312, #0512 and #0812	3.47	5.07	No
2nd rows		3.29	5.07	No		4.36	5.07	No

The sieving parameters of the first and second row shots with a nominal delay of 140 µs can be seen in Table 24 and in Appendix 15.

Table 24: Fragmentation of shots with a delay of 140 µs in the 1st and 2nd row

		k_{30} [mm]	k_{50} [mm]	k_{80} [mm]	Uniformity Coefficient
#0212	Row 1	19.6	37.8	84.2	4.30
	Row 2	11.3	21.8	63.8	5.63
#0412	Row 1	16.9	35.8	77.2	4.58
	Row 2	11.7	22.3	65.3	5.57
#0912	Row 1	16.5	36.5	75.6	4.58
	Row 2	9.3	19.4	52.4	5.66

The statistical evaluation of the sieving parameters (Table 25) showed that there were no significant differences between the identically blasted blocks.

Table 25: Statistical evaluation of the sieving parameters with the KW-ANOVA (α = 0.05; 3 x 2 data)

	H	X^2	Significant Difference
k_{30}	0.86	4.57	No
k_{50}	0.29	4.57	No
k_{80}	0.86	4.57	No
Unif. Coeff.	0.29	4.57	No

The sieving parameters of the testing blocks with a delay of 140 µs in the 1st and 0 µs in the 2nd row can be seen in Table 26 and in Appendix 15.

Table 26: Fragmentation of shots with a delay of 140 µs in the 1st and 0 µs in the 2nd row

		k_{30} [mm]	k_{50} [mm]	k_{80} [mm]	Uniformity Coefficient
#0312	Row 1	18.0	36.3	78.8	4.37
	Row 2	15.5	30.2	72.6	4.69
#0512	Row 1	18.5	33.9	79.2	4.29
	Row 2	14.5	28.6	66.3	4.57
#0812	Row 1	12.5	26.7	66.2	5.32
	Row 2	10.3	24.0	61.1	5.95

The statistical evaluation of the sieving parameters (Table 27) showed that there were no significant differences between the comparably blasted blocks.

Table 27: Statistical evaluation of the sieving parameters with the KW-ANOVA (α = 0.05; 3 x 2 data)

	H	X^2	Significant Difference
k_{30}	3.43	4.57	No
k_{50}	3.71	4.57	No
k_{80}	3.43	4.57	No
Unif. Coeff.	3.71	4.57	No

4.1.2.2 Production Cycle #02

The results of the two cylinder blasts from production cycle #02 (Table 28) showed that they had nearly the same fragmentation (see Appendix 3).

Table 28: Sieving parameters for cylinder-blasts of production cycle #02

Cylinder Number	Sieving parameters [mm] k_{30}	k_{50}	k_{80}	Uniformity Coefficient
#0102	8.8	15.9	26.4	3.01
#0202	8.0	14.3	22.8	2.86
Average	**8.4**	**15.1**	**24.6**	**2.93**
Std. dev.	0.4	0.8	1.8	0.07

Additionally the identically blasted testing blocks can be compared. As mentioned in chapter 3.3.3 four testing blocks were blasted with the same nominal delay of 28 µs in their first rows. Figure 85 shows the bench faces after blasting.

Figure 85: Front view of block #0213 (top left), #0513 (top right), #0613 (bottom left) and #0713 (bottom right) after blasting of the 1st row with 28 µs delay

The surface characteristics of all four testing blocks were similar. The statistical evaluation of the D_{Mean} values from the first rows (see also Appendix 10) showed no significant differences between the specimens (Table 29).

Table 29: Statistical evaluation of D_{Mean} of the 28 µs delayed first row shots of stage 2 with the KW-ANOVA (α = 0.05; 4 x 3 data)

	H	X^2	Significant Difference
1st rows	5.05	7.81	No

In contrast to that the statistical evaluation of the S_{Norm} values from the first rows showed significant differences between the specimens (Table 30). Again the usefulness of this parameter for a comparison of the bench face characteristics is questioned.

Table 30: Statistical evaluation of S_{Norm} of the 28 µs delayed first row shots of stage 2 with the KW-ANOVA (α = 0.05; 4 x 3 data)

	H	X^2	Significant Difference
1st rows	9.97	7.81	Yes

The sieving parameters of the first row shots of stage 2 (Table 31 and Appendix 16) showed small variations in the values with an outlier in the k_{30} of testing block #0513 and hence in the corresponding uniformity coefficient.

Table 31: Fragmentation of the 1st rows of stage 2 with a delay of 28 µs

	k_{30} [mm]	k_{50} [mm]	k_{80} [mm]	Uniformity Coefficient
#0213	40.2	67.0	94.4	2.35
#0513	28.7	65.8	96.1	3.35
#0613	40.7	76.7	100.5	2.47
#0713	40.3	77.5	97.5	2.42
Average	**37.5**	**71.7**	**97.1**	**2.65**
Std. dev.	5.1	5.4	2.3	0.41

4.1.2.3 Production Cycle #03

The results of the cylinder blasts from production cycle #03 (Table 32) showed that all four cylinders had almost the same fragmentation (see also Appendix 3).

Table 32: Sieving parameters for cylinder-blasts of production cycle #03

Cylinder Number	Sieving parameters [mm] k_{30}	k_{50}	k_{80}	Uniformity Coefficient
#0103	8.1	13.2	22.2	2.74
#0203	8.4	13.3	22.1	2.63
#0303	8.1	13.6	24.4	3.03
#0403	7.6	13.5	23.3	3.08
Average	**8.0**	**13.4**	**23.0**	**2.87**
Std. dev.	0.3	0.2	1.0	0.22

In addition to the fragmentation characteristics of the cylinder blasts results from identically blasted testing blocks can be compared. As mentioned in chapter 3.3.4 two testing blocks (#0114 and #0314) were blasted with the same nominal delay of 28 µs in their first and second rows. The statistical evaluation of the D_{Mean} values (Table 33) showed no significant differences between the specimens. The S_{Norm} values of the first rows were on the verge of being significantly different (Table 34). This result is related to the small amount of data (see chapter 3.6.1). The complete set of data can be found in Appendix 10.

Table 33: Statistical evaluation of D_{Mean} of the 28 µs delayed shots of stage 3 with the MWU-Test ($\alpha = 0.05$; $Q_L = 6$; $Q_U = 15$; 2 x 3 data)

	T_1	T_2	Significant Difference
1st rows	11.0	10.0	No
2nd rows	11.0	10.0	No

Table 34: Statistical evaluation of S_{Norm} of the 28 µs delayed shots of stage 3 with the MWU-Test (α = 0.05; Q_L = 6; Q_U = 15; 2 x 3 data)

	T_1	T_2	Significant Difference
1st rows	6.0	15.0	No
2nd rows	11.0	10.0	No

The sieving parameters of the first and second row shots with a nominal delay of 28 µs were nearly the same (see Table 35 and Appendix 17).

Table 35: Fragmentation of testing blocks from stage 3 with 28 µs delay

		k_{30} [mm]	k_{50} [mm]	k_{80} [mm]	Uniformity Coefficient
#0114	Row 1	36.1	72.0	107.9*	2.99*
	Row 2	15.6	40.7	97.0	6.24
#0314	Row 1	38.0	71.0	112.3*	2.96*
	Row 2	18.5	43.9	92.7	5.02

*…extrapolated value

The statistical evaluation of the sieving parameters (Table 36) showed that there were no significant differences between the identically blasted blocks.

Table 36: Statistical evaluation of the sieving parameters with the MWU-Test (α = 0.05; Q_L = 3; Q_U = 12; 2 x 2 data)

	T_1	T_2	Significant Difference
k_{30}	4.0	6.0	No
k_{50}	5.0	5.0	No
k_{80}	5.0	5.0	No
Unif. Coeff.	6.0	4.0	No

4.1.2.4 Findings

The findings of chapter 4.1.2 showed comparable fragmentation characteristics for the blasted cylinders from the same production cycle.

The D_{Mean} values and the sieving data of blasted testing blocks from the production cycles #01 and #02, which was evaluated with the KW-ANOVA, were not significantly different for specimens that were shot the same way. In contrast to that the S_{Norm} values showed inconsistent results and sometimes significant differences.

The comparison of the D_{Mean} values and the S_{Norm} values as well as the sieving data within production cycle #03, which was done with the MWU-Test, showed no significant differences of the results.

Due to these results it is judged that the S_{Norm} values are not useful as comparative figures for a description of the bench face characteristics and they are therefore not used in the further analysis of the blasting tests.

Additionally it seems that the MWU-Test, which is comparing two groups (see chapter 3.6.1), is not a suitable method for identification of significant differences when there are so few data in each group (see chapter 3.6.1). As no other method seems to work in these conditions, this is a strong argument for using more tests with identical blasting conditions.

Finally it can be stated that a comparison of test-results within the production cycles is useful as their results, except S_{Norm}, are repeatable when test conditions are the same.

4.1.3 Are neighbouring Holes influencing the Backbreak or the Cracks created?

During the preliminary stage of the blasting tests (chapter 3.3.1) different arrangements of the neighbouring blastholes of single-hole shots were tested for the investigation of their influence on the breakout and the cracks created. When blasting a single-hole in the middle of the 1st row the neighbouring holes, which were filled with wooden sticks, were completely split open. A dominant crack had grown through them until the end of the block. When the holes of the 2nd row weren't filled with any material a single-hole-shot in the middle of this row also split the neighbouring holes open but the dominant crack through the other holes until the end of the block did not develop (see Figure 86).

Figure 86: Front view after single-hole-shot in the middle of the 1st (left) and 2nd row (right)

Then the blastholes on the right side of the next testing block were drilled in the laboratory and filled with fast hardening cement while on the left side just a shallow collar was drilled. The blasting result was that the neighbouring holes were split open and a dominant crack through the entire block had developed. The crack at the right side grew slightly towards the back while on the left side the crack grew parallel to the free surface. During blasting the hole in the middle of the 2nd row the neighbouring blastholes were also split open but no dominant crack through the entire block was detected (see Figure 87).

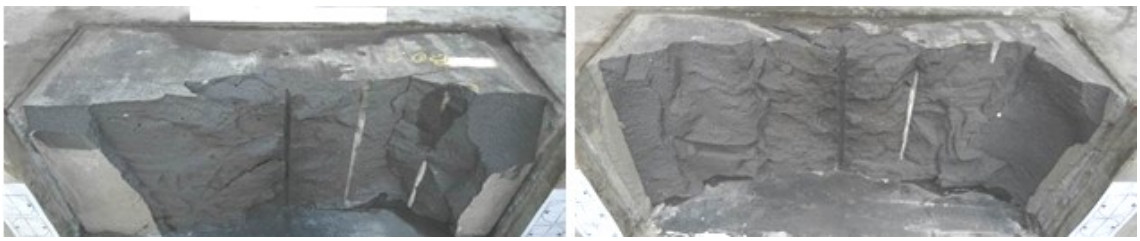

Figure 87: Front view after single-hole-shot in the middle of the 1st (left) and 2nd row (right)

The next two testing blocks were blasted with a cut-away-corner arrangement at the first blasted hole. After blasting the first hole of block #0511 (Figure 88) the breakout at the top of the block was larger than at the bottom and a thin slice around the top of the blasthole broke off. A dominant crack, which cut through the neighbouring holes, developed. This crack went directly through the second blasthole, then it propagated between the second and third blasthole towards the back side of the testing block with a sharp change in direction (kink) near the middle between the two holes. After a further kink between the 3rd and 4th blasthole this crack propagated towards the front side of the block.

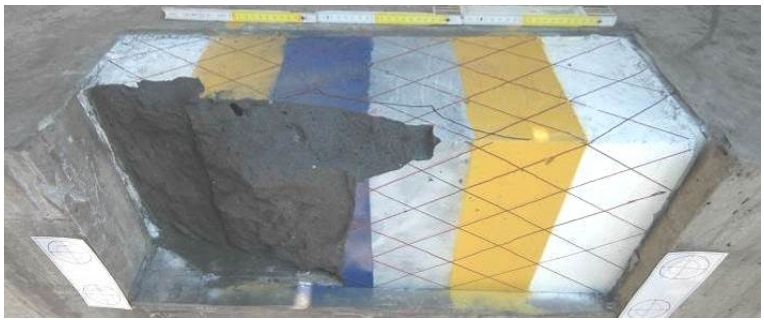

Figure 88: Testing block #0511 after blasting of the 1st blasthole

A similar crack development was detected by Petropoulos (2011) when a row of holes was blasted with delay-times longer than 218 µs (Figure 89 and Figure 90). He stated "*that there was a kind of interaction between the shock wave/crack propagation and the gas expansion.*" Further Petropoulos (2011) explained "*that the back breakage appears after the initiation of the second hole and before or after the initiation of the third hole.*"

Figure 89: Extensive back breakage damage (B4R3, confined) (Petropoulos, 2011)

Figure 90: Extensive back breakage damage (B5R1, free face) (Petropoulos, 2011)

Petropoulos (2011) found that the "*phenomenon happened in both conditions (confined and free face), in smaller extent in the confined condition because of a part of the energy was absorbed by the confined material. In the free face shot, the phenomenon was in greater extent because all the amount of energy was released to the magnetite block and came back as tensile wave. The direction of the cracks is in the direction of the firing pattern.*"

Since the neighbouring holes of block #0511 were filled with fast hardening cement they had to be redrilled before the following blasts. During several of these drilling steps the previously created cracks were activated and the burden of some blastholes was loosened, but put back in place to be able to do the blast. With this method all 5 holes of the 1st row were blasted.

When blasting a single hole in the middle of the 2nd row the neighbouring holes, which were not drilled in that case, would have been destroyed (see Figure 91).

Figure 91: Front view after blasting a single hole shot in the middle of the 2nd row

The holes of the next testing block with the cut-away corner arrangement (#0611) weren't filled with any material (Figure 92).

Figure 92: Testing block #0611 after blasting of the 1st blasthole

The result of the first shot was similar to that for the previous block (see Figure 88). The larger breakout at the top of the block and even the dominant crack at the top were nearly the same. Out of the next 4 blastholes of row 1 only three could be blasted due to the removed burden.

Before blasting the 2nd row the corner of this row was cut-away to get comparable results to the 1st row. While blasting the 1st hole the 2nd hole was split open (see Figure 93) and no blasting in this hole was possible. The other three holes of the 2nd row were blasted in the normal way.

Figure 93: Block #0611 after blasting the 1st hole in the 2nd row

When comparing the results of blasts with not drilled neighbouring blastholes to results of blasts with different properties of the neighbouring holes (filled with wooden sticks, without filling material, fast hardening cement filling), the influence of the neighbouring blastholes on or attraction of the generation of dominant cracks can be excluded.

4.1.4 Is a Detachment of the Testing Block influencing the Results?

Since in two cases of stage 3 (#0114 and #0214) a joint of about 1 mm at the back of the testing block was observed after blasting the third rows, their results can be used as an indication of the influence of a detachment of the testing blocks on the results. They can be compared to two further testing blocks of stage 3, where this detachment was not observed. In all testing blocks of stage 3 an inter-hole-delay of 28 µs was used. The following figures show the results of block #0114 with detachment and block #0314 without detachment.

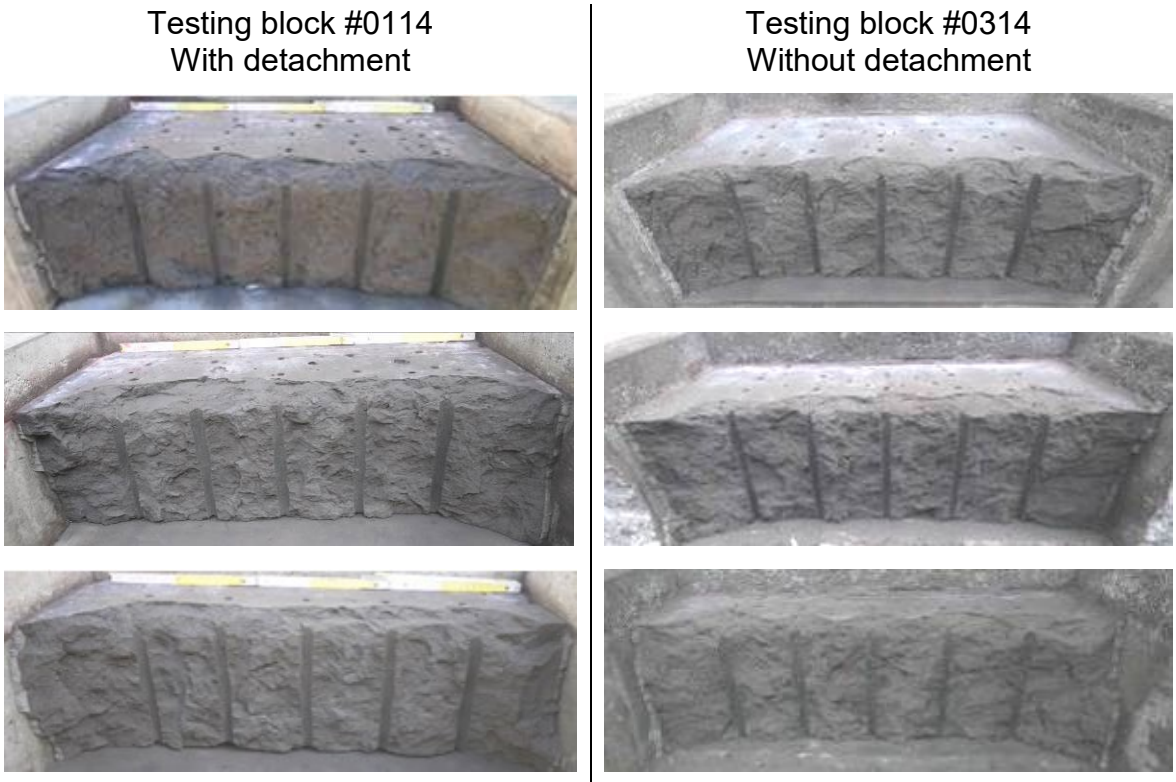

Figure 94: Bench face after blasting the 1st (top), 2nd (middle) and 3rd (bottom) row from testing blocks with (left) and without detachment (right)

In both cases the bench surface, the half-casts of the blastholes and the broken off thin slab at the top of the blastholes looked almost the same. The evaluation of the D_{Mean} values (Figure 95) showed that the first row blast of testing block #0114 produced a small overbreak while in testing block #0314 the average D_{Mean} value was nearly zero (see also Appendix 10). The large scatter of the values in the 1st row of testing block #0314 is worth noting. The second row blasts' average D_{Mean} values showed a small overbreak. While for testing block #0314 the blasts of the third row resulted in similar D_{Mean} values as for the previous rows the values for the

third row blast of testing block #0114 produced more backbreak. This result might have been influenced by the above mentioned detachment of the testing block from the yoke.

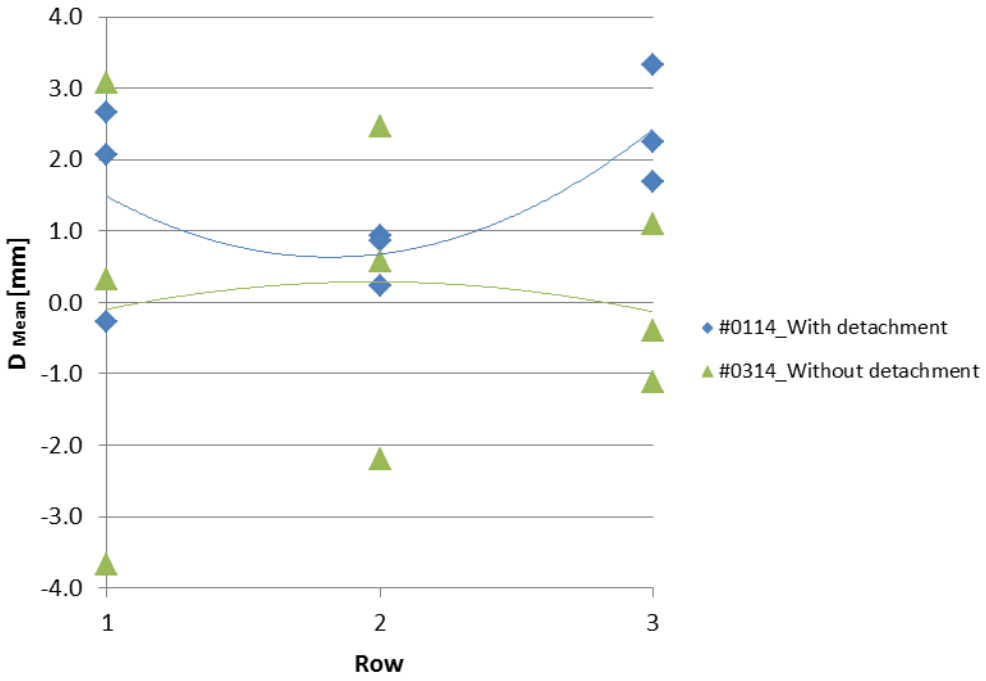

Figure 95: D_{Mean} for testing blocks with (#0114) and without (#0314) detachment

The statistical evaluation of the D_{Mean} values from the individual rows (Table 37) showed no significant differences between the testing blocks. The result for the comparison of the third rows was on the verge of being significant. This may be related to the small amount of data and the limitation of the MWU-Test (see chapter 3.6.1) but might also be an indication that the 3rd row blast was done in an already detached testing block.

Table 37: Statistical evaluation of D_{Mean} of the detached (#0114) and undetached (#0314) testing block with the MWU-Test ($\alpha = 0.05$; $Q_L = 6$; $Q_U = 15$; 2 x 3 data)

	T_1	T_2	Significant Difference
1st rows	11.0	10.0	No
2nd rows	11.0	10.0	No
3rd rows	15.0	6.0	No

Table 38 shows that the fragmentation values of the first and second rows of both testing blocks were almost the same while the third rows gave different values (see also Appendix 17). Since the third row blast of testing block #0114 gave a

finer fragmentation, it seems that the detachment of the back of testing block #0114 from the yoke may have happened during the blast of the 2nd row. This would mean that the 3rd row blast was done in an already detached (free) specimen. Then blasting waves weren't able to escape from the specimen and the fragmentation improved. The trend of the coefficient of uniformity from row 1 to row 3 was the same for both testing blocks, i.e. low-high-low. Testing block #0114 produced larger coefficients.

Table 38: Fragmentation of testing blocks from stage 3 with 28 µs delay

		k_{30} [mm]	k_{50} [mm]	k_{80} [mm]	Uniformity Coefficient
#0114	Row 1	36.1	72.0	107.9*	2.99*
	Row 2	15.6	40.7	97.0	6.24
	Row 3	11.0	23.6	51.5	4.68
#0314	Row 1	38.0	71.0	112.3*	2.96*
	Row 2	18.5	43.9	92.7	5.02
	Row 3	16.7	36.6	61.5	3.68

*…extrapolated value

The comparison of detached (#0114) and confined (#0314) testing blocks showed that the characteristics of the bench face after blasting and the fragmentation results might be influenced by a detachment of the testing block from the yoke.

4.1.5 Which Method is best suitable to quantify the Damage created?

Since the cracks created after every blast were traced by using dye-penetrant spray and categorized in 10 crack families followed by the calculation of the mean crack density (MCD) and the mean crack intersection density (MCID) these measures (see also chapter 3.4.2.1) have to be evaluated according to their added value to the description of the damage created.

Figure 96 shows the comparison of the totally created cracks in the testing block remains and the calculated MCD and MCID values. The complete set of data can be found in Appendix 13.

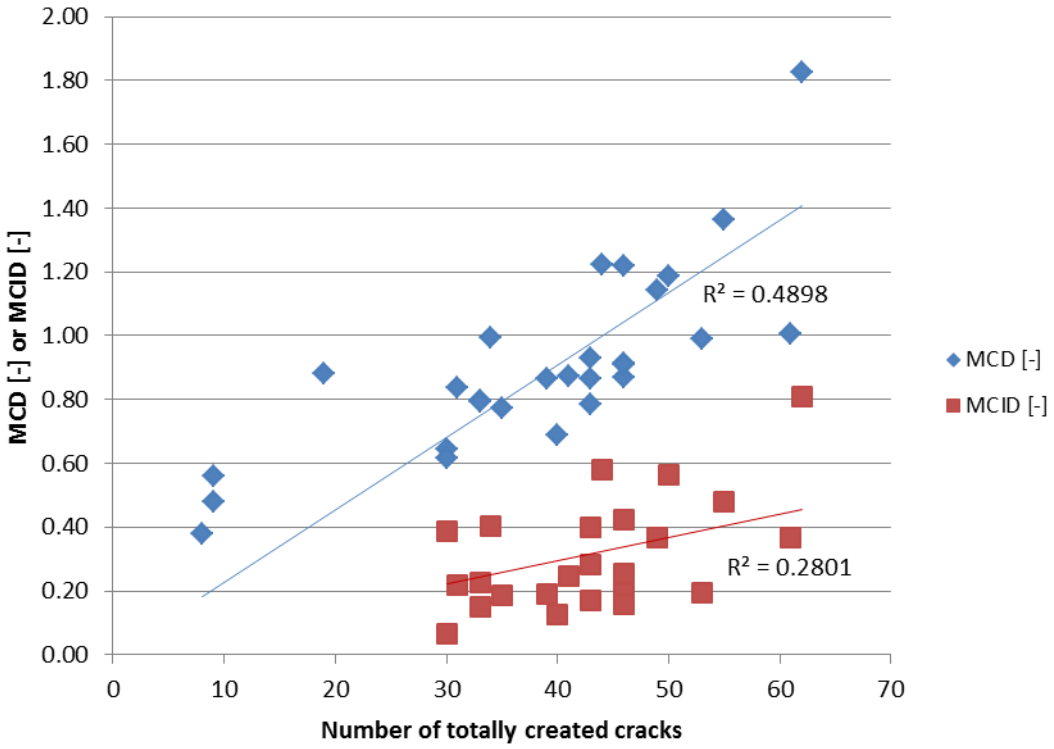

Figure 96: Number of totally created cracks in combination with MCD and MCID from testing blocks of stage 2 and 3 which were blasted with normal pattern

The presented R^2 values of the correlation of the MCD and MCID with the number of totally created cracks are less than the square of the correlation values shown in Table 39 since the regression line in Figure 96 is originating at zero.

The MCD values have a better correlation with the totally created cracks than the MCID values. This can also be seen in Table 39 where the good correlation between MCD and MCID is also shown.

Table 39: Correlation matrix for totally created cracks, MCD and MCID from testing blocks of stage 2 and 3 which were blasted with normal pattern

	Total Cracks	*MCD [-]*	*MCID [-]*
Total Cracks	1.00		
MCD [-]	0.78	1.00	
MCID [-]	0.56	0.86	1.00

Due to this good correlation of MCD and MCID it is decided that for the further analysis of the blasting tests the MCID values are skipped.

The totally created cracks in the testing block remains are meaningful as a comparison figure for the number of cracks created while the MCD values are meaningful for a quantification of the spatial and length distribution of the cracks created.

4.2 Research Questions

4.2.1 RQ 1: Is the Delay-Time influencing the Fragmentation and Backbreak in Specimens with given Pre-Conditioning?

Johansson & Ouchterlony (2013) found in their blasting tests, where all rows were fired with the same delays but different from block to block "*that the scatter in the data from row 1 is much larger.*" To exclude this scatter in the fragmentation and the backbreak, two sets of testing blocks were blasted with a nominal delay of either 28 or 140 µs in their first rows to answer research question 1 (RQ 1). This pre-conditioning ensured comparable conditions for the investigations of the 2nd and 3rd row shots which were blasted with different delay-times.

4.2.1.1 Pre-Conditioning of 28 µs (0.04 ms/m)

The 1st rows of the testing blocks in Figure 97 had an identical pre-conditioning by use of a 28 µs delay. The delay-times for the 2nd and 3rd rows were 0, 28 or 73 µs.

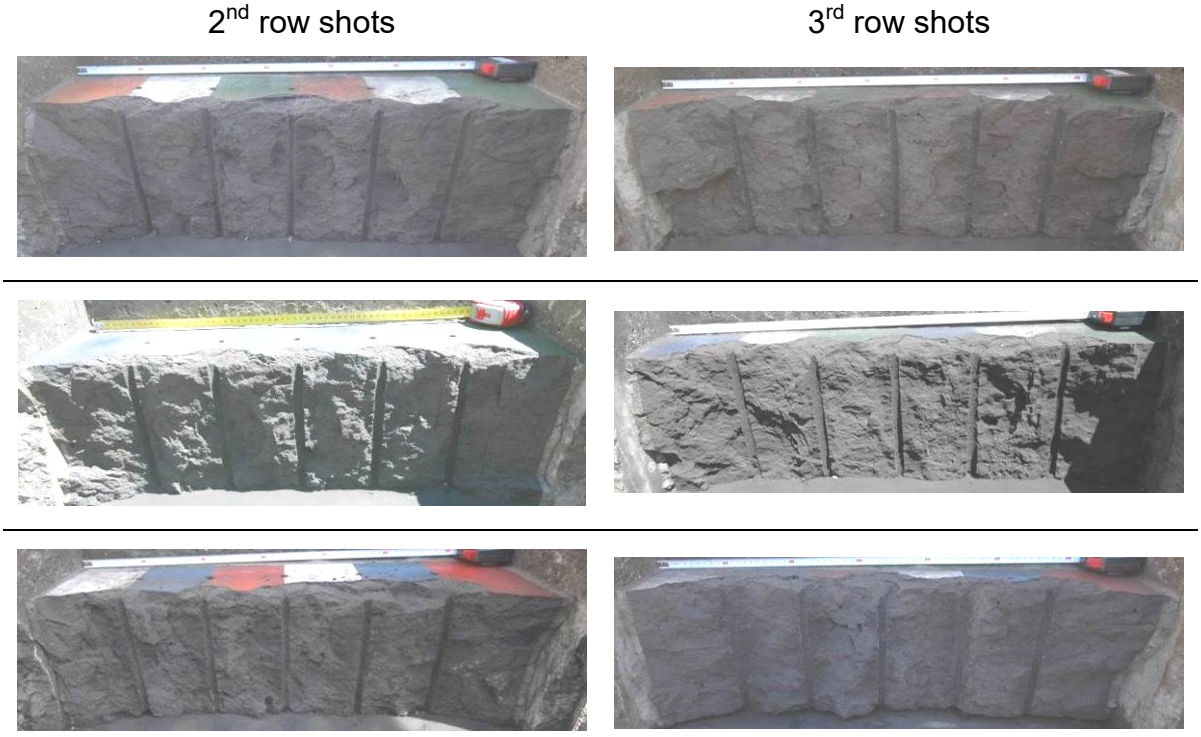

Figure 97: Bench face after blasting with a nominal delay in the 2nd and 3rd rows of 0 µs (#0613 – top), 28 µs (#0213 – middle) and 73 µs (#0713 – bottom)

The surfaces behind the 2nd rows showed no large differences for the different delay-times although with the longer delay of 73 µs small vertical trenches became

visible. The comparison of the third rows showed that the longest delay-time of 73 µs produced the largest backbreak.

The evaluation of the D_{Mean} values (see Figure 98) shows that already the identically blasted 1st rows produced a relatively large scatter although the statistical evaluation of the D_{Mean} values showed no significant difference (see Table 40 and Appendix 10). Testing block #0613 with 0 µs delay for the 2nd and 3rd row showed an increasing backbreak while for the short (28 µs) and long (73 µs) delay-times the backbreak for the 2nd row increased but for the 3rd row it decreased. The D_{Mean} values for the third row of testing block #0213 (28 µs delay) were very small and the surface created very flat.

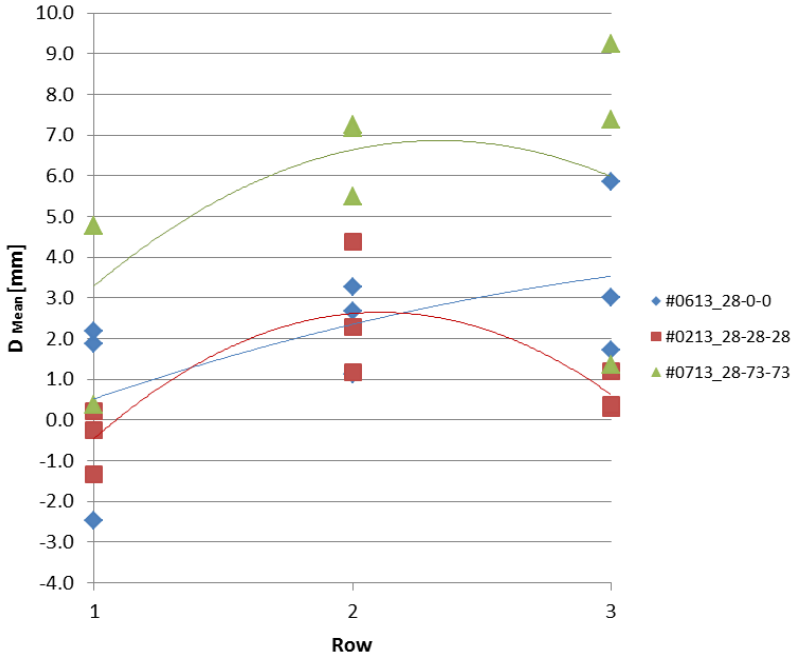

Figure 98: D_{Mean} for blocks with similar pre-conditioning but different arrangements for rows 2 and 3

The statistical evaluation of D_{Mean} from the comparisons of the individual rows gave the results in Table 40.

Table 40: Statistical evaluation of D_{Mean} with the KW-ANOVA (α = 0.05; 3 x 3 data)

	H	X^2	Significant Difference
1st rows	3.82	5.07	No
2nd rows	5.42	5.07	Yes
3rd rows	5.60	5.07	Yes

While the D_{Mean} values of the 1st rows showed no significant differences the 2nd and 3rd row values were significantly different. This result indicates an influence of the delay-times on the backbreak of the newly blasted bench face.

Table 41 shows that the 28 µs delay for row #2 and row #3 after the pre-conditioning of 28 µs delay for the 1st row gave the coarsest fragmentation (block #0213). The delay of 0 µs (block #0613) gave a finer fragmentation and the 73 µs delay (block #0713) gave the finest fragmentation. Note that block #0213 was from another batch than the blocks #0613 and #0713 and that the properties of these batches were judged to be comparable (see chapter 4.1.2). The complete set of data can be found in Appendix 16.

Table 41: Fragmentation parameters for blocks with the same pre-conditioning (28 µs delay)

		k_{30} [mm]	k_{50} [mm]	k_{80} [mm]	Uniformity Coefficient	Planned delay [µs]	Delay per m of burden [ms/m]
	Row 1	40.7	76.7	100.5	2.47	28	0.40
#0613	Row 2	20.7	45.4	79.2	3.83	0	0.00
	Row 3	17.2	36.7	73.3	4.27	0	0.00
	Row 1	40.2	67.0	94.4	2.35	28	0.40
#0213	Row 2	24.4	63.2	101.6	4.17	28	0.40
	Row 3	19.9	43.5	74.1	3.72	28	0.40
	Row 1	40.3	77.5	97.5	2.42	28	0.40
#0713	Row 2	16.0	32.9	74.0	4.63	73	1.04
	Row 3	11.9	22.1	48.1	4.03	73	1.04

In all cases the uniformity coefficient of the 2nd row was larger than of the 1st row. With simultaneous initiation the coefficient of the 3rd row was again larger, while for 28 and 73 µs the coefficient of the 3rd row was smaller than that of the 2nd row.

Figure 99 shows the total number of cracks created behind the third row (see chapter 3.4.2.1 and Appendix 13).

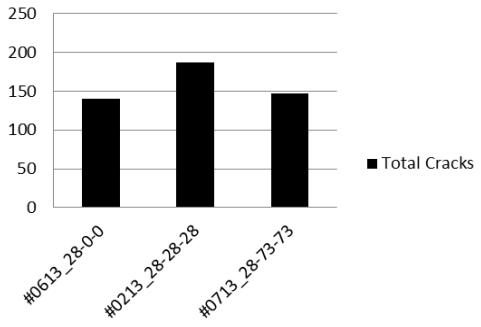

Figure 99: Totally created cracks in blocks with a 1st row pre-conditioning of 28 µs

The largest number of totally created cracks behind the third row occurred for the delay-time of 28 µs for all three rows. The 0 µs and 73 µs delays for the 2nd and 3rd rows created almost the same number of cracks.

The statistical evaluation of the detected cracks for the different crack families (see chapter 3.4.2.1) showed no significant differences between the delay-time sequences in any of the crack families (Table 42).

Table 42: Statistical analysis of crack families with the KW-ANOVA (α = 0.05; 3 x 4 data)

	H	X^2	Significant Difference
Total Cracks	4.16	5.65	No
CB 90-80	0.30	5.65	No
CB 80-30	0.93	5.65	No
CB 30-0	4.27	5.65	No
CD 90-80	1.08	5.65	No
CD 80-30	2.18	5.65	No
CD 30-0	1.05	5.65	No
Parallel	2.67	5.65	No
Connection	2.38	5.65	No
SCB	4.72	5.65	No
Short	0.78	5.65	No

Figure 100 shows that testing block #0613 with simultaneous initiation for the 2nd and 3rd row blasts produced about the same number of cracks on slice 1, 2 and 4 while the number of cracks on the 3rd slice was about 50 % higher. The short delay-time (28 µs) created the highest number of cracks on slice 1 (highest level) while the smallest number was detected on slice 2. In testing block #0713 the number of cracks on slices 1 and 3 was roughly 25 % smaller than that on the slices 2 and 4.

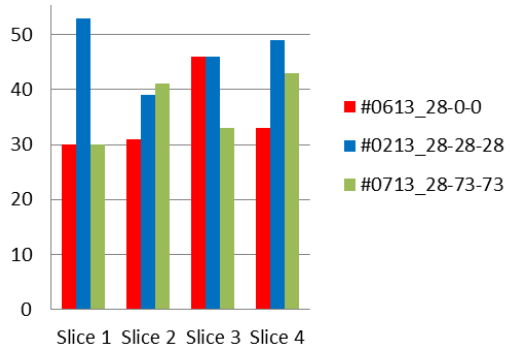

Figure 100: Totally detected cracks on the different slices

The results of the damage measure MCD (see chapter 3.4.2.1) can be seen in Table 43.

Table 43: Mean crack density (MCD) for testing blocks with same pre-conditioning of 28 µs

	#0613 28-0-0	#0213 28-28-28	#0713 28-73-73
Slice 1	0.65	0.99	0.62
Slice 2	0.84	0.86	0.87
Slice 3	0.91	0.91	0.79
Slice 4	0.80	1.14	0.86
Average	**0.80**	**0.98**	**0.79**
Std. dev.	0.10	0.11	0.10

The mean crack density (MCD) values of the testing blocks #0613 and #0713 were nearly the same for all four slices. While the 2nd and 3rd slice of testing block #0213 showed comparable MCD-values to the other two blocks, the first and fourth slice showed higher values. The average values of MCD means that the damage in testing block #0213 was the largest. The statistical evaluation of MCD (Table 44) confirmed this result of significant differences.

Table 44: Statistical analysis of MCD with the KW-ANOVA (α = 0.05; 3 x 4 data)

	H	X^2	Significant Difference
MCD	5.69	5.65	Yes

The conclusion which can be drawn from these statistical analyses are that the short delay of 28 µs, where the shock wave of the first detonating blasthole arrives when the second hole detonates, generates significantly higher damage than 0 and 73 µs delay.

The statistical analysis of the totally created cracks and the MCD on the different slices (Table 45), which showed no significant differences, is an indication that the damage is not height dependent in these three tests.

Table 45: Statistical analysis of damage on the different slices with the KW-ANOVA (α = 0.05; 4 x 3 data)

	H	X^2	Significant Difference
Total cracks on different slices	1.65	7.81	No
MCD on different slices	1.17	7.81	No

4.2.1.2 Pre-Conditioning of 140 µs (2.00 ms/m)

The 1st rows of the testing blocks in Figure 101 had the same pre-conditioning by use of a 140 µs delay. The delay-times for the rows 2 and 3 were 0, 28, 73 or 140 µs.

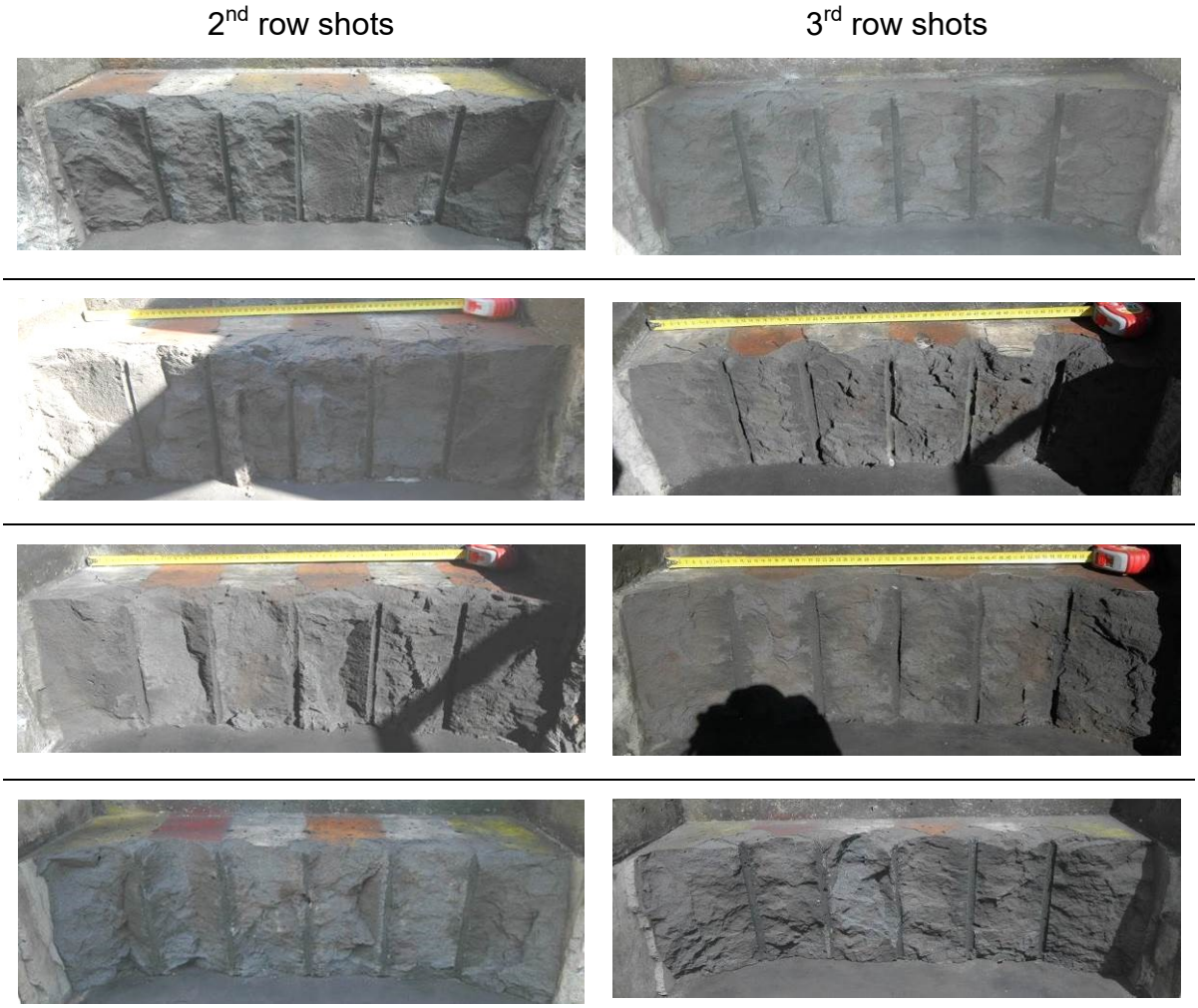

Figure 101: Bench face after blasting with a nominal delay in the 2nd and 3rd rows of 0 µs (#0312 – top), 28 µs (#0712 – middle top), 73 µs (#0612 – middle bottom) and 140 µs (#0212 – bottom)

While the simultaneously initiated 2nd row (#0312) showed the smallest backbreak, the 28 µs delay showed small vertical trenches and the longest delays of 73 and 140 µs produced several deep trenches on the left side of the bench face. The surfaces behind the 3rd row shots were quite similar for the 0 and 73 µs delays. The 28 µs delay (block #0712) even produced underbreak, i.e. less breakage than defined by the reference line through the centres of the blastholes. The longest delay of 140 µs produced some vertical trenches on the left side.

The comparison of the 2nd and 3rd row shots of testing block #0312 with 0 µs delay (simultaneous initiation) showed almost no difference. Both had a flat surface and insignificant backbreak.

The 3rd row blasts with the delay-times of 28, 73 and 140 µs resulted in a flatter surface than their 2nd row shots.

The D_{Mean} values of the four different delay-time combinations (0, 28, 73 and 140 µs), which were used for the blasts of the 2nd and 3rd rows, confirmed the visible observations (see Figure 102). The complete set of data can be found in Appendix 10.

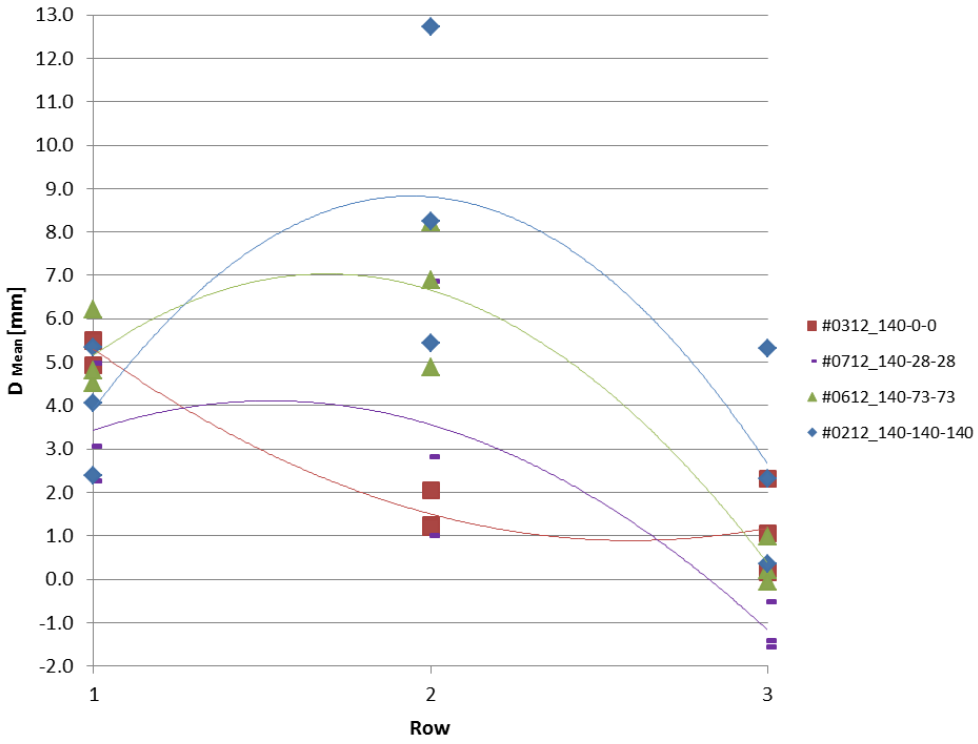

Figure 102: Development of D_{Mean} for testing blocks with 3 rows in stage 2

For all 4 testing blocks the D_{Mean} values behind the 1st row blasts showed only a small scatter.

Behind the 2nd row blasts the longest delay of 140 µs (2 ms/m of burden) gave the largest backbreak while the simultaneous initiation (0 µs delay) gave the smallest backbreak. The scatter in the individual values of D_{Mean} is larger than for the row 1 blasts.

The surface after blasting of the 3rd rows showed a flattening of the previously rougher surfaces. The delay of 28 µs, where an interaction of the blasting waves is possible, even resulted in underbreak. The scatter in the values was again smaller.

While the statistical evaluation of D_{Mean} from the comparisons of the individual rows (Table 46) showed no significant differences in between the 1st and the 2nd rows the 3rd rows did.

Table 46: Statistical evaluation of D_{Mean} with the KW-ANOVA (α = 0.05; 4 x 3 data)

	H	X^2	Significant Difference
1st rows	4.13	7.81	No
2nd rows	7.21	7.81	No
3rd rows	7.82	7.81	Yes

The fragmentation parameters for the blocks with the same pre-conditioning of 140 µs in the first row shots can be seen in Table 47 (see also Appendix 15).

Table 47: Fragmentation parameters for blocks with the same pre-conditioning (140 µs delay)

		k_{30} [mm]	k_{50} [mm]	k_{80} [mm]	Uniformity Coefficient	Planned delay [µs]	Delay per m of burden [ms/m]
#0312	Row 1	18.0	36.3	78.8	4.37	140	2.00
	Row 2	15.5	30.2	72.6	4.69	0	0.00
	Row 3	17.1	35.1	66.1	3.86	0	0.00
#0712	Row 1	18.8	36.4	80.6	4.29	140	2.00
	Row 2	15.0	31.4	76.7	5.11	28	0.40
	Row 3	13.5	27.9	60.0	4.46	28	0.40
#0612	Row 1	14.3	28.0	66.6	4.66	140	2.00
	Row 2	12.2	23.9	57.1	4.68	73	1.04
	Row 3	9.6	19.7	43.6	4.53	73	1.04
#0212	Row 1	19.6	37.8	84.2	4.30	140	2.00
	Row 2	11.3	21.8	63.8	5.63	140	2.00
	Row 3	8.4	16.2	38.2	4.54	140	2.00

The comparable 1st row shots resulted in similar fragmentation parameters, except for testing block #0612, which produced a finer fragmentation. The evaluation of the fragmentation from the following rows has to be done in consideration of possible differences due to this finer fragmentation. While the second row shots with simultaneous initiation and short delay of 28 µs showed similar fragmentation

parameters the longer delay of 73 µs showed a finer and the longest delay of 140 µs the finest fragmentation. With exception of the simultaneously initiated blastholes the third row shots showed coarser fragmentation for the shortest delays while the longest delay generated the finest material.

A comparison of the cracks created was not possible as the dye-penetration method was developed just after the blasts of the 1st stage.

4.2.1.3 Findings for RQ 1

The results of chapter 4.2.1 showed that the first row blasts, which were done with the same nominal delay-times, produced no significant difference in the D_{Mean}, i.e. backbreak values. This implies a high repeatability of the small scale blasting tests in the magnetic mortar used with the chosen delay sequences. In specimens with the same pre-conditioning longer delay-times resulted in a larger backbreak. Although the statistical evaluation of the D_{Mean} values behind the 2nd row shots didn't show significant differences in all cases the values from the 3rd row shots did so.

The simultaneously initiated tests produced a flat surface while some deep trenches were visible after blasts with 140 µs delay (2.0 ms/m of burden). The second row showed similar results to those of the first row. The long delays of 73 and 140 µs generated irregular results with some deep trenches. This phenomenon was also observed by Ivanova (2015) where specimens of the same material and size but with a smaller side-spacing of the blastholes were blasted with a delay of 73 µs. The third row blasts showed as a general trend a flattening of the surface. The conclusions that larger backbreak has to be expected when longer delay-times are chosen can be drawn for the first and second row blasts.

With exception of the simultaneously initiated blastholes the 2nd row blasts showed coarser fragmentation for the shortest delays while the longest delay generated the finest material. This result was also observed for the third row blasts when they had the same delay-time as the previous 2nd row blasts.

It was found that the crack families were not influenced by the chosen delay-time. The evaluation of the damage introduced to the testing block remains showed that there are significant differences in the MCD. This is an indication for different spatial and length distributions of the cracks created

4.2.2 RQ 2: How far does the Pre-Conditioning of the 1st Row Blasts reach?

Two sets of testing blocks were blasted to investigate research question 2 (RQ 2): the influence of different 1st row pre-conditionings on subsequent rows. While the delay-times of the first rows of three testing blocks varied between 0, 28 and 140 µs delay, the subsequent 2nd and 3rd rows were blasted simultaneously. Two other blocks had delay-times of 28 or 73 µs in their first rows while their 2nd and 3rd rows were blasted with 73 µs delay.

4.2.2.1 Simultaneously initiated 2nd and 3rd Row Shots

The three rows of testing block #0113 were blasted with a delay-time of 0 µs and produced bench faces which looked the same (see Figure 103).

Figure 103: Front view of block #0113 after blasting of the 1st (top), 2nd (middle) and 3rd (bottom) row with 0 µs delay

Testing block #0613 was blasted with a delay-time of 28 µs in the first row while the 2nd and 3rd rows were again blasted simultaneously. The newly blasted bench surface (Figure 104) looked the same for all three blasted rows.

Figure 104: Front view of block #0613 after blasting of the 1st row (top) with 28 µs delay, the 2nd (middle) and 3rd (bottom) row with 0 µs delay

The first row of the third testing block (#0313) of this group, which was blasted with a delay of 140 µs, showed deep trenches on the left side (Figure 105). The 2nd and 3rd rows, which were blasted simultaneously, resulted in a flatter bench surface with less backbreak.

The different delay-times for the 1st rows showed that the newly blasted bench surface looked more irregular for longer delays. The simultaneous initiation gave a flatter bench surface than the short 28 µs delay. The 140 µs delay created deep trenches and a very large backbreak.

Figure 105: Front view of block #0313 after blasting of the 1st row (top) with 140 µs delay, the 2nd (middle) and 3rd (bottom) row with 0 µs delay

Figure 106 shows the D_{Mean} values for the blocks with different pre-conditioning in the first row blasts but similar arrangements for the other rows (see Appendix 10).

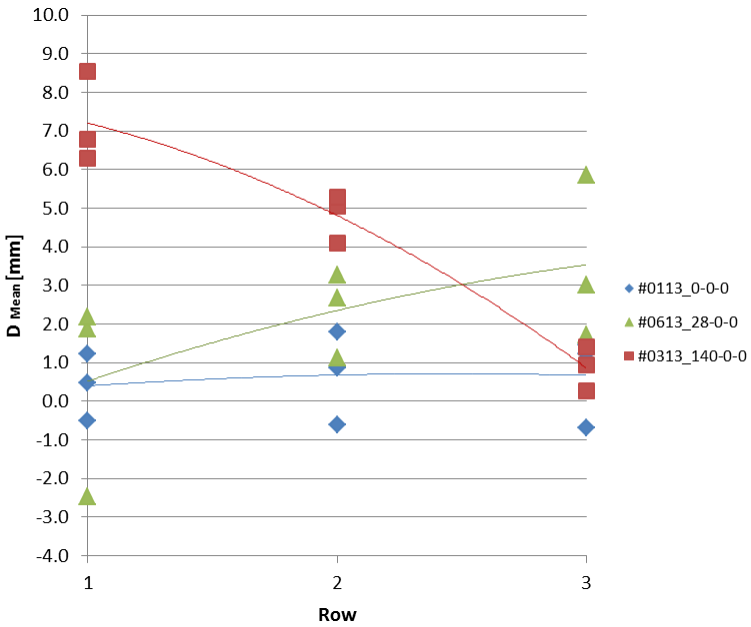

Figure 106: D_{Mean} for blocks with different pre-conditioning of row 1 but identical 2nd and 3rd row shots

The first row blasts with the longest delay of 140 µs produced a large overbreak while the short delay (28 µs) and simultaneous initiation (0 µs delay) produced nearly no overbreak. The difference between the D_{Mean} values of the testing blocks #0113 and #0313 decreased until the results of the 3rd row blasts were almost the same with almost no overbreak. Testing block #0613 showed in contrast to that increasing D_{Mean} values when the blasting progressed although this increase was statistically not significant.

The statistical evaluation of the D_{Mean} values from the individual rows showed significant differences (Table 48).

Table 48: Statistical evaluation of D_{Mean} of the individual rows with the KW-ANOVA (α = 0.05; 3 x 3 data)

	H	X^2	Significant Difference
1st rows	5.60	5.07	Yes
2nd rows	6.49	5.07	Yes
3rd rows	5.42	5.07	Yes

Table 49 shows the fragmentation results of the blasting tests with different pre-conditioning but identical delay-times for the 2nd and 3rd row blasts.

Table 49: Fragmentation of blocks with different pre-conditioning (similar 2nd and 3rd row)

		k_{30} [mm]	k_{50} [mm]	k_{80} [mm]	Uniformity Coefficient	Planned delay [µs]	Delay per m of burden [ms/m]
#0113	Row 1	27.1	47.5	85.5	3.16	0	0.00
	Row 2	28.8	81.5	147.5*	5.12*	0	0.00
	Row 3	16.1	32.1	64.7	4.02	0	0.00
#0613	Row 1	40.7	76.7	100.5	2.47	28	0.40
	Row 2	20.7	45.4	79.2	3.83	0	0.00
	Row 3	17.2	36.7	73.3	4.27	0	0.00
#0313	Row 1	20.6	40.3	79.8	3.87	140	2.00
	Row 2	15.9	36.7	70.2	4.41	0	0.00
	Row 3	18.2	36.1	65.7	3.61	0	0.00

*…extrapolated value

The fragmentation of the 2nd and 3rd rows was strongly dependent on the delay-time of the 1st row. A pre-conditioning of 140 µs delay in the 1st row resulted in similar fragmentation of the 2nd and 3rd rows. If the 1st row was blasted with 28 µs then the 3rd row fragmentation was finer than that of the 2nd row. The

fragmentation results of the testing block with 0 µs delay for each row were unclear due to a large boulder in row 2 which was not fragmented (Figure 107).

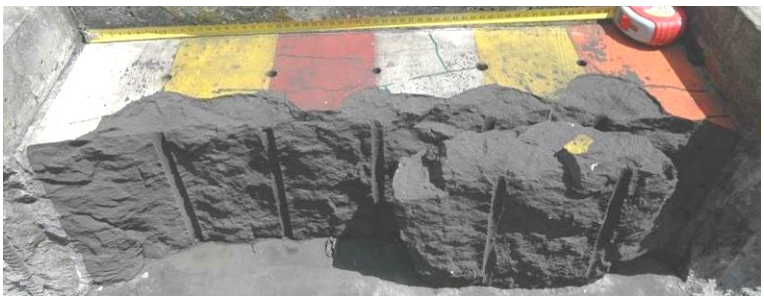

Figure 107: Front view of block #0113 after blasting of the 2nd row with 0 µs delay with replaced large boulder

The coefficients of uniformity for the different 1st row blasts were varying between the lowest value of 2.47 for the 28 µs delay shot and the largest value of 3.87 for the 140 µs blast. The coefficients of the second row blasts were in all cases larger than for the first row blasts. The 0 and 140 µs delay gave a smaller coefficient for the third rows than for the second rows while the 28 µs delay gave a larger value. However all three values for the third row blasts lay in a narrow range.

The largest number of cracks behind the third row (see Appendix 13) was created with the longest delay-time of 140 µs for the first row (#0313), while the short delay of 28 µs created the smallest number of cracks (Figure 108).

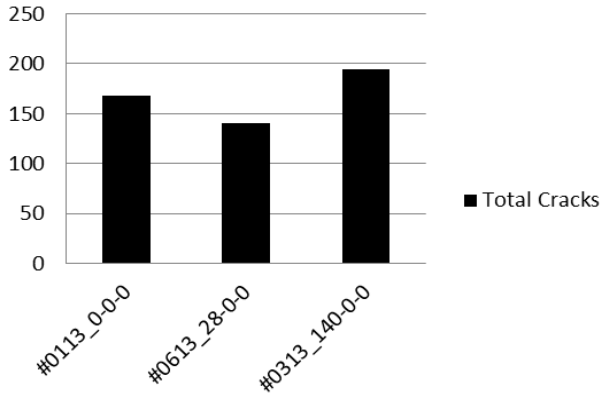

Figure 108: Totally created cracks in testing block remains with different pre-conditioning but similar 2nd and 3rd rows

The KW-ANOVA showed significant differences in the detected number of cracks for the crack families “CB 90-80”, “Parallel” and “Connection” (Table 50). The

number of detected cracks in the other crack families and the total number of detected cracks were not significantly different for the three delay sequences.

Table 50: Statistical analysis of crack families with the KW-ANOVA (α = 0.05; 3 x 4 data)

	H	X^2	Significant Difference
Total Cracks	3.59	5.65	No
CB 90-80	6.93	5.65	Yes
CB 80-30	1.19	5.65	No
CB 30-0	4.45	5.65	No
CD 90-80	3.13	5.65	No
CD 80-30	1.86	5.65	No
CD 30-0	2.58	5.65	No
Parallel	7.63	5.65	Yes
Connection	6.07	5.65	Yes
SCB	2.92	5.65	No
Short	2.58	5.65	No

The number of cracks for the crack families which were identified to be significant different can be seen in Table 51.

Table 51: Number of cracks created for significant different crack families

	#0113 0-0-0	#0613 28-0-0	#0313 140-0-0
CB 90-80	13	19	11
Parallel	9	12	31
Connection	13	10	6

While the testing blocks #0113 and #0313 had almost the same number of cracks in the crack family “CB 90-80” block #0613 had a much larger number. While the number of “Parallel” cracks in the blocks #0113 and #0613 were almost the same block #0313 created nearly three times as many. The “Connection” cracks were the highest for block #0113 and the lowest for block #0313.

Figure 109 shows the total number of cracks subdivided into the different slices of the testing blocks. The order of the first to the fourth slice is from the top to the bottom of the testing block remains.

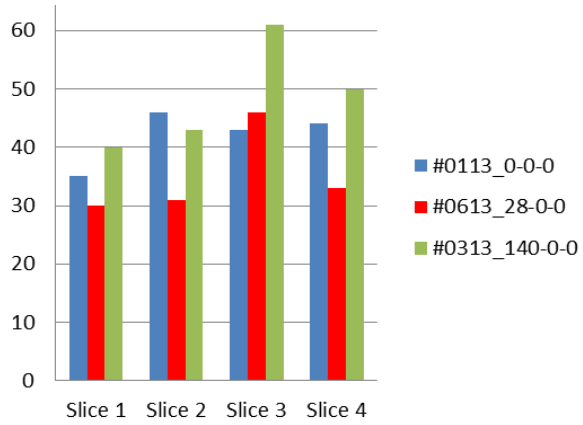

Figure 109: Totally detected cracks on the different slices

Slice 1 of testing block #0113 contained a smaller number of cracks than the other three slices for which the numbers were almost the same. Testing block #0613 contained almost the same number of cracks created on the slices 1, 2 and 4 while on slice 3 the crack number was 45 % higher. Testing block #0313 gave a higher crack number than testing block #0613 but the same ranking of the slices and the highest number of cracks was created on slice 3.

The results of the analyses of the mean crack density (MCD) of the cracks created on the individual slices are shown in Table 52.

Table 52: Mean crack density (MCD) for testing blocks with different pre-conditioning but similar 2nd and 3rd rows

	#0113 0-0-0	#0613 28-0-0	#0313 140-0-0
Slice 1	0.77	0.65	0.69
Slice 2	0.87	0.84	0.78
Slice 3	0.93	0.91	1.00
Slice 4	1.22	0.80	1.19
Average	**0.95**	**0.80**	**0.92**
Std. dev.	0.17	0.10	0.19

The mean crack density (MCD) showed similar trends with slice number in the comparison of these three testing blocks. The values for slices 1, 2 and 3 were similar but for testing block #0613 the value decreased for slice 4 while the damage in the testing blocks #0113 and #0313 increased. The average values of MCD showed that testing block #0113 had the highest degree of damage and testing block #0613 the lowest.

The statistical analysis showed no significant differences between the three testing blocks (Table 53).

Table 53: Statistical analysis of MCD with the KW-ANOVA (α = 0.05; 3 x 4 data)

	H	X^2	Significant Difference
MCD	1.19	5.65	No

While the statistical analysis of the total number of cracks created on the different slices (Table 54) showed no significant differences the mean MCD values on the different slices were significantly different.

Table 54: Statistical analysis of damage on the different slices with the KW-ANOVA (α = 0.05; 4 x 3 data)

	H	X^2	Significant Difference
Total cracks on different slices	4.38	7.81	No
MCD on different slices	8.13	7.81	Yes

4.2.2.2 73 µs (1.04 ms/m) delayed 2nd and 3rd Row Shots

The first testing block of this group was blasted with a delay-time of 28 µs in the first row and 73 µs in the 2nd and 3rd rows (Figure 110).

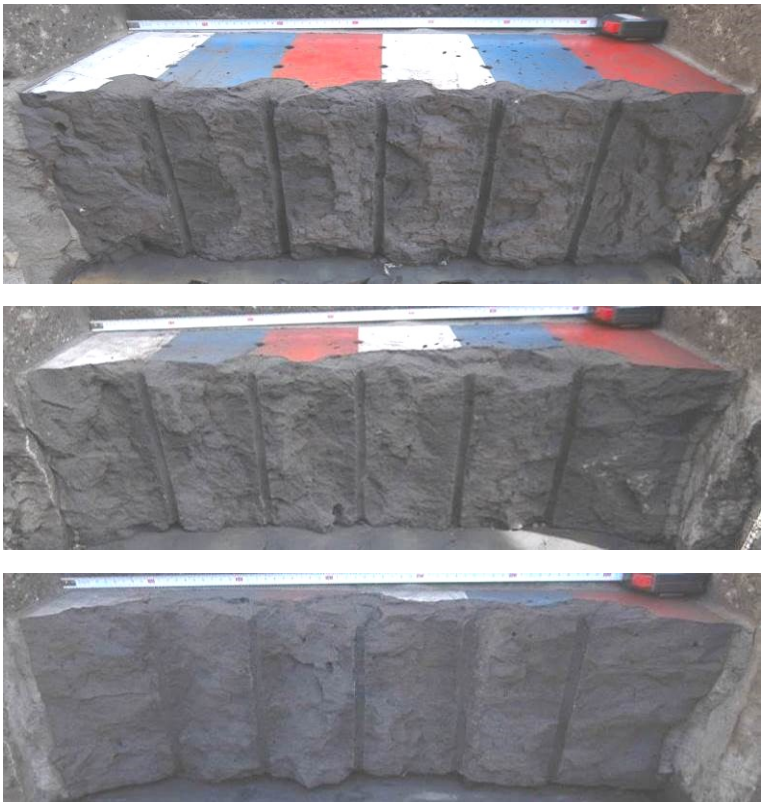

Figure 110: Front view of block #0713 after blasting of the 1st row (top) with 28 µs delay, the 2nd (middle) and 3rd (bottom) rows with 73 µs delay

Several small vertical trenches were visible behind every blasted row but no clear difference between the individual rows was detected.

The tests in Figure 111 used the same delay-times in rows 2 and 3 (73 µs) as the tests shown in Figure 110, but the 1st row was blasted with a delay of 73 µs (instead of 28 µs). After blasting of the 1st row small trenches were seen. In contrast to that the 2nd row shot produced several deep trenches while this wasn't observed for the 28 µs pre-conditioned testing block. The surface after blasting the 3rd row with 73 µs delay was flat.

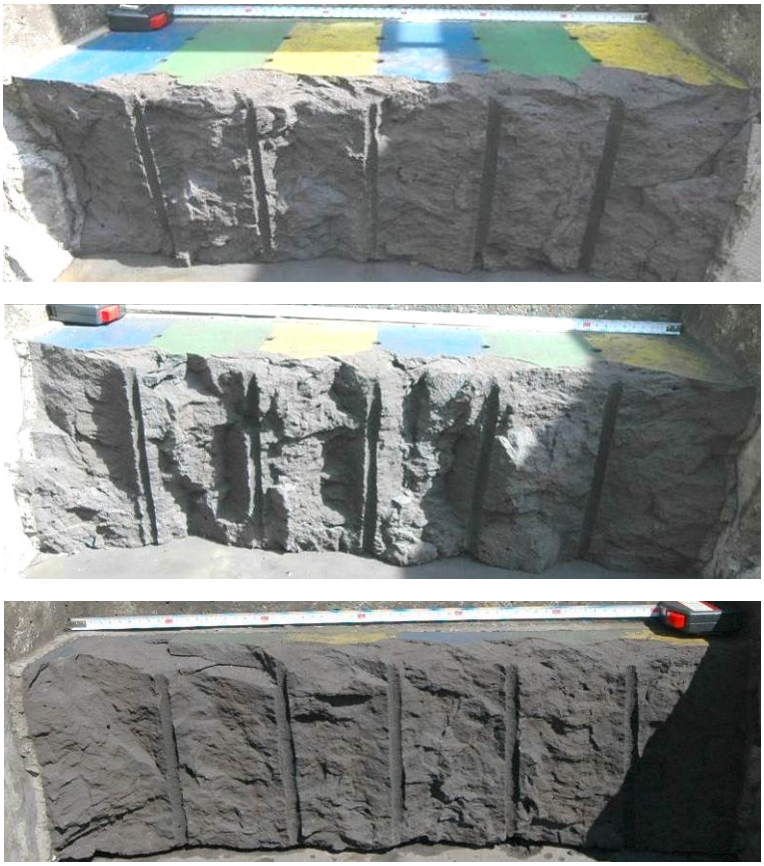

Figure 111: Front view of block #0413 after blasting of the 1st (top), 2nd (middle) and 3rd (bottom) row all with 73 µs delay

Figure 112 shows the D_{Mean} values for the testing blocks #0713 and #0413 (see Appendix 10).

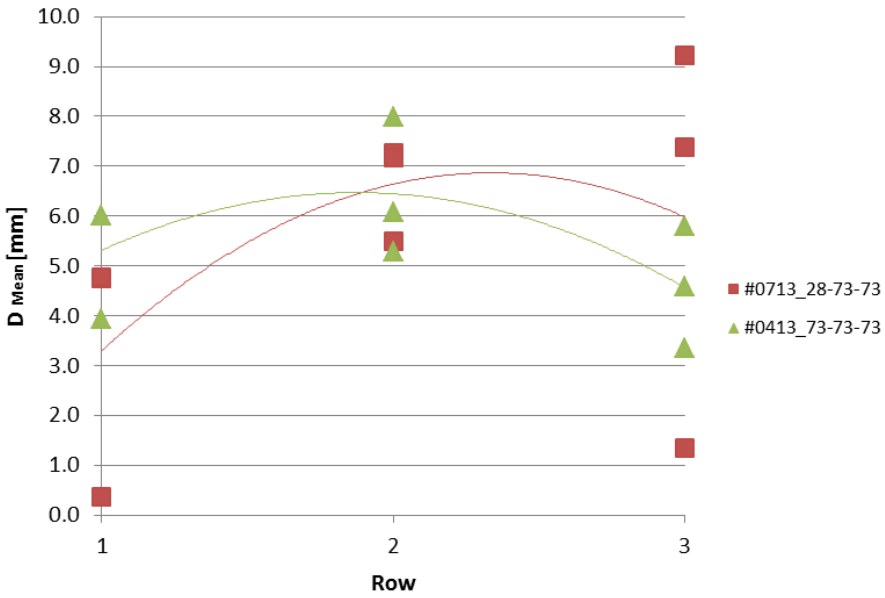

Figure 112: D_{Mean} for blocks with different pre-conditioning of row 1 but similar arrangements for rows 2 and 3

The first row blast with the longer delay of 73 µs produced a larger overbreak than the shorter delay of 28 µs. The second row blasts showed an increasing backbreak for both cases while the third row blast gave smaller D_{Mean} values. The statistical evaluation of the D_{Mean} values (Table 55) showed no significant differences between the individual rows of the testing blocks.

Table 55: Statistical evaluation of D_{Mean} of the individual rows with the MWU-Test (α = 0.05; Q_L = 6; Q_U = 15; 2 x 3 data)

	T_1	T_2	Significant Difference
1st rows	13.0	8.0	No
2nd rows	10.0	11.0	No
3rd rows	9.0	12.0	No

Table 56 shows the fragmentation results of the blasting tests with different pre-conditioning but the same delay-times of 73 µs for the 2nd and 3rd rows.

Table 56: Fragmentation of blocks with different pre-conditioning (similar 2nd and 3rd rows)

		k_{30} [mm]	k_{50} [mm]	k_{80} [mm]	Uniformity Coefficient	Planned delay [µs]	Delay per m of burden [ms/m]
#0713	Row 1	40.3	77.5	97.5	2.42	28	0.40
	Row 2	16.0	32.9	74.0	4.63	73	1.04
	Row 3	11.9	22.1	48.1	4.03	73	1.04
#0413	Row 1	23.2	45.0	84.7	3.65	73	1.04
	Row 2	13.9	27.2	61.4	4.41	73	1.04
	Row 3	12.8	23.8	47.7	3.72	73	1.04

The pre-conditioning with shorter delays (28 µs) gave a coarser fragmentation in row 1. As the blasting proceeds with further rows the similar medium range delay of 73 µs showed similar results. The uniformity coefficient for the 1st row blast with 73 µs delay was larger than for the blast with 28 µs delay. The comparable second and third row blasts gave almost the same uniformity coefficient values.

Figure 113 shows that the longer delay-time in the first row created a higher number of cracks behind the third row than the shorter delay-time (see also Appendix 13).

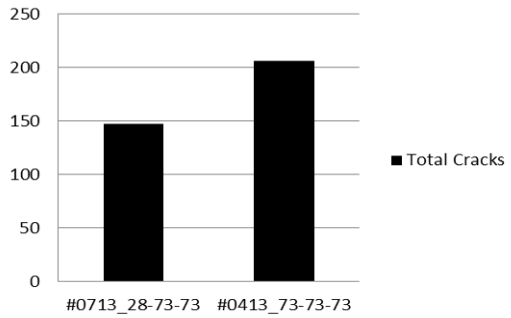

Figure 113: Totally created cracks in testing block remains with different pre-conditioning (similarly blasted 2nd and 3rd rows)

The statistical evaluation of the crack families is shown in Table 57.

Table 57: Statistical analysis of crack families with the MWU-Test (α = 0.05; Q_L = 11; Q_U = 25; 2 x 4 data)

	T_1	T_2	Significant Difference
Total Cracks	12.0	24.0	No
CB 90-80	19.5	16.5	No
CB 80-30	11.0	25.0	No
CB 30-0	19.5	16.5	No
CD 90-80	15.0	21.0	No
CD 80-30	17.0	19.0	No
CD 30-0	20.0	16.0	No
Parallel	10.0	26.0	Yes
Connection	20.0	16.0	No
SCB	12.0	24.0	No
Short	18.5	17.5	No

The MWU-Test showed significant differences of the number of cracks in the crack family “Parallel”. The number of cracks in the other crack families and for the totally detected cracks was not significantly different from each other. The reason for the borderline case of the crack family “CB 80-30” is the small amount of data (see chapter 3.6.1). The number of cracks created in “CB 80-30” and “Parallel” is much larger in block #0413 (Table 58).

Table 58: Number of cracks created for significant different crack families

	#0713 28-73-73	#0413 73-73-73
CB 80-30	21	37
Parallel	14	33

When the above mentioned number of cracks is subdivided into the different slices of the testing blocks Figure 114 can be seen.

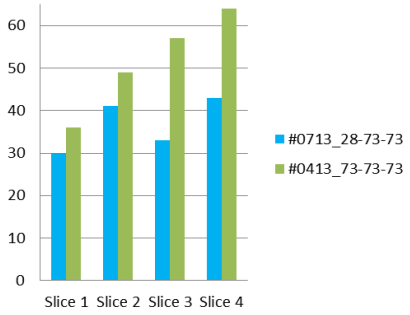

Figure 114: Totally detected cracks on the different slices

While testing block #0713 showed no clear trend in the number of cracks created per slice, an increasing trend with depth for testing block #0413 was detected.

The results of the analysis of the mean crack density (MCD) of the cracks created on the individual slices are shown in Table 59.

Table 59: Mean crack density (MCD) for testing blocks with different pre-conditioning (same delays in 2nd and 3rd row)

	#0713 28-73-73	#0413 73-73-73
Slice 1	0.62	0.99
Slice 2	0.87	1.22
Slice 3	0.79	1.36
Slice 4	0.86	1.83
Average	**0.79**	**1.35**
Std. dev.	0.10	0.30

The mean crack density (MCD) on the cut slices of testing block #0413 increased with depth. This trend was not observed for testing block #0713 although the slices 2, 3 and 4 had higher MCD values than slice 1. The gap of the MCD values between the two delay-time sequences became larger for increasing depth. The average of MCD showed a higher damage for testing block #0413. This was confirmed by the statistical evaluation of MCD, which showed significant differences between the two testing blocks (see Table 60).

Table 60: Statistical analysis of MCD with the MWU-Test (α = 0.05; Q_L = 11; Q_U = 25; 2 x 4 data)

	T_1	T_2	Significant Difference
MCD	10.0	26.0	Yes

4.2.2.3 Findings for RQ 2

The findings of chapter 4.2.2 were that the fragmentation of the third rows already seems to be independent of the pre-conditioning of the first row blasts while the backbreak and the cracks created behind the third row are dependent on the pre-conditioning.

The simultaneously initiated 2nd and 3rd row shots after different pre-conditionings of 0, 28 and 140 µs delay for the first rows produced significantly different backbreak values.

While the fragmentation of the 2nd row was strongly dependent on the delay-time of the 1st row the fragmentation of the third row became almost the same independent of the pre-conditioning.

The conclusions which can be drawn from the investigations of the crack development on cut surfaces (see also Navarro, 2015) are that some of the detected crack families were influenced by the chosen delay-time while others were not. Three crack families ("CB 90-80", "Parallel" and "Connection") showed significant differences but the total number of cracks created on the different slices showed no significant differences. While the statistical analysis showed no significant differences between the MCD values, their values on the different slices were significantly different.

The 73 µs delayed 2nd and 3rd row shots after a pre-conditioning of 28 and 73 µs delay didn't produce significantly different backbreak values.

While the fragmentation of the 2nd row was strongly dependent on the delay-time of the 1st row the fragmentation of the third row became almost the same independent of the pre-conditioning.

The number of cracks in the crack family "Parallel" was found to be significantly different while the number of cracks in the crack family "CB 80-30" was almost significantly different. Also the MCD showed significant differences between the two testing blocks.

4.2.3 RQ 3: How many Rows have to be blasted before the Pre-Conditioning becomes constant?

Johansson & Ouchterlony (2013) found in their blasting tests that the fragmentation in row #2 was finer than in row #1. To investigate research question 3 (RQ 3), the extent of different pre-conditionings, a set of testing blocks was blasted with the same nominal delay of 0, 28, 73 or 140 µs in all three rows.

4.2.3.1 Three Rows blasted

Figure 115 shows the D_{Mean} values for the testing blocks where three rows were blasted with the same nominal delay (see also Appendix 10). Note that testing block #0212 was from a different mortar production cycle.

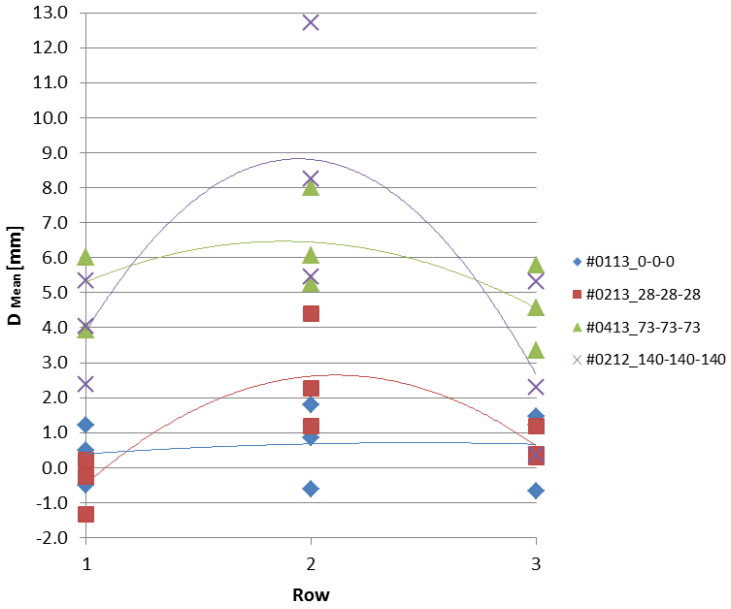

Figure 115: D_{Mean} of testing blocks with the same delay for all three rows

The D_{Mean} values of the three rows were constant for the simultaneous initiation (0 µs delay) with almost no over-/ or underbreak even though the second row blast produced a large boulder (see Figure 107). The second row blast with the short delay of 28 µs produced a larger backbreak than the first row. The D_{Mean} values of the third row were almost the same as those of the first row blast and almost the same as those for the simultaneous initiation. The longer delays of 73 and 140 µs resulted in more backbreak than the shorter delays. The second row blasts produced more backbreak than the first rows while the third rows gave smaller backbreak than both previous rows.

The statistical evaluation of the D_{Mean} values (Table 61) showed that the 0 µs (#0113) and the 73 µs (#0413) didn't generate significantly different backbreak for the individual rows but the 28 µs (#0213) and 140 µs (#0212) delays did.

Table 61: Statistical evaluation of D_{Mean} with the KW-ANOVA (α = 0.05; 3 x 3 data)

	H	X^2	Significant Difference
#0113_0-0-0	0.27	5.07	No
#0213_28-28-28	6.49	5.07	Yes
#0413_73-73-73	3.20	5.07	No
#0212_140-140-140	5.96	5.07	Yes

The fragmentation of the testing blocks where all three rows were blasted with the same delay can be seen in Table 62 (see also Appendix 15 and 16). Note that testing block #0212 was from a different mortar production cycle.

Table 62: Fragmentation of testing blocks with the same delay for the 1st, 2nd and 3rd row

		k_{30} [mm]	k_{50} [mm]	k_{80} [mm]	Uniformity Coefficient	Planned delay [µs]	Delay per m of burden [ms/m]
#0113	Row 1	27.1	47.5	85.5	3.16	0	0.00
	Row 2	28.8	81.5	147.5*	5.12*	0	0.00
	Row 3	16.1	32.1	64.7	4.02	0	0.00
#0213	Row 1	40.2	67.0	94.4	2.35	28	0.40
	Row 2	24.4	63.2	101.6	4.17	28	0.40
	Row 3	19.9	43.5	74.1	3.72	28	0.40
#0413	Row 1	23.2	45.0	84.7	3.65	73	1.04
	Row 2	13.9	27.2	61.4	4.41	73	1.04
	Row 3	12.8	23.8	47.7	3.72	73	1.04
#0212	Row 1	19.6	37.8	84.2	4.30	140	2.00
	Row 2	11.3	21.8	63.8	5.63	140	2.00
	Row 3	8.4	16.2	38.2	4.54	140	2.00

*…extrapolated value

The fragmentation of the testing blocks with a specific delay of 28, 73 or 140 µs showed that the k_{50} of the blasted material in all three cases was getting finer as the blasts proceeded. The fragmentation of the second row blast with simultaneous initiation (#0113) was influenced by the large boulder which was formed (see Figure 107). The k_{50} for this row was coarser than for the first row. The third row fragmentation was finer than that for both previous rows.

The comparison of the different delay-times showed that the longest delay gave the finest fragmentation. The fragmentation for the 0 µs delay lay in between.

While for 0 and 28 µs delay the coefficients of uniformity of the third row blasts had, compared to the coefficients of the first row blasts, increased, for longer delays the coefficient values for the 1st and 3rd row blasts lay on the same level.

The coefficient of uniformity of the first row blasts resulted in increasing values with increasing delay-time. The results for simultaneous initiation lay in between. For the non-zero second row delays the coefficient of uniformity values showed the same trend as for the first row values. For the third rows the coefficient values were smaller than those of the 2nd rows.

4.2.3.2 Four Rows blasted

Figure 116 shows the D_{Mean} values for testing block #0314 where all four rows were blasted with the same nominal delay of 28 µs (see also Appendix 10). While the average D_{Mean} values of the rows was constant with nearly no over-/ or underbreak the scatter of the individual rows decreased as the blast proceeded.

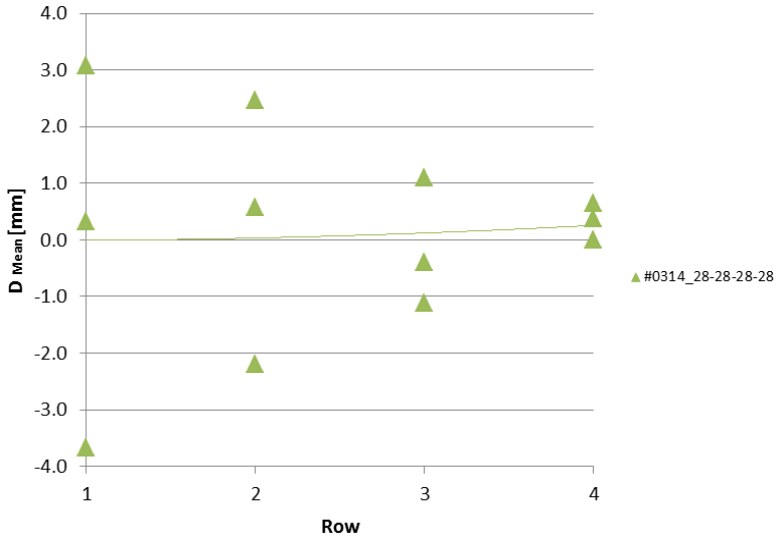

Figure 116: D_{Mean} of testing block #0314 with four rows blasted (28 µs)

The statistical analysis of the D_{Mean} values (Table 63) showed that there were no significant differences between the blasted rows.

Table 63: Statistical evaluation of D_{Mean} with the KW-ANOVA (α = 0.05; 4 x 3 data)

	H	X^2	Significant Difference
#0314_28-28-28-28	0.28	7.81	No

The procedure of crack detection at the top of the testing blocks (see chapter 3.4.2.1) makes it possible to investigate the cracks created after every blasted row (see also Appendix 12). Figure 117 shows that one crack was detected already before the 1st row was blasted. After the following blasts a gradual net increase of the totally detected cracks can be seen.

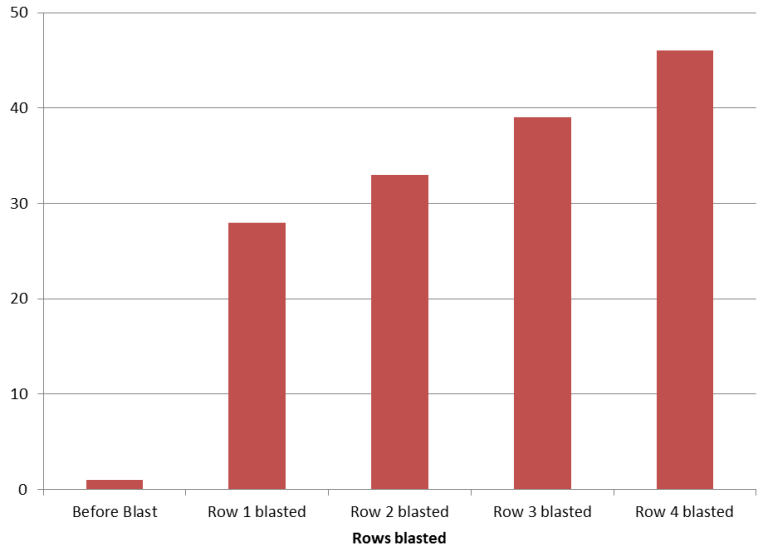

Figure 117: Totally detected cracks in block #0314 after blasting the individual rows

These cracks from Figure 117, when split up into the different areas where they were detected, can be seen in Figure 118. Every shot created the highest number of cracks directly behind the blasted row. The number of cracks created increased constantly as the blasts proceeded.

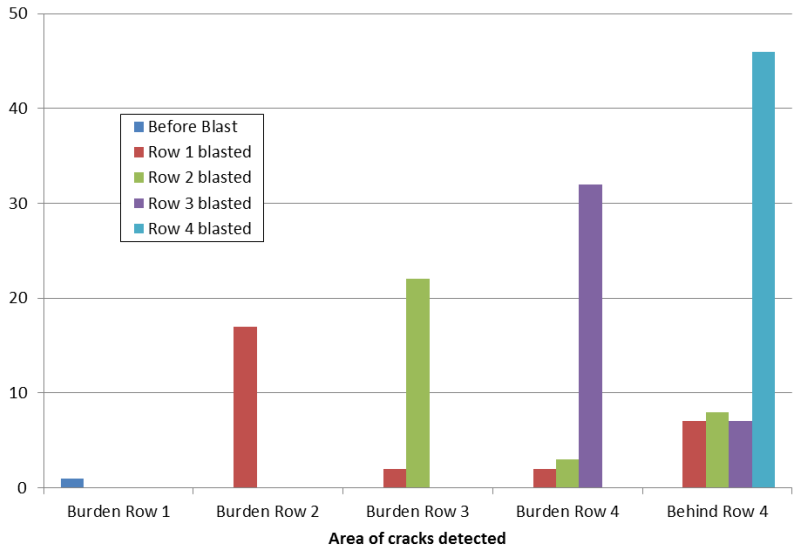

Figure 118: Totally detected cracks in the different regions of block #0314

Table 64 shows the fragmentation of testing block #0314 where all four rows were blasted with the same nominal delay of 28 µs (see also Appendix 17).

Table 64: Fragmentation of testing block #0314 with 28 µs delay in all four rows

		k30 [mm]	k50 [mm]	k80 [mm]	Uniformity Coefficient
#0314	Row 1	38.02	71.03	112.3*	2.96*
	Row 2	18.48	43.85	92.69	5.02
	Row 3	16.72	36.64	61.54	3.68
	Row 4	16.00	37.01	64.65*	4.04*

*…extrapolated value

Similar to the tests described in chapter 4.2.3.1 the fragmentation with a specific delay of 28 µs was getting finer until the third row blast. The fourth row blasted showed almost the same fragmentation as the third row.

The uniformity coefficient values for the third and fourth rows were nearly the same while the 1st row produced a smaller but extrapolated coefficient of uniformity and the 2nd row produced a larger coefficient.

4.2.3.3 Findings for RQ 3

The fragmentation results showed that the material after delayed first-row blasts was always coarser than the fragmentation of the second-row shots (see also Johansson and Ouchterlony, 2013). If the third row was blasted with a specific delay, the fragmentation was once again finer than for the previous rows. If the blastholes of any of the rows were blasted simultaneously, this is no longer true.

In the testing blocks with four blasted rows with a delay of 28 µs (0.4 ms/m of burden) an increase in the number of cracks created was observed as the blasts proceeded. The fragmentation of the third and fourth row was almost the same. Taking into account the small number of blasted specimens this is an indication for a constant level of pre-conditioning after the third row was blasted.

4.2.4 RQ 4: How is the Delay-Time influencing the Cracks created?

According to Lownds (1983) and Hustrulid (1999) the cracks created are influenced by interactions of blasting waves from neighbouring holes (see also chapter 2.2). To investigate research question 4 (RQ 4), the influence of delay-times on the cracks created, a set of testing blocks was blasted with the same nominal delay of 0, 28 or 73 µs in all of their rows. Figure 119 shows the total number of cracks created behind the third row.

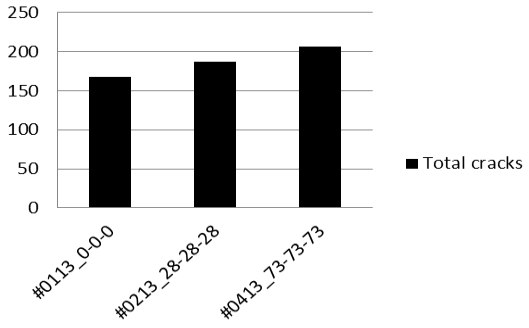

Figure 119: Totally created cracks in testing block remains with the same delay for all three rows

For longer delay-times an increase in the total number of cracks created was detected. The number of cracks created for the different delay-time arrangements was statistically evaluated according to the crack families (Table 65).

Table 65: Statistical analysis of crack families with the KW-ANOVA (α = 0.05; 3 x 4 data)

	H	X^2	Significant Difference
Total Cracks	2.89	5.65	No
CB 90-80	2.20	5.65	No
CB 80-30	6.93	5.65	Yes
CB 30-0	4.68	5.65	No
CD 90-80	0.18	5.65	No
CD 80-30	0.61	5.65	No
CD 30-0	1.74	5.65	No
Parallel	8.00	5.65	Yes
Connection	4.88	5.65	No
SCB	4.57	5.65	No
Short	2.81	5.65	No

The crack families “CB 80-30” and “Parallel” showed significant differences when the three delay sequences were compared. All other crack families and even the

total number of cracks created showed no significant difference between the delay-times.

The comparison of the crack families which were identified to be significant different showed that the longest delay-time of 73 µs created the largest number of cracks (Table 66).

Table 66: Number of cracks created for significant different crack families

	#0113 0-0-0	#0213 28-28-28	#0413 73-73-73
CB 80-30	15	23	37
Parallel	9	4	33

Figure 120 shows the total number of cracks in the block remains subdivided into the different slices. The order of the first to the fourth slice is from the top to the bottom of the remaining testing block.

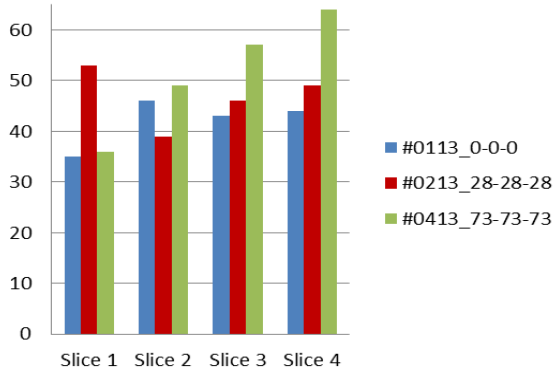

Figure 120: Totally detected cracks on the different slices

In case of simultaneous initiation (#0113) the top slice showed the smallest number of cracks while the number on the other three slices was almost the same. The testing block with the 28 µs delay showed in contrast to that the highest number of cracks in the top slice. The numbers for the other three slices of that delay-time were comparable to that for the simultaneous initiation. The longest delay-time of 73 µs showed that the number of cracks created was increasing the closer the slices were to the bottom.

The mean crack density (MCD) in slice 1 was similar for the short (28 µs) and long (73 µs) delay-time (Table 67). While the simultaneous and the short (28 µs) delay-time showed almost the same mean crack densities for the other slices the longest delay-time of 73 µs created a crack density that increased with depth.

Table 67: Mean crack density (MCD) for testing blocks with the same delay for all three rows

	#0113 0-0-0	#0213 28-28-28	#0413 73-73-73
Slice 1	0.77	0.99	0.99
Slice 2	0.87	0.86	1.22
Slice 3	0.93	0.91	1.36
Slice 4	1.22	1.14	1.83
Average	**0.95**	**0.98**	**1.35**
Std. dev.	0.17	0.11	0.30

The average values of MCD showed the largest damage for testing block #0413 and the lowest damage for block #0113. However, the statistical evaluation (Table 68) showed no significant differences between the different testing blocks.

Table 68: Statistical analysis of MCD with the Kruskal-Wallis one-way analysis of variance (α = 0.05; 3 x 4 data)

	H	X^2	Sign. Diff.
MCD	4.91	5.65	No

The conclusions which can be drawn from the investigations of the crack development on cut surfaces (see also Navarro, 2015) are that some of the detected crack families were influenced by the chosen delay-time while others were not. The damage of the material, which was based on the calculated mean crack density (MCD), showed that for longer delay-times more damage was generated. This was most likely caused by the longer time period which was available for the developing of the cracks.

4.2.5 RQ 5: Is there an Effect of a Staggered Pattern?

As described in chapter 3.3.4 the tests of stage 3 were used to investigate if the staggered pattern results in a finer fragmentation (Hustrulid, 1999; Cunningham, 2005). Since only two testing blocks were blasted under this research question any conclusions are not meaningful. The findings can be summarized as follows.

With the chosen delay-times of 28 µs no differences in backbreak between the individual rows and the different pattern arrangements were detected. This was confirmed by the D_{Mean} values of the individual rows (see Appendix 10).

The totally created surface cracks at the whole remaining top of the testing blocks (see Appendix 12) after blasting rows 1, 2 and 3 showed that the total number of cracks was much larger for the staggered pattern (#0414), after the 4^{th} row shot the number of cracks was nearly the same.

The fragmentation values of the first rows of both testing blocks were almost the same. The second rows showed different results with finer fragmentation for the testing block with a staggered pattern. For the following rows the staggered pattern again produced a finer fragmentation (see Appendix 17).

The changes in the coefficient of uniformity values for both testing blocks worked in the same direction. While those for the second row were larger than for the first rows the third rows blasted produced smaller coefficients than the second rows. The fourth rows produced once again larger values than the third rows.

The staggered pattern created almost twice as many interior cracks in the remaining part of the block as the blasts with the normal pattern (see Appendix 13).

The results of the analysis of the mean crack density (MCD) of the cracks created on the individual slices showed that the staggered pattern created a larger degree of damage in the different slices of the remaining testing block.

These results have to be proven in more detail due to investigations of Ivanova (2015), who blasted the same kind of testing blocks with 7 holes per row, but found that the staggered pattern generated coarser material than the normal pattern.

4.3 Concluding Remarks

The small-scale tests of this thesis allowed a large number of tests to be made and therefore delivered enough data for a detailed analysis of the research questions. However some aspects could only be superficially investigated and these need additional work.

The findings of the methodological questions can be summarised as follows:

- The different mortar production cycles gave significantly different results in the material properties and in the fragmentation of the cylinder shots. Together with the fragmentation and backbreak results from identically blasted testing blocks from different production cycles the conclusion can be drawn, that only a relative comparison of results from different production cycles is meaningful.
- The comparison of the blasted cylinders from the same production cycle showed comparable fragmentation characteristics. The evaluation of the D_{Mean} values and the sieving data of identically blasted testing blocks showed no significant differences. In contrast the S_{Norm} values showed inconsistent results and often significant differences. Hence it is judged that the S_{Norm} values are not useful as comparative figures for a description of the bench face characteristics. Summarizing these results it can be stated that a comparison of tests within the production cycles is meaningful.
- The comparison of blasts with not drilled neighbouring blastholes to blasts with different properties of the neighbouring holes (filled with wooden sticks, without filling material, fast hardening cement filling), showed that the influence of the neighbouring blastholes on or attraction of the generation of dominant cracks can be excluded.
- The characteristics of the bench face after blasting and the fragmentation results are most probably influenced by a detachment of the testing block from the yoke during testing.
- The totally created cracks are meaningful as a comparison figure for the number of cracks created while the MCD values are meaningful for a quantification of the spatial and length distribution of the cracks created.

The main conclusions of this thesis can be summarised under each research question:

RQ 1: Is the delay-time influencing the fragmentation and backbreak in specimens with given pre-conditioning?

Yes, to a certain extent. The 2nd and 3rd row blasts produced a coarser fragmentation for the shortest delays while the longest delays generated the finest material and the largest backbreak.

- The backbreak behind the 2nd row shots did not in all cases show significant differences for different 2nd row delay-times. The 3rd row shots produced a significantly different backbreak though.
- The first and second row shots produced a larger backbreak for longer delays. While the simultaneously initiated tests produced a flat surface, deep trenches were detected behind blasts with 140 µs delay (2.0 ms/m of burden). The third row blasts produced a flattening of the surface.
- Although the contents of the crack families were not influenced by the chosen delay-time the MCD showed significant differences between different delay-times. This is an indication for different spatial and length distributions of the cracks created.

RQ 2: How far does the pre-conditioning of the 1st row blasts reach?

It depends if the initiation is simultaneous or not. The fragmentation of the third row seems to be independent of the 1st row pre-conditioning while the backbreak and the cracks created in the testing block remains are dependent on the pre-conditioning.

- While the simultaneously initiated 2nd and 3rd row shots after different pre-conditionings produced significant variations in backbreak between blocks, the 73 µs delayed 2nd and 3rd row shots did not produce significant variations in backbreak between blocks.
- While the fragmentation of the 2nd row was strongly dependent on the delay-time of the 1st row the fragmentation of the 3rd row was independent of the pre-conditioning.

- Some of the detected crack families (“CB 90-80”, “CB 80-30”, “Parallel” and “Connection”) were influenced by the chosen delay-time while the others were not.
- While the damage in the testing block remain was not significantly different for simultaneously initiated 2nd and 3rd row shots, the 73 µs delayed 2nd and 3rd row shots produced significantly different damage.

RQ 3: How many rows have to be blasted before the pre-conditioning becomes constant?

A constant fragmentation after the third row was blasted was observed, but the small number of blasted specimens has to be taken into account.

- The delayed first-row blasts produced a coarser fragmentation than the second-row shots. If the third row was blasted with a non-zero delay, the fragmentation was once again finer. If the blastholes of any of the rows were blasted simultaneously, an improved fragmentation was not found.
- In the testing blocks with four blasted rows (delay of 0.4 ms/m) an increase in the number of cracks created was observed as the blasts proceeded. The fragmentation of the third and fourth rows was essentially the same.

RQ 4: How is the delay-time influencing the cracks created?

The number of cracks in the crack families “CB 80-30” and “Parallel” were larger for longer delays. The damage of the material, based on the calculated mean crack density (MCD), showed that for longer delay-times more damage was generated.

RQ 5: Is there an effect of a staggered pattern?

Perhaps, but the number of tests is too small. The staggered pattern introduced a larger number of cracks behind the blasted row and produced a better fragmentation.

5 Discussion of Results

Due to the differences in the material properties of the different production cycles, an absolute comparison of the blasting results was not made. This decision is further justified by that researchers have widely different views about how material properties affect the blasting results. Reichholf (2003) summarized in his literature review of the "*influence of rock and rock mass parameters on the blast results*" that contradictions exists with regard to the influence of the compressive strength on the blast result. Some authors stated that the "*blast result is strongly influenced by the compressive strength*" while others state "*that the uniaxial compressive strength is a worthless property to design a blast*". Other authors "*mentioned that the compressive strength is a parameter, which influences the mean fragment size k_{50} in blasting.*" Anyhow they "*were not able to find correlations between the k_{50} and the uniaxial compressive strength with their blast experiments.*" He further summarized "*that the rock mass density influences the blast energy transfer into the rock, and thus, affects the blastability and the fragmentation.*" (Reichholf, 2003)

Cunningham (1987) stated that the "*mechanical strength of intact rock is commonly rated by its uniaxial compressive strength (UCS), but better correlation with explosive fracturing is obtained from the uniaxial tensile strength (UTS), as measured in the Brazilian test.*"

Cunningham (1987) specifies that the "*Young's modulus (Y) is loosely linked to strength. This is possibly the best single indicator of rock blastability in weak rock types, since it governs the readiness with which the blasthole expands under explosive pressure.*" This mechanism might be the explanation for the observed broadened half-casts in the testing blocks of production cycle #03. Also the thin slab, which was thrown off at the top of each blasthole, seemed to be larger in the testing blocks of production cycle #03, for which the density was about 10 % lower.

Our different research questions use in several cases blocks from different mortar production cycles but with a few exceptions the same for each question. For this we used many combinations of in-row delay-times so the possibility of comparing statistically fragmentation, backbreak and crack damage in identically shot blocks

are very small. Furthermore our measurement methods developed during the work, which further hinders such comparisons.

Backbreak differences between blocks from different production cycles that were shot in the same way didn't seem to be significant (see chapters 4.1.1.3 and 4.1.1.4). For blocks shot the same way the fragmentation differences between production cycles do not seem to be so large (Table 15 and Table 17). Regarding crack contents the differences in block geometry, 3 and 4 rows respectively e.g. makes a serious comparison impossible. Thus the differences in blasting results between identically shot blocks from different mortar production cycles may in general not be very large. This points in the direction that the answers to our research questions are valid irrespective of the variations in material properties, not in the other direction.

An initiation in the middle of the row worked for holes shot in the same sequence but did not work for holes shot one by one due to the damage to the neighbouring holes of the row. These single-hole blasting tests showed a breakout angle which was larger than 90°. This result was observed for shots in the middle of the row as well as for shots at one corner of the block (with a cut-away corner). Ouchterlony & Moser (2013) summarized the results of single-hole blasts in rock-like material and found that earlier tests with similar arrangements produced breakout-angles between 120° and 180°.

The phenomenon of a broken off thin section at the top of every blasthole was also observed in other small scale blasts (Reichholf, 2003; Wimmer, 2007). Wimmer (2007) suspected reflections of tensile waves at the free surface to be the reason for broken off thin sections at the bottom of blasted cubes. A reason for the broken off thin sections at the top of the blastholes might be the 20 g/m detonating cord used for blasting, which stood out a few centimetres of the blastholes.

The average speed of crack development in the magnetite mortar used was estimated by the analysis of clearly visible trenches on the bench surface. For one testing block, which was blasted with the longest delay of 140 µs, the evaluated trenches resulted in an estimated speed of crack development of ~260 m/s. This is quite low compared to figures in the literature, with Wilson & Holloway (1987) determining the speed of radial cracks in concrete models between 1000 m/s (near the boreholes) slowing down to around 200 m/s far away from the boreholes.

In addition, Johansson & Ouchterlony (2013), who determined ridges on the surface of a blasted magnetite block as the meeting point of cracks, found a higher speed of crack development of about 650 m/s.

The differences observed in the characteristics of the newly blasted bench face might be influenced by the saturation of the specimen. Khormali (2012) investigated the properties of the material from production cycle #01 of this thesis. The quasi static Wedge-Split test in a saturated sample produced a flat surface while the dry specimen resulted in an irregular surface (Figure 121).

Figure 121: Results from the Wedge-Split test in a saturated (left) and a dry specimen (right) (Khormali, 2012)

For the blasting tests of this thesis the saturation conditions of the test specimen are not possible to state since the testing was done outdoors and the mounted specimens were left overnight for the cement around the specimens to harden.

The tests in which all three rows of the testing blocks were blasted with the same delay of 0, 28, 73 or 140 µs showed that the shortest delay of 28 µs gave the coarsest result while the longest delay of 140 µs gave the finest fragmentation. Johansson & Ouchterlony (2013) did similar tests where they evaluated the influence of delay-time on the fragmentation in the 2nd row. They found "*that the fragmentation of the simultaneously initiated row, x_{50} = 45.8 mm, is by far the coarsest.*" The finest fragmentation was found to be at a delay of 73 µs (1 ms/m).

Katsabanis et al. (2014) reanalysed these small scale tests and came to the conclusions "*that the range of delays, influenced by the interpretation of Rossmanith's work by Vanbrabant (2006), was small and the optimum, if there is one, could be at higher delay values.*"

In their (Katsabanis et al., 2014) opinion the "*outgoing cracks are initially driven by the stress wave but they are later assisted by gas, either through penetration of the crack or by means of modifying the stress field around the crack due to the pressurization of the borehole. The cracks are driven until the stress intensity factor at the crack tip is smaller than the critical value."* Furthermore they explained, that "*in small scale experiments, which utilize top initiation and no stemming, venting occurs immediately after initiation of the charge."* For large and full scale blasting "*this occurs later, after the stemming is ejected*". In their model "*the arrested crack can be extended from the action from the second hole*" and therefore they suggest a "*delay between holes of 145 µs*". Further they state that "*a certain delay is needed to take advantage of any possible interaction of outgoing waves with cracks.*" They (Katsabanis et al., 2014) found in their tests that "*instantaneous initiation favors the formation of large blocks with little back break"*. These results correlate with the findings of this thesis where a large boulder was formed during the simultaneously initiated 2nd row blast when the 1st row also was blasted simultaneously (see Figure 107). These blasts produced nearly no overbreak (see Figure 103 and Figure 106).

Finally Katsabanis et al. (2014) found that "v*ery long delays result in significantly more back break and the fragment size is not optimum."* They explained that for "*the type of blast conducted (top initiation, unstemmed holes) the optimum delay is between 400 and 700 µs, corresponding to 6 ms and 10 ms per meter of burden respectively."* Since the longest delay-time used for the blasting tests of this thesis was 2.0 ms per meter of burden, the optimum range for best fragmentation was probably not obtained for the arrangement chosen.

Further Johansson & Ouchterlony (2013) found that the fragmentation in the 2nd row was much more even than that of the first row (evaluating the residuals). These results, which were also observed in the results of this thesis, were most likely influenced by the fact, that the first row contained virgin material and the second row contained already cracked material. Winzer & Ritter (1980) also investigated pre-conditioned specimens. They stated that "*the pre-existing structural discontinuities in the rock play a critical and perhaps dominant role in the overall fragmentation of the rock by interacting with the stress waves to produce new fractures or to further develop themselves. These new fractures likely result*

from shear stresses that develop because of the passage of the P wave over the discontinuity, and a lesser number develop in tension at the free face with the reflection of the P wave." In the blasting tests of this thesis the existing cracks before blasting were evaluated during stage 3 with tracing the cracks created at the top of the testing block after every blast (see chapter 3.4.2.1). The correlation of the pre-existing cracks in the blasted rows with the resultant fragmentation showed that the blasts in material with a higher number of cracks produced, as expected, finer material compared to blasts in material with less cracks.

6 Recommendations for Future Blasting Tests

Although upscaling of the results of small-scale blasting tests is not easy, the advantages of a homogeneous mortar mass with repeatable material properties dominate even though already small variations in the ingredients might have a large influence on the physical material properties and the blastability (see chapter 4.1.1). The limiting factor for small scale blasting tests is the manual handling of the testing block. The chosen arrangements of three or four blasted rows resulted in a testing block with a weight of approximately 100 kg.

The chosen magnetite mortar had as an advantage a darker colour than that of the yoke and the fast hardening cement which was used for grouting the testing blocks into the yoke. The irrelevant lighter fragments could be removed directly after blasting.

The production of the test specimen in the precast concrete plant was expensive but had the advantage of giving up to 5 testing blocks for the same batch. The probability of similar fragmentation characteristics of these testing blocks was accordingly high. The production in the laboratory had the advantage that the ingredients were introduced exactly according to the recipe. The mixture of the ingredients had to be done in small batches though with the maximum size of 100 to 120 kg per batch. The availability of a climate chamber guaranteed the curing of the test specimen according to industry standards. Anyhow the findings of the tests showed that test specimens with comparable properties have advantages and therefore the production of large batches is recommended for future blasting tests.

There are two possibilities for the production of the blastholes which can be chosen. Johansson (2008) used a plastic stick which was pulled out of the curing mortar after 6 hours and resulted in "*a hole with a very small deviation from the centre line*" (Johansson, 2008). In this procedure the exact pull-out time of the stick is critical for the success of the method. The second possibility for the production of the blastholes is drilling. There are custom-built core drills available with which blasthole-diameters down to 10 mm can be drilled. The limiting factors in this case are the length of the blasthole and the related drill-hole-deviations.

The chosen fast hardening cement for grouting the testing blocks into the yoke was a proper choice. Except for the first two blocks in the 4-row arrangement, where a joint between the testing block and the yoke was detected after three blasted rows, the contacts on both sides of the layer of fast hardening cement seemed not to open up. In the two cases during stage #03 where these contacts opened up, this joint of about 1 mm might have been influenced by the gases which were generated during the detonation. They could have been trapped at the bottom of the block and activated a movement of the block. The use of silicone at the bottom of the block in the further stage #03 tests prevented the produced gases to flow backwards.

The delay-timing arrangement with the use of the 5 g/m detonating cord was critical due to several observed cut-offs. Especially in the case of longer delay-times the limited place above the testing blocks competed with the needed length of the delay-timing cord. In these cases the initiation procedure has to be improved either by choosing a detonating cord with a lower strength (1, 2 or 3 g/m) or another method of initiating of the blastholes.

In the post-blast photography of the blasts, almost identical camera positions for every blast-documentation were essential. Comparable light conditions would be of advantage for the generation of the 3D-models. A sun umbrella could be used during the sunny season as a simple tool of shading the bench face to avoid shadow lines.

The method of taking 3 horizontal contour lines along the blasted bench face for the calculation of reference figures for the characteristics of the blasted bench face was simple and fast. The parameter D_{Mean} gave reasonable results and a proper description of the backbreak after every blasted row. However S_{Norm} is not a suitable parameter for the description of the fresh blasted bench face. Due to the observed irregularities along the bench face the horizontal contour lines should be split up into smaller sections. Single parameters for the sections between the individual blastholes might result in a better description of the blasted bench face. The BlastMetrix^{3D} software generated a 3D-model with a dense mesh of data points along the bench face. Due to the known coordinates of these data points this mesh could be used for further analysis, e.g. along several lines at the surface (see also Kulatilake et al., 1995).

The procedure of crack detection by using dye penetrant spray worked although the repeatability of the results depends on the skills of the person who does the work. An automation of the analysis part is a possible solution. The box-counting method (Li et al. 2009) might be a solution for this automated approach of the image analysis.

The classification of the cracks in crack families was a proper choice although a smaller number of different crack families might be better for an efficient analysis, e.g. relating them to different ranges of fragment sizes. To be able to link the surface characteristics to the number of cracks created in the remaining testing block the heights used for cuts and backbreak lines should be the same.

As an alternative for the detection of cracks created and the damage in the remaining testing block a method which is able to detect cracks in-situ should be investigated. A damage of the testing block remains could be avoided with methods like e.g. P-/ S-wave or ultrasound measurements before the removal.

For the analysis of the fragmentation the complete collection of the particles has highest priority. The chosen arrangement with blasting mats on a wire mesh around the blasting site avoided secondary breakage and made this possible. Another possibility could be the use of a rubber lined container. This arrangement would mean independence on the weather conditions and comparable saturation conditions for all test specimens.

Finally a larger number of repetitions for the different arrangements are recommended since a proper statistical analysis needs a specific amount of repeated tests.

7 Bibliography

AECI Explosives and Chemicals Limited. 1978. Perimeter blasting techniques. Explosives Today. 2 (14): December.

Blair, D.P. 2010. Limitations of electronic delays for the control of blast vibration and fragmentation. In J. Sanchidrián (ed), Fragblast 9, *Proc. 9th Int. Symp. on Rock Fragmentation by Blasting*: 171 – 184. London: Taylor & Francis Group.

Cardu, M. & Giraudi, A. 2013. A review of benefits of electronic detonators. *Revista Escola de Minas*, Brazil, Vol. 66, Issue 3: 375 – 382, July – September 2013.

Conover, W.J. 1999. Practical Nonparametric Statistics, 3rd Edition. Wiley & Sons, ISBN 978-0-471-16068-7.

Cunningham, C.V.B. 1987. Fragmentation estimations and the Kuz-Ram model – four years on. In W L Fourney & R D Dick (eds), Fragblast 2, *Proc. 2nd Int. Symp. on Rock Fragmentation by Blasting*: 475 – 487. Colorado.

Cunningham, C.V.B. 2003. Use of blast timing to improve slope stability. African Explosives Limited. SME volume “Slope Stability in Surface Mining”: 131 – 134.

Cunningham, C.V.B. 2005. The Kuz-Ram fragmentation model – 20 years on. In R. Holmberg et al (eds), Third EFEE World Conference on Explosives and Blasting, European Federation of Explosives Engineers, Brighton Conference Proceedings: 201 – 210.

Field, J.E. & Ladegaard-Pedersen, A. 1971. The importance of the reflected stress wave in rock blasting. In *Int. J. Rock Mech. Min. Sci*. Vol. 8: 213 – 226.

Gertsch, L.S. 1995. Three-dimensional fracture network models from laboratory-scale rock samples. Technical Note. *Int. J. Rock Mech. Min. Sci. & Geomech. Abstr*., Vol. 32, Issue 1: 85 – 91.

Grasedieck, A. 2006. Die natürliche Bruchcharakteristik (NBC) von Gesteinen in der Sprengtechnik. Doctoral thesis, Leoben, Austria: Montanuniversitaet, Chair of Mining Engineering and Mineral Economics.

Holloway, D.C., Bjarnholt, G. and Wilson, W.H. 1987. A field study of fracture control techniques for smooth wall blasting. In W L Fourney & R D Dick (eds),

Fragblast 2, *Proc. 2nd Int. Symp. on Rock Fragmentation by Blasting*: 646 –656. Colorado.

Hustrulid, W. 1999. Blasting principles for open pit mining. 1 General design concepts. Rotterdam: Balkema.

Ivanova, R. 2015. Influence of distorted blasthole patterns on fragmentation as well as roughness of and blast damage behind remaining bench face in model scale blasting. Doctoral thesis in progress, Leoben, Austria: Montanuniversitaet, Chair of Mining Engineering and Mineral Economics.

Johansson, C. H. & Persson, P.A. 1970. Detonics of High Explosives. London: Academic Press Inc.

Johansson, D. 2008. Fragmentation and waste rock compaction in small-scale confined blasting. Licentiate thesis 2008:30, Lulea: Lulea University Techn.

Johansson, D. 2011. Effects of confinement and initiation delay on fragmentation and waste rock compaction. Doctoral thesis. Lulea: Lulea University Techn.

Johansson, D. & Ouchterlony, F. 2013. Shock wave interactions in rock blasting: the use of short delays to improve fragmentation in model-scale. In *Int. J. Rock Mech. and Rock Eng.,* Vol. 46, Issue 1: 1 – 28.

Katsabanis, P., Omidi, O., Rielo, O. & Ross, P. 2014. Examination of timing requirements for optimization of fragmentation using small scale grout samples. In *Fragblast: Int. J. for Blasting and Fragmentation*, Vol. 8, Issue 1: 35 – 53.

Katsabanis, P., Omidi, O. 2015. The effect of delay time on fragmentation distribution through small and medium scale testing and analysis. In A T Spathis, D P Gribble, A C Torrance & T N Little (eds), Fragblast 11, *Proc. 11th Int. Symp. on Rock Fragmentation by Blasting:* 715 – 720. Sydney, Australia: AusIMM

Khormali, R. 2012. An investigation into the natural breakage characteristics (NBC) of rock and rock-like materials in blasting, and model correlations in fragmentation phenomena. Scientific report, Leoben, Austria: Montanuniversitaet, Chair of Mining Engineering and Mineral Economics.

Kulatilake, P.H.S.W., Shou, G., Huang, T.H. & Morgan, R.M. 1995. New peak shear strength criteria for anisotropic rock joints. In *Int. J. Rock Mech. Min. Sci. & Geomech. Abstr.,* Vol. 32, Issue 7: 673 – 697.

Li, J., Du, Q. & Sun, C. 2009. An improved box-counting method for image fractal dimension estimation. In *Pattern Recognition,* Vol. 42, Issue 11: 2460 – 2469.

Lownds, C.M. 1983. Computer modelling of fragmentation from an array of shotholes. In R. Holmberg & A. Rustan (eds), Fragblast 1, *Proc. 1st Int. Symp. on Rock Fragmentation by Blasting:* 455-468. Sweden.

Lownds, C.M. & Seligmann, P.C. 1976. Primary fracture from an array of shotholes. In *J. South African Inst. Min. & Metallurgy.* January: 307 – 310.

Ma, G.W. & An, X.M. 2008. Numerical simulation of blasting-induced rock fractures. In *Int. J. Rock Mech. Min. Sci*., Vol. 45: 966 – 975.

Maierhofer, E. 2011. Development of a blasting area and blasting tests with mortar blocks in half scale to research different fragmentation phenomena. Master thesis, Leoben, Austria: Montanuniversitaet, Chair of Mining Engineering and Mineral Economics.

Moser, P., Grasedieck, A., Arsic, V. & Reichholf, G. 2003. Charakteristik der Korngrößenverteilung von Sprenghauwerk im Feinbereich. In *Berg- & Hüttenmännische Monatshefte*, Vol. 148: 205 – 216.

Navarro, J. 2015. Quantification of blast-induced cracks. Master thesis, Leoben, Austria: Montanuniversitaet, Chair of Mining Engineering and Mineral Economics.

Olsson, M. & Bergqvist, I. 1996. Crack lengths from explosives in multiple hole blasting. In B. Mohanty (ed), Fragblast 5, *Proc. 5th Int. Symp. on Rock Fragmentation by Blasting*: 187-191. Rotterdam: Balkema.

Ouchterlony, F. 2005. The Swebrec© function, linking fragmentation by blasting and crushing. In *Mining Technology (Trans. Inst. Min. Metal A*) 114: A29-A44.

Ouchterlony, F. 2010. Fragmentation characterization; the Swebrec function and its use in blast engineering. In J. Sanchidrián (ed), Fragblast 9, *Proc. 9th Int. Symp. on Rock Fragmentation by Blasting*: 3-22. London: Taylor & Francis Group.

Ouchterlony, F., Olsson, M. & Svärd, J. 2010. Crack lengths or blast damage from string emulsion and electronic detonators. In J. Sanchidrián (ed), Fragblast 9, *Proc. 9th Int. Symp. on Rock Fragmentation by Blasting*: 469-480. London: Taylor & Francis Group.

Ouchterlony, F. & Moser. P. 2013. Lessons from single-hole blasting in mortar, concrete and rocks. In P K Singh & A Sinha (eds), Fragblast 10, *Proc. 10th Int. Symp. on Rock Fragmentation by Blasting*: 3 – 14. London: Taylor & Francis Group.

Petropoulos, N. 2011. Influence of confinement on fragmentation and investigation of the burden movement – small scale tests. Master thesis. Lulea: Lulea Univ. Techn.

Petropoulos, N., Johansson, D., Nyberg, U., Novikov, E. & Beyglou, A. 2013. Improved blasting results through precise initiation – results from field trials at the Aitik open pit mine. Swebrec rpt 2013:1, Lulea: Swedish Blasting Research Centre at Lulea Univ. Techn.

Reichholf, G. 2003. Experimental investigation into the characteristic of particle size distributions of blasted material; Doctoral thesis, Leoben, Austria: Montanuniversitaet, Chair of Mining Engineering and Mineral Economics.

Roberts, D.K., & Wells, A.A. 1954. Velocity of brittle fracture. In *Engineering. 178:820-1*.

Rossmanith, H.P. 2002. The use of Lagrange diagrams in precise initiation blasting. Part I: Two interacting blast holes. In *Fragblast: Int. J. for Blasting and Fragmentation*, Vol. 6, Issue 1: 104 – 136.

Rossmanith, H.P., Hochholdinger-Arsic, V. & Uenishi, K. 2005. Understanding size and boundary effects in scaled model blasts – plane problems. In *Fragblast: Int. J. for Blasting and Fragmentation*, Vol. 9, Issue 2: 93 – 125.

Rossmanith, H.P. & Uenishi, K. 2006. On size and boundary effects in scaled model blasts – fractures and fragmentation patterns. In *Fragblast: Int. J. for Blasting and Fragmentation*, Vol. 10, Issue 3 – 4: 163 – 211.

Rustan, A., Vutukuri, V.S. & Naarttijärvi, T. 1983. The influence from specific charge, geometric scale and physical properties of homogeneous rock on fragmentation. In R Holmberg & A Rustan (eds), Fragblast 1, *Proc. 1st Int. Symp. on Rock Fragmentation by Blasting*: 115 – 142. Lulea: Lulea University Techn.

Rustan, A. 1998. Micro-sequential contour blasting – how does it influence the surrounding rock mass? In *Eng. Geology,* Vol. 49: 303 – 313.

Saharan, M.R., Mitri, H.S. & Jethwa, J.L. 2006. Rock fracturing by explosive energy: review of state-of-the-art. In *Fragblast: Int. J. for Blasting and Fragmentation*, Vol. 10, Issue 1: 61 – 81.

Sanchidrián, J.A., Segarra, P., López, L.M. & Ouchterlony, F. 2010. Evaluation of some distribution functions for describing rock fragmentation data. In J. Sanchidrián (ed), Fragblast 9, *Proc. 9th Int. Symp. on Rock Fragmentation by Blasting*: 239-248. London: Taylor & Francis Group.

Sanchidrián, J.A., Ouchterlony, F., Moser, P., Segarra, P. & Lopéz, L. 2012. Performance of some distributions to describe rock fragmentation data. In *Int. J. Rock Mech. Min. Sci*. Vol. 53: 18 – 31.

Sanchidrián, J.A., Ouchterlony, F., Segarra, P. & Moser, P. 2014. Size distribution functions for rock fragments. In *Int. J. Rock Mech. Min. Sci*., Vol. 71: 381 – 394.

Schimek, P., Ouchterlony, F. & Moser, P. 2013. Experimental blast fragmentation research in model-scale bench blasts. In J Sanchidrián & A K Singh (eds), Proc. Fragblast 10, *Measurement and Analysis of Blast Fragmentation*: 51 - 60. London: Taylor & Francis Group.

Schimek, P., Ouchterlony, F. & Moser, P. 2015. Influence of blasthole delay-timing on fragmentation as well as roughness of and blast damage behind a remaining bench face through model scale blasting. In A T Spathis, D P Gribble, A C Torrance & T N Little (eds), Fragblast 11, *Proc. 11th Int. Symp. on Rock Fragmentation by Blasting:* 257 – 265. Sydney, Australia: AusIMM.

Schuhmann, R. 1940. Principles of comminution, I-Size distribution and surface calculations. *Tech. Publs.,* Vol. 1189, 11 p, New York: American Institute of Mining, Metallurgical and Petroleum Engineers.

Sharma, P.D. 2009. Electronic detonators – Results in substantial techno-economic benefits for large mining operations. *Mining Engineers' Journal*, India.

Stagg, M.S. & Nutting, M.J. 1987. Influence of blast delay time on rock fragmentation: one-tenth-scale tests. BuMines IC 9135: 79 – 95, Chicago, USA.

Stagg, M.S. & Rholl, S.A. 1987. Effects of accurate delays on fragmentation for single row blasting in a 6.7 m bench. In W L Fourney & R D Dick (eds), Fragblast 2, *Proc. 2nd Int. Symp. on Rock Fragmentation by Blasting*: 210 – 230. Colorado.

Vanbrabant, F. & Espinosa, A. 2006. Impact of short delays sequence on fragmentation by means of electronic detonators: theoretical concepts and field validation. In Fragblast 8, *Proc. 8th Int. Symp. on Rock Fragmentation by Blasting*: 326 – 331, Santiago, Chile: Editec S.A.

Wagner, H. 2002. Bruchvorgänge im Gebirge – Erfahrungen aus dem Bergbau. *Proceedings of the 7th Conference on „Gefüge und Bruch“*: 6 – 19, Leoben: Montanuniversitaet Leoben.

Wilson, W.H. & Holloway, D.C. 1987. Fragmentation studies in instrumented concrete models; In Herget, G, Vongpaisal, S (eds), *Proc. 6th ISRM Int. Cong. on Rock Mechanics*, Vol. 1: 735 – 741, Rotterdam: Balkema.

Wimmer, M. 2007. An experimental investigation of blastability. Swebrec rpt 2007:1. Lulea: Swedish Blasting Research Centre at Lulea Univ. Techn.

Winzer, S.R., Anderson, D.A. & Ritter, A.P. 1983. Rock fragmentation by explosives. In R Holmberg & A Rustan (eds), Fragblast 1, *Proc. 1st Int. Symp. on Rock Fragmentation by Blasting*: 225 – 249. Lulea: Lulea Univ. Techn.

Winzer, S.R. & Ritter, A.P. 1980. The Role of Stress Waves and Discontinuities in Rock Fragmentation: A Study of Fragmentation in Large Limestone Blocks. *Proc. 21st U.S. Symposium on Rock Mechanics (USRMS)*, Missouri: American Rock Mechanics Association.

Wrienz, M.H. 2013. Untersuchung der Zerkleinerung und Rissausbreitung an Betonblöcken. Bachelor thesis, Leoben, Austria: Montanuniversitaet, Chair of Mining Engineering and Mineral Economics.

Zhu, Z., Mohanty, B., Xie, H. 2007. Numerical investigation of blasting-induced crack initiation and propagation in rocks. In *Int. J. Rock Mech. Min. Sci.*, Vol. 44: 412 – 424.

Zhu, Z., Xie, H., Mohanty, B. 2008. Numerical investigation of blasting-induced damage in cylindrical rocks. In *Int. J. Rock Mech. Min. Sci.*, Vol. 45: 111 – 121.

8 List of Figures

9 List of Tables

10 List of Abbreviations

2D	Two dimensional
3D	Three dimensional
α	Significance level (= 5 % = 0.05)
B	Burden of the blastholes
Bh	Blasthole
CB 90 – 80	Cracks originating from the borehole and an angle from 90° to 80°
CB 80 – 30	Cracks originating from the borehole and an angle from 80° to 30°
CB 30 – 0	Cracks originating from the borehole and an angle from 30° to 0°
CD 90 – 80	Cracks with no direct link to a blasthole but with direction to a blasthole and an angle between 90° and 80°
CD 80 – 30	Cracks with no direct link to a blasthole but with direction to a blasthole and an angle between 80° and 30°
CD 30 – 0	Cracks with no direct link to a blasthole but with direction to a blasthole and an angle between 30° and 0°
c_P	Longitudinal compressive (P-) wave speed
c_S	Shear (S-) wave speed
d+b	Dust and boulders
d	Centre of the “untouched” areas when using the cylindrical influence zones around a blasthole
d_i	Distance from the individual data points to the reference line
D_{Mean}	Mean distance of the individual data points to the reference line
H	Test statistic for the KW-ANOVA
k	Amount of groups (used in KW-ANOVA)
k-1	Degrees of freedom (used in KW-ANOVA)
k_{30}	Calculated grain size at cumulative mass passing of 30 %

k_{50}	Calculated grain size at cumulative mass passing of 50 %
k_{80}	Calculated grain size at cumulative mass passing of 80 %
k_L	Lower screen size
k_U	Upper screen size
KW-ANOVA	Kruskal-Wallis one-way analysis of variance
l	Length of contour line between 1st and last blasthole
MCD	Mean crack density
MCID	Mean crack intersection density
MP	Meeting point of detected cracks at the bench face
ms	Milliseconds
m	Number of observations in group 2 (used in MWU-Test)
MWU-Test	Mann-Whitney-U-Test
n	Number of observations in group 1 (used in MWU-Test)
n	Amount of observations (when used for statistical methods)
n_i	Number of observations in group i
NONEL	Non electrical detonator
ÖGI	Österreichisches Gießerei-Institut at the Montanuniversitaet Leoben
P	Mass passing through a specific mesh size
P_{50}	Cumulative mass passing at k_{50} (= 50 %)
P_E	End of longitudinal compressive (p-) wave
P_F	Front of longitudinal compressive (p-) wave
P_L	Cumulative mass passing at lower screen size
P_U	Cumulative mass passing at upper screen size
Q_L	Lower quantile (used in MWU-Test)
Q_U	Upper quantile (used in MWU-Test)
R	Radius of cylindrical influence zone around a blasthole

R^2	Coefficient of determination
R_i^2	Sum of the ranks of group i squared (used in Kruskal- Wallis one-way analysis of variance)
RQ	Research question
S	Side-spacing of the blastholes
SCB	Straight cracks between blastholes (from back or front of block)
S_E	End of shear (S-) wave
S_F	Front of shear (S-) wave
s_i	Inclination of the connection line between two data points
S_{Norm}	Normalized slope inclination of individual sections of the contour lines
T_0	Duration of the first half-wave at the blasted hole when the charge detonates
T_1	Duration of the first (negative) half-wave at the neighbouring hole
T_1	Sum of the ranks of group 1 (used in MWU-Test)
T_2	Sum of the ranks of group 2 (used in MWU-Test)
T_d	Time which the compressive wave needs to reach the next blasthole
T_{ideal}	Ideal delay-time between the individual blastholes
UCS	Uniaxial compressive strength
Unif.Coeff.	Uniformity coefficient = Coefficient of uniformity = k_{80} / k_{30}
VOD	Velocity of detonation
x_{max}	Maximum x-value along contour line
x_{min}	Minimum x-value along contour line
τ_P	Duration of longitudinal compressive (P-) wave
τ_S	Duration of shear (S-) wave
µs	Microseconds
χ^2	Critical value of the test statistic for the KW-ANOVA

Appendix 1 – Datasheets of Ingredients of Magnetite-Mortar

Schlieper & Heyng

Technisches Datenblatt

Aktualisiert: Mai 2006

Ferroxon® 618

Type:	Black iron oxide pigment
Form of delivery:	Powder, packed in PE-bags 25 kg or Big Bags

Characteristics		**Test methode**
Fe_3O_4-content:	90 - 95 M.-%	DIN ISO 1248
Matter volatile at 105 °C:	≤ 0,5 M.-%	DIN ISO 787-2
Water soluble content:	≤ 0,5 M.-%	DIN ISO 787-3
Loss on ignition:	≤ 1,0 M.-%	DIN ISO 4621
Oil absorption:	35 g/100 g	DIN ISO 787-5
pH-value:	5 – 8	DIN ISO 787-9
Sieving residue 46 µm-sieve:	≤ 0,1 M.-%	DIN ISO 787-7

Schlieper & Heyng GmbH + Co. KG, Postfach 27, 57647 Nistertal
Fon: 02661/940040, Fax: 02661/9400480

Quarzwerke

CE

Datenblatt

Quarzsand ME 31
MESK31

Quarzsand ME31 ist ein aufbereiteter natürlicher Rohstoff. Der Quarzsand wird attritiert, gewaschen, hydroklassiert, gesiebt und ist von Kalk und organischen Verunreinigungen befreit.
Durch sein gerundetes Korn und den chem. Inhaltsstoffen, ist diese Sorte speziell als Formgrundstoff für die Gießereiindustrie geeignet.
Durch laufende Kontrollen garantieren wir Ihnen eine hohe und gleichmäßige Qualität.

Lieferform : feucht oder trocken (feuergetrocknet)
lose, abgesackt in PE Säcken, foliert auf Palette

Korngrößenverteilung

	Siebrückstand in %		Siebdurchgang in %
Körnung in mm	Richtwert	Toleranz	Richtwert
0,71		max.0,5	100
0,5	1,5	max.3	98,5
0,355	26	20-35	72,5
0,25	49	40-60	23,5
0,125	23	18-28	0,5
0,063	0,5	max.2	
<		max.0,5	

Chemische Analyse (Gew.-%)

Element	Richtwert	Toleranz
SiO_2	97	96-98
Al_2O_3	1,7	max.2,2
Fe_2O_3	0,17	max.0,25

Physikalische Eigenschaften

Schüttgewicht	1,5t/m3	mittlere Korngröße	0,30 mm
Dichte	2,65t/m3	AFS-Nummer	51
Härte	7Mohs	Glühverlust	<0,3%
Schlämmstoffgehalt	<0,2%	Sinterbeginn*	~1420° C

*lt.ÖGI

Quarzsand ist ein aufbereiteter natürlicher Rohstoff. Alle Daten sind Richtwerte mit vorkommens- und produktionsbedingter Toleranz. Sie dienen nur zur Beschreibung und stellen keine zugesicherten Eigenschaften dar. Gröbere und feinere Anteile sind in Spuren möglich. Dem Benutzer obliegt es, die Tauglichkeit für seinen Verwendungszweck zu prüfen. Wir geben auf Wunsch gerne Auskunft über Toleranzbreiten und anwendungstechnische Erfahrungen. Verkäufe erfolgen gemäß unseren Verkaufs- und Lieferbedingungen.

QUARZWERKE Österreich GmbH
Wachbergstr. 1
A-3390 Melk
www.quarzwerke.at

Telefon (02752) 50040-0
Telefax (02752) 50040-30

O541 04/07

Quarzwerke

CE

Datenblatt

Quarzsand ME 0,1 - 0,4 mm

Quarzsand ME 0,1-0,4 ist ein aufbereiteter natürlicher Rohstoff. Der Quarzsand wird attritiert, gewaschen, hydroklassiert, gesiebt und ist von Kalk und organischen Verunreinigungen befreit.
Durch laufende Kontrollen garantieren wir Ihnen eine hohe und gleichmäßige Qualität.

Lieferform : feucht oder trocken (feuergetrocknet)
lose, abgesackt in PE Säcken, foliert auf Palette

Korngrößenverteilung

	Siebrückstand in %		Siebdurchgang in %
Körnung in mm	Richtwert	Toleranz	Richtwert
0,71	0	0	100
0,5	1	max.2	99
0,355	10	5-15	89
0,25	36	30-55	53
0,125	50	40-60	3
0,063	3	1-6	
<		max.1	

Chemische Analyse (Gew.-%)

Element	Richtwert		Toleranz
SiO_2	93		91-95
Al_2O_3	4		3-5
Fe_2O_3	0,2		0,1-0,4

Physikalische Eigenschaften

Schüttgewicht	1,5 t/m3		
Dichte	2,65 t/m3		
Härte	7 Mohs		

Quarzsand ist ein aufbereiteter natürlicher Rohstoff. Alle Daten sind Richtwerte mit vorkommens- und produktionsbedingter Toleranz. Sie dienen nur zur Beschreibung und stellen keine zugesicherten Eigenschaften dar. Gröbere und feinere Anteile sind in Spuren möglich. Dem Benutzer obliegt es, die Tauglichkeit für seinen Verwendungszweck zu prüfen. Wir geben auf Wunsch gerne Auskunft über Toleranzbreiten und anwendungstechnische Erfahrungen. Verkäufe erfolgen gemäß unseren Verkaufs- und Lieferbedingungen.

QUARZWERKE Österreich GmbH
Wachbergstr. 1
A-3390 Melk
www.quarzwerke.at

Telefon (02752) 50040-0
Telefax (02752) 50040-30

O535 04/07

Appendix 2 – Summary of Material Properties

Density

Production Cycle #01

Sample Nr. [-]	L [mm]	D [mm]	Mass [g]	L:D ratio [-]	Volume [cm³]	Density [g/cm³]
BBK-66-1	104.00	49.79	484.26	2.09	202.49	2.39
BBK-66-2	104.63	49.76	489.26	2.10	203.47	2.40
BBK-66-3	104.45	49.83	487.12	2.10	203.69	2.39
BBK-66-4	97.76	49.76	454.31	1.96	190.11	2.39
BBK-66-5	27.93	49.78	128.08	0.56	54.36	2.36
BBK-66-6	27.27	49.77	126.97	0.55	53.05	2.39
BBK-66-7	23.96	49.77	111.13	0.48	46.61	2.38
BBK-66-8	23.04	49.75	105.99	0.46	44.79	2.37
					Average	**2.38**
					Std. dev.	0.01

Production Cycle #02

Sample Nr. [-]	L [mm]	D [mm]	Mass [g]	L:D ratio [-]	Volume [cm³]	Density [g/cm³]
BBK-241-3/1	102.5	51.21	481.84	2.00	211.12	2.28
BBK-241-4/1	102.25	51.22	481.27	2.00	210.68	2.28
BBK-241-5/1	102.85	51.25	486.33	2.01	212.17	2.29
BBK-241-6/1	103.59	51.29	495.11	2.02	214.03	2.31
BBK-241-7/1	24.85	51.35	116.10	0.48	51.46	2.26
BBK-241-8/1	24.24	51.04	112.75	0.47	49.60	2.27
BBK-241-10/1	24.94	51.02	117.71	0.49	50.99	2.31
BBK-241-11/1	25.48	51.01	116.31	0.50	52.07	2.23
BBK-241-12/1	25.96	51.02	118.45	0.51	53.07	2.23
					Average	**2.28**
					Std. dev.	0.03

Production Cycle #03

Sample Nr. [-]	Density [g/cm³]
BG01	2.11
BG02	2.12
BG03	2.15
BG04	2.13
Average	**2.13**
Std. dev.	0.01

Young's Modulus, Uniaxial Compressive Strength

Production Cycle #01

Sample Nr. [-]	L [mm]	D [mm]	max Load [kN]	Young's-mod [GPa]	Poisson's ratio [-]	UCS [MPa]
BBK-66-1	104.00	49.79	116.96	24.74	0.16	60.07
BBK-66-2	104.63	49.79	127.94	25.16	0.16	65.79
BBK-66-3	104.45	49.83	122.34	25.65	0.17	62.73
BBK-66-4	97.76	49.79	120.66	24.57	0.17	62.05
			Average	**25.03**	**0.17**	**62.7**
			Std. dev.	0.42	0.01	2.1

Production Cycle #02

Sample Nr. [-]	L [mm]	D [mm]	Young's-mod [GPa]	Poisson's ratio [-]	UCS [MPa]
BBK-241-3/1	102.50	51.21	23.44	0.10	58.85
BBK-241-4/1	102.25	51.22	22.00	0.10	54.81
BBK-241-5/1	102.85	51.25	22.51	0.10	49.53
BBK-241-6/1	103.59	51.29	24.61	0.14	58.96
		Average	**23.14**	**0.11**	**55.5**
		Std. dev.	0.99	0.02	3.9

Production Cycle #03

Sample Nr. [-]	Young's-mod [GPa]	Poisson's ratio [-]	UCS [MPa]
BBK-262-1/1	12.58	0.16	30.01
BBK-262-2/1	14.26	0.15	40.77
BBK-262-3/1	14.08	0.16	40.49
BBK-262-4/1	13.89	0.18	33.99
BBK-263-1/1	13.10	0.17	31.43
BBK-263-2/1	13.80	0.15	29.27
BBK-263-3/1	16.15	0.26	27.62
BBK-264-1/1	14.11	0.17	35.27
BBK-264-2/1	13.91	0.13	36.54
BBK-264-3/1	13.97	0.17	38.49
BBK-264-4/1	12.66	0.17	36.14
BBK-264-9/1	14.55	0.18	40.89
BBK-264-10/1	14.32	0.17	39.85
BBK-264-11/1	14.39	0.17	39.88
Average	**13.98**	**0.17**	**35.8**
Std. dev.	0.84	0.03	4.5

P-Wave and S-Wave Velocity

Production Cycle #01

Sample Nr. [-]	L [mm]	P-wave velocity [m/s]	S-wave velocity [m/s]	P-wave velocity* [m/s]	c_P/c_S [-]
BBK-66-1	104.00	3837	2315	3796	
BBK-66-2	104.63	3869	2335	3807	
BBK-66-3	104.45	3834	2313	3789	
BBK-66-4	97.76	3795	2290	3758	
BBK-66-5	27.93	3869	2382	3890	1.62
BBK-66-6	27.27	3933	2339	3872	1.68
BBK-66-7	23.96	3883	2362	3780	1.64
BBK-66-8	23.04	3898	2304	3756	1.69
	Average	**3865**	**2330**	**3806**	**1.66**
	Std. dev.	40	29	46	0.03

* Measurement at the chair of Mining Engineering

Production Cycle #02

Sample Nr. [-]	P-wave velocity [m/s]
CH02B02	3676
CH02B03	3685
CH02B04	3698
CH02B05	3706
CH03B01	3647
CH03B02	3761
CH03B03	3794
CH03B04	3786
CH03B05	3786
Average	**3727**
Std. dev.	52

Production Cycle #03

Sample Nr. [-]	P-wave velocity [m/s]	S-wave velocity [m/s]	c_P/c_S [-]
BG01	2895		
BG01	2869		
BG01	2928		
BG02	2831		
BG02	2838		
BG02	2861		
BG03	2873	1768	1.63
BG03	2938	1778	1.65
BG03	2917	1769	1.65

BG04	2958	1781	1.66
BG04	2913	1788	1.63
BG04	2905	1784	1.63
Average	**2894**	**1778**	**1.64**
Std. dev.	38	7	0.01

Brazilian Tensile Strength

Production Cycle #01

Sample Nr. [-]	L [mm]	D [mm]	max Load [kN]	Tensile Strength [MPa]
BBK-66-5	27.93	49.78	8.90	4.08
BBK-66-6	27.27	49.77	11.19	5.25
BBK-66-7	23.96	49.77	9.92	5.30
BBK-66-8	23.04	49.75	9.50	5.28
			Average	**4.98**
			Std. dev.	0.52

Production Cycle #02

Sample Nr. [-]	L [mm]	D [mm]	Tensile Strength [MPa]
BBK-241-7/1	24.85	51.35	5.13
BBK-241-8/1	24.24	51.04	5.76
BBK-241-10/1	24.94	51.02	5.62
BBK-241-11/1	25.48	51.01	5.87
BBK-241-12/1	25.96	51.02	5.99
		Average	**5.67**
		Std. dev.	0.30

Production Cycle #03

Sample Nr. [-]	Tensile Strength [MPa]
BBK-264-5/1	2.78
BBK-264-6/1	3.26
BBK-264-7/1	3.34
BBK-264-8/1	3.76
BBK-264-12/1	3.25
BBK-264-13/1	3.73
BBK-264-14/1	3.71
BBK-264-15/1	4.67
Average	**3.56**
Std. dev.	0.52

Appendix 3 – Sieving Data Cylinder Shots

Production Cycle #01

Sample-ID	CH01Z03		Screen size [mm]	Mass passing [%]
Blasting date	14.07.2011		125	100.00
Blasting type	Cylinder Shot		100	100.00
Blasthole diameter	10	[mm]	80	100.00
Charge type	20	[g/m]	63	100.00
Diameter Cylinder	138.5	[mm]	50	100.00
			40	100.00
			31.5	97.54
			25	94.40
			20	82.89
			14	58.77
			12.5	53.69
			10	45.13
			6.3	30.98
			4	20.70
			2	12.11
			1	7.60
			0.5	5.22
			0.25	2.06
			<0.25	0.00

Sample-ID	CH02Z01		Screen size [mm]	Mass passing [%]
Blasting date	14.07.2011		125	100.00
Blasting type	Cylinder Shot		100	100.00
Blasthole diameter	10	[mm]	80	100.00
Charge type	20	[g/m]	63	100.00
Diameter Cylinder	138.5	[mm]	50	100.00
			40	96.32
			31.5	91.69
			25	88.34
			20	78.87
			14	56.93
			12.5	50.94
			10	41.66
			6.3	28.45
			4	18.90
			2	10.89
			1	6.69
			0.5	4.51
			0.25	1.83
			<0.25	0.00

Sample-ID	CH03Z01		Screen size [mm]	Mass passing [%]
Blasting date	14.07.2011		125	100.00
Blasting type	Cylinder Shot		100	100.00
Blasthole diameter	10	[mm]	80	100.00
Charge type	20	[g/m]	63	100.00
Diameter Cylinder	138.5	[mm]	50	100.00
			40	100.00
			31.5	98.24
			25	95.30
			20	86.61
			14	62.93
			12.5	57.82
			10	44.87
			6.3	31.26
			4	20.54
			2	11.57
			1	6.95
			0.5	4.58
			0.25	1.91
			<0.25	0.00

Sample-ID	CH04Z01		Screen size [mm]	Mass passing [%]
Blasting date	14.07.2011		125	100.00
Blasting type	Cylinder Shot		100	100.00
Blasthole diameter	10	[mm]	80	100.00
Charge type	20	[g/m]	63	100.00
Diameter Cylinder	138.5	[mm]	50	100.00
			40	100.00
			31.5	97.35
			25	93.03
			20	83.44
			14	61.29
			12.5	55.15
			10	44.86
			6.3	30.49
			4	19.69
			2	10.84
			1	6.25
			0.5	3.97
			0.25	1.69
			<0.25	0.00

Production Cycle #02

Sample-ID	CH01Z03		Screen size [mm]	Mass passing [%]
Blasting date	27.06.2013		125	100.00
Blasting type	Cylinder Shot		100	100.00
Blasthole diameter	10	[mm]	80	100.00
Charge type	20	[g/m]	63	100.00
Diameter Cylinder	141	[mm]	50	100.00
			40	96.28
			31.5	92.93
			25	81.28
			20	65.02
			14	45.20
			12.5	41.76
			10	35.02
			6.3	23.20
			4	13.81
			2	8.21
			1	4.97
			0.5	2.98
			< 0.5	0.00

Sample-ID	CH02Z03		Screen size [mm]	Mass passing [%]
Blasting date	27.06.2013		125	100.00
Blasting type	Cylinder Shot		100	100.00
Blasthole diameter	10	[mm]	80	100.00
Charge type	20	[g/m]	63	100.00
Diameter Cylinder	142	[mm]	50	100.00
			40	97.82
			31.5	89.71
			25	77.25
			20	61.70
			14	44.49
			12.5	40.92
			10	33.89
			6.3	22.07
			4	13.50
			2	8.66
			1	5.34
			0.5	3.20
			< 0.5	0.00

Sample-ID	CH03Z03		Screen size [mm]	Mass passing [%]
Blasting date	27.06.2013		125	100.00
Blasting type	Cylinder Shot		100	100.00
Blasthole diameter	10	[mm]	80	100.00
Charge type	20	[g/m]	63	100.00
Diameter Cylinder	144	[mm]	50	100.00
			40	99.11
			31.5	96.35
			25	88.01
			20	69.95
			14	49.10
			12.5	45.24
			10	37.26
			6.3	24.05
			4	14.57
			2	8.71
			1	5.34
			0.5	3.13
			< 0.5	0.00

Production Cycle #03

Sample-ID	CH01Z01		Screen size [mm]	Mass passing [%]
Blasting date	21.08.2014		125	100.00
Blasting type	Cylinder Shot		100	100.00
Blasthole diameter	10	[mm]	80	100.00
Charge type	20	[g/m]	63	100.00
Diameter Cylinder	141	[mm]	50	100.00
			40	100.00
			31.5	95.77
			25	86.76
			20	74.57
			14	53.02
			12.5	47.05
			10	37.15
			6.3	23.24
			4	14.38
			2	8.52
			1	5.45
			0.5	3.72
			<0.5	0.00

Sample-ID	CH01Z02		Screen size [mm]	Mass passing [%]
Blasting date	21.08.2014		125	100.00
Blasting type	Cylinder Shot		100	100.00
Blasthole diameter	10	[mm]	80	100.00
Charge type	20	[g/m]	63	100.00
Diameter Cylinder	142	[mm]	50	100.00
			40	99.21
			31.5	95.24
			25	87.20
			20	74.98
			14	52.69
			12.5	46.60
			10	35.86
			6.3	22.36
			4	13.72
			2	8.23
			1	5.18
			0.5	3.40
			<0.5	0.00

Sample-ID	CH02Z01		Screen size [mm]	Mass passing [%]
Blasting date	21.08.2014		125	100.00
Blasting type	Cylinder Shot		100	100.00
Blasthole diameter	10	[mm]	80	100.00
Charge type	20	[g/m]	63	100.00
Diameter Cylinder	141	[mm]	50	100.00
			40	97.93
			31.5	90.91
			25	81.40
			20	69.13
			14	51.59
			12.5	45.43
			10	36.65
			6.3	23.97
			4	15.93
			2	10.57
			1	7.56
			0.5	5.69
			<0.5	0.00

Sample-ID	CH02Z02		Screen size [mm]	Mass passing [%]
Blasting date	21.08.2014		125	100.00
Blasting type	Cylinder Shot		100	100.00
Blasthole diameter	10	[mm]	80	100.00
Charge type	20	[g/m]	63	100.00
Diameter Cylinder	142	[mm]	50	100.00
			40	98.92
			31.5	95.06
			25	84.20
			20	71.66
			14	51.45
			12.5	46.69
			10	38.69
			6.3	25.44
			4	17.44
			2	10.85
			1	7.86
			0.5	5.87
			<0.5	0.00

Appendix 4 – Swebrec-Fits Cylinder Shots

Production Cycle #01

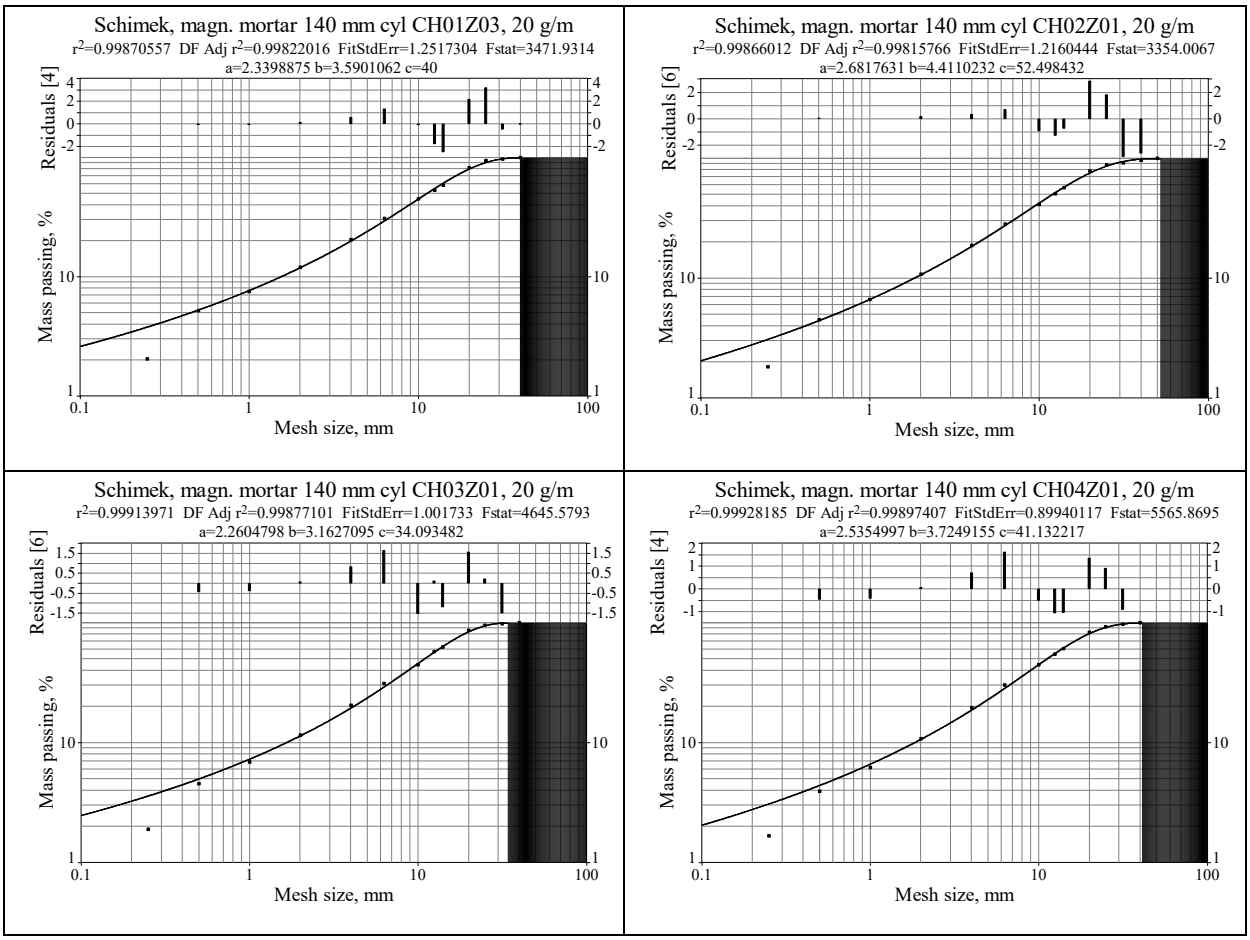

Production Cycle #02

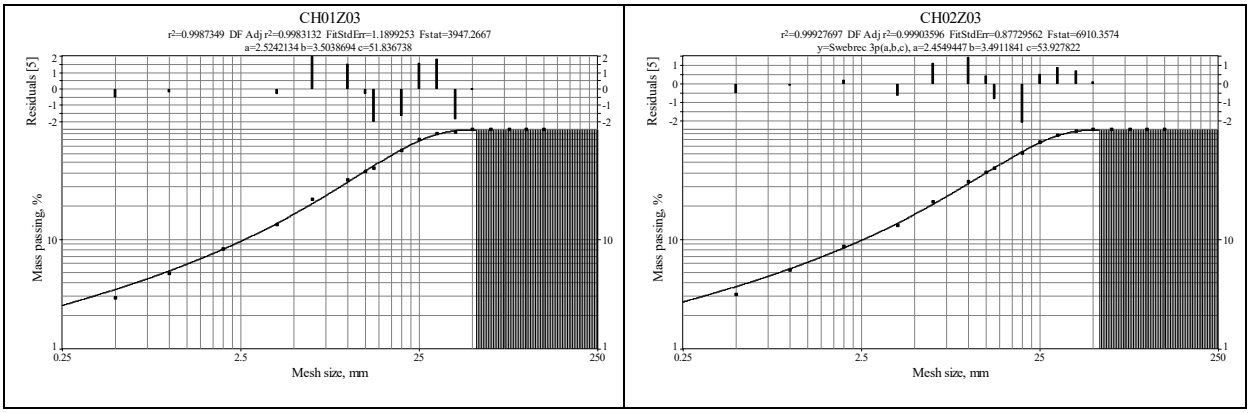

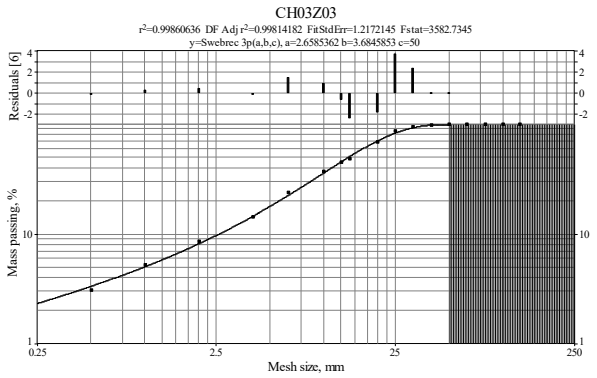

Production Cycle #03

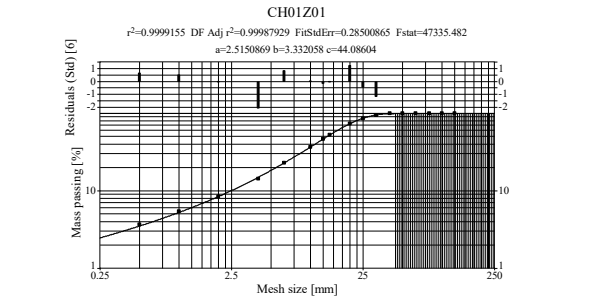

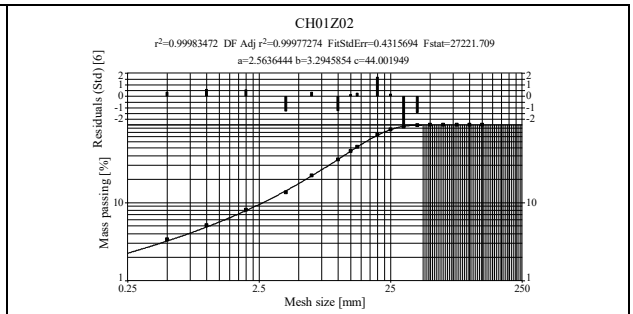

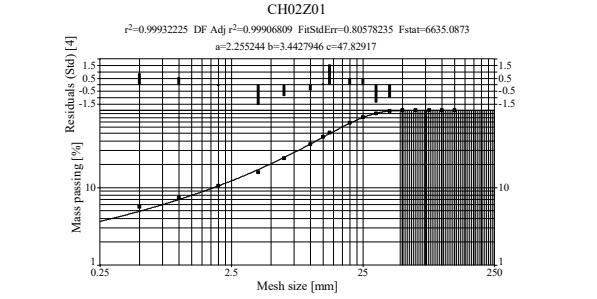

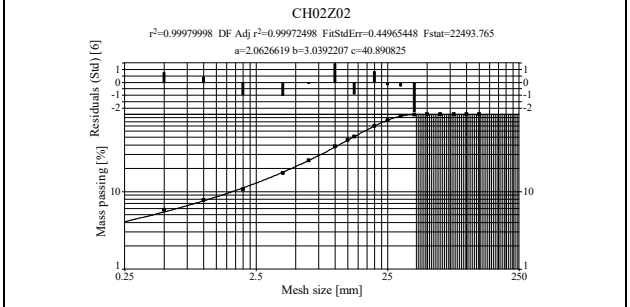

Appendix 5 – Documentation of Preliminary Blasting Tests

#0111: Row 1: 140 µs delay

Row 2: 140 µs delay

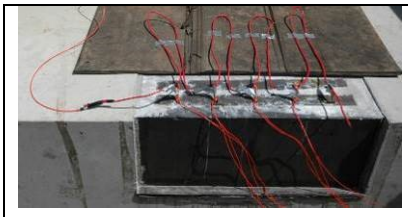
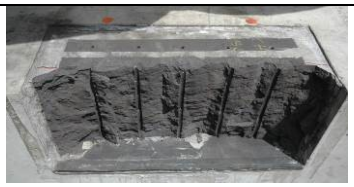



#0211: Row 1: 140 µs delay

Row 2: 140 µs delay






#0311: Row 1: Single Hole Shot in the middle of the row with wooden sticks in neighbouring holes

Row 2: Single Hole Shot in the middle of the row without any filling in neighbouring holes

#0411: Row 1: Single Hole Shot in the middle of the row with fast hardening cement in the neighbouring holes on the right side and no filling material in the neighbouring holes on the left side.

Row 2: Single Hole Shot in the middle of the row with fast hardening cement in the neighbouring holes on the right side and no filling material in the neighbouring holes on the left side.

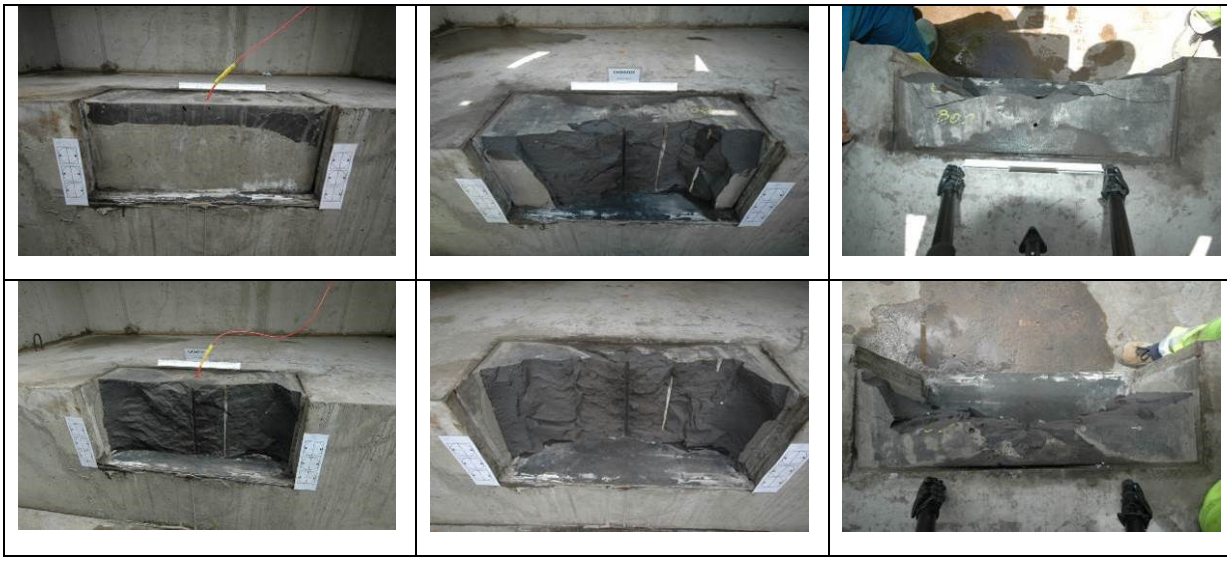

#0511: Row 1: Single Hole Shots with cut-away-corner arrangement and fast hardening cement in the neighbouring holes of the row.

Row 2: Single Hole Shot in the middle of the row without any drilled neighbouring holes.

#0611: Row 1: Single Hole Shots with cut-away-corner arrangement. Neighbouring holes without any filling material.

Row 2: Single Hole Shots with cut-away-corner arrangement. Neighbouring holes without any filling material.

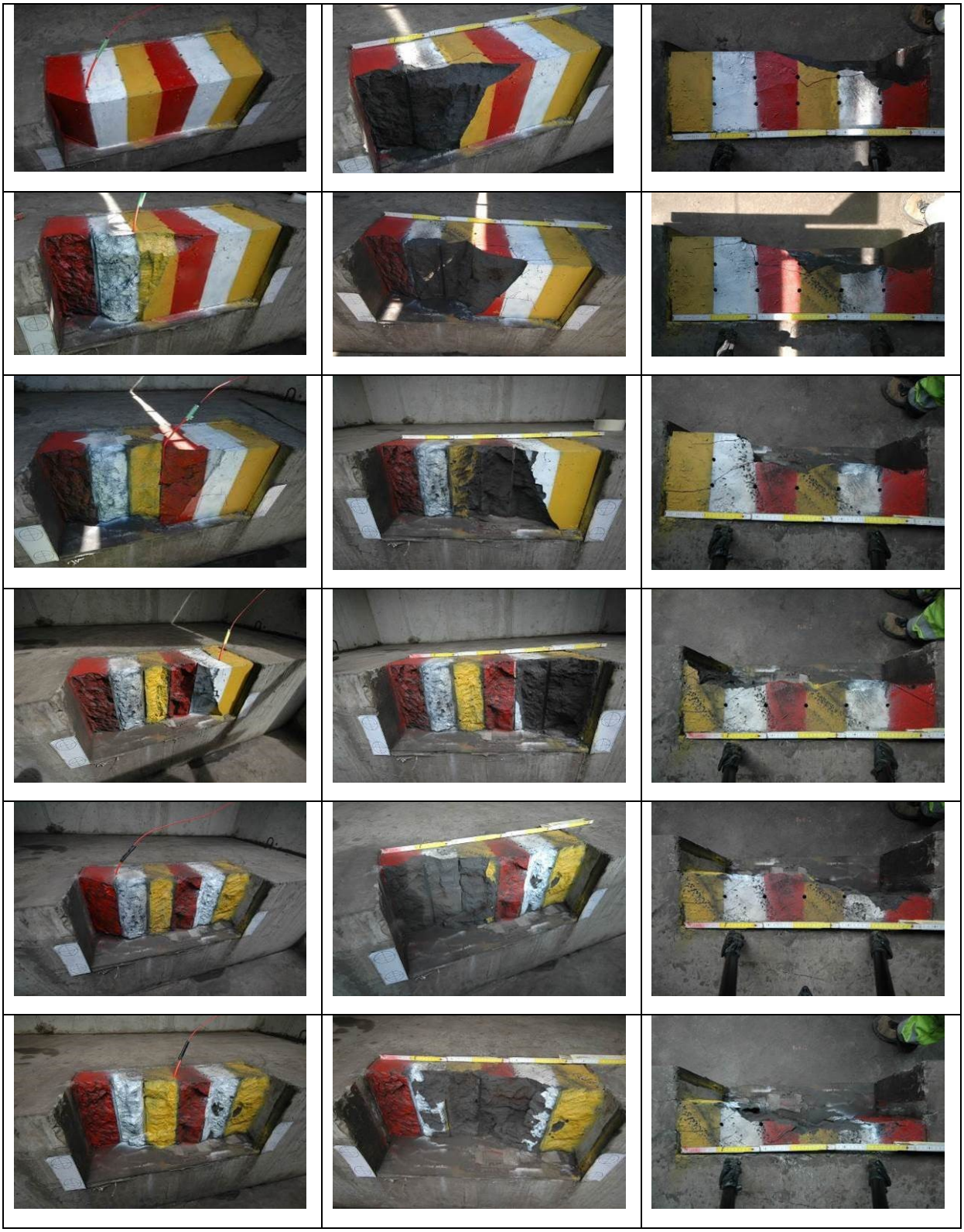






Appendix 6 – Documentation of Blasting Tests – Stage 1

#0212: Row 1: 140 µs delay; Row 2: 140 µs delay; Row 3: 140 µs delay

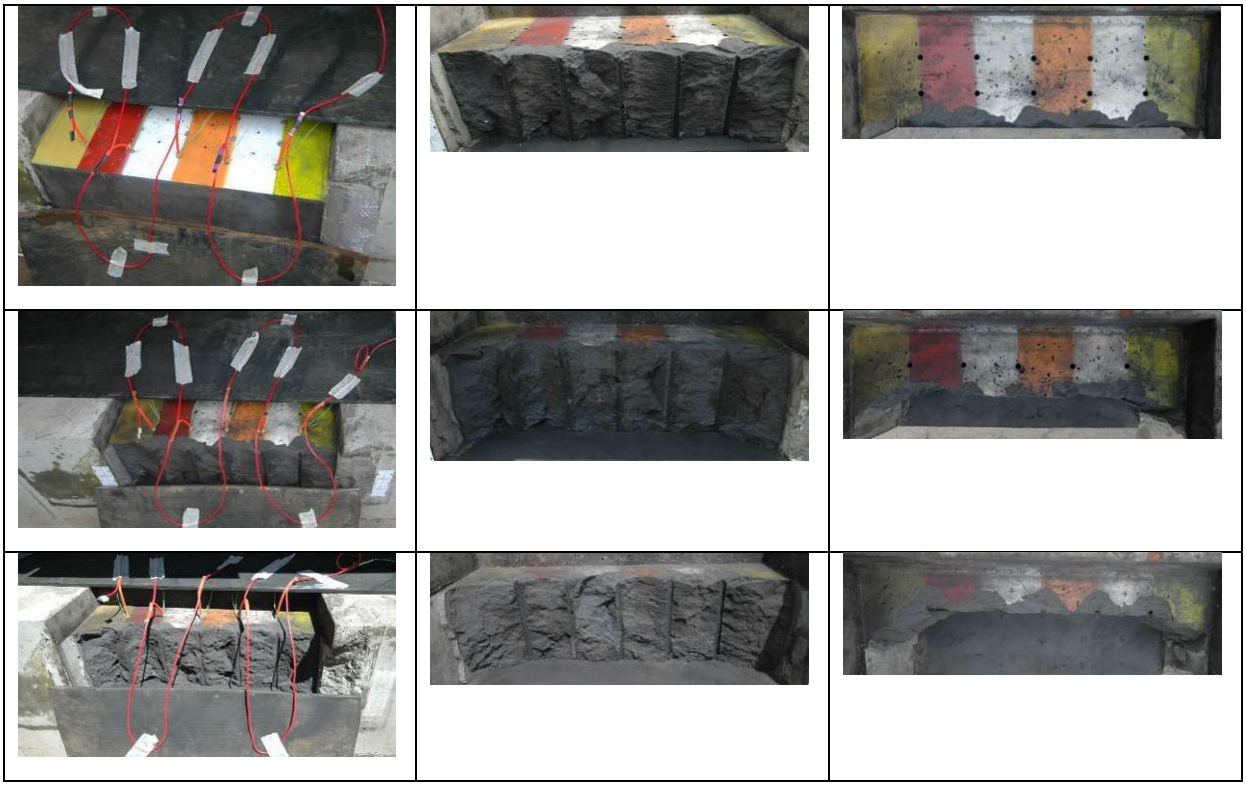

#0312: Row 1: 140 µs delay; Row 2: 0 µs delay; Row 3: 0 µs delay

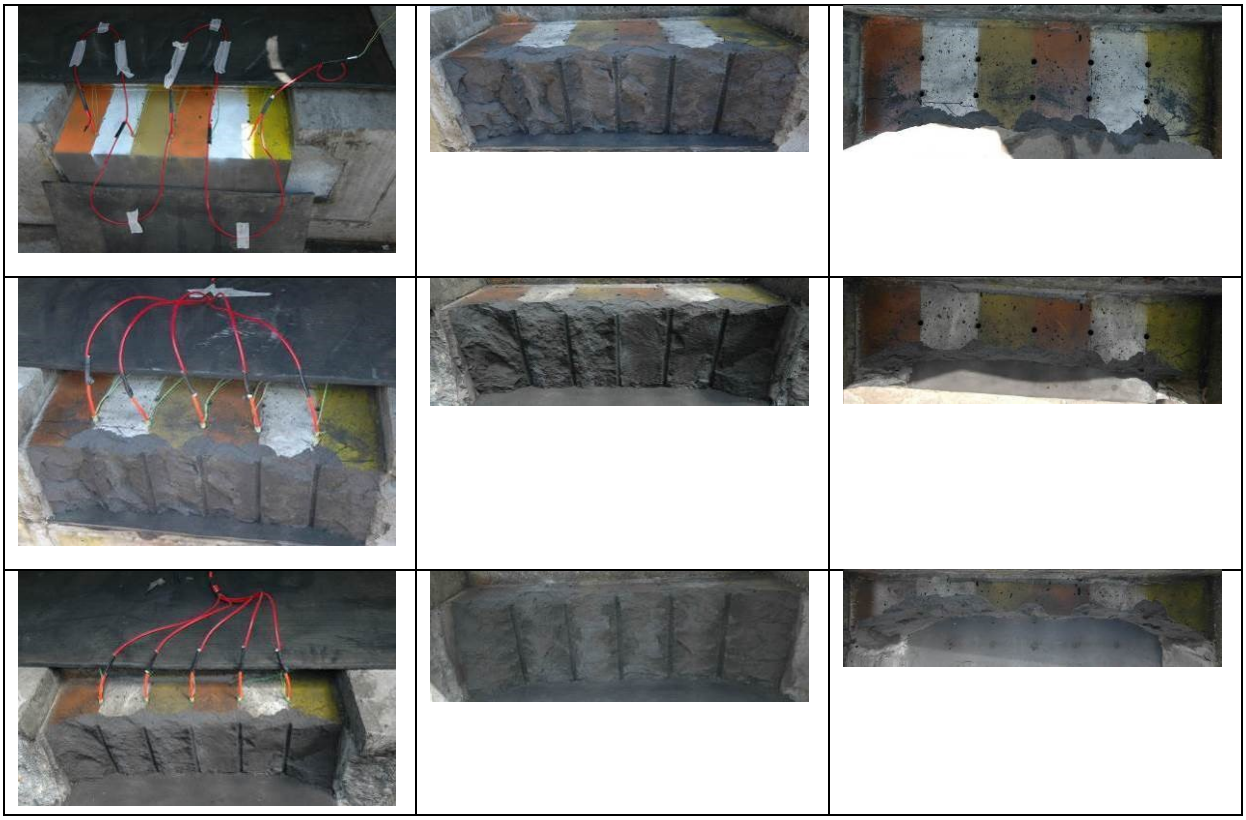

#0412: Row 1: 140 µs delay; Row 2: 140 µs delay

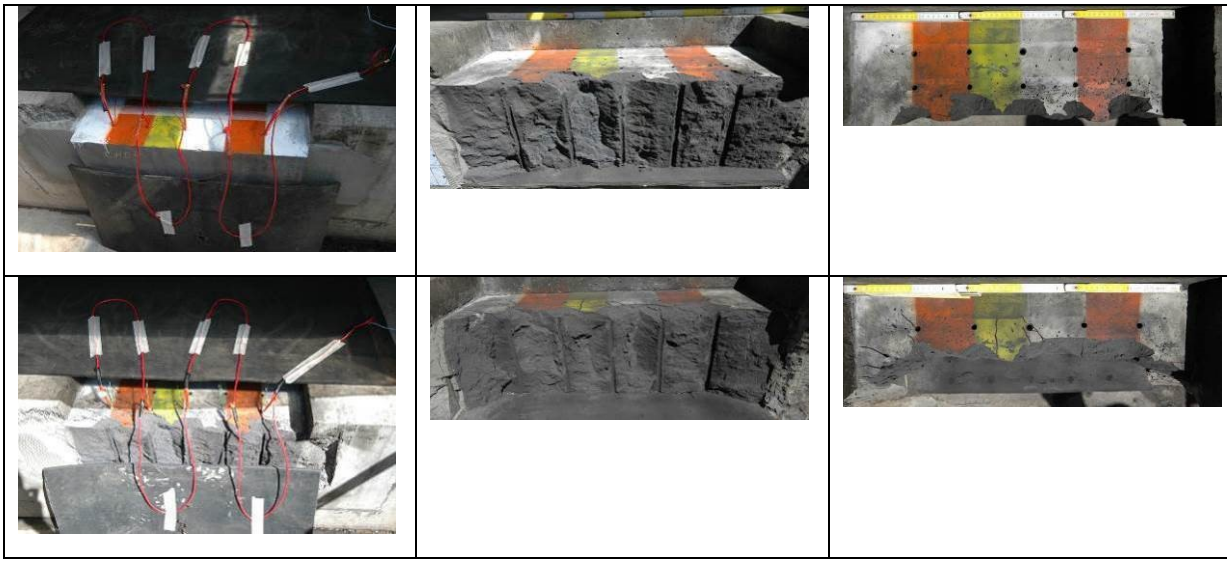

#0512: Row 1: 140 µs delay; Row 2: 0 µs delay

#0612: Row 1: 140 µs delay; Row 2: 73 µs delay; Row 3: 73 µs delay

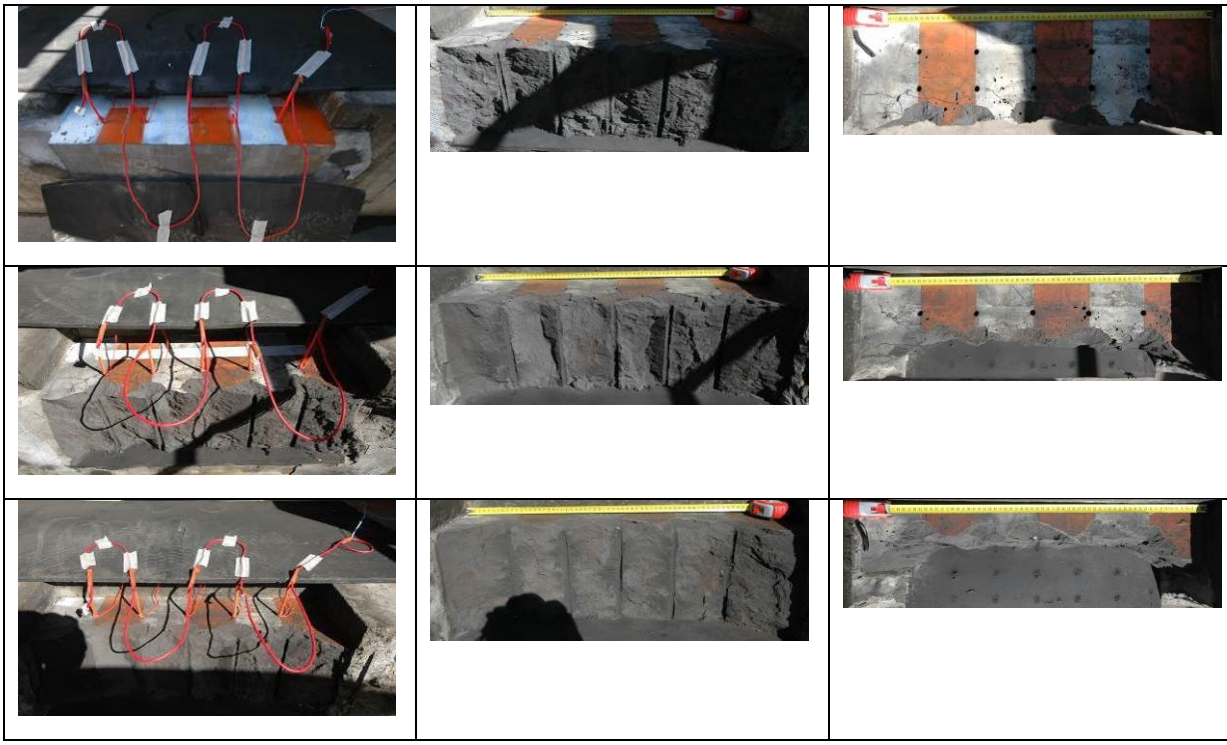

#0712: Row 1: 140 µs delay; Row 2: 28 µs delay; Row 3: 28 µs delay

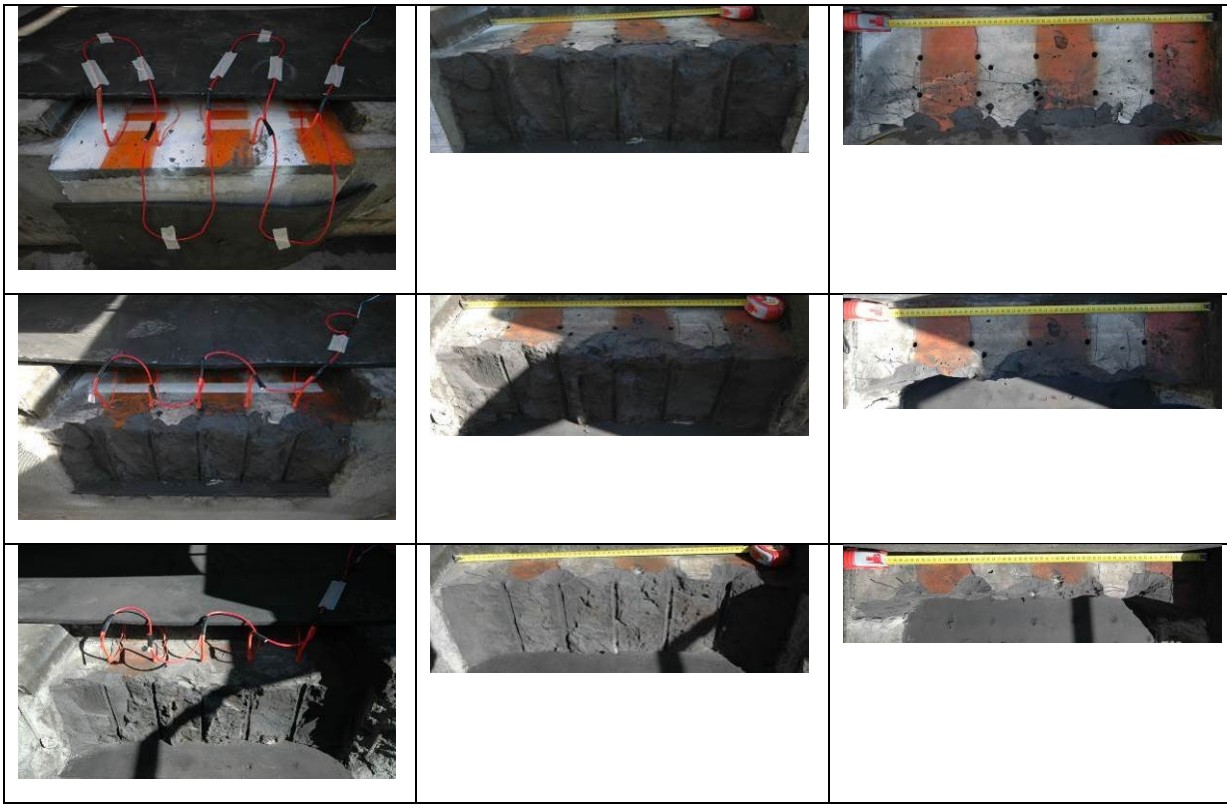

#0812: Row 1: 140 µs delay; Row 2: 0 µs delay; Row 3: 140 µs delay

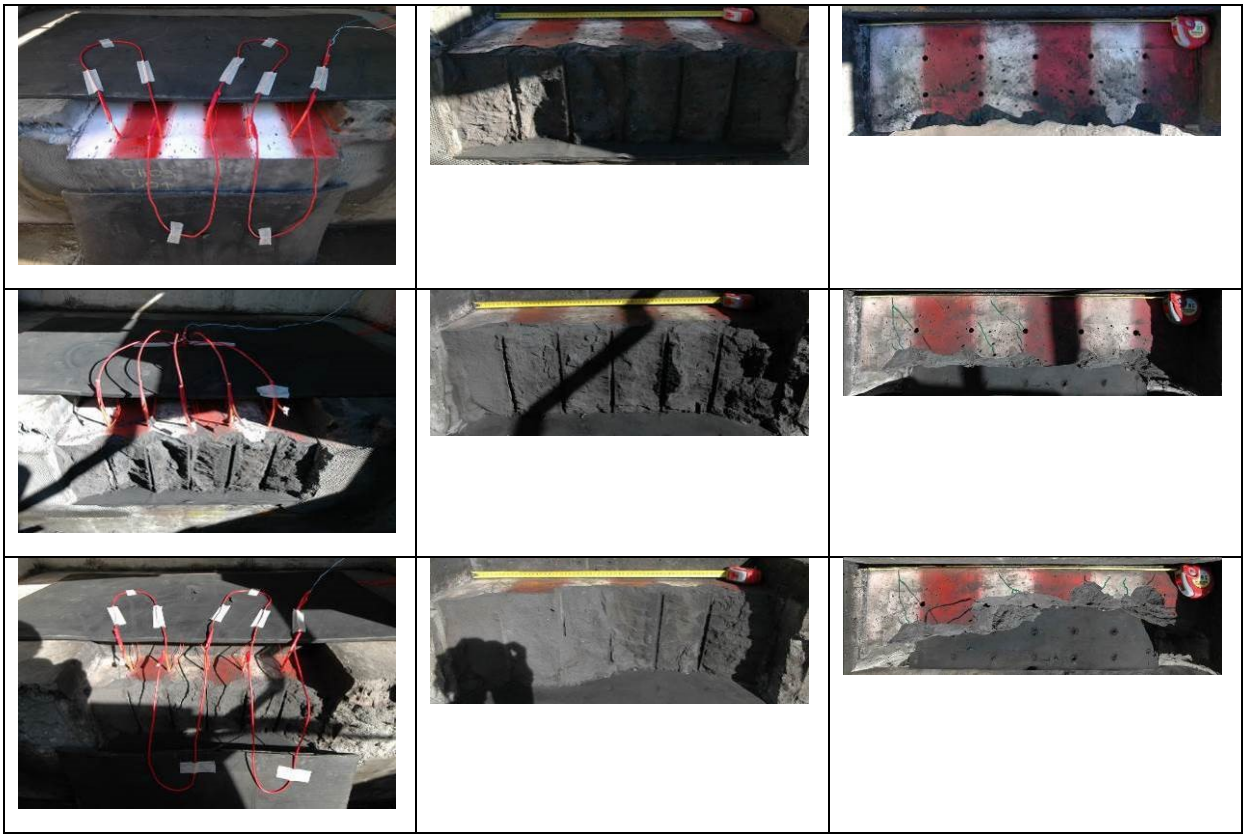

#0912: Row 1: 140 µs delay; Row 2: 140 µs delay; Row 3: 140 µs delay

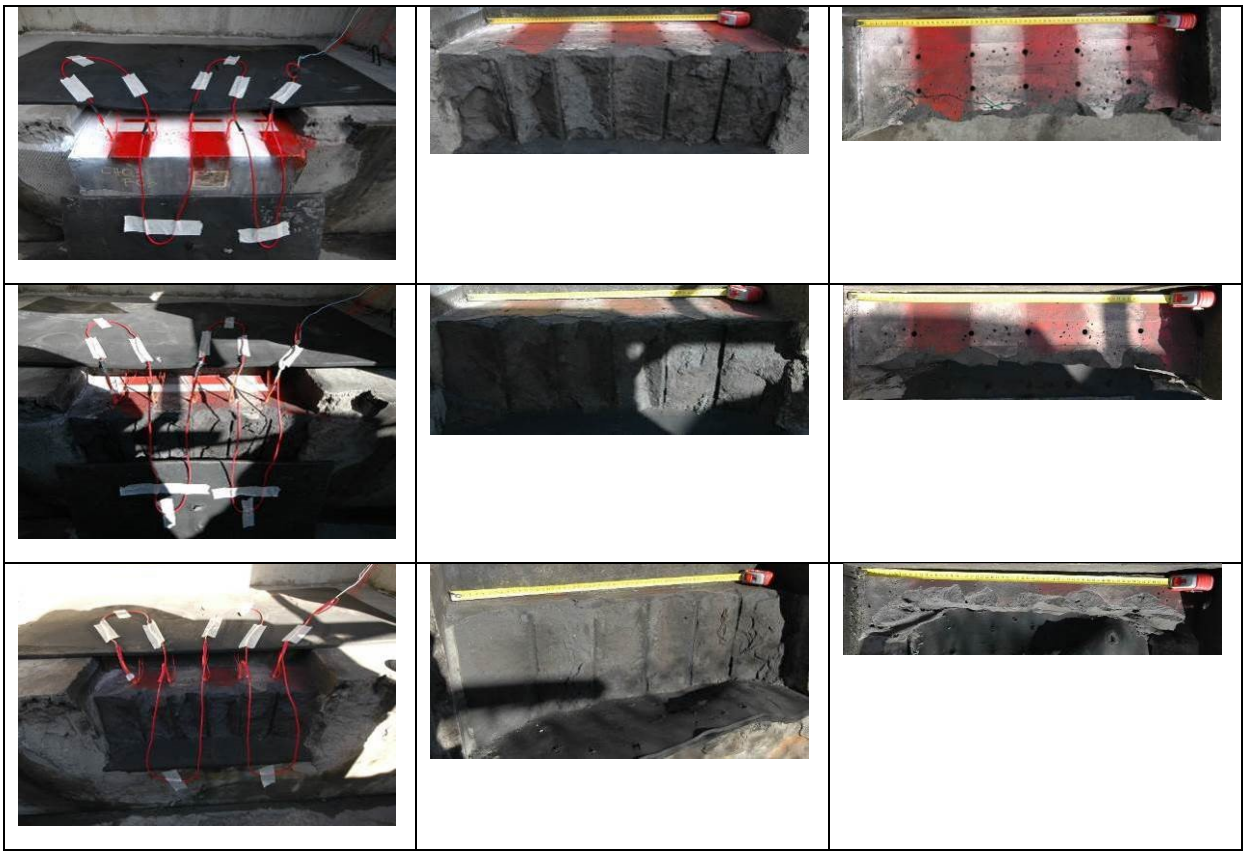

Appendix 7 – Documentation of Blasting Tests – Stage 2

#0113: Row 1: 0 µs delay; Row 2: 0 µs delay; Row 3: 0 µs delay

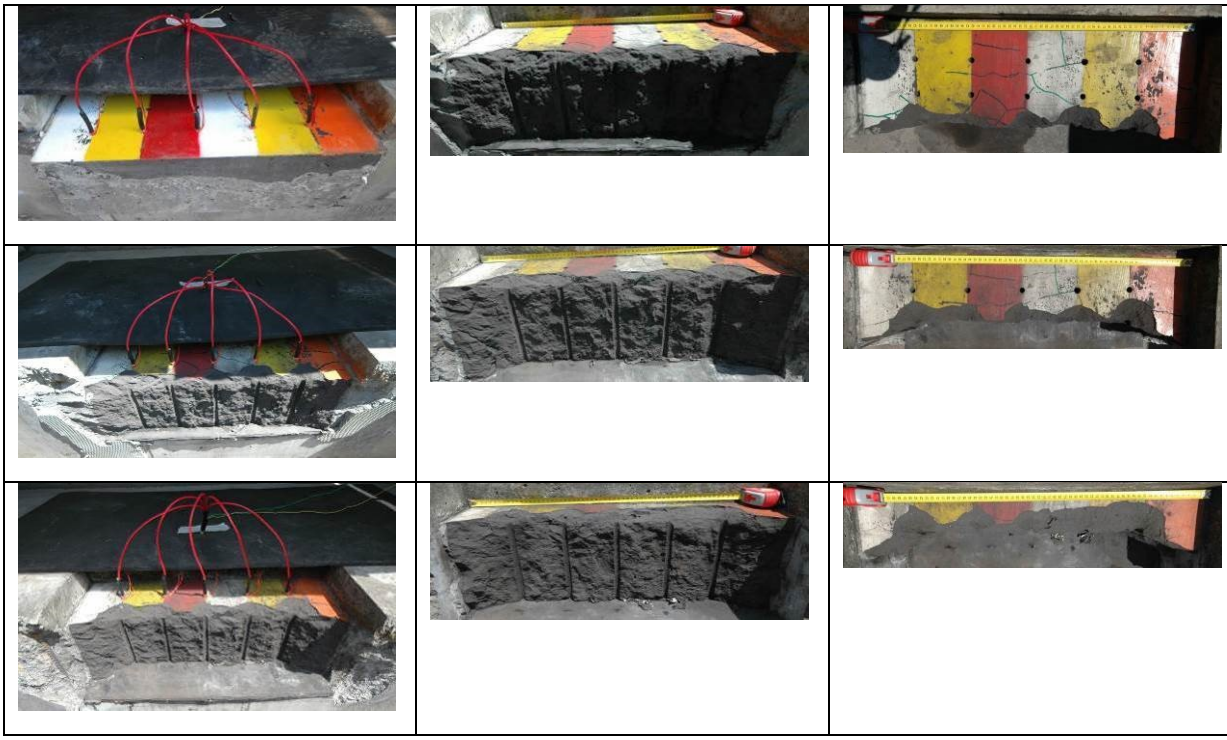

#0213: Row 1: 28 µs delay; Row 2: 28 µs delay; Row 3: 28 µs delay

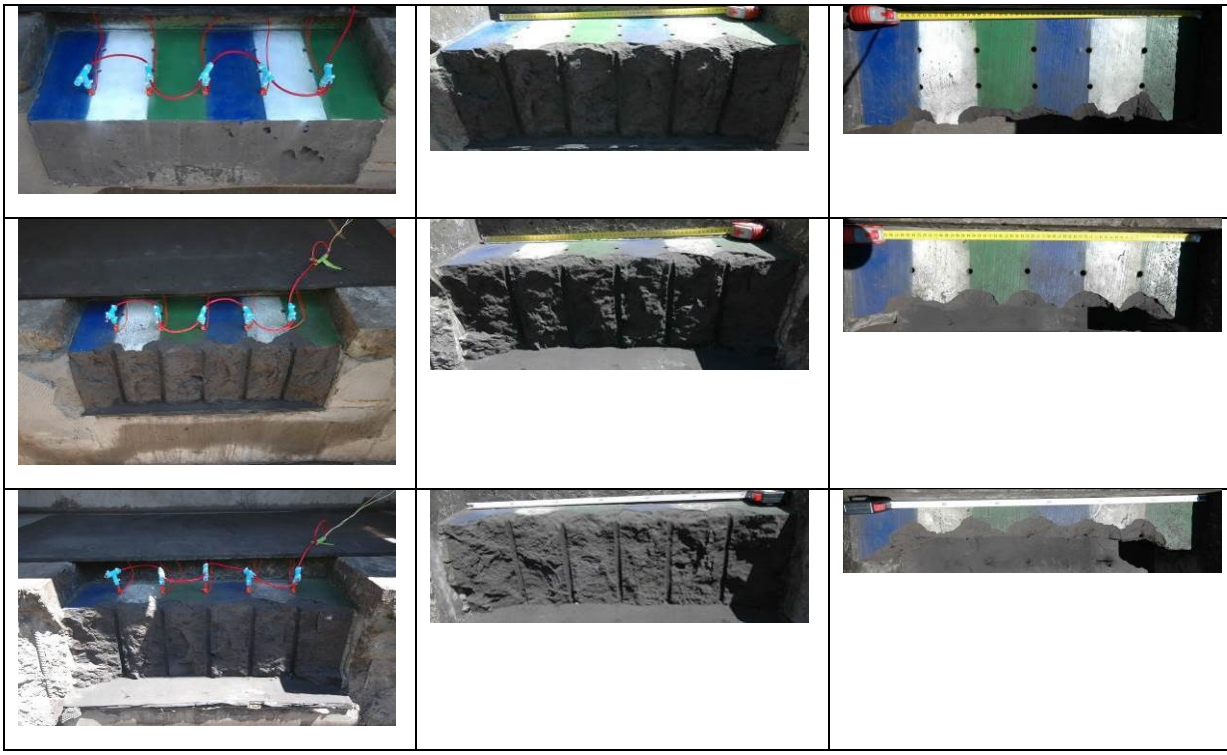

#0313: Row 1: 140 µs delay; Row 2: 0 µs delay; Row 3: 0 µs delay

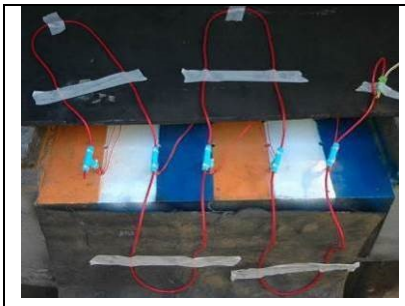

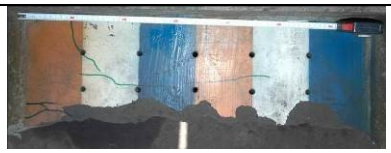
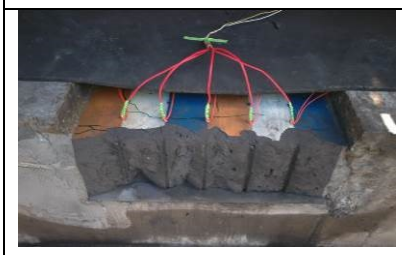

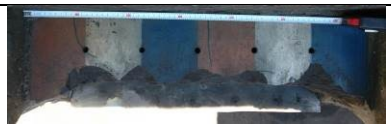
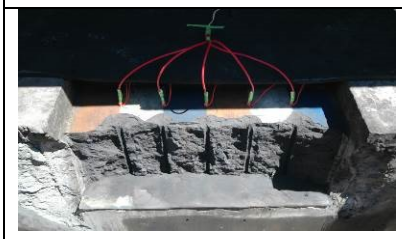

#0413: Row 1: 73 µs delay; Row 2: 73 µs delay; Row 3: 73 µs delay

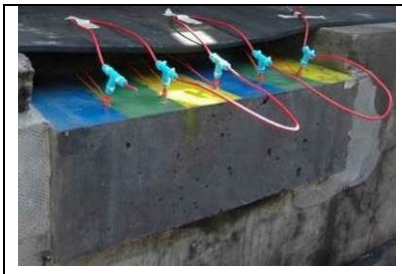


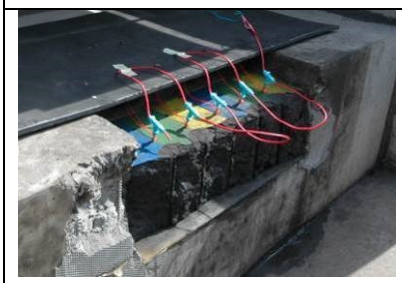


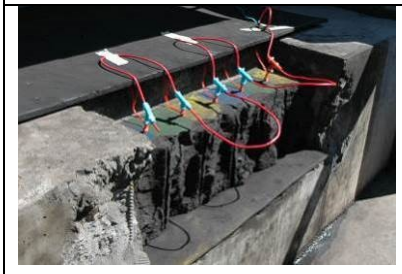
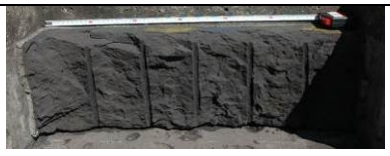


#0513: Row 1: 28 µs delay; Row 2: 140 µs delay




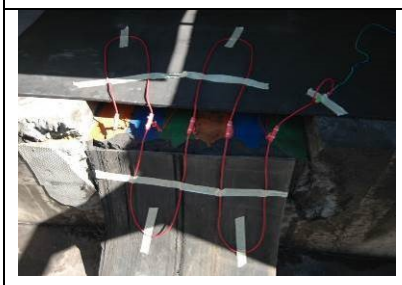

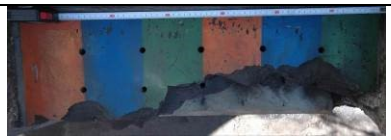

#0613: Row 1: 28 µs delay; Row 2: 0 µs delay; Row 3: 0 µs delay

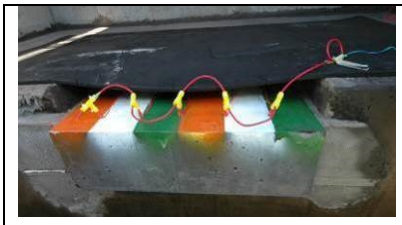


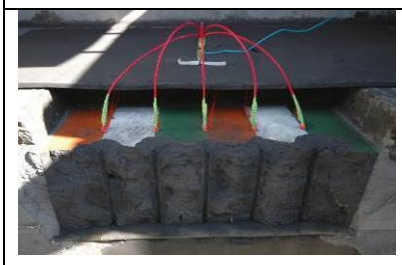
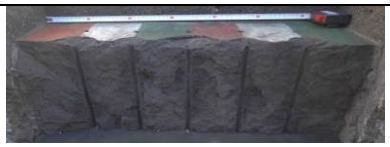



#0713: Row 1: 28 µs delay; Row 2: 73 µs delay; Row 3: 73 µs delay

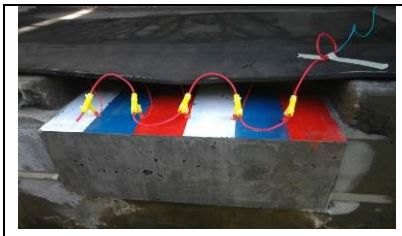		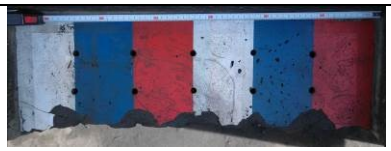
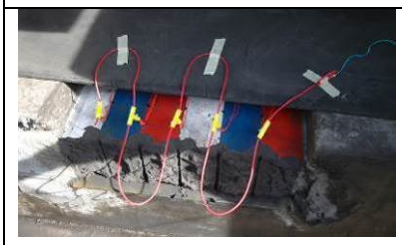	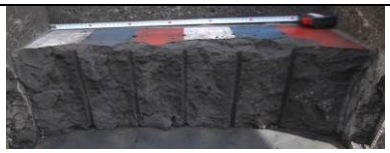	
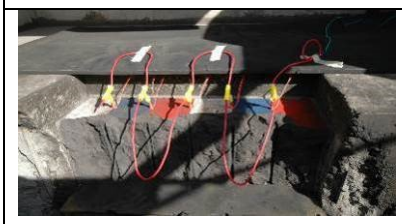	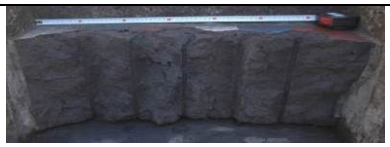	

Appendix 8 – Documentation of Blasting Tests – Stage 3

#0114: Row 1: 28 µs delay; Row 2: 28 µs delay; Row 3: 28 µs delay

#0214: Staggered Pattern

Row 1: 28 µs delay, Row 2: 28 µs delay, Row 3: 28 µs delay

#0314: Row 1: 28 µs delay; Row 2: 28 µs delay; Row 3: 28 µs delay; Row 4: 28 µs delay

#0414: Staggered Pattern

Row 1: 28 µs delay; Row 2: 28 µs delay; Row 3: 28 µs delay; Row 4: 28 µs delay

Appendix 9 – Methodology for Bench Surface Analysis

Source: Thomas SEIDL

1) Blast Metrix

- Generate 3D-model from images using Blast Metrix.
- Export surface model as .dxf for 3D analysis (used later)
- Create three sections (at 5cm, 10cm, and 15cm) and export contour as .dxf file for 2D-analysis.
- See Blast Metrix Manual for detailed information

2) Place drillhole reference in AutoCAD®

- Open contour.dxf
- If available for current drill pattern, copy & paste block template into contour file. Place template in x-y-plane using the left bottom front corner as centre of coordinate system. (x=0 ,y=0 ,z=0)
- A block template should consist of:
    - Planned drill grid
    - Circles (10mm diameter) representing the holes
    - Polyline connecting the centres of the circles (at z=0)

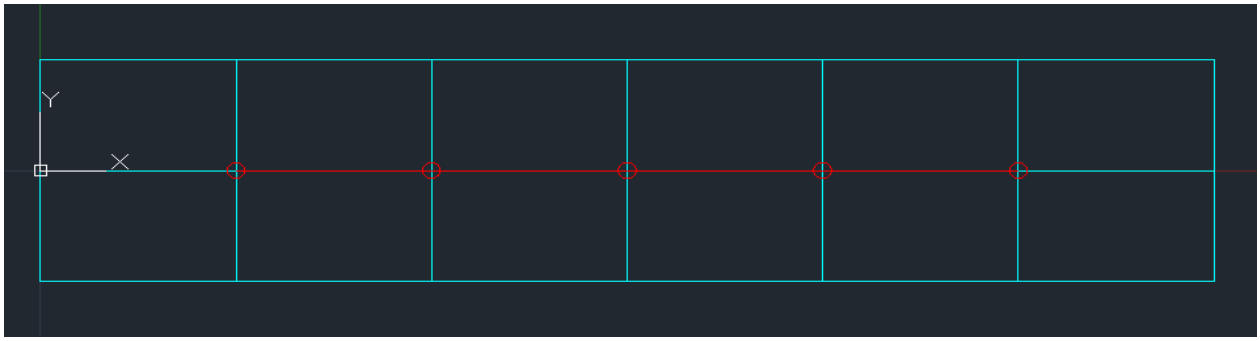

- Place drill holes on actual position, with regard to the half cast pattern in the contour line.
- Suggested workflow using a template (relevant tools marked):
    - Paste block template matching the block-coordinate system
    - Move contours, fitting at least one hole to its half cast
    - If required, rotate contours around matched hole (make sure to be in top-view)
    - If required, scale contours (NOTE: z-coordinates are affected as well)
    - If required, move single holes from the defined pattern to the actual position. Check image of block taken before blasting to identify inaccurate drill holes.
      Also move corresponding point of Polyline to new centre of drillhole.

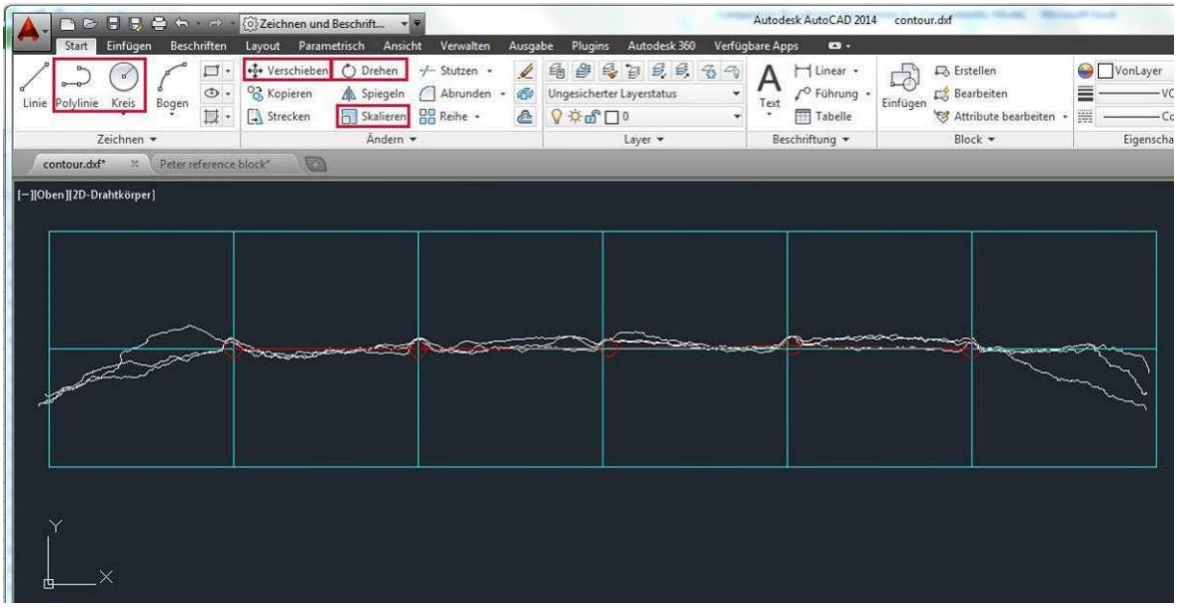

- Save as DWG-file
- Delete everything except drillhole-polyline and profiled and save as DXF-file
- Optional all rows of one block can be place in one DWG-file (recommended for blocks with irregular pattern). Create an individual DXF-file for each row. Use “delete” and “UnDo” to create the DXF files containing only profiles and drillhole-polyline.

3) Preparation of Data

Conversion of DXF-files to XYZ-files is done using the freeware tool “dxf2xyz” by “Guthrie CAD/GIS Software”

- Open dxf2xyz.exe
- Select files to be converted
- Save XYZ-file. Name is taken from original file, or can be specified using “Save As…”

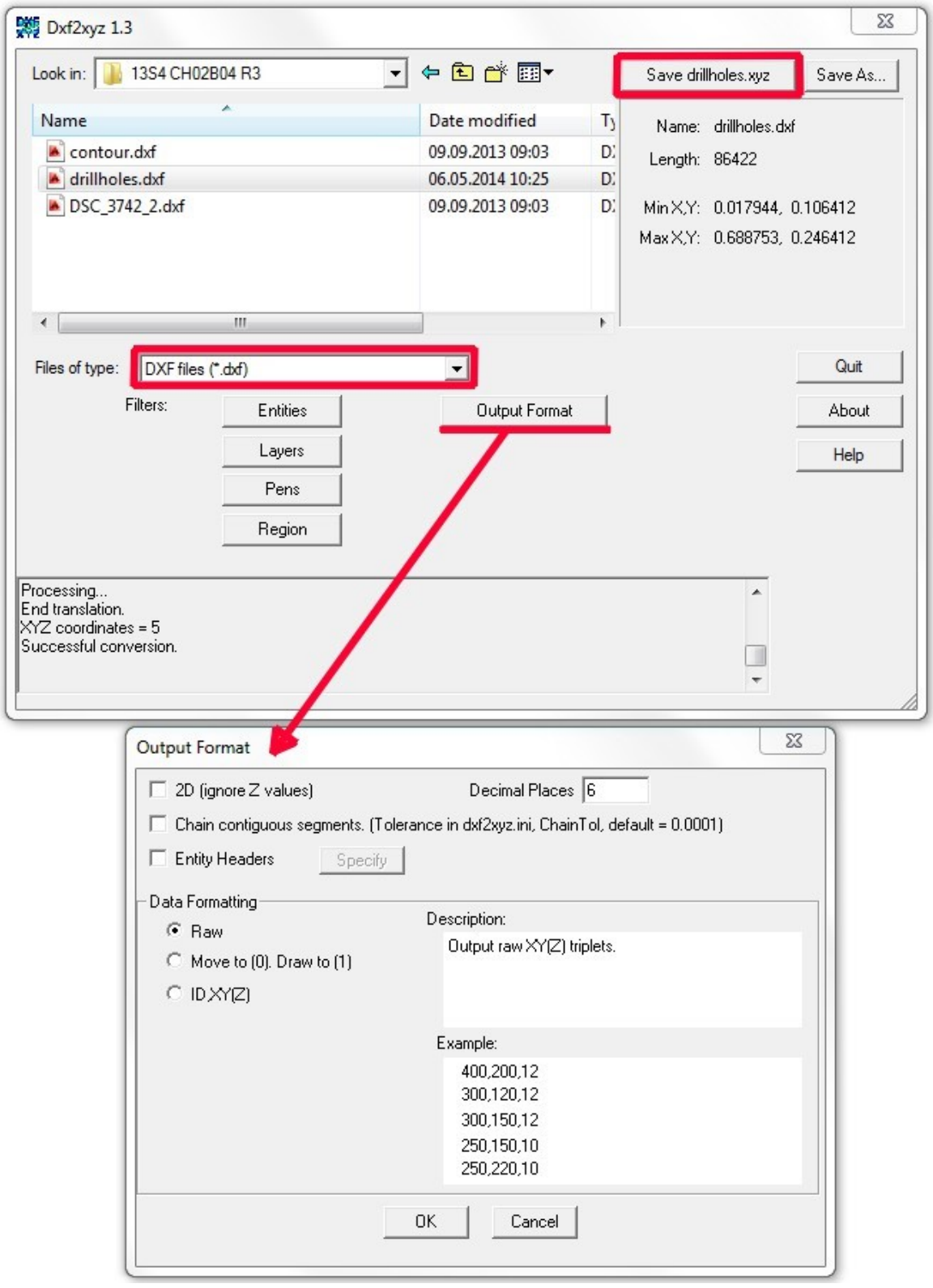

- Open new Excel file
- Open XYZ-file with “Editor”, “Notepad” or similar
- Copy all (Shortcuts: “Ctrl+A” + “Ctrl+C”)
- Paste data to Excel (“Ctrl+V”)
- Use function “Data” - “Text to Columns” with comma as delimiter when pasting (Sometimes the conversion to columns works directly when pasting the data, sometimes it has to be initiated manually)

- Split drill holes (z=0, mostly at top or bottom) from contour data (z≠0)
- Save Excel file
- NOTE: Points with z-coordinate other then 0.05, 0.10 or 0.15 can be deleted, but they can also remain as they are ignored by the processing algorithms anyway.
- NOTE: In case the contour data was scaled in AutoCAD®, the z-values are not exactly at 5cm intervals and would be ignored by the processing algorithms. Therefor the profiles need to be shifted using the “Find and Replace” function in Excel.

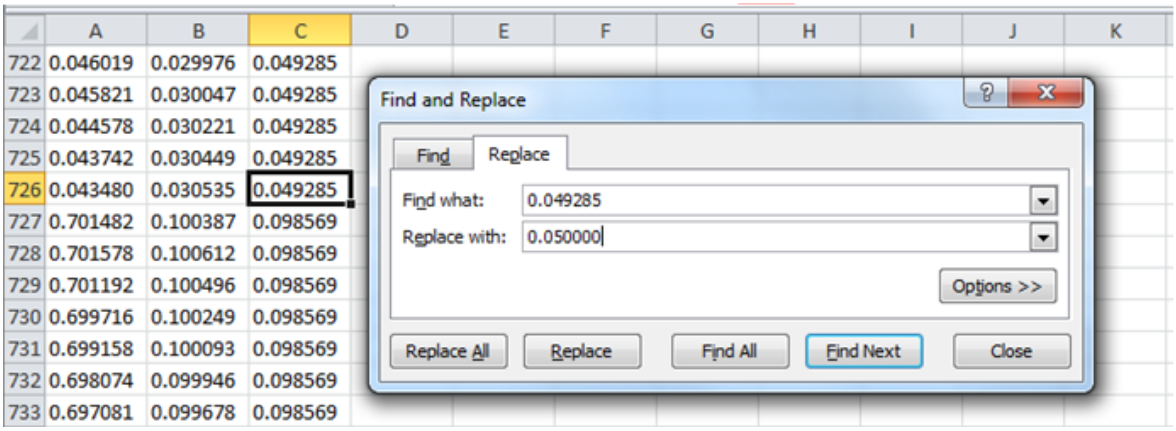

4) Short general introduction to MATLAB® GUI

[1] Path of current folder

[2] Content of current folder

[3] Preview of file or description of function

[4] Workspace (list of active variables)

[5] Variables editor (activated by double clicking of variable in workspace)

[6] Command window

[7] Command history

[red] Command buttons for workspace handling

- All MATLAB® files have to be in the Current folder. Its path is indicated (and can be changed) at [1], and its contents are listed in [2].
- This Manual is based on MATLAB® Version “R2013b”

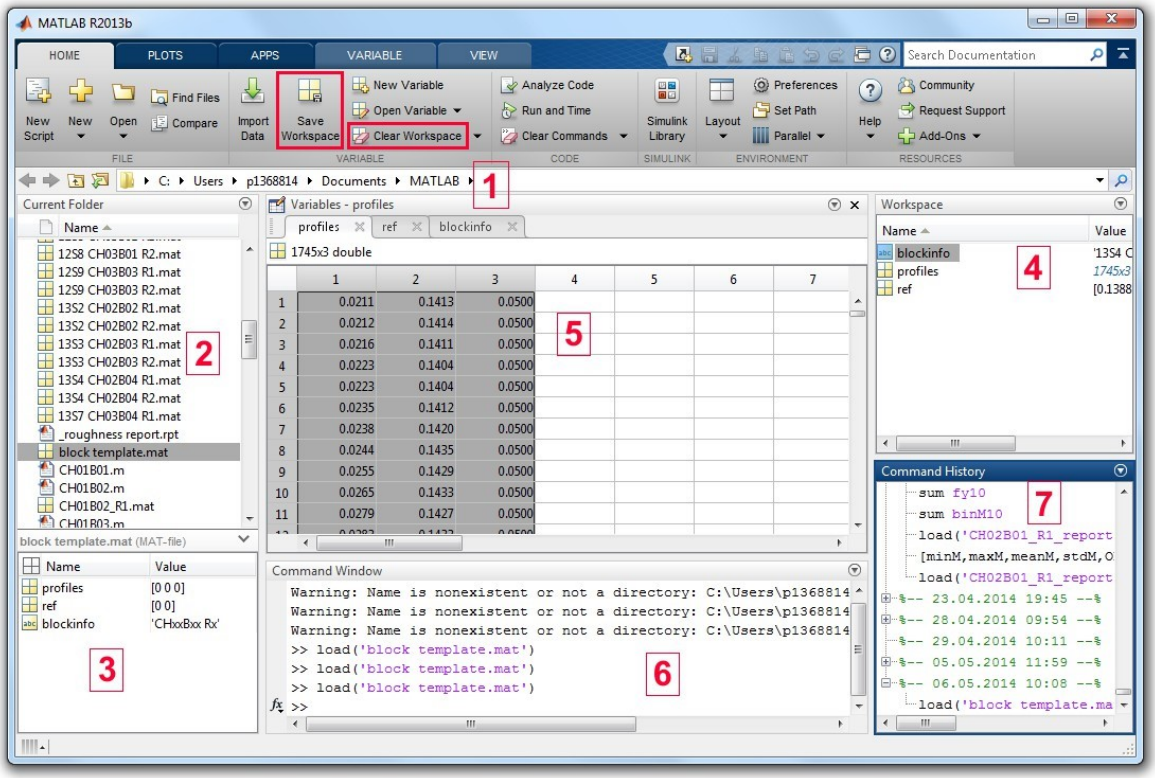

5) Report generation in MATLAB® (automated)

- Clear workspace first in case of existing variables
- Create variables “blockinfo”, “profiles” and “ref” for basic information in workspace. This task is performed when opening “block template.mat” NOTE: Names of variables have to be **exactly** like mentioned above
- Enter name of block and blasted row in “blockinfo”. This name will be displayed on the report and the graphs. Filename and saving location of the result files also use this name.
- Enter x, y, z coordinates into “profiles” (copy & paste from Excel file)
- Enter x, y coordinates of drill holes in “ref” (copy & paste from Excel file). Drill holes must be sorted ascending in x-direction
- Save workspace (recommendation: use same name as stored in “blockinfo”)

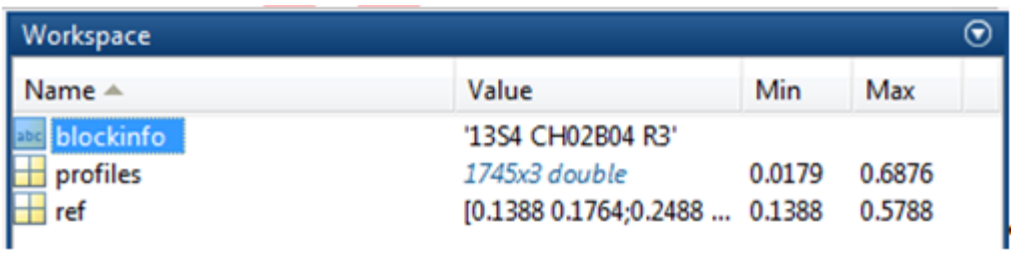

- Open “_roughness report.rpt” -> Report Explorer launches
- Run report generation by clicking the “flash”-symbol
- NOTE: all MATLAB® files have to be in current MATLAB® working directory (path [1])

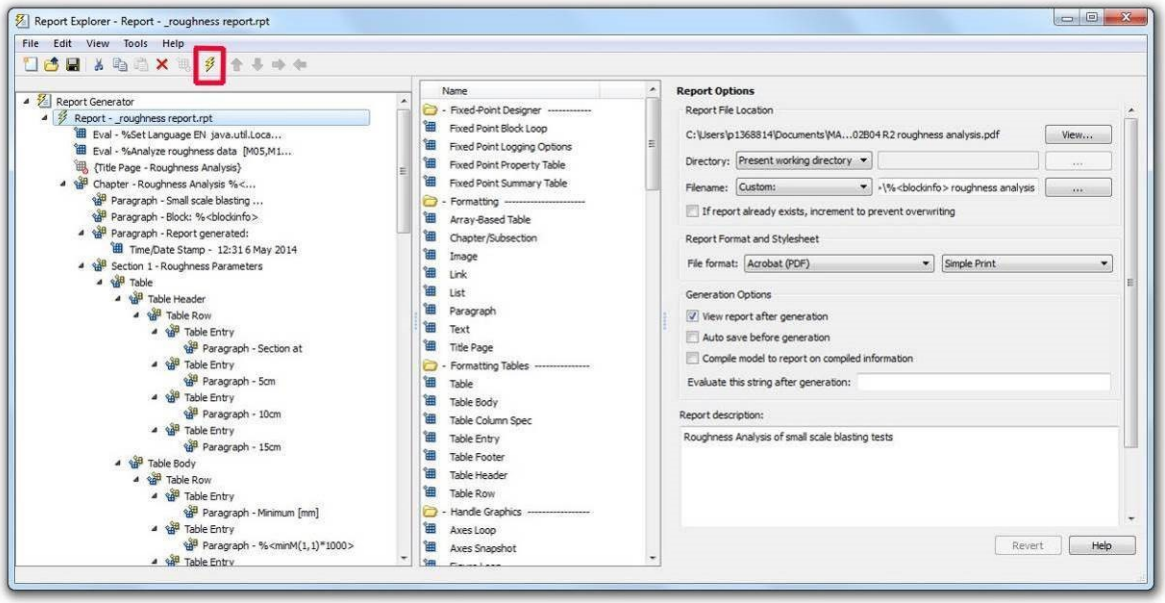

- The following tasks are performed by the report generator:
  - Analysis of the data and generation of graphs
  - Creation of folder named according to “blockinfo” for result files as a subdirectory of the current working directory
  - Saving of PDF report
  - Saving of graphs in PNG format
  - Creation of export-variable for further use of data in Excel
  - Saving of analysed workspace
- The data in the export-variable can now be copied into an Excel-file

  NOTE: “Use Text import wizard” in Excel and choose “Tab” as delimiter when pasting into Excel-sheet.

- The export variable contains 15x4 values (5, 10, 15 cm & combined), sorted as follows:
  - Number of Points [-]
  - Length of section [-]
  - Distance Minimum [mm]
  - Distance Maximum [mm]
  - Distance Mean [mm]
  - Distance Standard Deviation [mm]
  - Overbreak [mm²/mm]
  - Underbreak [mm²/mm]
  - Total Area [mm²/mm]
  - Area Replacement [mm²/mm]
  - Inclination Normalized [-]
  - Inclination Minimum [-]
  - Inclination Maximum [-]
  - Inclination Mean [-]
  - Inclination Standard Deviation [-]

6) *Histogram comparison from multiple rows*

- Open saved analysed workspace of first row to compare ("*blockname* analyzed**.mat**" in folder containing the pdf-report and saved histograms)
- Run "plothistocomparisonStart.m" to initiate plot and add first curve. Therefore type as follows in Command Window [6]:

```
plothistocomparisonStart(ME05,ME10,ME15,blockinfo);
```

- Load next analysed workspace and run "plothistocomparisonAdd.m":

```
plothistocomparisonAdd(ME05,ME10,ME15,blockinfo);
```

- Repeat previous step until second to last data set.
- Load last analysed workspace
- Run "plothistocomparisonFinish.m" to add last data set and save plot:

```
plothistocomparisonFinish(ME05,ME10,ME15,blockinfo);
```

- Desired formatting of plot (e.g. fixed range of axis) can be applied by adopting the code-section "complete plot" of "plothistocomparisonFinish.m". All available parameters are listed in the MATLAB® documentation of "plot" (2-D line plot).
- For comparison of 2 rows, only "Start" and "Finish" are required.
- NOTE: The created histograms are saved to the folder "Histogram Comparison" in the MATLAB® working directory. If this folder doesn't exist and problems occur while saving the histogram: create the folder manually.
- NOTE: The comparison code is programmed for 7 curves with individual colour for each (caused by 7 available colours in MATLAB®). The 8th curve will be black again, more than 8 curves are not possible and will cause an error.

Appendix 10 – Data Set from Bench Surface Analysis

Preliminary Tests

	Row	Delay	Points [-]				Length [mm]				D_{Mean} [mm]				S_{Norm} [-]			
	Nr.	[µs]	5 cm	10 cm	15 cm	comb.	5 cm	10 cm	15 cm	comb.	5 cm	10 cm	15 cm	comb.	5 cm	10 cm	15 cm	comb.
#0111	1	140	516	507	513	1536	438.37	438.30	437.29	1313.96	3.892	2.637	1.838	2.792	0.440	0.387	0.436	0.421
	2	140	328	354	356	1038	328.89	328.84	327.31	985.04	2.576	5.692	7.264	5.246	0.373	0.393	0.356	0.374
#0211	1	140	562	613	624	1799	568.60	568.22	568.64	1705.46	2.810	2.461	4.775	3.373	0.313	0.331	0.388	0.344
	2	140	544	562	581	1687	568.30	568.93	569.24	1706.46	4.555	1.520	0.079	2.002	0.407	0.409	0.449	0.422

Stage 1

	Row	Delay	Points [-]				Length [mm]				D_{Mean} [mm]				S_{Norm} [-]			
	Nr.	[µs]	5 cm	10 cm	15 cm	comb.	5 cm	10 cm	15 cm	comb.	5 cm	10 cm	15 cm	comb.	5 cm	10 cm	15 cm	comb.
#0212	1	140	539	580	571	1690	440.57	439.73	437.03	1317.33	5.350	2.380	4.048	3.891	0.315	0.282	0.324	0.307
	2	140	464	449	477	1390	437.84	436.21	438.80	1312.85	12.723	8.254	5.444	8.782	0.465	0.407	0.396	0.423
	3	140	399	398	398	1195	436.94	439.00	439.50	1315.44	0.355	2.306	5.322	2.659	0.428	0.374	0.407	0.403
#0312	1	140	542	584	606	1732	437.21	439.17	439.79	1316.16	5.505	5.485	4.921	5.294	0.360	0.390	0.362	0.371
	2	0	483	507	514	1504	438.06	438.92	438.48	1315.46	1.243	2.059	1.211	1.507	0.344	0.346	0.352	0.347
	3	0	406	455	452	1313	437.74	437.88	439.62	1315.24	1.062	0.160	2.310	1.179	0.357	0.416	0.344	0.372
#0412	1	140	585	586	605	1776	437.41	436.47	438.27	1312.15	4.079	5.335	3.415	4.268	0.399	0.389	0.353	0.380
	2	140	489	486	501	1476	439.56	434.84	437.80	1312.20	8.557	11.641	10.299	10.164	0.398	0.460	0.405	0.421
#0512	1	140	641	653	706	2000	435.81	436.18	435.83	1307.81	4.553	2.120	1.662	2.738	0.408	0.366	0.401	0.392
	2	0	476	484	464	1424	438.41	438.17	438.55	1315.13	1.008	-0.761	-0.396	-0.050	0.452	0.476	0.347	0.425
#0612	1	140	553	610	599	1762	437.52	438.42	438.48	1314.42	6.200	4.513	4.798	5.140	0.338	0.374	0.376	0.363
	2	73	534	553	568	1655	434.53	438.16	439.82	1312.51	4.890	8.216	6.886	6.686	0.453	0.438	0.446	0.446
	3	73	305	434	456	1195	291.49	437.89	434.40	1163.77	0.985	0.219	-0.068	0.305	0.339	0.359	0.405	0.371
#0712	1	140	602	613	654	1869	448.89	449.81	449.45	1348.15	4.975	3.071	2.265	3.402	0.396	0.365	0.379	0.380
	2	28	503	471	520	1494	439.25	438.94	440.26	1318.46	1.014	2.813	6.859	3.616	0.440	0.440	0.397	0.426
	3	28	479	485	455	1419	439.38	440.64	442.15	1322.17	-1.410	-0.529	-1.561	-1.157	0.402	0.440	0.383	0.408
#0812	1	140	514	541	580	1635	432.38	431.75	431.42	1295.54	7.502	5.706	3.919	5.637	0.404	0.388	0.413	0.402
	2	0	480	522	524	1526	437.80	436.76	436.77	1311.33	3.338	-0.819	0.185	0.833	0.389	0.423	0.394	0.402
#0912	1	140	571	587	600	1758	437.06	438.92	439.23	1315.21	5.148	6.005	5.355	5.505	0.448	0.506	0.404	0.453
	2	140	467	478	447	1392	439.16	437.44	438.40	1315.00	7.756	9.744	9.660	9.050	0.548	0.482	0.438	0.490

Stage 2

	Row	Delay	Points [-]				Length [mm]				D_{Mean} [mm]				S_{Norm} [-]			
	Nr.	[µs]	5 cm	10 cm	15 cm	comb.	5 cm	10 cm	15 cm	comb.	5 cm	10 cm	15 cm	comb.	5 cm	10 cm	15 cm	comb.
#0113	1	0	535	537	563	1635	445.03	444.23	444.52	1333.78	-0.510	0.486	1.217	0.412	0.347	0.344	0.319	0.337
	2	0	483	503	511	1497	441.53	442.41	442.42	1326.37	-0.611	0.851	1.801	0.704	0.325	0.354	0.317	0.332
	3	0	411	439	437	1287	443.02	443.12	439.12	1325.26	-0.678	1.462	1.226	0.698	0.389	0.372	0.332	0.365
#0213	1	28	531	518	563	1612	437.48	438.86	439.56	1315.89	-1.324	0.216	-0.250	-0.454	0.413	0.540	0.417	0.457
	2	28	413	464	496	1373	438.74	437.84	436.02	1312.59	1.181	2.277	4.391	2.711	0.314	0.376	0.344	0.345
	3	28	442	447	468	1357	440.22	441.85	442.55	1324.62	0.305	0.377	1.199	0.637	0.403	0.431	0.411	0.415
#0313	1	140	543	559	587	1689	437.08	434.70	438.55	1310.33	8.548	6.284	6.771	7.181	0.443	0.380	0.466	0.430
	2	0	453	469	500	1422	439.16	438.43	437.96	1315.55	4.100	5.058	5.274	4.829	0.352	0.363	0.373	0.363
	3	0	406	397	408	1211	442.38	440.53	440.76	1323.67	0.265	0.929	1.400	0.865	0.372	0.387	0.370	0.376
#0413	1	73	559	605	591	1755	436.67	439.48	439.30	1315.45	3.937	6.008	5.999	5.346	0.350	0.411	0.367	0.376
	2	73	443	450	459	1352	438.12	438.94	436.03	1313.09	6.070	7.993	5.271	6.439	0.520	0.515	0.459	0.498
	3	73	403	416	395	1214	438.99	439.36	438.12	1316.47	5.784	3.336	4.580	4.554	0.341	0.429	0.354	0.375
#0513	1	28	482	567	555	1604	439.50	438.14	437.54	1315.17	0.570	2.379	1.717	1.606	0.285	0.269	0.272	0.275
#0613	1	28	591	586	632	1809	439.51	439.45	439.63	1318.59	-2.479	1.867	2.184	0.558	0.384	0.355	0.401	0.380
	2	0	517	561	579	1657	440.52	440.84	439.33	1320.69	1.129	2.672	3.255	2.394	0.330	0.330	0.298	0.319
	3	0	447	468	509	1424	437.52	438.60	436.02	1312.14	1.729	3.019	5.848	3.625	0.293	0.314	0.300	0.302
#0713	1	28	562	548	612	1722	439.57	436.64	438.60	1314.81	0.373	4.756	4.768	3.330	0.306	0.293	0.280	0.293
	2	73	502	543	570	1615	439.62	433.43	438.82	1311.87	7.258	7.168	5.491	6.604	0.325	0.363	0.339	0.342
	3	73	418	436	476	1330	436.24	434.26	437.21	1307.70	1.346	7.371	9.232	6.143	0.346	0.351	0.345	0.347

Stage 3

	Row	Delay	Points [-]				Length [mm]				D_{Mean} [mm]				S_{Norm} [-]			
	Nr.	[µs]	5 cm	10 cm	15 cm	comb.	5 cm	10 cm	15 cm	comb.	5 cm	10 cm	15 cm	comb.	5 cm	10 cm	15 cm	comb.
#0114	1	28	769	767	796	2332	444.68	446.87	446.49	1338.04	2.072	2.663	-0.279	1.464	0.300	0.320	0.333	0.318
	2	28	688	726	745	2159	441.61	441.80	440.89	1324.30	0.935	0.869	0.229	0.669	0.362	0.319	0.393	0.358
	3	28	510	504	541	1555	434.29	433.45	435.17	1302.91	1.694	3.324	2.254	2.417	0.279	0.262	0.322	0.288
#0214	1	28	793	851	898	2542	439.24	439.26	438.49	1316.98	-1.018	-1.628	0.080	-0.834	0.373	0.387	0.327	0.362
	2	28	707	727	743	2177	436.00	430.23	437.13	1303.36	0.280	0.969	1.944	1.078	0.398	0.407	0.387	0.397
	3	28	657	667	690	2014	442.83	442.89	442.68	1328.41	0.054	0.779	1.296	0.720	0.345	0.374	0.405	0.375
#0314	1	28	545	573	608	1726	439.64	439.71	440.34	1319.69	-3.679	0.319	3.076	0.028	0.354	0.342	0.353	0.350
	2	28	487	507	538	1532	439.40	443.50	443.53	1326.43	-2.189	0.581	2.471	0.364	0.344	0.382	0.339	0.355
	3	28	410	417	435	1262	437.78	439.45	438.94	1316.18	-1.111	-0.393	1.103	-0.111	0.402	0.368	0.339	0.369
	4	28	372	407	406	1185	442.22	445.26	447.26	1334.74	0.649	0.374	0.003	0.333	0.359	0.353	0.405	0.373
#0414	1	28	523	542	573	1638	447.58	445.27	446.10	1338.94	0.081	1.889	-0.116	0.611	0.388	0.352	0.357	0.366
	2	28	482	506	545	1533	440.77	441.37	438.77	1320.91	0.372	-0.624	1.351	0.391	0.408	0.420	0.439	0.422
	3	28	425	414	441	1280	443.14	443.23	442.99	1329.35	2.938	-0.385	-1.667	0.276	0.434	0.420	0.427	0.427
	4	28	367	363	369	1099	442.25	442.86	443.95	1329.07	2.650	0.936	-0.778	0.933	0.436	0.389	0.374	0.400

Appendix 11 – Diagrams from Bench Surface Analysis

Preliminary Tests

#0111

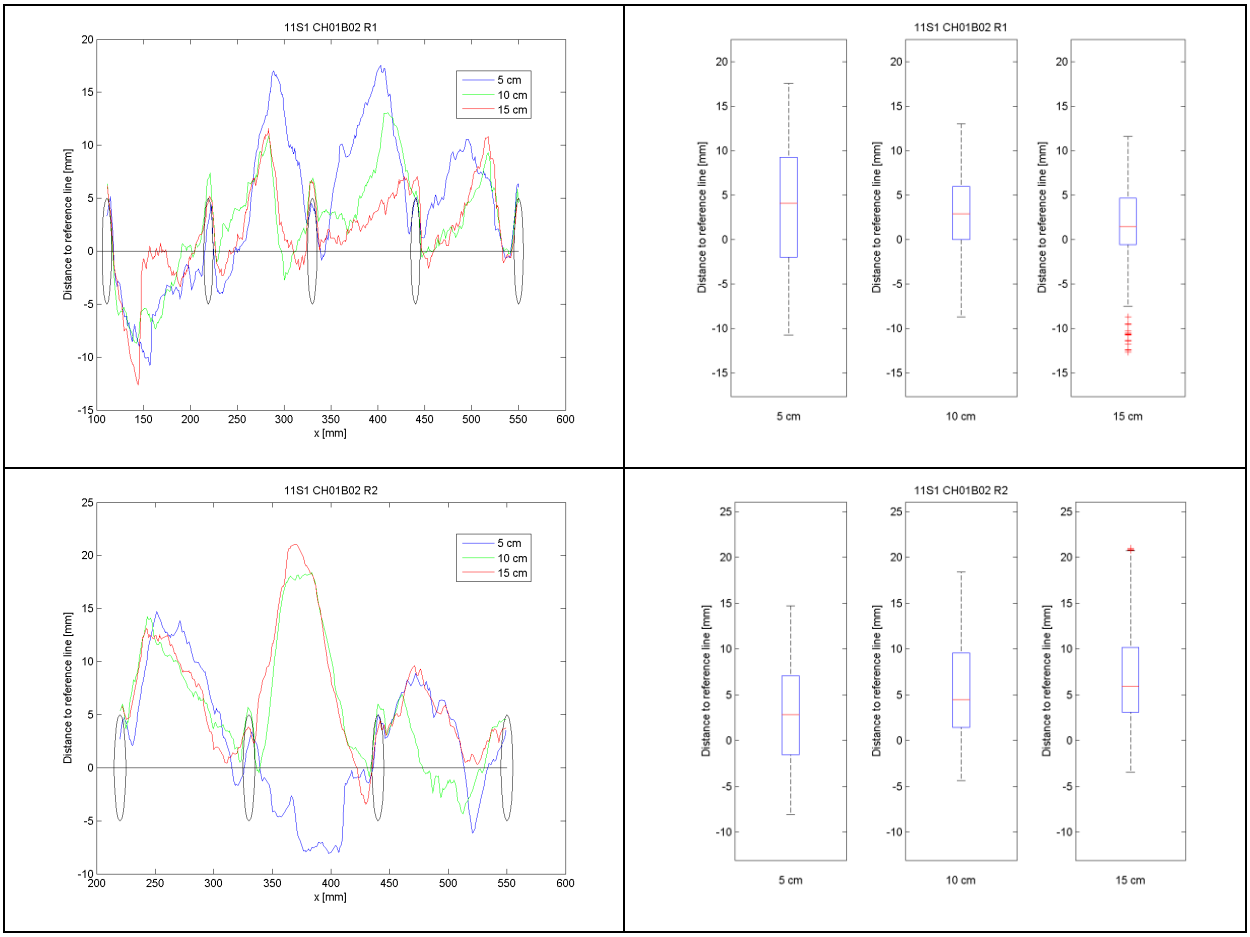

#0211

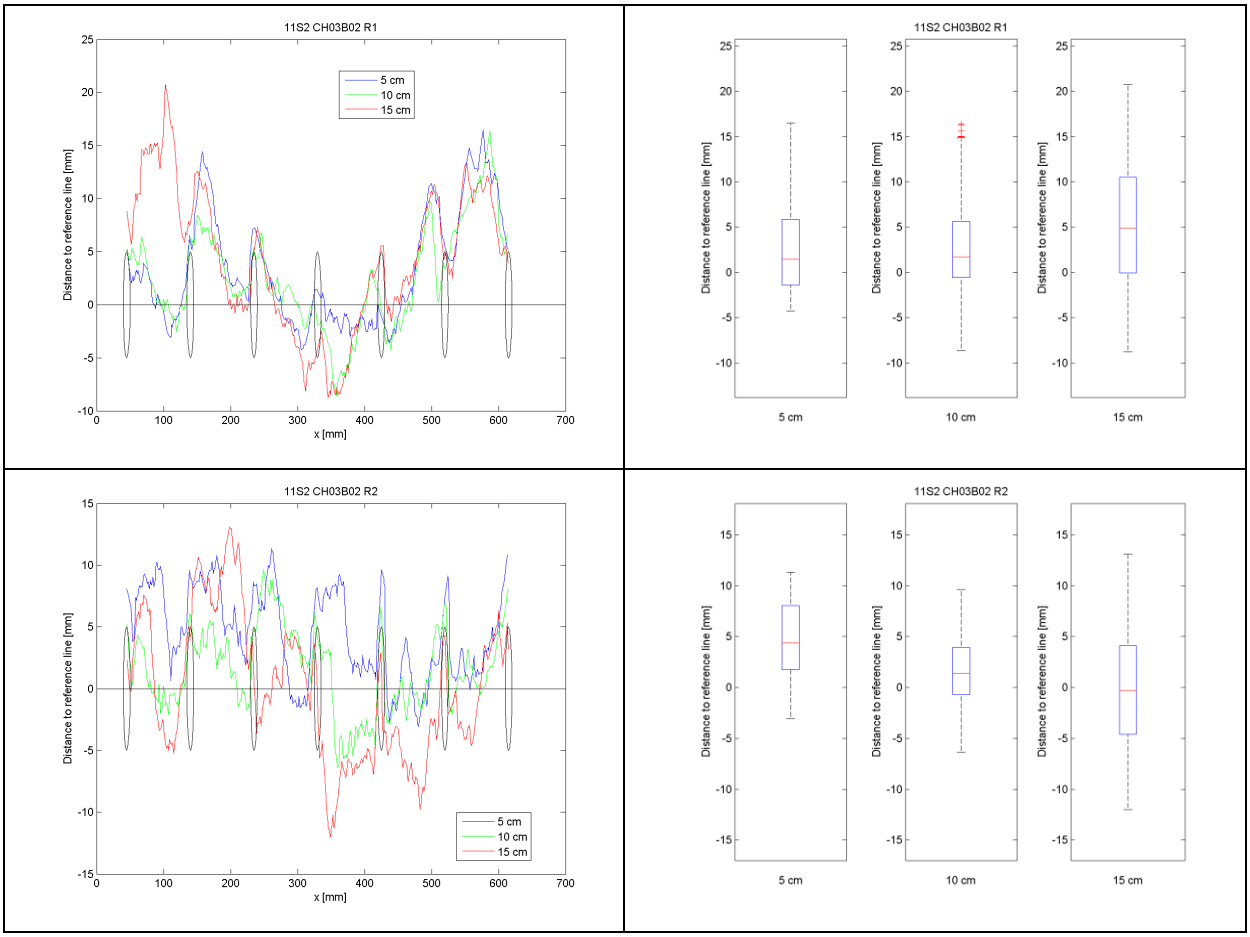
11S2 CH03B02 R1
5 cm
10 cm
15 cm
Distance to reference line [mm]
x [mm]
11S2 CH03B02 R1
Distance to reference line [mm]
5 cm
10 cm
15 cm
11S2 CH03B02 R2
Distance to reference line [mm]
x [mm]
5 cm
10 cm
15 cm
11S2 CH03B02 R2
Distance to reference line [mm]
5 cm
10 cm
15 cm

Stage 1

#0212

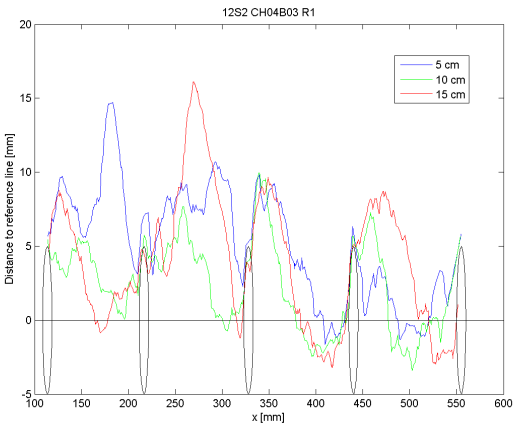
12S2 CH04B03 R1
5 cm
10 cm
15 cm
Distance to reference line [mm]
x [mm]

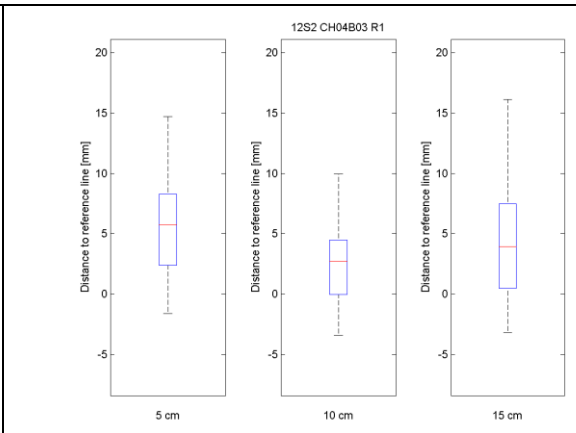
12S2 CH04B03 R1
Distance to reference line [mm]
5 cm
10 cm
15 cm

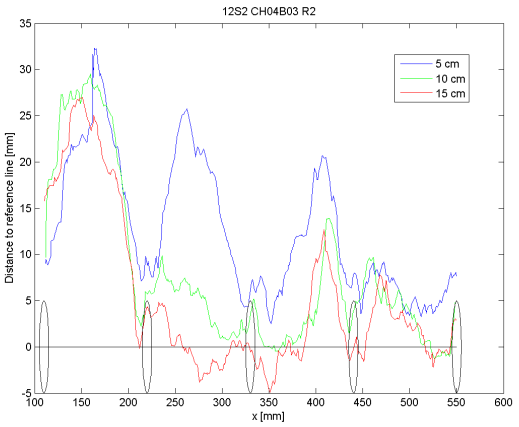
12S2 CH04B03 R2
5 cm
10 cm
15 cm
Distance to reference line [mm]
x [mm]

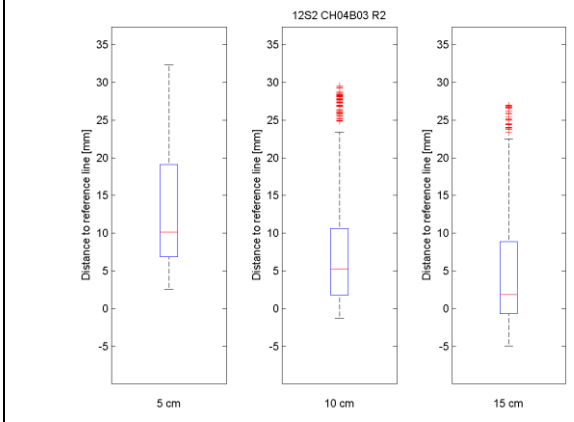
12S2 CH04B03 R2
Distance to reference line [mm]
5 cm
10 cm
15 cm

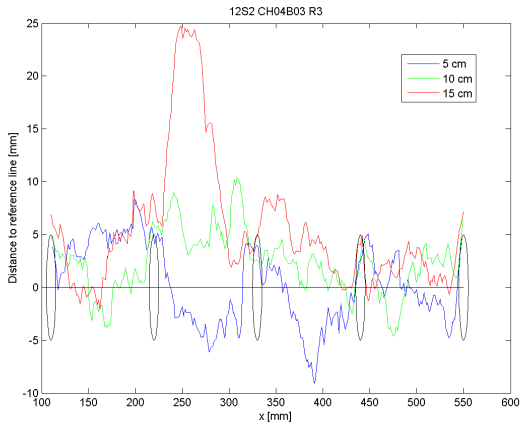
12S2 CH04B03 R3
5 cm
10 cm
15 cm
Distance to reference line [mm]
x [mm]

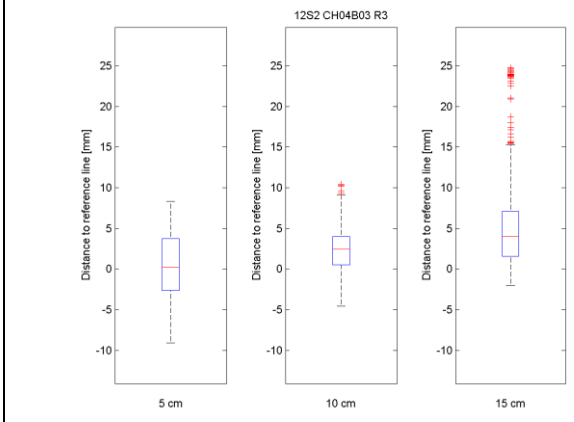
12S2 CH04B03 R3
Distance to reference line [mm]
5 cm
10 cm
15 cm

#0312

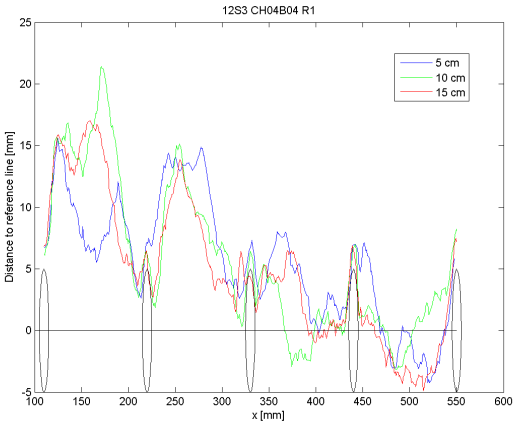
12S3 CH04B04 R1
5 cm
10 cm
15 cm
Distance to reference line [mm]
x [mm]

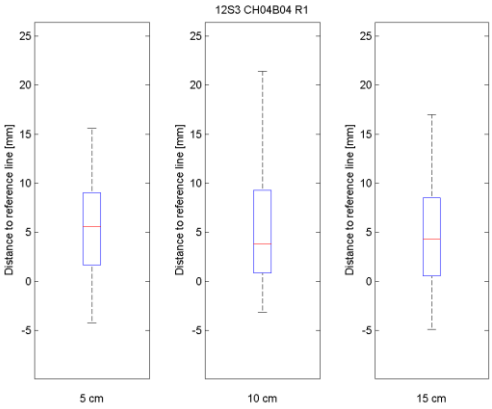
12S3 CH04B04 R1
Distance to reference line [mm]
5 cm
10 cm
15 cm

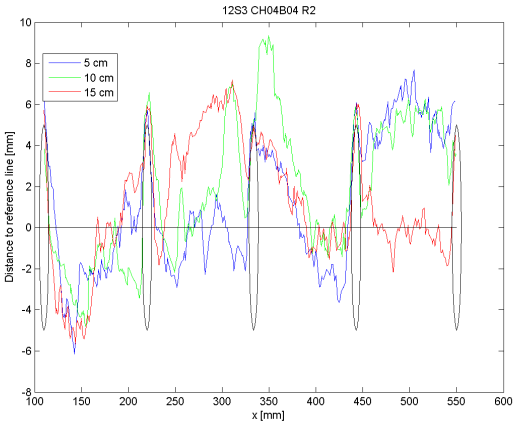
12S3 CH04B04 R2
5 cm
10 cm
15 cm
Distance to reference line [mm]
x [mm]

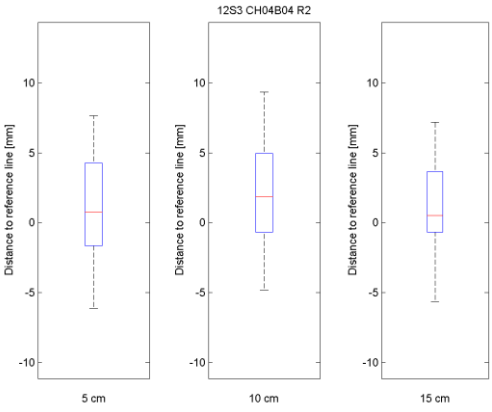
12S3 CH04B04 R2
Distance to reference line [mm]
5 cm
10 cm
15 cm

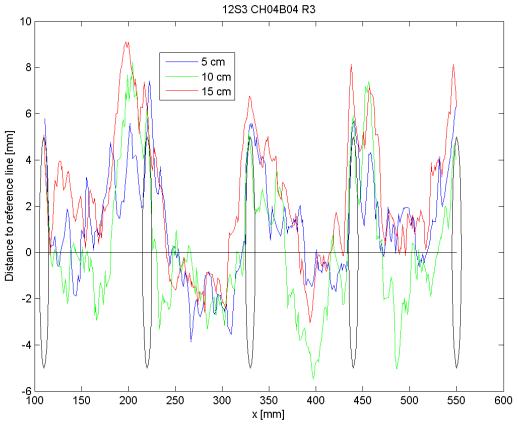
12S3 CH04B04 R3
5 cm
10 cm
15 cm
Distance to reference line [mm]
x [mm]

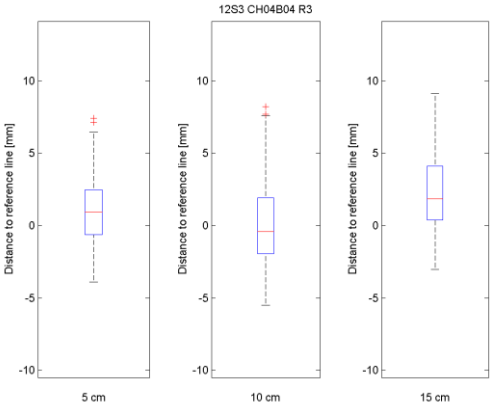
12S3 CH04B04 R3
Distance to reference line [mm]
5 cm
10 cm
15 cm

#0412

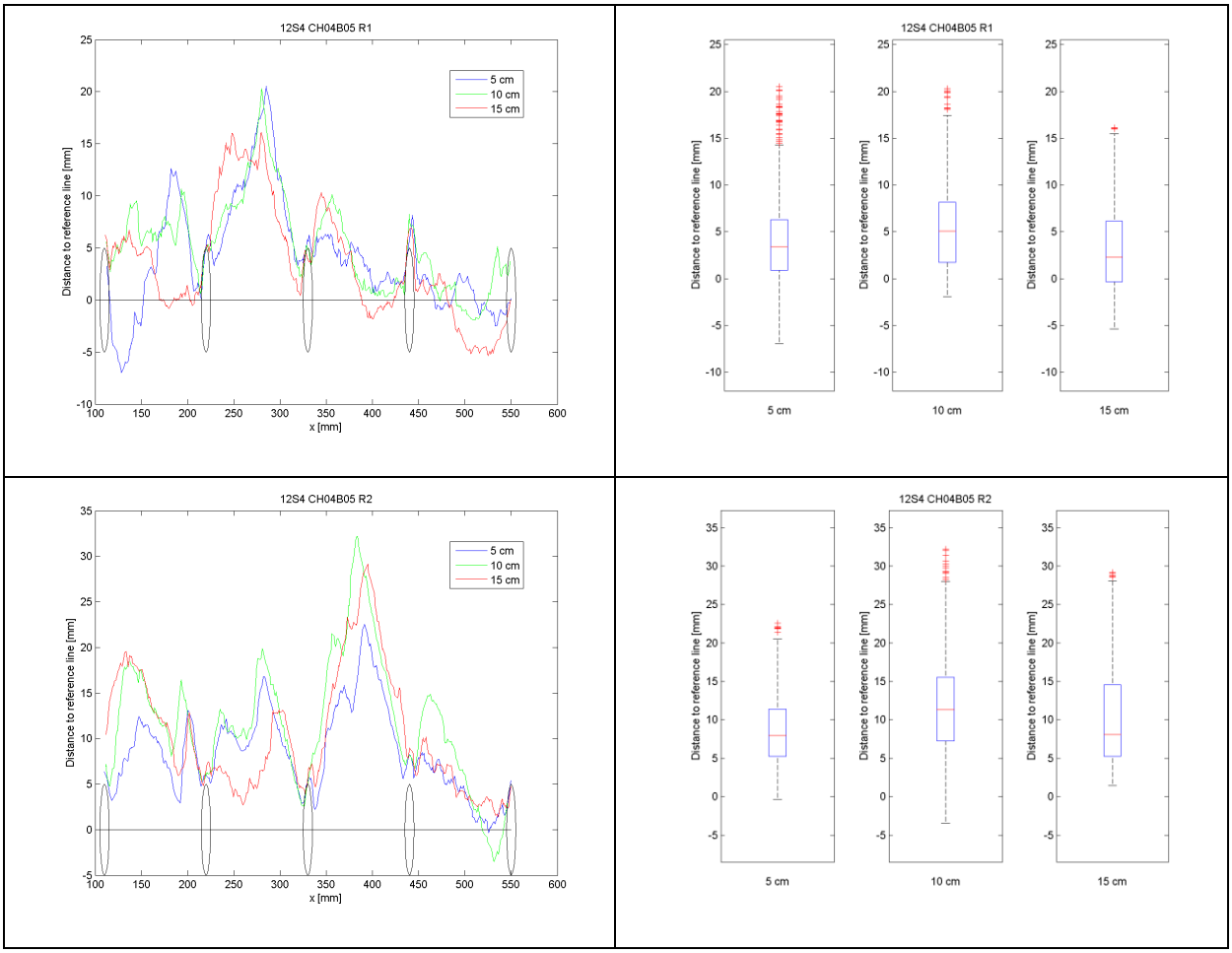
12S4 CH04B05 R1
5 cm
10 cm
15 cm
Distance to reference line [mm]
x [mm]
12S4 CH04B05 R1
Distance to reference line [mm]
5 cm
10 cm
15 cm
12S4 CH04B05 R2
5 cm
10 cm
15 cm
Distance to reference line [mm]
x [mm]
12S4 CH04B05 R2
Distance to reference line [mm]
5 cm
10 cm
15 cm

#0512

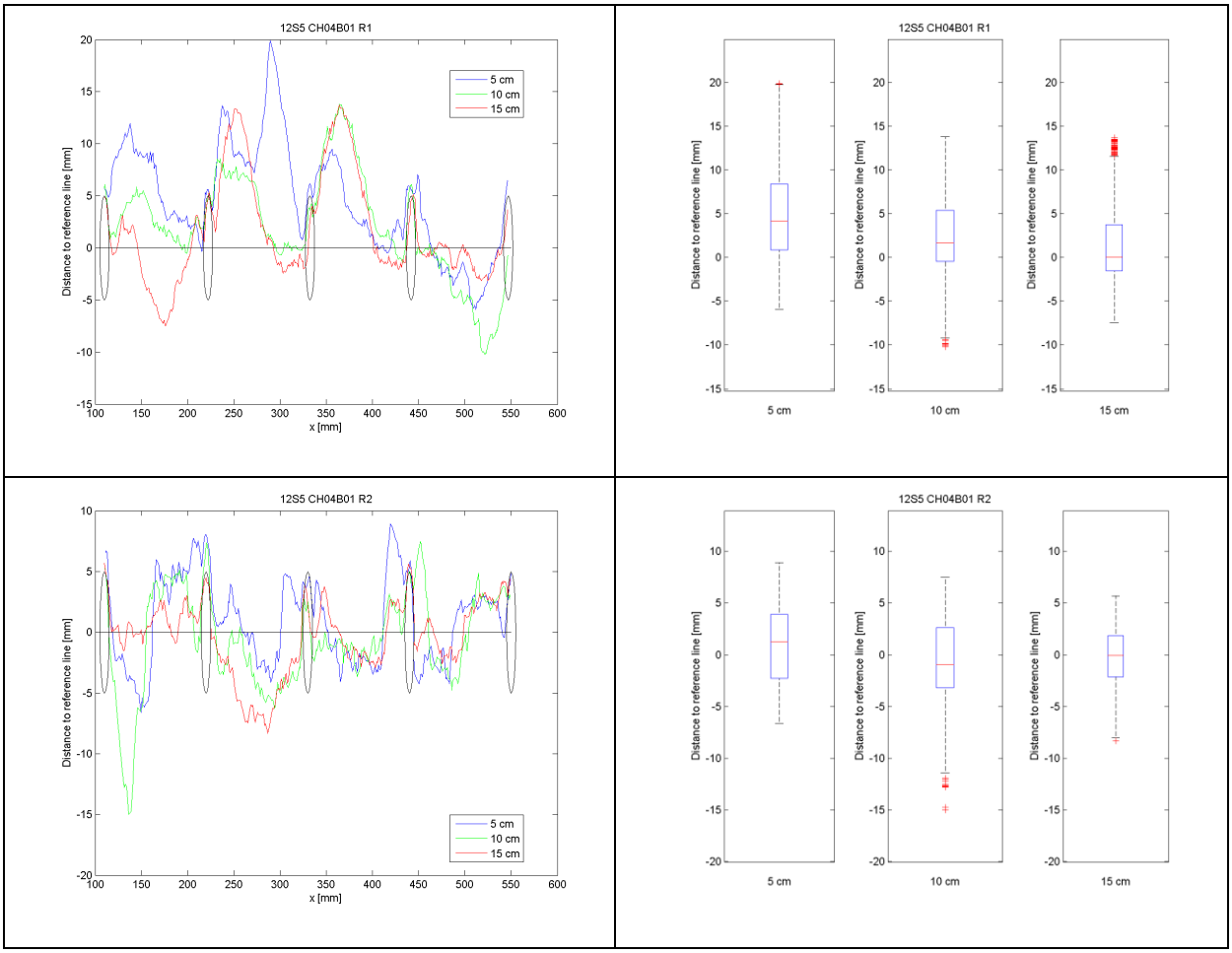
12S5 CH04B01 R1
Distance to reference line [mm]
x [mm]
5 cm
10 cm
15 cm
12S5 CH04B01 R1
Distance to reference line [mm]
5 cm
10 cm
15 cm
12S5 CH04B01 R2
Distance to reference line [mm]
x [mm]
5 cm
10 cm
15 cm
12S5 CH04B01 R2
Distance to reference line [mm]
5 cm
10 cm
15 cm

#0612

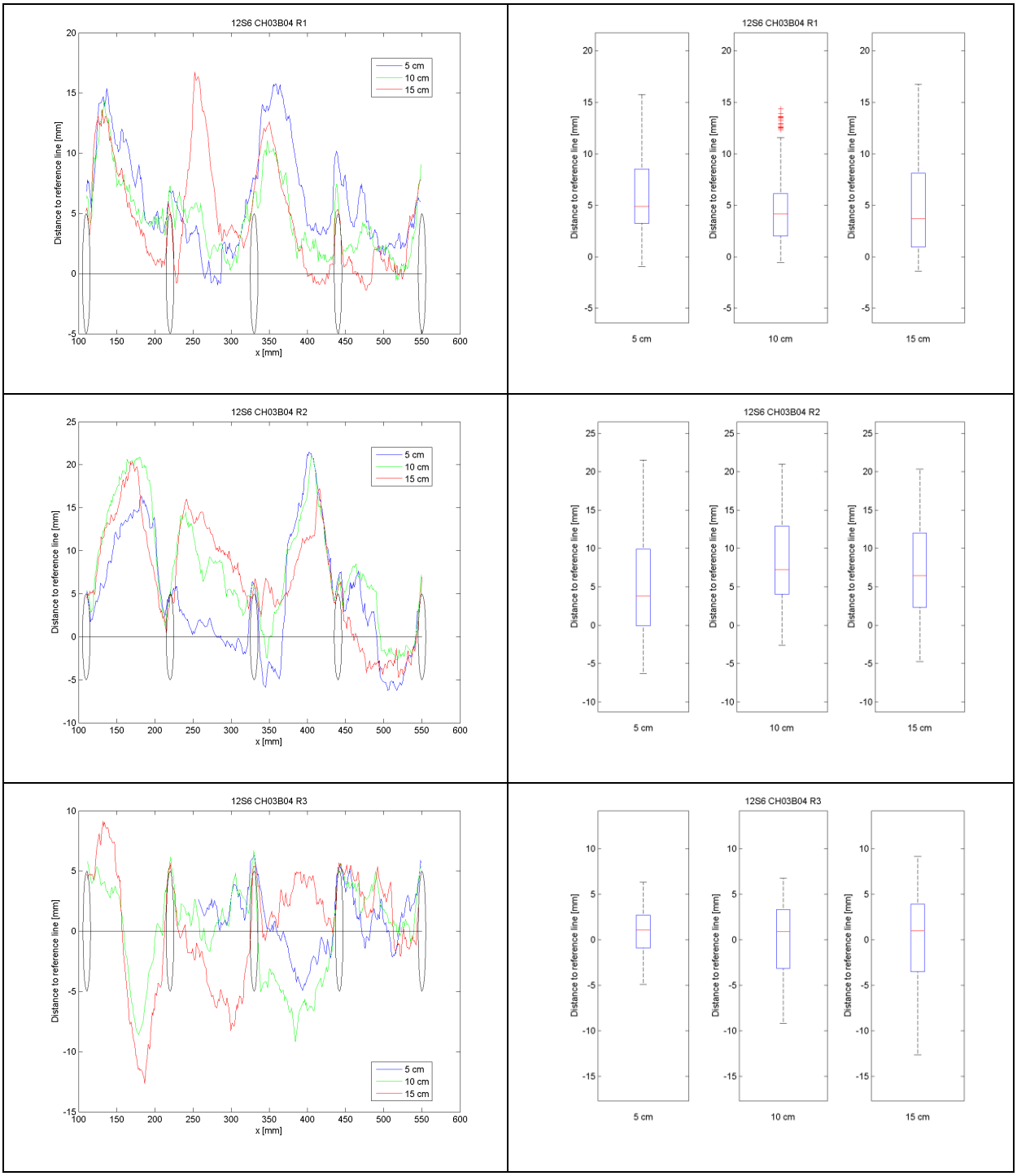
12S6 CH03B04 R1
Distance to reference line [mm]
x [mm]
5 cm
10 cm
15 cm
12S6 CH03B04 R1
12S6 CH03B04 R2
12S6 CH03B04 R2
12S6 CH03B04 R3
12S6 CH03B04 R3

#0712

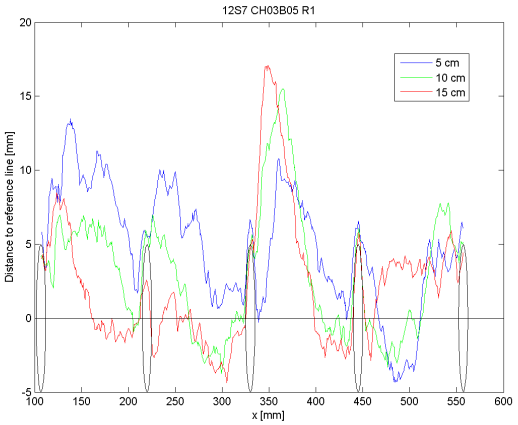
12S7 CH03B05 R1
5 cm
10 cm
15 cm
Distance to reference line [mm]
x [mm]

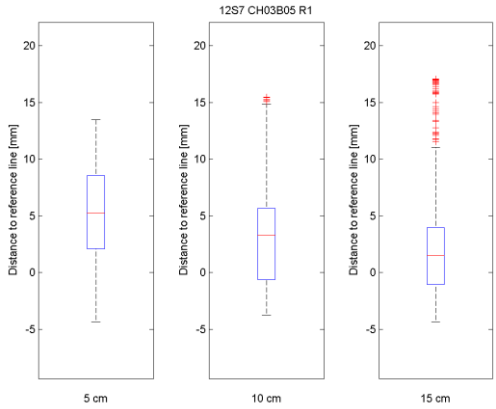
12S7 CH03B05 R1
Distance to reference line [mm]
5 cm
10 cm
15 cm

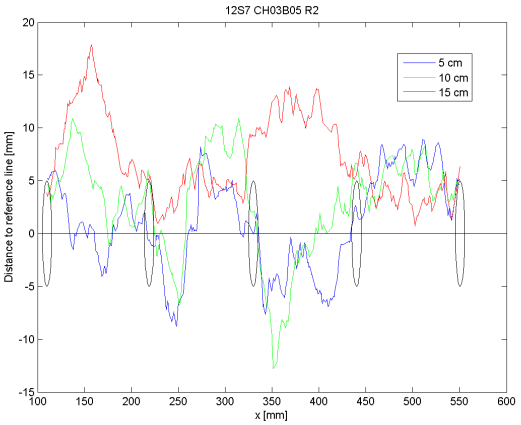
12S7 CH03B05 R2
5 cm
10 cm
15 cm
Distance to reference line [mm]
x [mm]

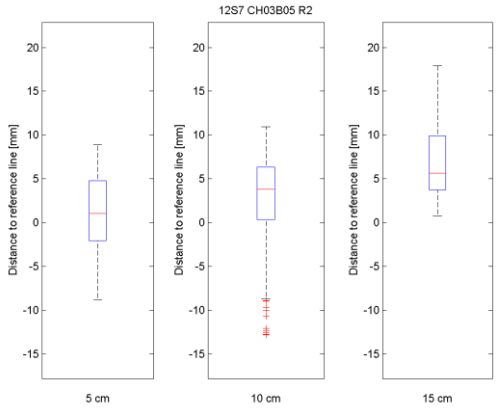
12S7 CH03B05 R2
Distance to reference line [mm]
5 cm
10 cm
15 cm

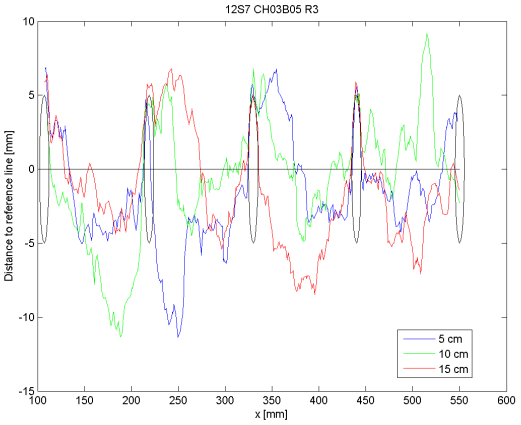
12S7 CH03B05 R3
5 cm
10 cm
15 cm
Distance to reference line [mm]
x [mm]

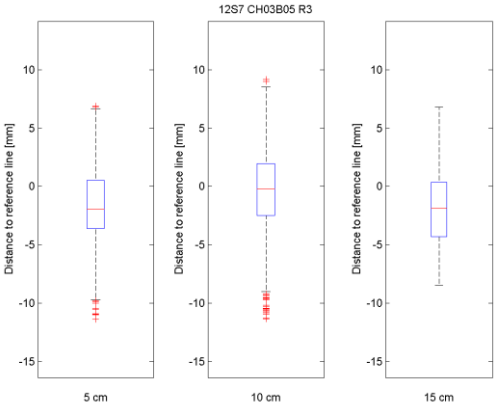
12S7 CH03B05 R3
Distance to reference line [mm]
5 cm
10 cm
15 cm

#0812

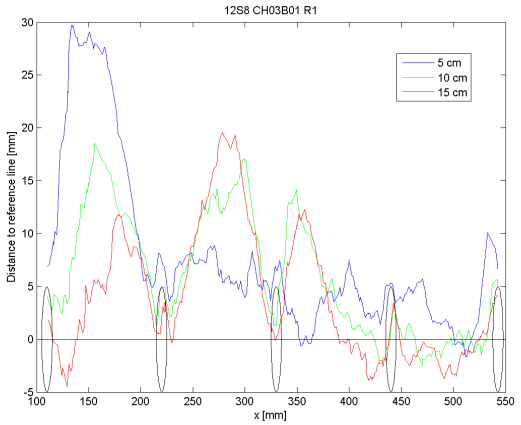
12S8 CH03B01 R1
5 cm
10 cm
15 cm
Distance to reference line [mm]
x [mm]

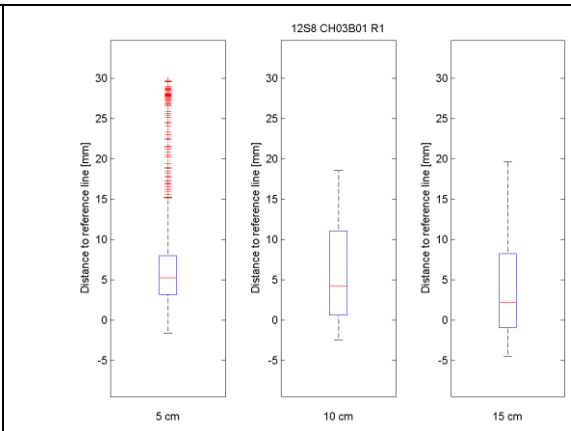
12S8 CH03B01 R1
Distance to reference line [mm]
5 cm
10 cm
15 cm

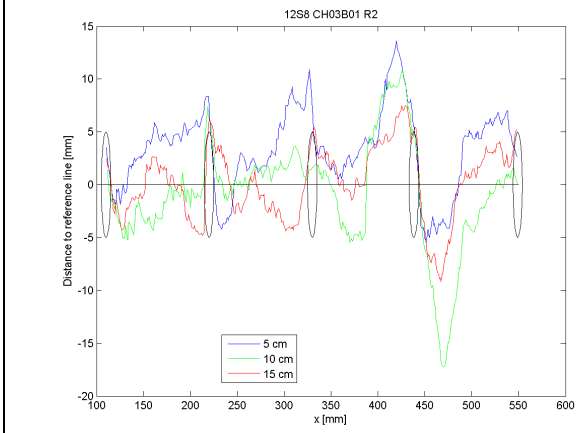
12S8 CH03B01 R2
5 cm
10 cm
15 cm
Distance to reference line [mm]
x [mm]

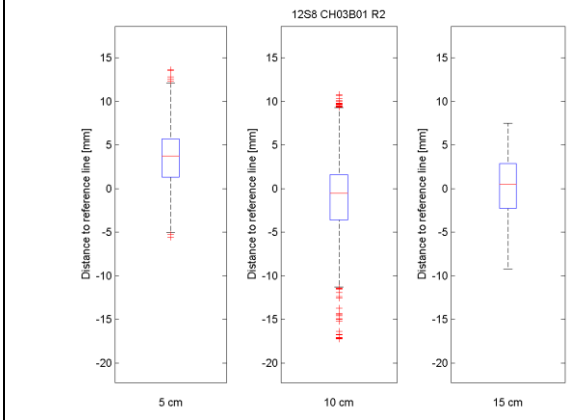
12S8 CH03B01 R2
Distance to reference line [mm]
5 cm
10 cm
15 cm

#0912

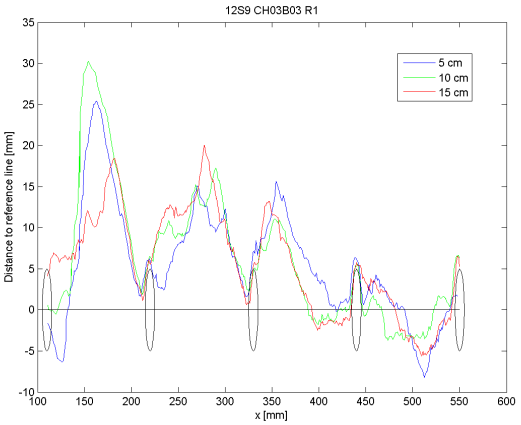
12S9 CH03B03 R1
5 cm
10 cm
15 cm
Distance to reference line [mm]
x [mm]

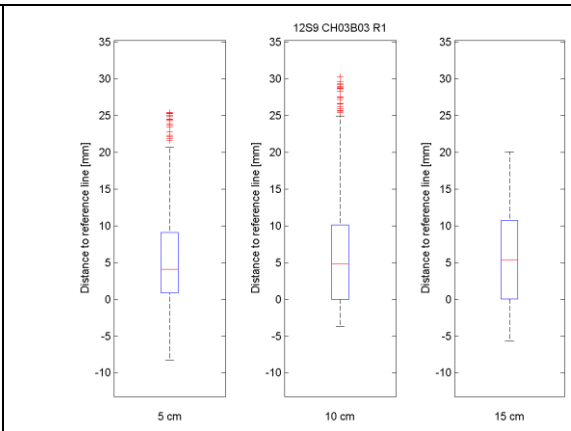
12S9 CH03B03 R1
Distance to reference line [mm]
5 cm
10 cm
15 cm

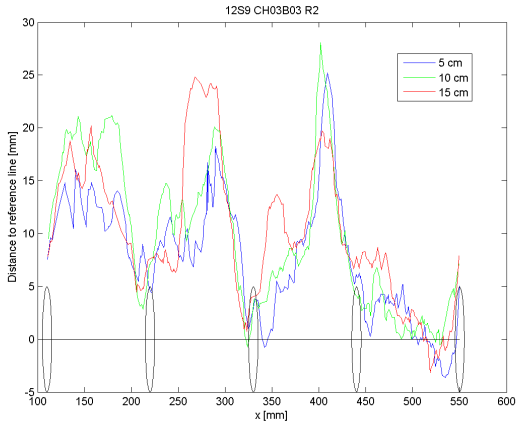
12S9 CH03B03 R2
5 cm
10 cm
15 cm
Distance to reference line [mm]
x [mm]

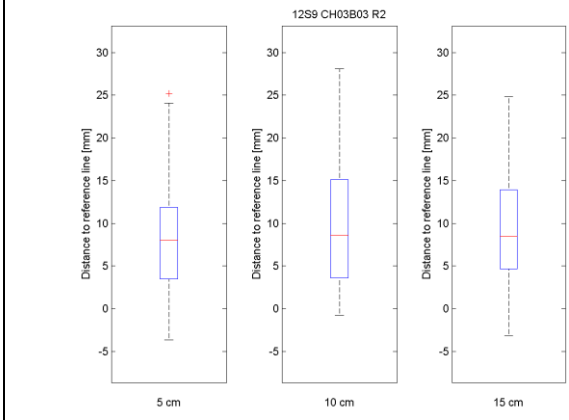
12S9 CH03B03 R2
Distance to reference line [mm]
5 cm
10 cm
15 cm

Stage 2

#0113

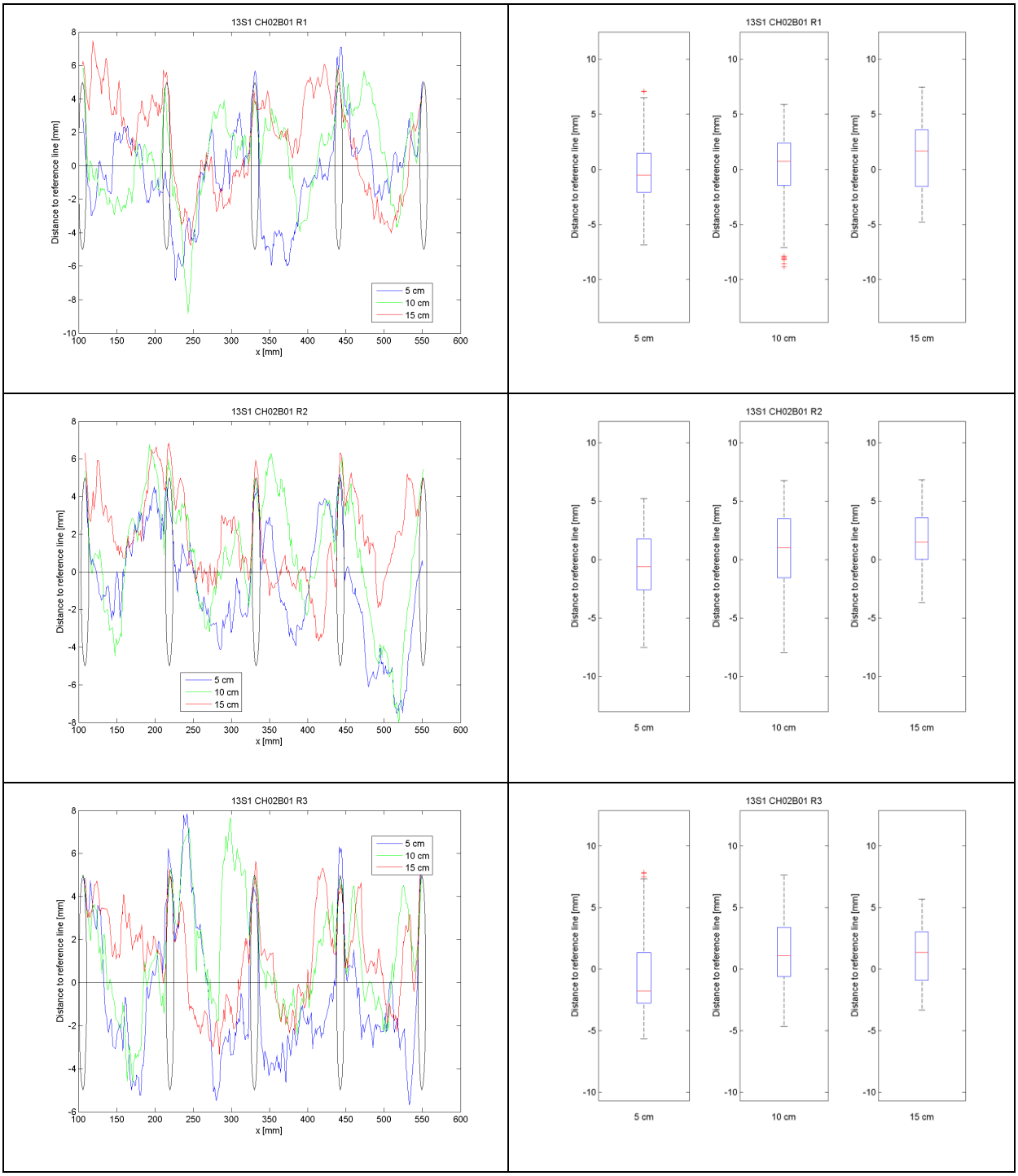
13S1 CH02B01 R1
Distance to reference line [mm]
x [mm]
5 cm
10 cm
15 cm
13S1 CH02B01 R1
Distance to reference line [mm]
5 cm
10 cm
15 cm
13S1 CH02B01 R2
Distance to reference line [mm]
x [mm]
5 cm
10 cm
15 cm
13S1 CH02B01 R2
Distance to reference line [mm]
5 cm
10 cm
15 cm
13S1 CH02B01 R3
Distance to reference line [mm]
x [mm]
5 cm
10 cm
15 cm
13S1 CH02B01 R3
Distance to reference line [mm]
5 cm
10 cm
15 cm

#0213

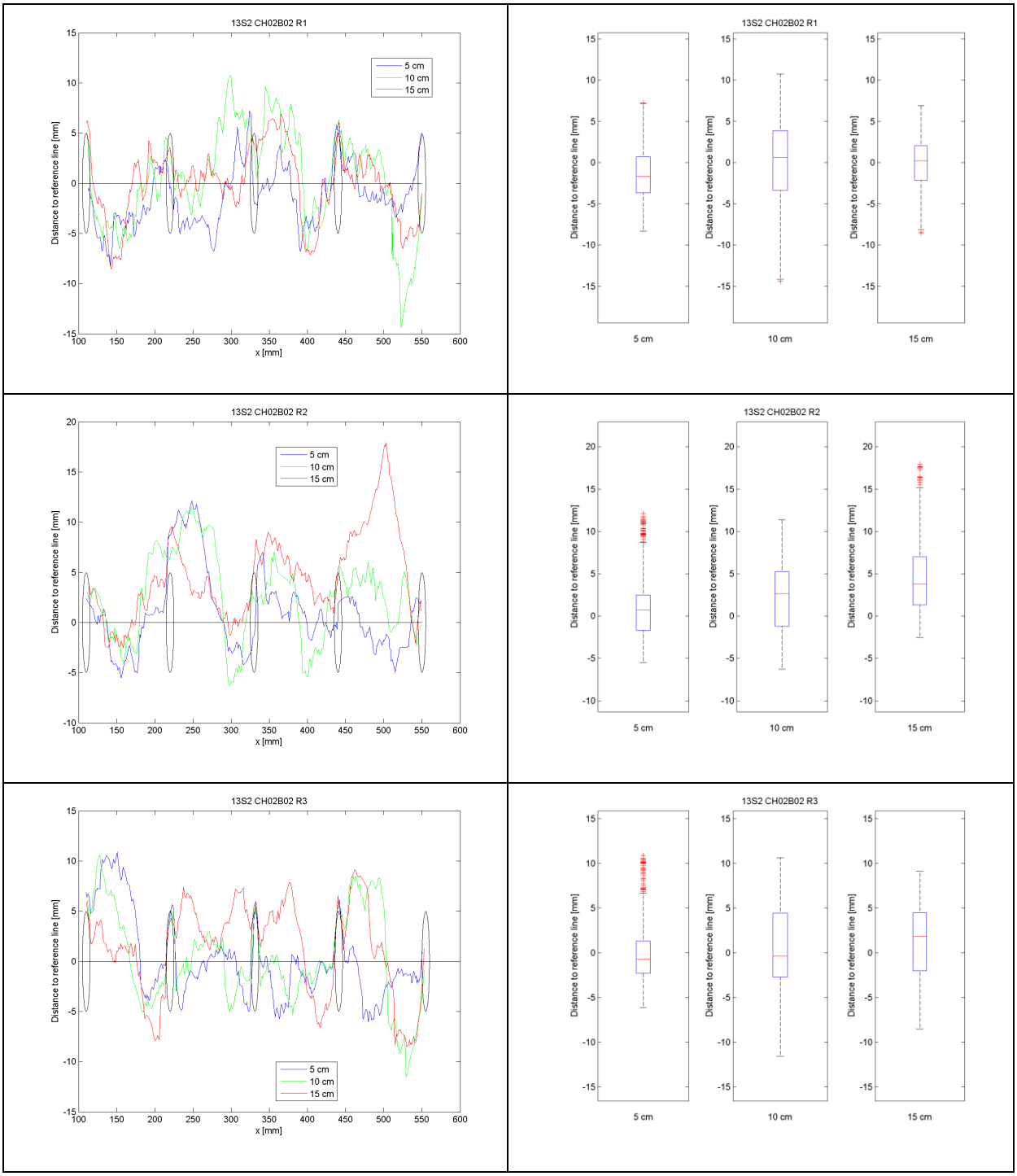
13S2 CH02B02 R1
5 cm
10 cm
15 cm
Distance to reference line [mm]
x [mm]
13S2 CH02B02 R1
Distance to reference line [mm]
5 cm
10 cm
15 cm
13S2 CH02B02 R2
5 cm
10 cm
15 cm
Distance to reference line [mm]
x [mm]
13S2 CH02B02 R2
Distance to reference line [mm]
5 cm
10 cm
15 cm
13S2 CH02B02 R3
5 cm
10 cm
15 cm
Distance to reference line [mm]
x [mm]
13S2 CH02B02 R3
Distance to reference line [mm]
5 cm
10 cm
15 cm

#0313

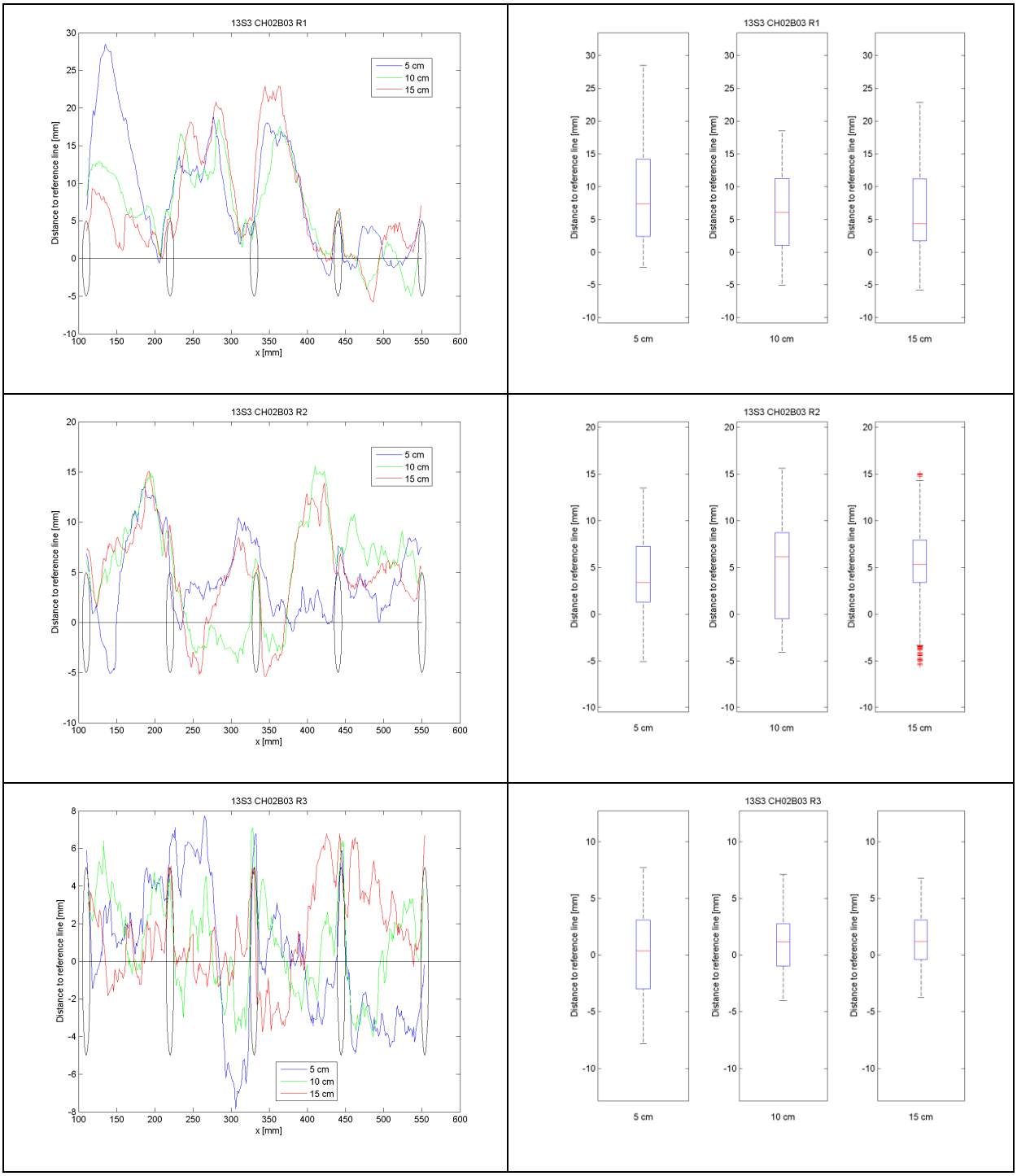
13S3 CH02B03 R1
Distance to reference line [mm]
x [mm]
5 cm
10 cm
15 cm
13S3 CH02B03 R1
Distance to reference line [mm]
5 cm
10 cm
15 cm
13S3 CH02B03 R2
Distance to reference line [mm]
x [mm]
5 cm
10 cm
15 cm
13S3 CH02B03 R2
Distance to reference line [mm]
5 cm
10 cm
15 cm
13S3 CH02B03 R3
Distance to reference line [mm]
x [mm]
5 cm
10 cm
15 cm
13S3 CH02B03 R3
Distance to reference line [mm]
5 cm
10 cm
15 cm

#0413

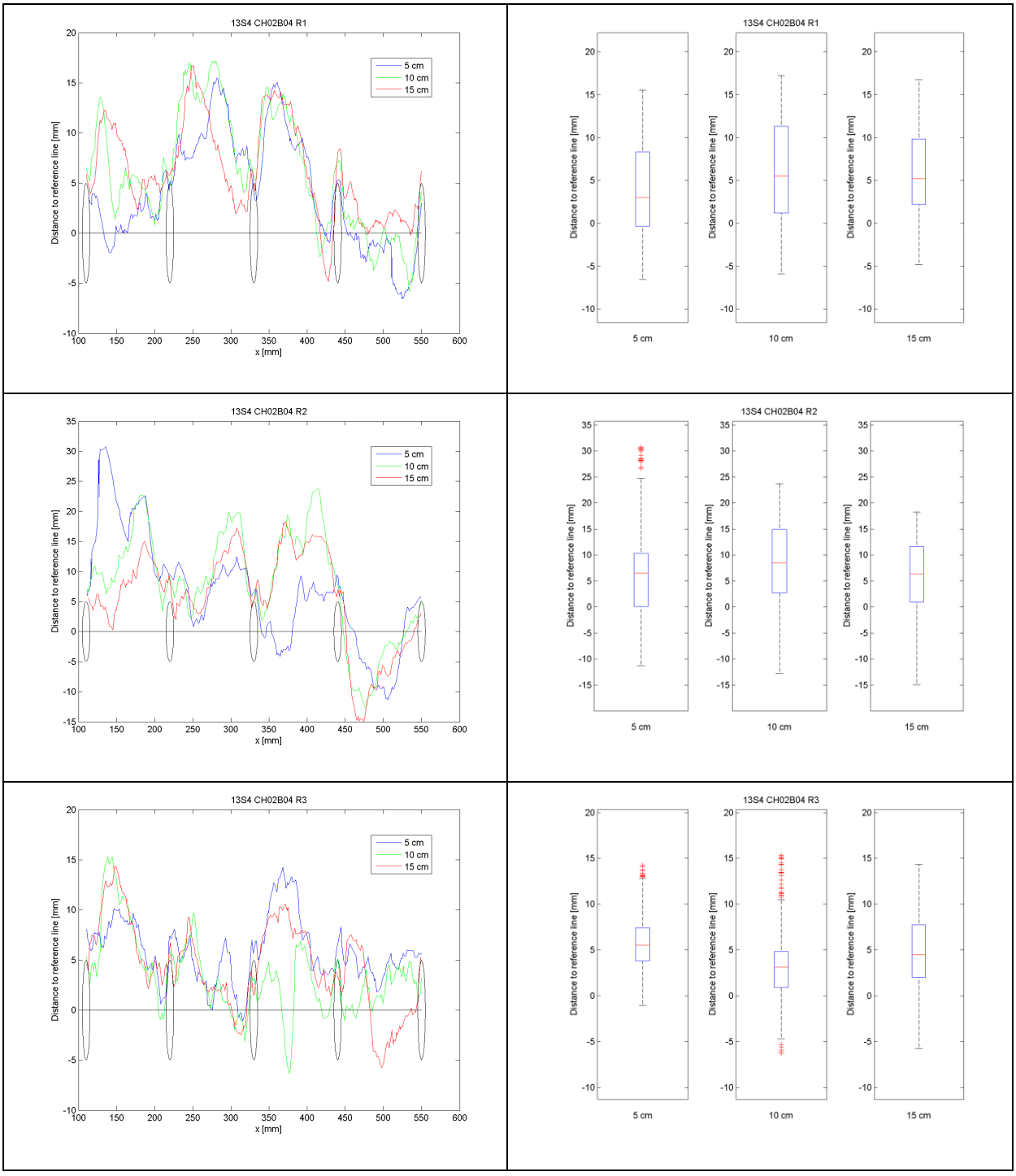
13S4 CH02B04 R1
5 cm
10 cm
15 cm
Distance to reference line [mm]
x [mm]
13S4 CH02B04 R1
Distance to reference line [mm]
5 cm
10 cm
15 cm
13S4 CH02B04 R2
5 cm
10 cm
15 cm
Distance to reference line [mm]
x [mm]
13S4 CH02B04 R2
Distance to reference line [mm]
5 cm
10 cm
15 cm
13S4 CH02B04 R3
5 cm
10 cm
15 cm
Distance to reference line [mm]
x [mm]
13S4 CH02B04 R3
Distance to reference line [mm]
5 cm
10 cm
15 cm

#0513

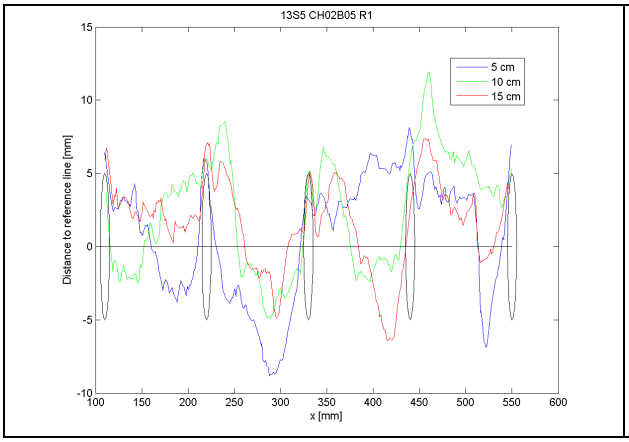
13S5 CH02B05 R1
5 cm
10 cm
15 cm
Distance to reference line [mm]
x [mm]

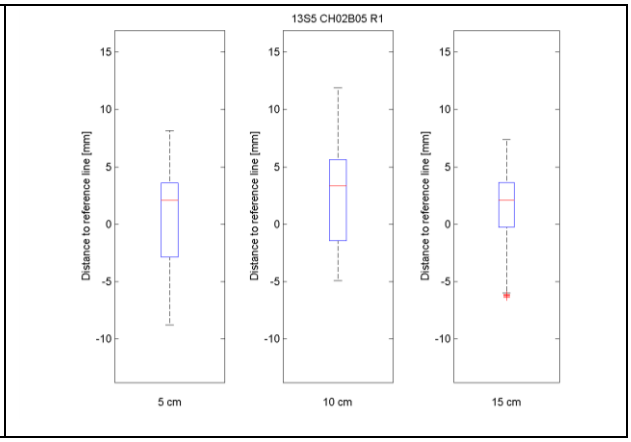
13S5 CH02B05 R1
Distance to reference line [mm]
5 cm
10 cm
15 cm

#0613

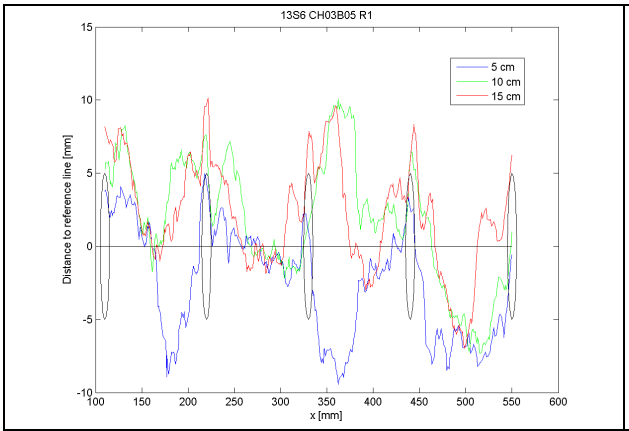
13S6 CH03B05 R1
5 cm
10 cm
15 cm
Distance to reference line [mm]
x [mm]

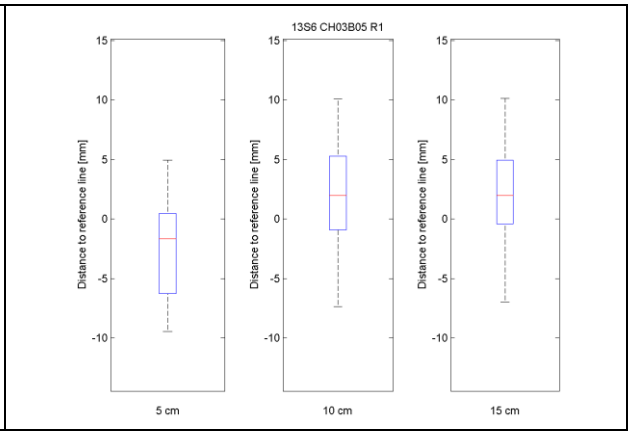
13S6 CH03B05 R1
Distance to reference line [mm]
5 cm
10 cm
15 cm

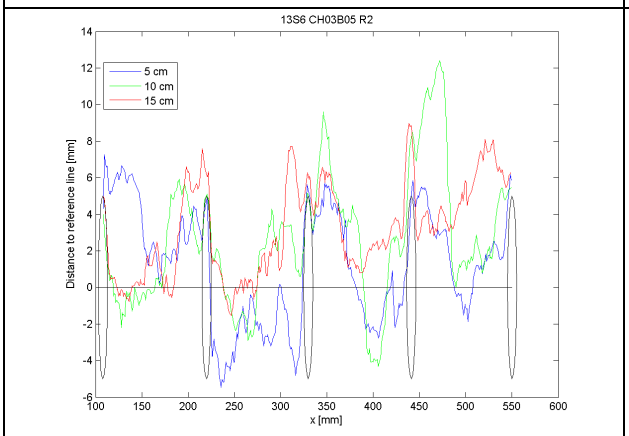
13S6 CH03B05 R2
5 cm
10 cm
15 cm
Distance to reference line [mm]
x [mm]

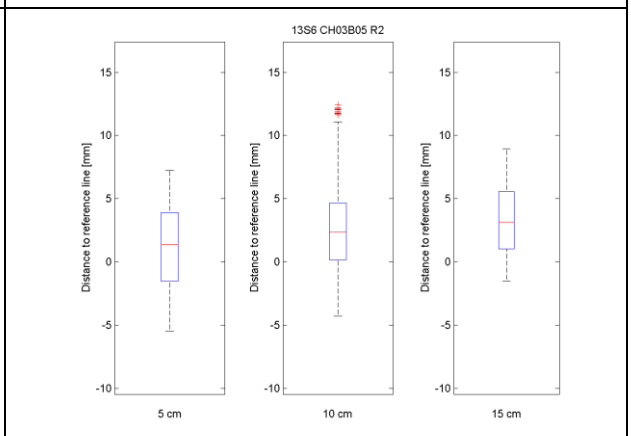
13S6 CH03B05 R2
Distance to reference line [mm]
5 cm
10 cm
15 cm

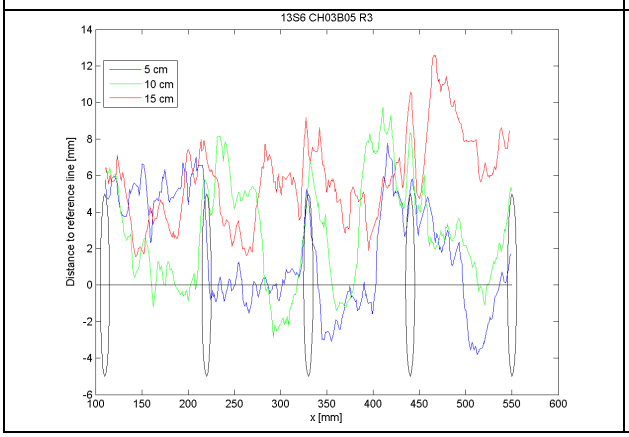
13S6 CH03B05 R3
5 cm
10 cm
15 cm
Distance to reference line [mm]
x [mm]

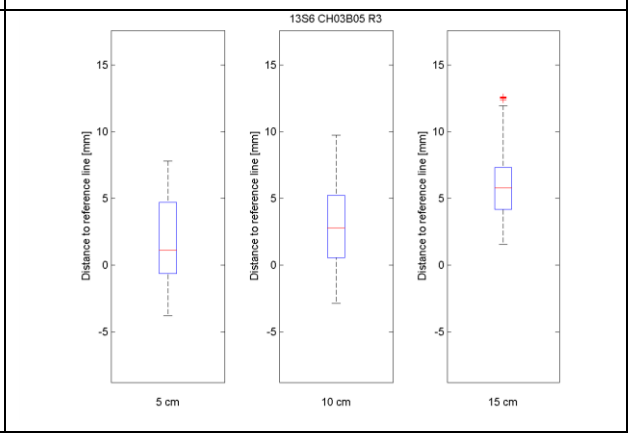
13S6 CH03B05 R3
Distance to reference line [mm]
5 cm
10 cm
15 cm

#0713

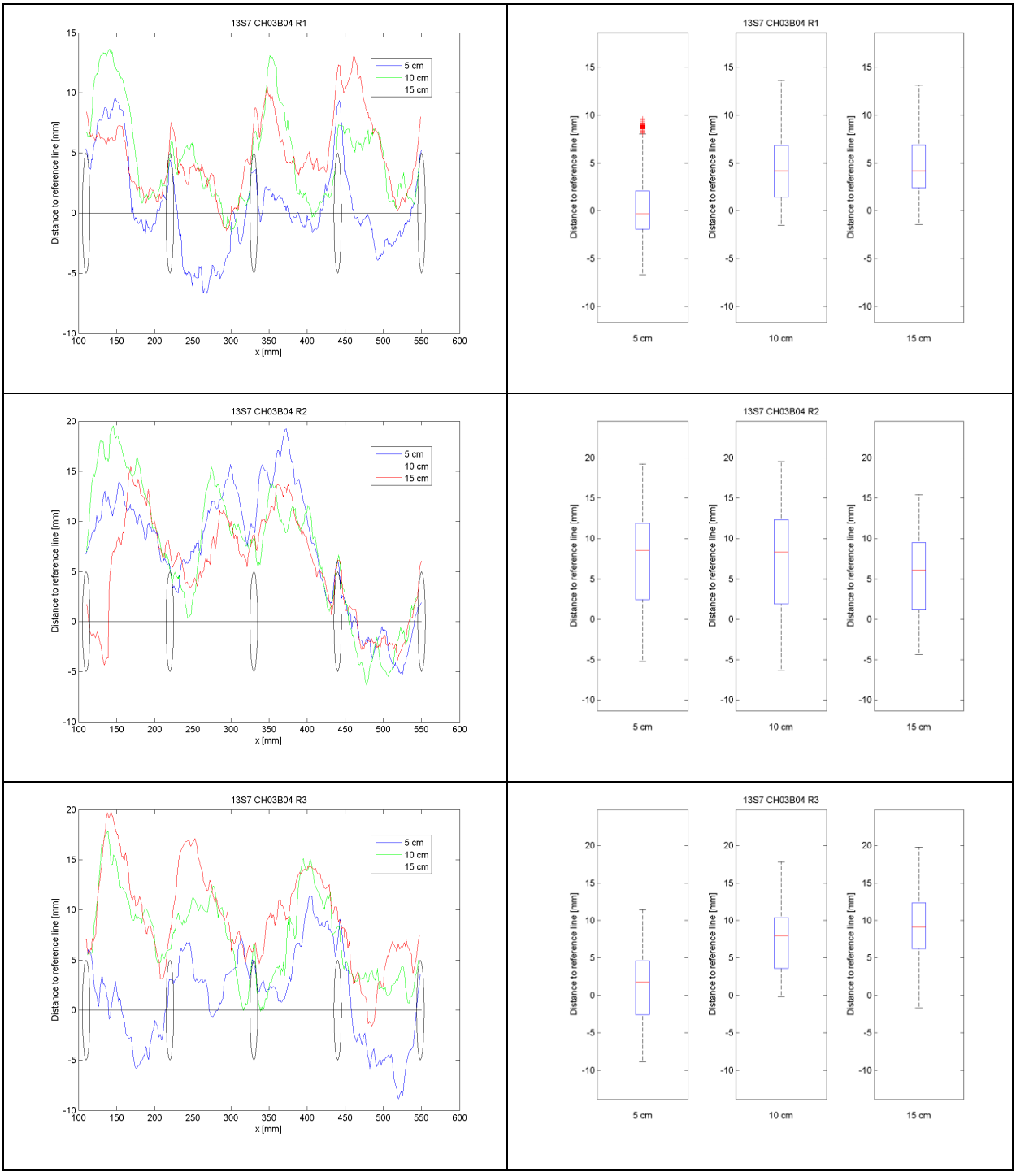
13S7 CH03B04 R1
5 cm
10 cm
15 cm
Distance to reference line [mm]
x [mm]
13S7 CH03B04 R1
Distance to reference line [mm]
5 cm
10 cm
15 cm
13S7 CH03B04 R2
5 cm
10 cm
15 cm
Distance to reference line [mm]
x [mm]
13S7 CH03B04 R2
Distance to reference line [mm]
5 cm
10 cm
15 cm
13S7 CH03B04 R3
5 cm
10 cm
15 cm
Distance to reference line [mm]
x [mm]
13S7 CH03B04 R3
Distance to reference line [mm]
5 cm
10 cm
15 cm

Stage 3

#0114

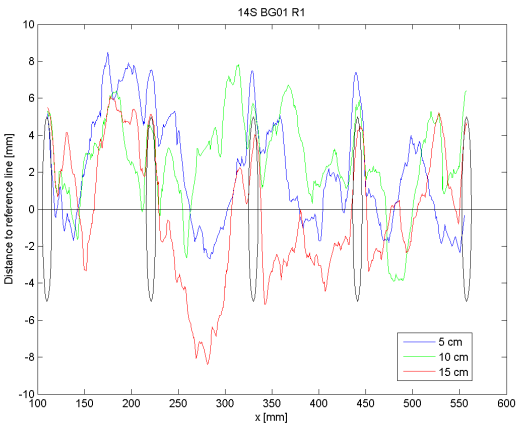
14S BG01 R1
Distance to reference line [mm]
x [mm]
5 cm
10 cm
15 cm

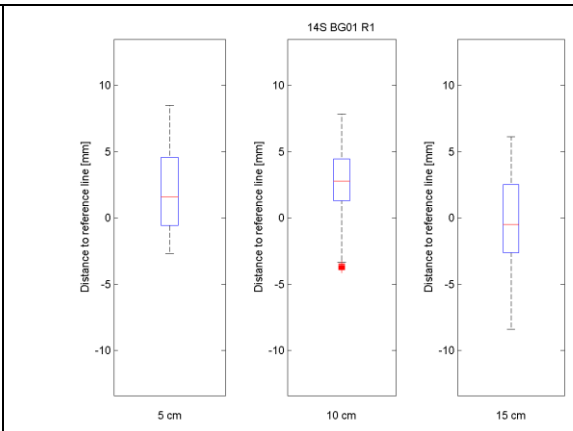
14S BG01 R1
Distance to reference line [mm]
5 cm
10 cm
15 cm

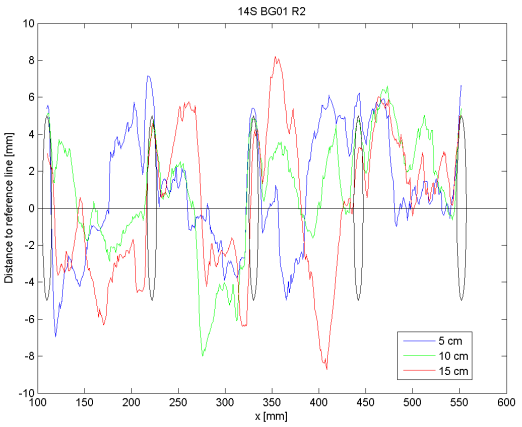
14S BG01 R2
Distance to reference line [mm]
x [mm]
5 cm
10 cm
15 cm

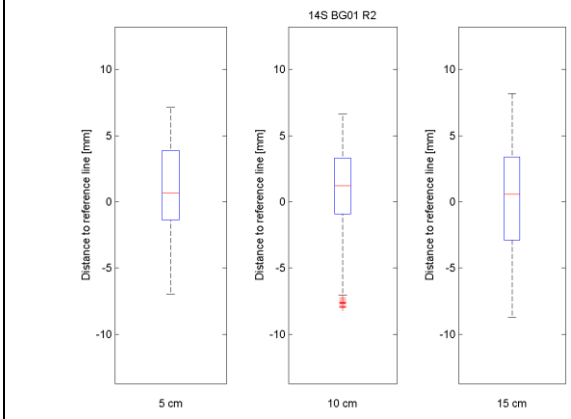
14S BG01 R2
Distance to reference line [mm]
5 cm
10 cm
15 cm

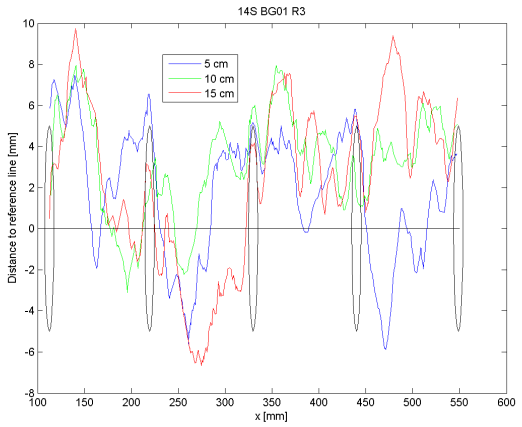
14S BG01 R3
Distance to reference line [mm]
x [mm]
5 cm
10 cm
15 cm

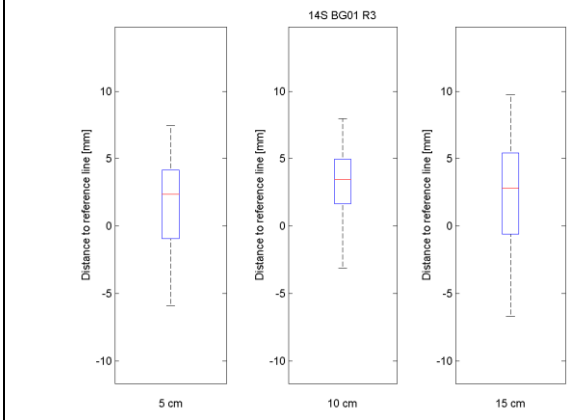
14S BG01 R3
Distance to reference line [mm]
5 cm
10 cm
15 cm

#0214

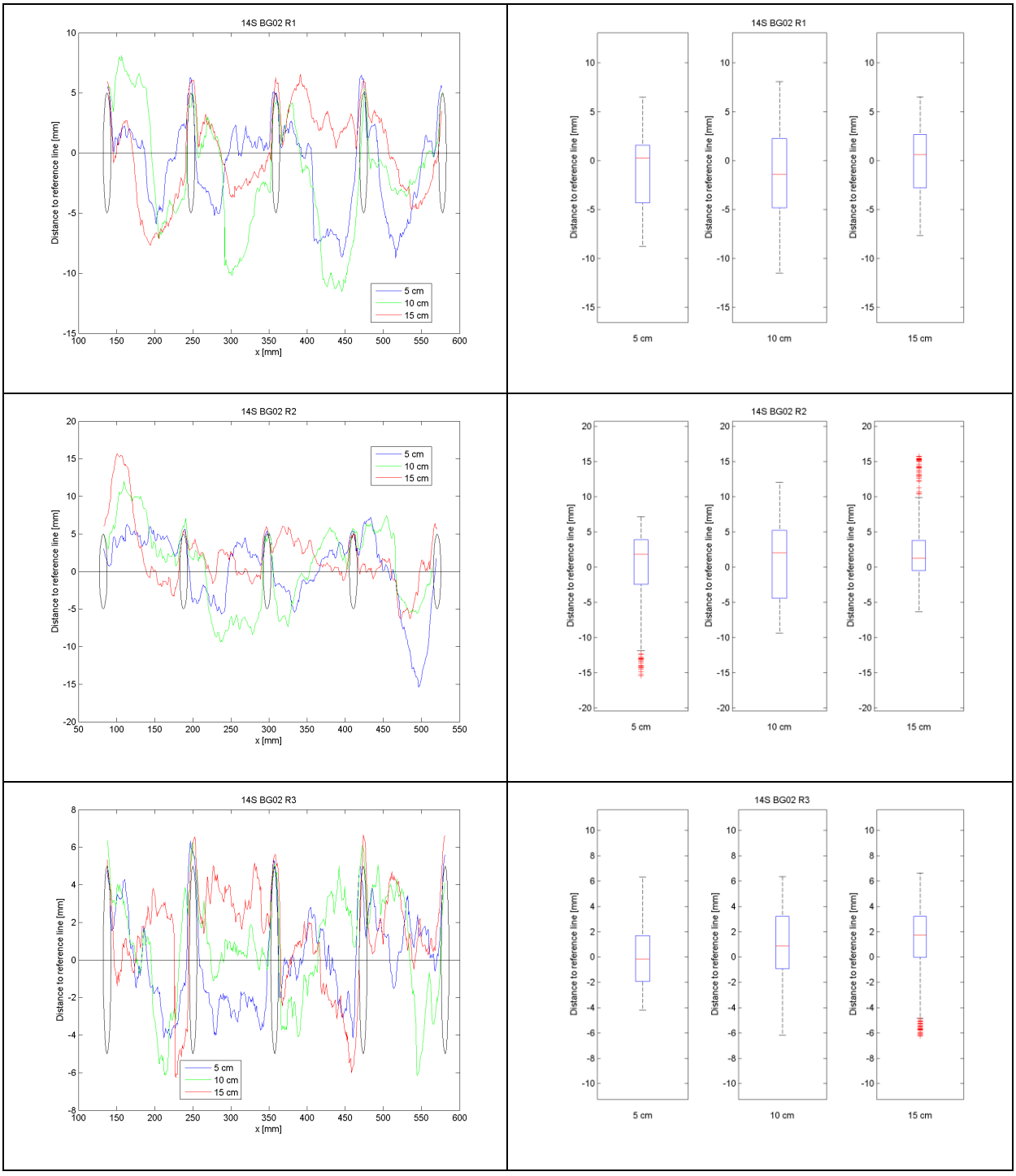
14S BG02 R1
Distance to reference line [mm]
x [mm]
5 cm
10 cm
15 cm
14S BG02 R1
Distance to reference line [mm]
5 cm
10 cm
15 cm
14S BG02 R2
Distance to reference line [mm]
x [mm]
5 cm
10 cm
15 cm
14S BG02 R2
Distance to reference line [mm]
5 cm
10 cm
15 cm
14S BG02 R3
Distance to reference line [mm]
x [mm]
5 cm
10 cm
15 cm
14S BG02 R3
Distance to reference line [mm]
5 cm
10 cm
15 cm

#0314

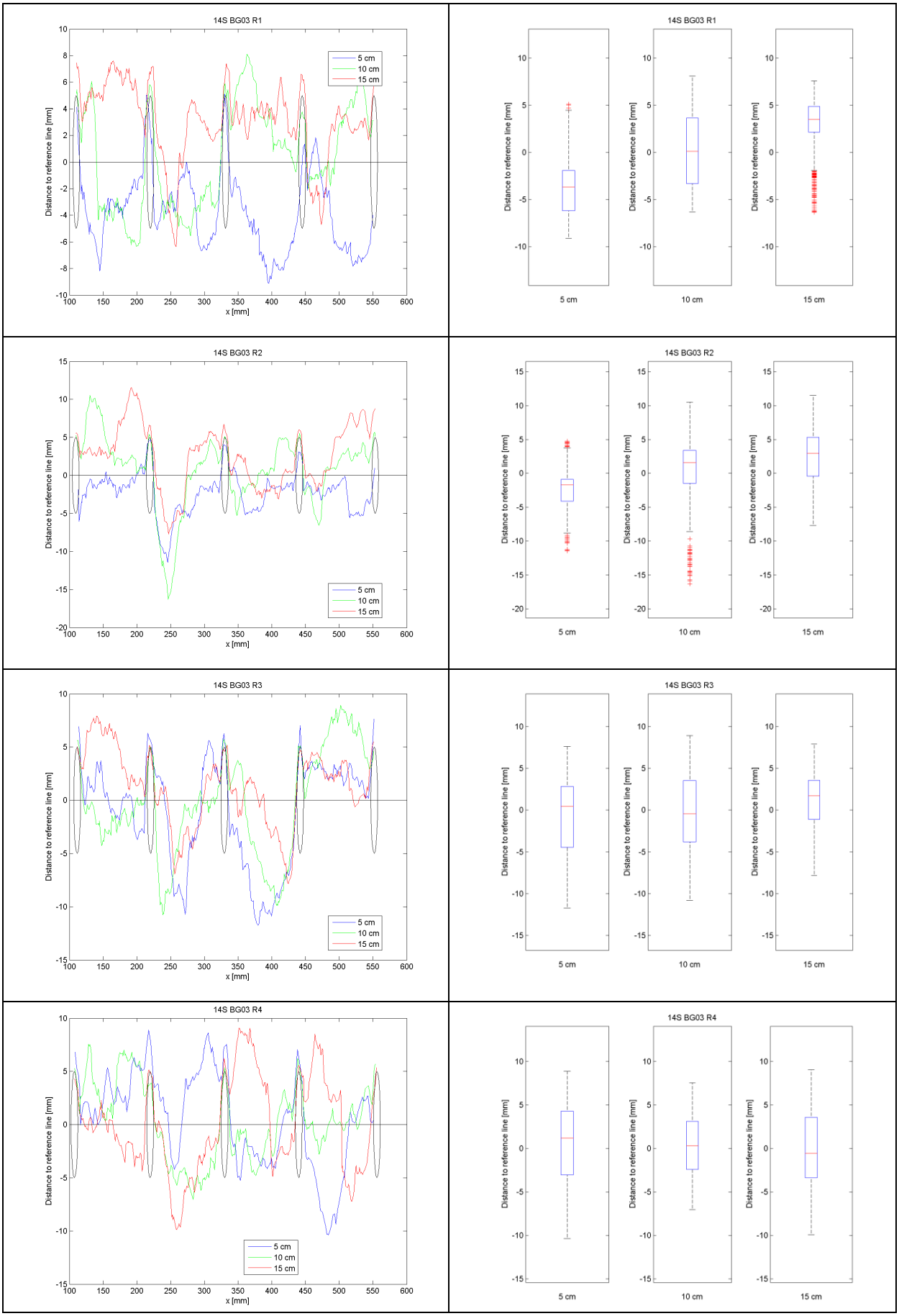
14S BG03 R1
5 cm
10 cm
15 cm
Distance to reference line [mm]
x [mm]
14S BG03 R1
Distance to reference line [mm]
5 cm
10 cm
15 cm
14S BG03 R2
Distance to reference line [mm]
x [mm]
5 cm
10 cm
15 cm
14S BG03 R2
Distance to reference line [mm]
5 cm
10 cm
15 cm
14S BG03 R3
Distance to reference line [mm]
x [mm]
5 cm
10 cm
15 cm
14S BG03 R3
Distance to reference line [mm]
5 cm
10 cm
15 cm
14S BG03 R4
Distance to reference line [mm]
x [mm]
5 cm
10 cm
15 cm
14S BG03 R4
Distance to reference line [mm]
5 cm
10 cm
15 cm

#0414

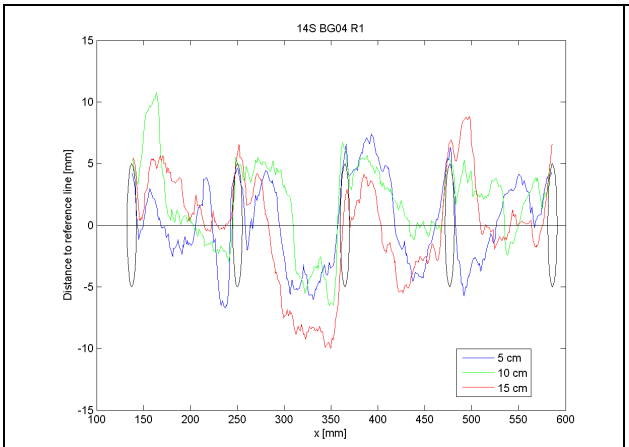
14S BG04 R1
Distance to reference line [mm]
x [mm]
5 cm
10 cm
15 cm

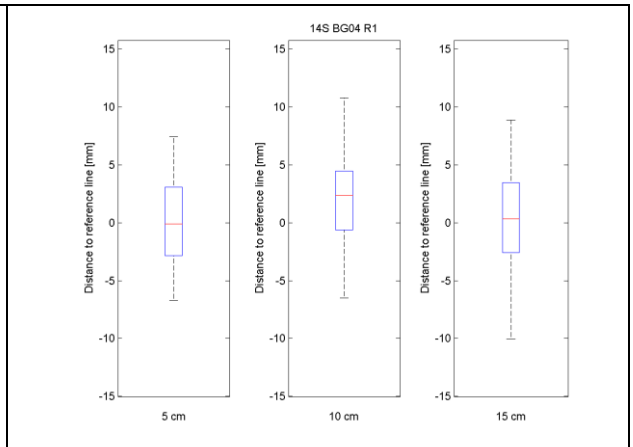
14S BG04 R1
Distance to reference line [mm]
5 cm
10 cm
15 cm

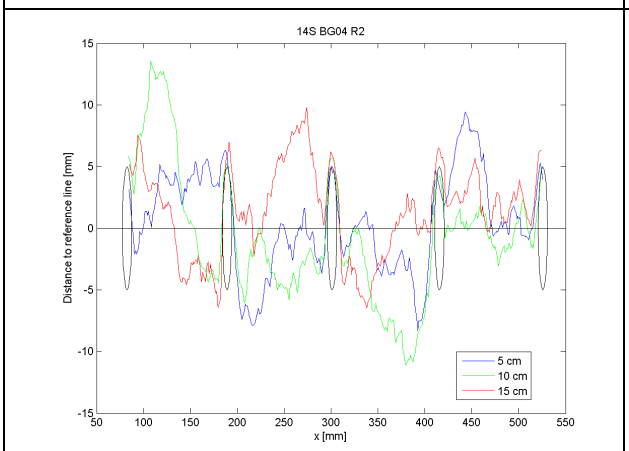
14S BG04 R2
Distance to reference line [mm]
x [mm]
5 cm
10 cm
15 cm

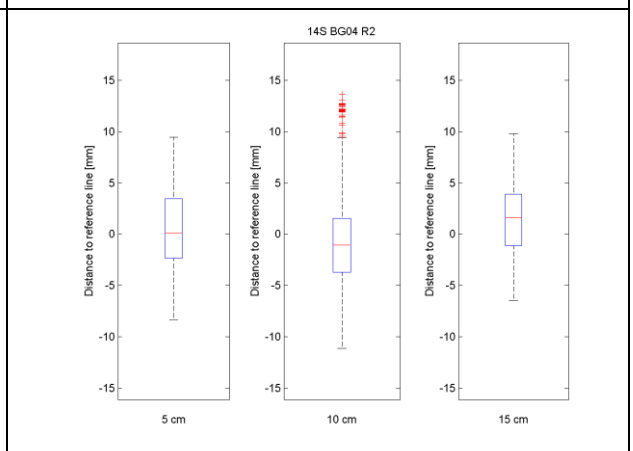
14S BG04 R2
Distance to reference line [mm]
5 cm
10 cm
15 cm

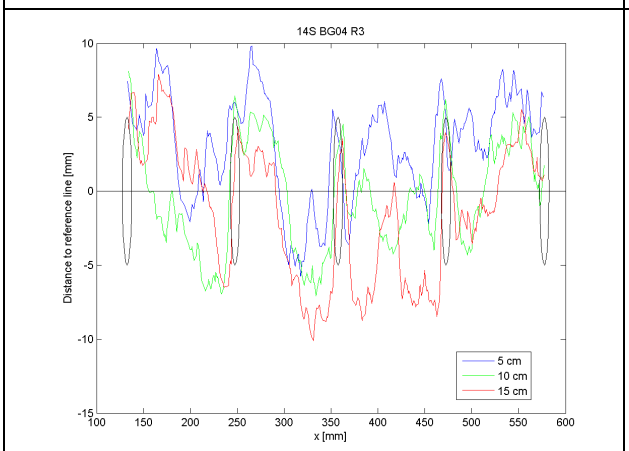
14S BG04 R3
Distance to reference line [mm]
x [mm]
5 cm
10 cm
15 cm

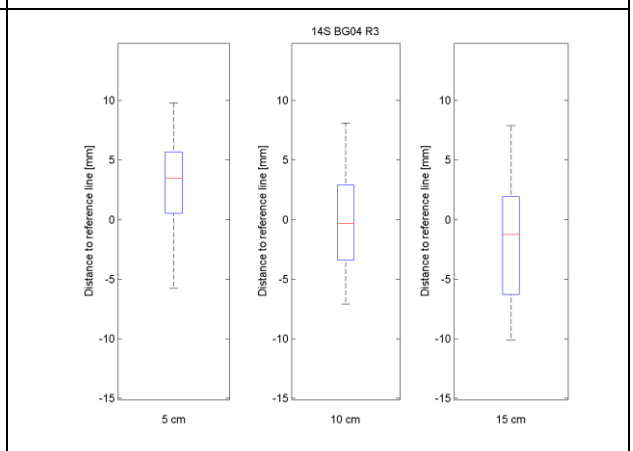
14S BG04 R3
Distance to reference line [mm]
5 cm
10 cm
15 cm

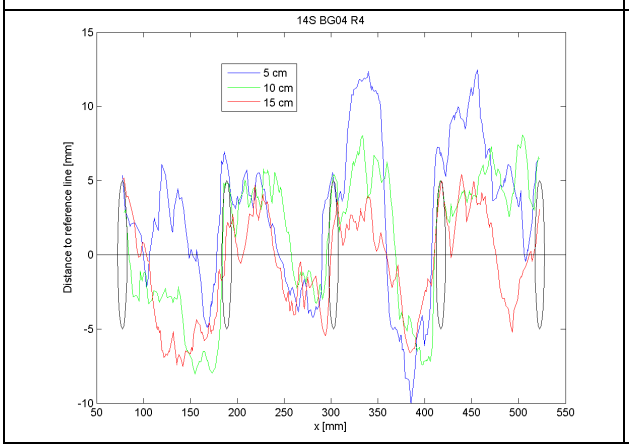
14S BG04 R4
Distance to reference line [mm]
x [mm]
5 cm
10 cm
15 cm

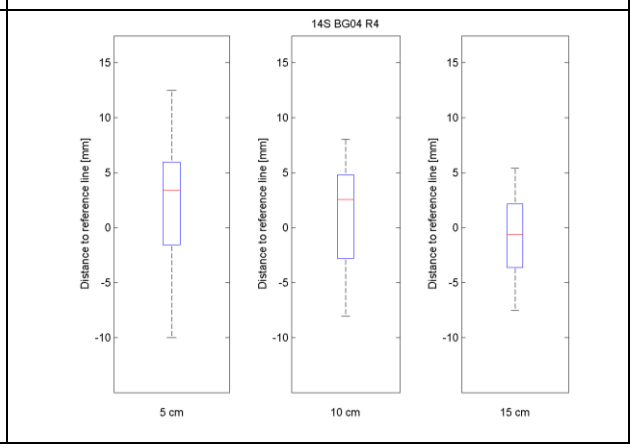
14S BG04 R4
Distance to reference line [mm]
5 cm
10 cm
15 cm

Appendix 12 – Cracks at the Top of the Testing Blocks

#0114

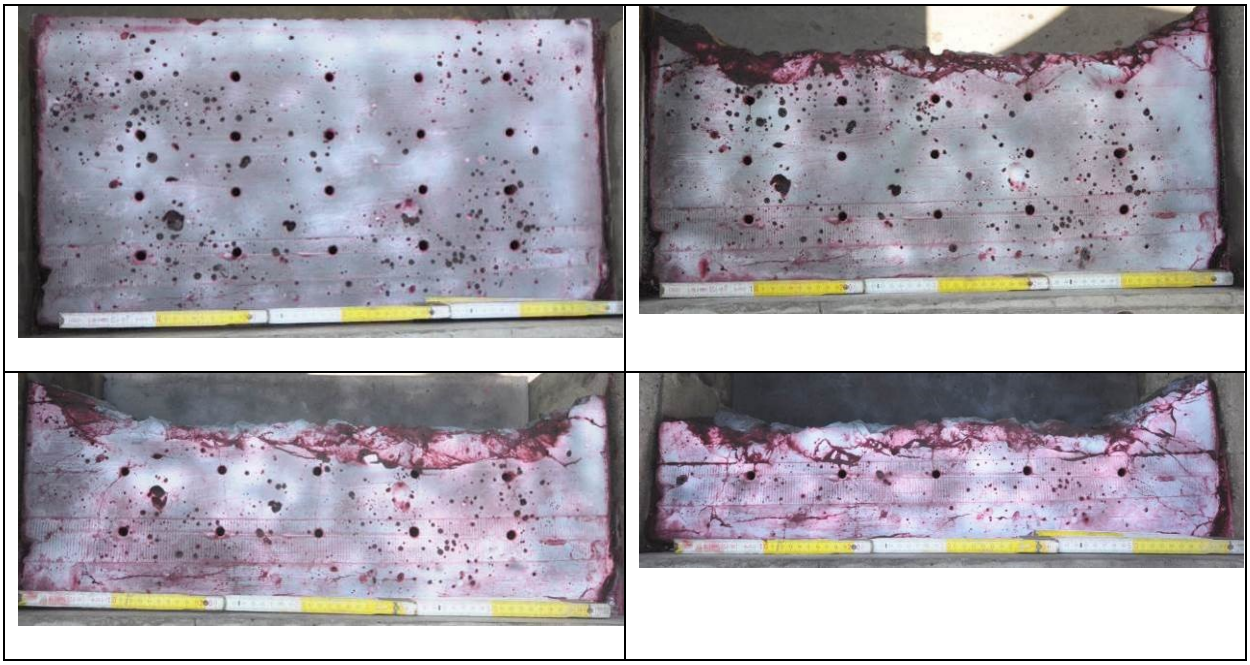

#0114	Before Blast							1st row blasted					
Crack Family	Burden Row 1	Burden Row 2	Burden Row 3	Burden Row 4	Behind Row 4	Total Cracks		Burden Row 1	Burden Row 2	Burden Row 3	Burden Row 4	Behind Row 4	Total Cracks
CB 90-80	0	0	0	0	0	0		-	3	5	4	0	12
CB 80-30	0	0	0	0	0	0		-	2	0	1	0	3
CB 30-0	0	1	0	0	0	1		-	4	0	0	1	5
SCB	4	1	3	1	0	9		-	2	1	0	6	9
Connect	0	0	0	0	0	0		-	0	0	0	0	0
Parallel	2	1	0	0	4	7		-	0	0	0	7	7
CD 90-80	0	0	1	0	0	1		-	1	3	0	1	5
CD 80-30	0	0	1	0	0	1		-	3	0	0	2	5
CD 30-0	0	0	0	0	0	0		-	0	0	0	0	0
Short	0	0	0	1	0	1		-	3	0	0	0	3
Totals	6	3	5	2	4	20		-	18	9	5	17	49

#0114	2nd row blasted							3rd row blasted					
Crack Family	Burden Row 1	Burden Row 2	Burden Row 3	Burden Row 4	Behind Row 4	Total Cracks		Burden Row 1	Burden Row 2	Burden Row 3	Burden Row 4	Behind Row 4	Total Cracks
CB 90-80	-	-	1	4	1	6		-	-	-	4	2	6
CB 80-30	-	-	3	2	0	5		-	-	-	6	0	6
CB 30-0	-	-	10	1	0	11		-	-	-	2	2	4
SCB	-	-	0	2	9	11		-	-	-	7	8	15
Connect	-	-	0	0	0	0		-	-	-	0	0	0
Parallel	-	-	3	1	7	11		-	-	-	9	9	18
CD 90-80	-	-	4	0	0	4		-	-	-	1	2	3
CD 80-30	-	-	6	2	3	11		-	-	-	5	1	6
CD 30-0	-	-	5	0	0	5		-	-	-	0	1	1
Short	-	-	3	0	0	3		-	-	-	0	0	0
Totals	-	-	35	12	20	67		-	-	-	34	25	59

#0214

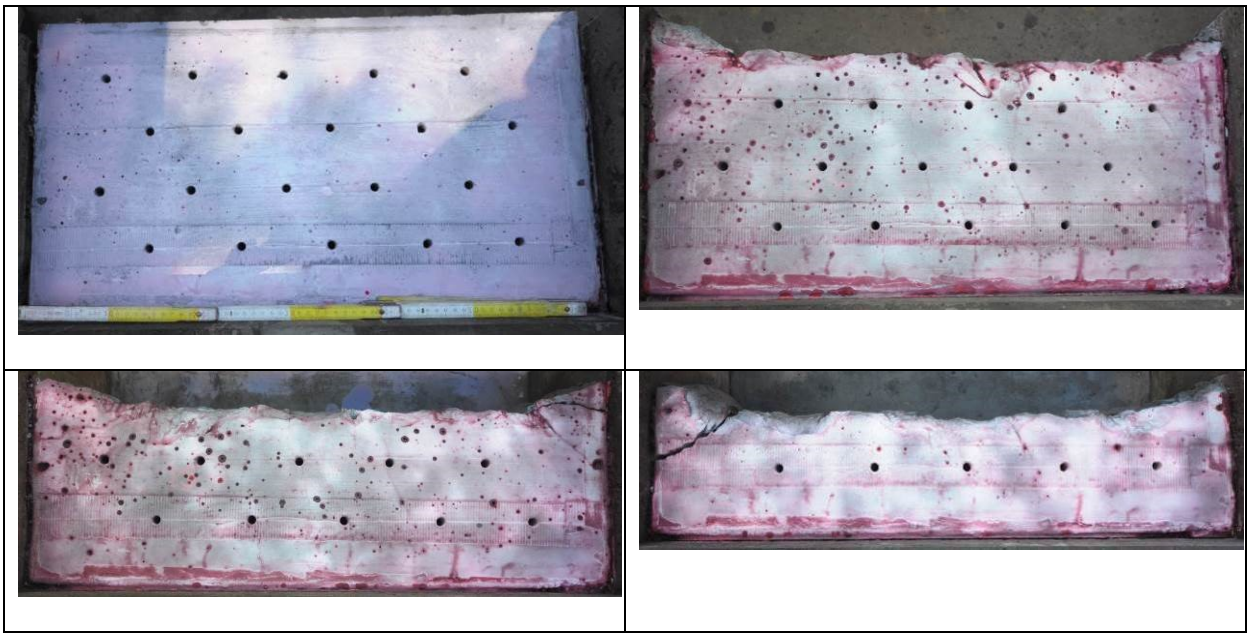

#0214	Before Blast							1st row blasted					
Crack Family	Burden Row 1	Burden Row 2	Burden Row 3	Burden Row 4	Behind Row 4	Total Cracks		Burden Row 1	Burden Row 2	Burden Row 3	Burden Row 4	Behind Row 4	Total Cracks
CB 90-80	0	0	0	0	0	0		-	3	2	2	2	9
CB 80-30	0	0	0	0	0	0		-	5	1	0	0	6
CB 30-0	0	0	0	0	0	0		-	4	0	0	0	4
SCB	0	0	1	0	0	1		-	1	2	1	3	7
Connect	0	0	0	0	0	0		-	0	0	0	0	0
Parallel	0	0	1	0	0	1		-	0	0	0	0	0
CD 90-80	0	0	0	0	2	2		-	0	0	0	0	0
CD 80-30	0	0	0	0	1	1		-	2	0	0	0	2
CD 30-0	0	0	0	0	0	0		-	0	0	0	0	0
Short	0	0	0	0	0	0		-	0	0	0	0	0
Totals	0	0	2	0	3	5		-	15	5	3	5	28

#0214	2nd row blasted							3rd row blasted					
Crack Family	Burden Row 1	Burden Row 2	Burden Row 3	Burden Row 4	Behind Row 4	Total Cracks		Burden Row 1	Burden Row 2	Burden Row 3	Burden Row 4	Behind Row 4	Total Cracks
CB 90-80	-	-	5	1	1	7		-	-	-	4	2	6
CB 80-30	-	-	6	1	0	7		-	-	-	5	0	5
CB 30-0	-	-	9	0	0	9		-	-	-	1	0	1
SCB	-	-	2	2	3	7		-	-	-	2	6	8
Connect	-	-	0	0	0	0		-	-	-	0	0	0
Parallel	-	-	1	0	0	1		-	-	-	0	0	0
CD 90-80	-	-	0	0	0	0		-	-	-	0	0	0
CD 80-30	-	-	2	0	0	2		-	-	-	0	0	0
CD 30-0	-	-	0	0	0	0		-	-	-	1	0	1
Short	-	-	0	0	0	0		-	-	-	2	0	2
Totals	-	-	25	4	4	33		-	-	-	15	8	23

#0314

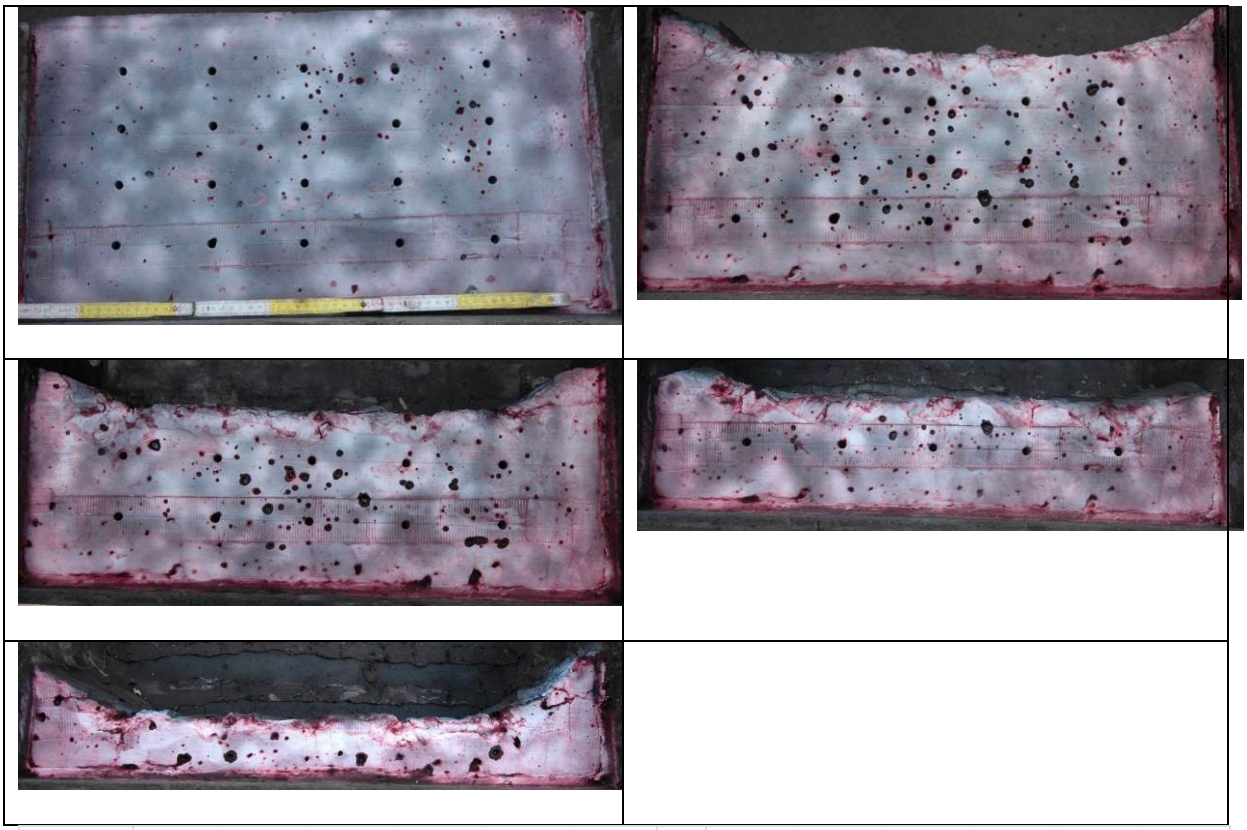

	Before Blast							1st row blasted					
#0314													
Crack Family	Burden Row 1	Burden Row 2	Burden Row 3	Burden Row 4	Behind Row 4	Total Cracks		Burden Row 1	Burden Row 2	Burden Row 3	Burden Row 4	Behind Row 4	Total Cracks
CB 90-80	0	0	0	0	0	0		-	2	2	2	1	7
CB 80-30	0	0	0	0	0	0		-	2	0	0	0	2
CB 30-0	0	0	0	0	0	0		-	9	0	0	0	9
SCB	1	0	0	0	0	1		-	3	0	0	3	6
Connect	0	0	0	0	0	0		-	1	0	0	0	1
Parallel	0	0	0	0	0	0		-	0	0	0	3	3
CD 90-80	0	0	0	0	0	0		-	0	0	0	0	0
CD 80-30	0	0	0	0	0	0		-	0	0	0	0	0
CD 30-0	0	0	0	0	0	0		-	0	0	0	0	0
Short	0	0	0	0	0	0		-	0	0	0	0	0
Totals	1	0	0	0	0	1		-	17	2	2	7	28

	2nd row blasted							3rd row blasted					
#0314													
Crack Family	Burden Row 1	Burden Row 2	Burden Row 3	Burden Row 4	Behind Row 4	Total Cracks		Burden Row 1	Burden Row 2	Burden Row 3	Burden Row 4	Behind Row 4	Total Cracks
CB 90-80	-	-	4	3	2	9		-	-	-	4	2	6
CB 80-30	-	-	5	0	0	5		-	-	-	5	0	5
CB 30-0	-	-	6	0	0	6		-	-	-	7	0	7
SCB	-	-	1	0	3	4		-	-	-	3	2	5
Connect	-	-	0	0	0	0		-	-	-	0	0	0
Parallel	-	-	0	0	3	3		-	-	-	1	3	4
CD 90-80	-	-	0	0	0	0		-	-	-	1	0	1
CD 80-30	-	-	2	0	0	2		-	-	-	5	0	5
CD 30-0	-	-	0	0	0	0		-	-	-	2	0	2
Short	-	-	4	0	0	4		-	-	-	4	0	4
Totals	-	-	22	3	8	33		-	-	-	32	7	39

	4th row blasted					
#0314						
Crack Family	Burden Row 1	Burden Row 2	Burden Row 3	Burden Row 4	Behind Row 4	Total Cracks
CB 90-80	-	-	-	-	5	5
CB 80-30	-	-	-	-	11	11
CB 30-0	-	-	-	-	10	10
SCB	-	-	-	-	7	7
Connect	-	-	-	-	1	1
Parallel	-	-	-	-	5	5
CD 90-80	-	-	-	-	0	0
CD 80-30	-	-	-	-	2	2
CD 30-0	-	-	-	-	1	1
Short	-	-	-	-	4	4
Totals	-	-	-	-	46	46

#0414

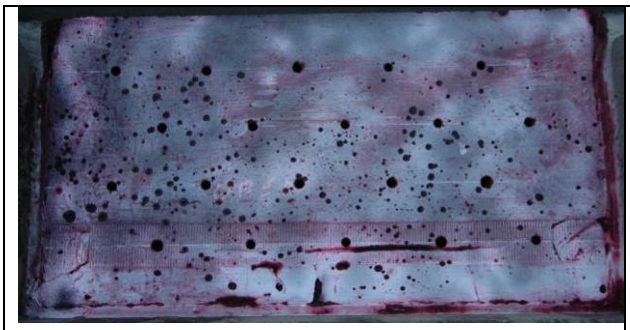

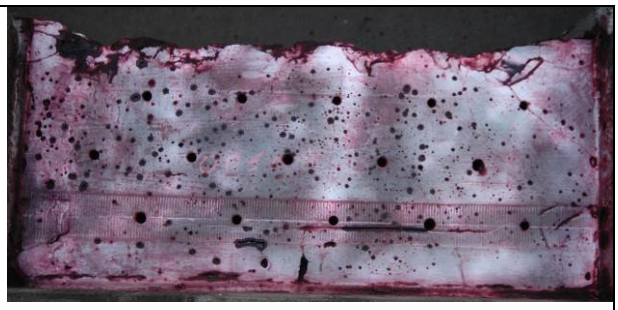

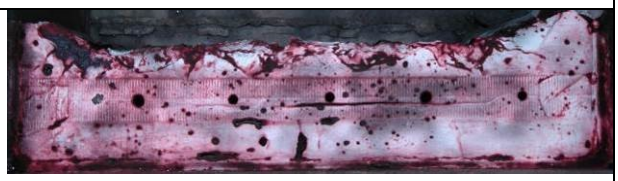

	Before Blast							1st row blasted					
#0414													
Crack Family	Burden Row 1	Burden Row 2	Burden Row 3	Burden Row 4	Behind Row 4	Total Cracks		Burden Row 1	Burden Row 2	Burden Row 3	Burden Row 4	Behind Row 4	Total Cracks
CB 90-80	0	0	0	0	0	0		-	2	3	3	0	8
CB 80-30	0	0	0	0	1	1		-	5	2	0	1	8
CB 30-0	0	0	0	0	0	0		-	1	0	0	0	1
SCB	1	0	0	0	7	8		-	21	3	5	8	37
Connect	0	0	0	0	0	0		-	0	0	0	0	0
Parallel	0	0	0	4	10	14		-	13	0	2	14	29
CD 90-80	0	0	0	0	0	0		-	3	0	0	2	5
CD 80-30	0	0	0	0	1	1		-	10	0	0	3	13
CD 30-0	0	0	0	0	0	0		-	1	0	0	0	1
Short	0	0	0	0	0	0		-	2	0	0	0	2
Totals	1	0	0	4	19	24		-	58	8	10	28	104

	2nd row blasted							3rd row blasted					
#0414													
Crack Family	Burden Row 1	Burden Row 2	Burden Row 3	Burden Row 4	Behind Row 4	Total Cracks		Burden Row 1	Burden Row 2	Burden Row 3	Burden Row 4	Behind Row 4	Total Cracks
CB 90-80	-	-	3	2	1	6		-	-	-	4	1	5
CB 80-30	-	-	5	2	0	7		-	-	-	12	0	12
CB 30-0	-	-	4	0	0	4		-	-	-	10	0	10
SCB	-	-	27	7	9	43		-	-	-	14	9	23
Connect	-	-	1	0	0	1		-	-	-	1	0	1
Parallel	-	-	14	4	11	29		-	-	-	4	11	15
CD 90-80	-	-	1	0	0	1		-	-	-	0	1	1
CD 80-30	-	-	6	0	0	6		-	-	-	3	0	3
CD 30-0	-	-	7	0	0	7		-	-	-	5	0	5
Short	-	-	12	0	0	12		-	-	-	11	0	11
Totals	-	-	80	15	21	116		-	-	-	64	22	86

	4th row blasted					
#0414						
Crack Family	Burden Row 1	Burden Row 2	Burden Row 3	Burden Row 4	Behind Row 4	Total Cracks
CB 90-80	-	-	-	-	4	4
CB 80-30	-	-	-	-	10	10
CB 30-0	-	-	-	-	9	9
SCB	-	-	-	-	12	12
Connect	-	-	-	-	0	0
Parallel	-	-	-	-	11	11
CD 90-80	-	-	-	-	1	1
CD 80-30	-	-	-	-	2	2
CD 30-0	-	-	-	-	0	0
Short	-	-	-	-	3	3
Totals	-	-	-	-	52	52

Appendix 13 – Cracks behind the last Row blasted

Stage 2

	#0113_0-0-0				#0213_28-28-28				#0313_140-0-0			
	Slice 1	Slice 2	Slice 3	Slice 4	Slice 1	Slice 2	Slice 3	Slice 4	Slice 1	Slice 2	Slice 3	Slice 4
CB 90-80	4	4	4	1	5	5	4	4	3	3	3	2
CB 80-30	2	6	3	4	8	7	6	2	4	5	5	6
CB 30-0	7	11	13	11	10	6	9	8	4	6	15	9
SCB	1	3	2	6	3	7	8	10	3	4	8	4
Parallel	1	3	1	4	2	0	0	2	9	6	10	6
Connect	3	4	3	3	2	2	3	2	0	1	3	2
CD 90-80	0	2	0	3	3	1	1	1	1	3	4	4
CD 80-30	5	6	7	7	10	7	4	10	8	7	4	6
CD 30-0	4	2	3	1	6	2	6	3	4	6	2	8
Short	8	5	7	4	4	2	5	7	4	2	7	3
Totals	35	46	43	44	53	39	46	49	40	43	61	50

	#0413_73-73-73				#0613_28-0-0				#0713_28-73-73			
	Slice 1	Slice 2	Slice 3	Slice 4	Slice 1	Slice 2	Slice 3	Slice 4	Slice 1	Slice 2	Slice 3	Slice 4
CB 90-80	5	5	4	2	5	5	5	4	5	5	5	2
CB 80-30	9	7	11	10	2	3	7	5	3	4	6	8
CB 30-0	4	9	7	6	4	5	7	5	4	7	8	9
SCB	4	8	4	8	3	1	2	4	1	5	0	2
Parallel	7	8	9	9	2	4	3	3	2	5	3	4
Connect	2	3	2	2	2	2	2	1	2	3	2	3
CD 90-80	1	0	3	2	0	3	3	1	1	0	0	2
CD 80-30	3	4	14	9	4	2	8	0	4	4	8	5
CD 30-0	1	2	0	9	3	2	4	3	2	5	1	4
Short	0	3	3	7	5	4	5	7	6	3	0	4
Totals	34	46	55	62	30	31	46	33	30	41	33	43

Stage 3

	#0314				#0414			
	Slice 1	Slice 2	Slice 3	Slice 4	Slice 1	Slice 2	Slice 3	Slice 4
CB 90-80	2	1	3	2	0	1	1	1
CB 80-30	0	3	3	1	0	2	0	5
CB 30-0	0	1	0	0	3	1	3	2
SCB	4	1	2	5	5	5	7	6
Parallel	2	0	0	0	1	0	4	9
Connect	0	3	1	1	0	0	0	2
CD 90-80	0	0	0	0	0	0	0	0
CD 80-30	0	0	0	4	1	0	6	3
CD 30-0	0	0	0	6	4	3	6	7
Short	0	0	0	0	0	0	0	0
Totals	8	9	9	19	14	12	27	35

Summary

		Total Cracks	MCD [-]	MCID [-]
#0113_0-0-0	Slice 1	35	0.77	0.19
	Slice 2	46	0.87	0.16
	Slice 3	43	0.93	0.40
	Slice 4	44	1.22	0.58
#0213_28-28-28	Slice 1	53	0.99	0.19
	Slice 2	39	0.86	0.19
	Slice 3	46	0.91	0.22
	Slice 4	49	1.14	0.37
#0313_140-0-0	Slice 1	40	0.69	0.13
	Slice 2	43	0.78	0.17
	Slice 3	61	1.00	0.37
	Slice 4	50	1.19	0.56
#0413_73-73-73	Slice 1	34	0.99	0.40
	Slice 2	46	1.22	0.42
	Slice 3	55	1.36	0.48
	Slice 4	62	1.83	0.81
#0613_28-0-0	Slice 1	30	0.65	0.06
	Slice 2	31	0.84	0.22
	Slice 3	46	0.91	0.25
	Slice 4	33	0.80	0.23
#0713_28-73-73	Slice 1	30	0.62	0.39
	Slice 2	41	0.87	0.25
	Slice 3	33	0.79	0.15
	Slice 4	43	0.86	0.28
#0314 Normal	Slice 1	8	0.38	
	Slice 2	9	0.56	
	Slice 3	9	0.48	
	Slice 4	19	0.88	
#0414 Staggered	Slice 1	14	0.75	
	Slice 2	12	1.19	
	Slice 3	27	1.61	
	Slice 4	35	1.84	

Appendix 14 – Sieving Data Preliminary Tests

Sample-ID	#0111 - CH01B02		Screen size [mm]	Mass passing [%]
Blasting date	07.06.2011		125	100.00
Blasting type	Shots in a row		100	89.38
Row-#	1		80	87.39
Shot-#	1		63	72.75
Blasthole diameter	10	[mm]	50	65.07
Burden	70	[mm]	40	58.30
Side-spacing	110	[mm]	31.5	52.90
Charge type	20	[g/m]	25	45.75
			20	39.60
			14	30.76
			12.5	28.12
			10	23.34
			6.3	15.89
			4	11.26
			2	7.24
			1	4.90
			0.5	3.55
			0.25	1.48
			<0.25	0.00

Sample-ID	#0111 - CH01B02		Screen size [mm]	Mass passing [%]
Blasting date	07.06.2011		125	100.00
Blasting type	Shots in a row		100	100.00
Row-#	2		80	100.00
Shot-#	1		63	96.55
Blasthole diameter	10	[mm]	50	93.82
Burden	70	[mm]	40	85.01
Side-spacing	110	[mm]	31.5	74.14
Charge type	20	[g/m]	25	65.67
			20	56.61
			14	44.65
			12.5	41.25
			10	35.07
			6.3	24.61
			4	17.67
			2	11.23
			1	7.38
			0.5	5.23
			0.25	1.96
			<0.25	0.00

Sample-ID	#0211 - CH03B02		Screen size [mm]	Mass passing [%]
Blasting date	27.06.2011		125	100.00
Blasting type	Shots in a row		100	100.00
Row-#	1		80	94.30
Shot-#	1		63	86.45
Blasthole diameter	10	[mm]	50	82.53
Burden	70	[mm]	40	75.38
Side-spacing	95	[mm]	31.5	67.45
Charge type	20	[g/m]	25	60.23
			20	54.11
			14	43.99
			12.5	40.42
			10	34.75
			6.3	23.88
			4	17.27
			2	10.72
			1	6.91
			0.5	4.83
			0.25	1.86
			<0.25	0.00

Sample-ID	#0211 - CH03B02		Screen size [mm]	Mass passing [%]
Blasting date	27.06.2011		125	100.00
Blasting type	Shots in a row		100	100.00
Row-#	2		80	100.00
Shot-#	1		63	98.43
Blasthole diameter	10	[mm]	50	94.50
Burden	70	[mm]	40	86.81
Side-spacing	95	[mm]	31.5	82.03
Charge type	20	[g/m]	25	74.79
			20	67.38
			14	54.69
			12.5	51.14
			10	44.19
			6.3	30.85
			4	23.20
			2	15.64
			1	10.53
			0.5	7.55
			0.25	3.15
			<0.25	0.00

Sample-ID	#0411 - CH04B02		Screen size [mm]	Mass passing [%]
Blasting date	09.08.2011		125	79.92
Blasting type	Single Hole Shots		100	65.34
Row-#	1		80	59.91
Shot-#	1		63	52.75
Blasthole diameter	10	[mm]	50	47.78
Burden		[mm]	40	40.91
Side-spacing		[mm]	31.5	32.75
Charge type	20	[g/m]	25	25.53
			20	20.13
			14	14.03
			12.5	12.50
			10	9.84
			6.3	6.06
			4	4.10
			2	2.49
			1	1.55
			0.5	1.00
			0.25	0.42
			<0.25	0.00

Sample-ID	#0411 - CH04B02		Screen size [mm]	Mass passing [%]
Blasting date	09.08.2011		125	100.00
Blasting type	Single Hole Shots		100	100.00
Row-#	2		80	82.67
Shot-#	1		63	62.14
Blasthole diameter	10	[mm]	50	50.83
Burden		[mm]	40	42.11
Side-spacing		[mm]	31.5	36.62
Charge type	20	[g/m]	25	26.84
			20	21.69
			14	15.10
			12.5	13.33
			10	10.23
			6.3	6.73
			4	4.49
			2	2.70
			1	1.63
			0.5	1.05
			<0.5	0.00

Sample-ID	#0511 - CH02B04		Screen size [mm]	Mass passing [%]
Blasting date	31.08.2011		125	100.00
Blasting type	Single Hole Shots		100	100.00
Row-#	1		80	100.00
Shot-#	1		63	95.43
Blasthole diameter	10	[mm]	50	84.00
Burden		[mm]	40	74.17
Side-spacing		[mm]	31.5	66.59
Charge type	20	[g/m]	25	59.46
			20	50.33
			14	39.00
			12.5	35.89
			10	29.74
			6.3	20.24
			4	13.66
			2	7.91
			1	4.71
			0.5	3.06
			<0.5	0.00

Sample-ID	#0511 - CH02B04		Screen size [mm]	Mass passing [%]
Blasting date	31.08.2011		125	100.00
Blasting type	Single Hole Shots		100	79.92
Row-#	1		80	79.92
Shot-#	2		63	59.41
Blasthole diameter	10	[mm]	50	50.96
Burden		[mm]	40	43.86
Side-spacing		[mm]	31.5	36.28
Charge type	20	[g/m]	25	30.36
			20	25.84
			14	20.37
			12.5	18.60
			10	15.40
			6.3	11.31
			4	8.22
			2	5.51
			1	3.89
			0.5	2.87
			<0.5	0.00

Sample-ID	#0511 - CH02B04		Screen size [mm]	Mass passing [%]
Blasting date	31.08.2011		125	100.00
Blasting type	Single Hole Shots		100	100.00
Row-#	1		80	100.00
Shot-#	3		63	100.00
Blasthole diameter	10	[mm]	50	81.36
Burden		[mm]	40	70.26
Side-spacing		[mm]	31.5	64.71
Charge type	20	[g/m]	25	56.52
			20	49.38
			14	40.86
			12.5	37.59
			10	33.18
			6.3	25.89
			4	20.88
			2	15.12
			1	11.03
			0.5	8.31
			<0.5	0.00

Sample-ID	#0511 - CH02B04		Screen size [mm]	Mass passing [%]
Blasting date	01.09.2011		125	100.00
Blasting type	Single Hole Shots		100	100.00
Row-#	1		80	100.00
Shot-#	4		63	100.00
Blasthole diameter	10	[mm]	50	76.96
Burden		[mm]	40	53.80
Side-spacing		[mm]	31.5	34.61
Charge type	20	[g/m]	25	26.46
			20	23.19
			14	15.67
			12.5	14.35
			10	12.14
			6.3	8.46
			4	6.04
			2	3.96
			1	2.67
			0.5	1.84
			<0.5	0.00

Sample-ID	#0511 - CH02B04		Screen size [mm]	Mass passing [%]
Blasting date	01.09.2011		125	100.00
Blasting type	Single Hole Shots		100	100.00
Row-#	1		80	100.00
Shot-#	5		63	100.00
Blasthole diameter	10	[mm]	50	100.00
Burden		[mm]	40	85.39
Side-spacing		[mm]	31.5	76.92
Charge type	20	[g/m]	25	66.45
			20	57.20
			14	42.11
			12.5	38.92
			10	31.44
			6.3	21.77
			4	15.38
			2	9.41
			1	5.97
			0.5	4.05
			<0.5	0.00

Sample-ID	#0511 - CH02B04		Screen size [mm]	Mass passing [%]
Blasting date	01.09.2011		125	100.00
Blasting type	Single Hole Shots		100	100.00
Row-#	2		80	96.01
Shot-#	1		63	96.01
Blasthole diameter	10	[mm]	50	93.50
Burden		[mm]	40	78.03
Side-spacing		[mm]	31.5	68.78
Charge type	20	[g/m]	25	56.04
			20	46.82
			14	32.14
			12.5	28.54
			10	23.23
			6.3	15.77
			4	10.84
			2	6.52
			1	4.26
			0.5	2.94
			<0.5	0.00

Sample-ID	#0611 - CH02B03		Screen size [mm]	Mass passing [%]
Blasting date	07.09.2011		125	100.00
Blasting type	Single Hole Shots		100	100.00
Row-#	1		80	100.00
Shot-#	1		63	100.00
Blasthole diameter	10	[mm]	50	100.00
Burden	70	[mm]	40	83.61
Side-spacing		[mm]	31.5	72.26
Charge type	20	[g/m]	25	63.72
			20	55.97
			14	43.39
			12.5	39.09
			10	33.11
			6.3	22.49
			4	15.59
			2	9.47
			1	5.99
			0.5	4.05
			<0.5	0.00

Sample-ID	#0611 - CH02B03		Screen size [mm]	Mass passing [%]
Blasting date	07.09.2011		125	79.31
Blasting type	Single Hole Shots		100	71.57
Row-#	1		80	71.57
Shot-#	2		63	71.57
Blasthole diameter	10	[mm]	50	68.32
Burden	70	[mm]	40	59.23
Side-spacing		[mm]	31.5	51.06
Charge type	20	[g/m]	25	44.17
			20	39.20
			14	31.01
			12.5	28.84
			10	25.29
			6.3	19.05
			4	14.26
			2	9.65
			1	6.64
			0.5	4.79
			<0.5	0.00

Sample-ID	#0611 - CH02B03		Screen size [mm]	Mass passing [%]
Blasting date	07.09.2011		125	100.00
Blasting type	Single Hole Shots		100	53.97
Row-#	1		80	40.17
Shot-#	3		63	40.17
Blasthole diameter	10	[mm]	50	32.32
Burden		[mm]	40	26.72
Side-spacing		[mm]	31.5	22.20
Charge type	20	[g/m]	25	18.93
			20	16.31
			14	13.23
			12.5	11.93
			10	10.51
			6.3	8.47
			4	6.78
			2	5.13
			1	3.95
			0.5	3.06
			<0.5	0.00

Sample-ID	#0611 - CH02B03		Screen size [mm]	Mass passing [%]
Blasting date	07.09.2011		125	100.00
Blasting type	Single Hole Shots		100	100.00
Row-#	1		80	93.32
Shot-#	4		63	93.32
Blasthole diameter	10	[mm]	50	81.99
Burden		[mm]	40	77.34
Side-spacing		[mm]	31.5	66.12
Charge type	20	[g/m]	25	58.00
			20	49.77
			14	39.26
			12.5	35.93
			10	30.50
			6.3	21.47
			4	15.38
			2	9.87
			1	6.68
			0.5	4.89
			<0.5	0.00

Sample-ID	#0611 - CH02B03		Screen size [mm]	Mass passing [%]
Blasting date	07.09.2011		125	100.00
Blasting type	Single Hole Shots		100	100.00
Row-#	2		80	90.06
Shot-#	1		63	90.06
Blasthole diameter	10	[mm]	50	90.06
Burden	70	[mm]	40	83.12
Side-spacing		[mm]	31.5	73.09
Charge type	20	[g/m]	25	64.01
			20	56.56
			14	43.97
			12.5	40.16
			10	33.60
			6.3	23.41
			4	16.30
			2	10.26
			1	6.80
			0.5	4.86
			<0.5	0.00

Sample-ID	#0611 - CH02B03		Screen size [mm]	Mass passing [%]
Blasting date	07.09.2011		125	100.00
Blasting type	Single Hole Shots		100	100.00
Row-#	2		80	100.00
Shot-#	2		63	96.55
Blasthole diameter	10	[mm]	50	83.48
Burden	70	[mm]	40	74.17
Side-spacing		[mm]	31.5	64.15
Charge type	20	[g/m]	25	52.36
			20	44.04
			14	32.74
			12.5	29.61
			10	24.70
			6.3	17.10
			4	12.30
			2	7.89
			1	5.31
			0.5	3.82
			<0.5	0.00

Sample-ID	#0611 - CH02B03		Screen size [mm]	Mass passing [%]
Blasting date	07.09.2011		125	100.00
Blasting type	Single Hole Shots		100	100.00
Row-#	2		80	100.00
Shot-#	3		63	100.00
Blasthole diameter	10	[mm]	50	100.00
Burden		[mm]	40	92.43
Side-spacing		[mm]	31.5	80.52
Charge type	20	[g/m]	25	73.98
			20	67.26
			14	53.58
			12.5	48.83
			10	43.55
			6.3	32.99
			4	26.27
			2	19.24
			1	14.67
			0.5	11.60
			<0.5	0.00

Sample-ID	#0611 - CH02B03		Screen size [mm]	Mass passing [%]
Blasting date	07.09.2011		125	100.00
Blasting type	Single Hole Shots		100	72.39
Row-#	2		80	72.39
Shot-#	4		63	67.00
Blasthole diameter	10	[mm]	50	60.18
Burden		[mm]	40	60.18
Side-spacing		[mm]	31.5	57.35
Charge type	20	[g/m]	25	49.52
			20	43.38
			14	34.55
			12.5	31.77
			10	26.37
			6.3	18.36
			4	12.98
			2	7.85
			1	5.22
			0.5	3.74
			<0.5	0.00

Appendix 15 – Sieving Data Stage 1

Sample-ID	#0212 - CH04B03		Screen size [mm]	Mass passing [%]
Blasting date	18.07.2012		125	100.00
Blasting type	Shots in a row		100	93.38
Row-#	1		80	76.45
Blasthole diameter	10	[mm]	63	61.80
Burden	70	[mm]	50	59.11
Side-spacing	110	[mm]	40	51.79
Charge type	20	[g/m]	31.5	44.77
Planned delay	140	[µs]	25	36.81
			20	30.54
			14	22.46
			12.5	19.93
			10	15.76
			6.3	10.12
			4	6.78
			2	4.15
			1	2.65
			0.5	1.61
			0.25	0.61
			<0.25	0.00

Sample-ID	#0212 - CH04B03		Screen size [mm]	Mass passing [%]
Blasting date	18.07.2012		125	100.00
Blasting type	Shots in a row		100	92.94
Row-#	2		80	89.22
Blasthole diameter	10	[mm]	63	79.56
Burden	70	[mm]	50	76.56
Side-spacing	110	[mm]	40	72.08
Charge type	20	[g/m]	31.5	63.57
Planned delay	140	[µs]	25	55.18
			20	47.18
			14	35.34
			12.5	32.49
			10	27.15
			6.3	18.99
			4	13.14
			2	8.09
			1	5.28
			0.5	3.29
			0.25	1.28
			<0.25	0.00

Sample-ID	#0212 - CH04B03		Screen size [mm]	Mass passing [%]
Blasting date	18.07.2012		125	100.00
Blasting type	Shots in a row		100	89.69
Row-#	3		80	89.69
Blasthole diameter	10	[mm]	63	89.69
Burden	70	[mm]	50	87.87
Side-spacing	110	[mm]	40	81.29
Charge type	20	[g/m]	31.5	75.19
Planned delay	140	[µs]	25	66.60
			20	58.60
			14	45.16
			12.5	41.67
			10	35.12
			6.3	23.11
			4	15.60
			2	9.39
			1	6.18
			0.5	4.07
			0.25	1.70
			<0.25	0.00

Sample-ID	#0312 - CH04B04		Screen size [mm]	Mass passing [%]
Blasting date	24.07.2012		125	100.00
Blasting type	Shots in a row		100	90.02
Row-#	1		80	80.68
Blasthole diameter	10	[mm]	63	70.92
Burden	70	[mm]	50	61.21
Side-spacing	110	[mm]	40	53.30
Charge type	20	[g/m]	31.5	45.70
Planned delay	140	[µs]	25	39.96
			20	32.93
			14	23.94
			12.5	21.36
			10	17.00
			6.3	10.81
			4	7.81
			2	4.80
			1	3.28
			0.5	2.15
			0.25	0.94
			<0.25	0.00

Sample-ID	#0312 - CH04B04		Screen size [mm]	Mass passing [%]
Blasting date	24.07.2012		125	100.00
Blasting type	Shots in a row		100	87.88
Row-#	2		80	84.96
Blasthole diameter	10	[mm]	63	73.62
Burden	70	[mm]	50	70.46
Side-spacing	110	[mm]	40	61.60
Charge type	20	[g/m]	31.5	51.82
Planned delay	0	[µs]	25	42.86
			20	36.30
			14	27.94
			12.5	25.65
			10	22.20
			6.3	14.61
			4	10.71
			2	6.43
			1	4.30
			0.5	2.84
			<0.5	1.23

Sample-ID	#0312 - CH04B04		Screen size [mm]	Mass passing [%]
Blasting date	24.07.2012		125	100.00
Blasting type	Shots in a row		100	92.79
Row-#	3		80	92.79
Blasthole diameter	10	[mm]	63	77.18
Burden	70	[mm]	50	62.24
Side-spacing	110	[mm]	40	54.26
Charge type	20	[g/m]	31.5	46.85
Planned delay	0	[µs]	25	39.85
			20	32.86
			14	26.90
			12.5	24.17
			10	20.29
			6.3	14.51
			4	10.58
			2	6.77
			1	4.53
			0.5	3.06
			<0.5	0.00

Sample-ID	#0412 - CH04B05		Screen size [mm]	Mass passing [%]
Blasting date	28.08.2012		125	100.00
Blasting type	Shots in a row		100	82.98
Row-#	1		80	82.98
Blasthole diameter	10	[mm]	63	64.83
Burden	70	[mm]	50	59.40
Side-spacing	110	[mm]	40	53.53
Charge type	20	[g/m]	31.5	46.48
Planned delay	140	[µs]	25	40.18
			20	34.79
			14	25.65
			12.5	22.92
			10	18.86
			6.3	12.53
			4	8.62
			2	5.25
			1	3.42
			0.5	2.29
			<0.5	0.00

Sample-ID	#0412 - CH04B05		Screen size [mm]	Mass passing [%]
Blasting date	28.08.2012		125	100.00
Blasting type	Shots in a row		100	92.17
Row-#	2		80	89.84
Blasthole diameter	10	[mm]	63	78.46
Burden	70	[mm]	50	73.65
Side-spacing	110	[mm]	40	69.41
Charge type	20	[g/m]	31.5	61.43
Planned delay	140	[µs]	25	54.01
			20	46.49
			14	35.05
			12.5	31.81
			10	26.02
			6.3	17.86
			4	12.20
			2	7.22
			1	4.64
			0.5	3.07
			<0.5	0.00

Sample-ID	#0512 - CH04B01		Screen size [mm]	Mass passing [%]
Blasting date	14.09.2012		125	100.00
Blasting type	Shots in a row		100	95.12
Row-#	2		80	80.38
Blasthole diameter	10	[mm]	63	72.05
Burden	70	[mm]	50	66.81
Side-spacing	110	[mm]	40	57.03
Charge type	20	[g/m]	31.5	47.17
Planned delay	140	[µs]	25	40.51
			20	32.54
			14	25.32
			12.5	22.50
			10	18.41
			6.3	12.37
			4	8.47
			2	5.02
			1	3.14
			0.5	1.98
			<0.5	0.00

Sample-ID	#0512 - CH04B01		Screen size [mm]	Mass passing [%]
Blasting date	14.09.2012		125	100.00
Blasting type	Shots in a row		100	93.49
Row-#	2		80	88.04
Blasthole diameter	10	[mm]	63	78.05
Burden	70	[mm]	50	67.88
Side-spacing	110	[mm]	40	61.16
Charge type	20	[g/m]	31.5	53.19
Planned delay	0	[µs]	25	45.98
			20	37.57
			14	29.29
			12.5	27.12
			10	22.56
			6.3	16.02
			4	11.17
			2	6.83
			1	4.45
			0.5	2.91
			<0.5	0.00

Sample-ID	#0612 - CH03B04		Screen size [mm]	Mass passing [%]
Blasting date	03.10.2012		125	100.00
Blasting type	Shots in a row		100	94.89
Row-#	1		80	85.58
Blasthole diameter	10	[mm]	63	78.48
Burden	70	[mm]	50	74.08
Side-spacing	110	[mm]	40	62.00
Charge type	20	[g/m]	31.5	53.54
Planned delay	140	[µs]	25	47.02
			20	39.73
			14	29.51
			12.5	26.98
			10	21.65
			6.3	14.43
			4	9.58
			2	5.52
			1	3.62
			0.5	2.41
			<0.5	0.00

Sample-ID	#0612 - CH03B04		Screen size [mm]	Mass passing [%]
Blasting date	03.10.2012		125	100.00
Blasting type	Shots in a row		100	94.42
Row-#	2		80	91.05
Blasthole diameter	10	[mm]	63	84.88
Burden	70	[mm]	50	74.07
Side-spacing	110	[mm]	40	63.85
Charge type	20	[g/m]	31.5	58.16
Planned delay	73	[µs]	25	51.64
			20	44.17
			14	33.76
			12.5	30.53
			10	25.71
			6.3	18.00
			4	12.57
			2	7.59
			1	5.11
			0.5	3.50
			<0.5	0.00

Sample-ID	#0612 - CH03B04		Screen size [mm]	Mass passing [%]
Blasting date	03.10.2012		125	100.00
Blasting type	Shots in a row		100	100.00
Row-#	3		80	95.07
Blasthole diameter	10	[mm]	63	91.05
Burden	70	[mm]	50	86.90
Side-spacing	110	[mm]	40	76.15
Charge type	20	[g/m]	31.5	65.62
Planned delay	73	[µs]	25	57.01
			20	50.60
			14	39.17
			12.5	36.26
			10	30.94
			6.3	21.84
			4	15.13
			2	9.08
			1	6.01
			0.5	4.06
			<0.5	0.00

Sample-ID	#0712 - CH03B05		Screen size [mm]	Mass passing [%]
Blasting date	05.10.2012		125	100.00
Blasting type	Shots in a row		100	90.40
Row-#	1		80	79.70
Blasthole diameter	10	[mm]	63	69.60
Burden	70	[mm]	50	60.62
Side-spacing	110	[mm]	40	54.37
Charge type	20	[g/m]	31.5	44.07
Planned delay	140	[µs]	25	36.67
			20	31.59
			14	23.65
			12.5	20.86
			10	17.11
			6.3	11.57
			4	8.16
			2	4.94
			1	3.33
			0.5	2.29
			<0.5	0.00

Sample-ID	#0712 - CH03B05		Screen size [mm]	Mass passing [%]
Blasting date	05.10.2012		125	100.00
Blasting type	Shots in a row		100	93.28
Row-#	3		80	82.70
Blasthole diameter	10	[mm]	63	68.74
Burden	70	[mm]	50	62.07
Side-spacing	110	[mm]	40	54.30
Charge type	20	[g/m]	31.5	50.09
Planned delay	28	[µs]	25	43.68
			20	37.11
			14	28.54
			12.5	26.29
			10	21.96
			6.3	15.40
			4	11.12
			2	6.85
			1	4.53
			0.5	3.10
			<0.5	0.00

Sample-ID	#0712 - CH03B05		Screen size [mm]	Mass passing [%]
Blasting date	05.10.2012		125	100.00
Blasting type	Shots in a row		100	100.00
Row-#	3		80	84.02
Blasthole diameter	10	[mm]	63	82.50
Burden	70	[mm]	50	71.66
Side-spacing	110	[mm]	40	61.89
Charge type	20	[g/m]	31.5	54.57
Planned delay	28	[µs]	25	46.36
			20	39.98
			14	31.01
			12.5	28.18
			10	23.88
			6.3	17.46
			4	12.62
			2	8.02
			1	5.54
			0.5	3.96
			<0.5	0.00

Sample-ID	#0812 - CH03B01		Screen size [mm]	Mass passing [%]
Blasting date	17.10.2012		125	100.00
Blasting type	Shots in a row		100	100.00
Row-#	1		80	84.02
Blasthole diameter	10	[mm]	63	82.50
Burden	70	[mm]	50	71.66
Side-spacing	110	[mm]	40	61.89
Charge type	20	[g/m]	31.5	54.57
Planned delay	140	[µs]	25	46.36
			20	39.98
			14	31.01
			12.5	28.18
			10	23.88
			6.3	17.46
			4	12.62
			2	8.02
			1	5.54
			0.5	3.96
			<0.5	0.00

Sample-ID	#0812 - CH03B01		Screen size [mm]	Mass passing [%]
Blasting date	17.10.2012		125	100.00
Blasting type	Shots in a row		100	100.00
Row-#	2		80	84.02
Blasthole diameter	10	[mm]	63	82.50
Burden	70	[mm]	50	71.66
Side-spacing	110	[mm]	40	61.89
Charge type	20	[g/m]	31.5	54.57
Planned delay	0	[µs]	25	46.36
			20	39.98
			14	31.01
			12.5	28.18
			10	23.88
			6.3	17.46
			4	12.62
			2	8.02
			1	5.54
			0.5	3.96
			<0.5	0.00

Sample-ID	#0812 - CH03B01		Screen size [mm]	Mass passing [%]
Blasting date	17.10.2012		125	100.00
Blasting type	Shots in a row		100	100.00
Row-#	3		80	84.02
Blasthole diameter	10	[mm]	63	82.50
Burden	70	[mm]	50	71.66
Side-spacing	110	[mm]	40	61.89
Charge type	20	[g/m]	31.5	54.57
Planned delay	140	[µs]	25	46.36
			20	39.98
			14	31.01
			12.5	28.18
			10	23.88
			6.3	17.46
			4	12.62
			2	8.02
			1	5.54
			0.5	3.96
			<0.5	0.00

Sample-ID	#0912 - CH03B03		Screen size [mm]	Mass passing [%]
Blasting date	25.10.2012		125	100.00
Blasting type	Shots in a row		100	100.00
Row-#	1		80	82.97
Blasthole diameter	10	[mm]	63	71.39
Burden	70	[mm]	50	60.83
Side-spacing	110	[mm]	40	52.65
Charge type	20	[g/m]	31.5	46.16
Planned delay	140	[µs]	25	39.48
			20	34.69
			14	26.61
			12.5	24.46
			10	19.92
			6.3	13.93
			4	9.69
			2	6.01
			1	4.05
			0.5	2.78
			<0.5	0.00

Sample-ID	#0912 - CH03B03		Screen size [mm]	Mass passing [%]
Blasting date	25.10.2012		125	100.00
Blasting type	Shots in a row		100	89.45
Row-#	3		80	85.91
Blasthole diameter	10	[mm]	63	84.02
Burden	70	[mm]	50	79.11
Side-spacing	110	[mm]	40	69.16
Charge type	20	[g/m]	31.5	63.25
Planned delay	140	[µs]	25	56.56
			20	51.15
			14	40.28
			12.5	37.88
			10	32.01
			6.3	22.06
			4	14.73
			2	8.89
			1	5.97
			0.5	3.95
			<0.5	0.00

Sample-ID	#0912 - CH03B03		Screen size [mm]	Mass passing [%]
Blasting date	25.10.2012		125	100.00
Blasting type	Shots in a row		100	89.45
Row-#	3		80	84.21
Blasthole diameter	10	[mm]	63	84.21
Burden	70	[mm]	50	83.18
Side-spacing	110	[mm]	40	77.64
Charge type	20	[g/m]	31.5	71.02
Planned delay	140	[µs]	25	65.05
			20	59.04
			14	46.37
			12.5	43.06
			10	35.84
			6.3	24.32
			4	16.62
			2	10.18
			1	6.79
			0.5	4.64
			<0.5	0.00

Appendix 16 – Sieving Data Stage 2

Sample-ID	#0113 - CH02B01		Screen size [mm]	Mass passing [%]
Blasting date	03.07.2013		125	100.00
Blasting type	Shots in a row		100	93.70
Row-#	1		80	74.75
Blasthole diameter	10	[mm]	63	60.20
Burden	70	[mm]	50	52.61
Side-spacing	110	[mm]	40	42.37
Charge type	20	[g/m]	31.5	33.80
Planned delay	0	[µs]	25	28.22
			20	23.82
			14	18.16
			12.5	17.15
			10	14.44
			6.3	10.36
			4	7.29
			2	5.43
			1	3.99
			0.5	2.78
			< 0.5	0.00

Sample-ID	#0113 - CH02B01		Screen size [mm]	Mass passing [%]
Blasting date	03.07.2013		125	72.01
Blasting type	Shots in a row		100	63.12
Row-#	2		80	48.96
Blasthole diameter	10	[mm]	63	44.46
Burden	70	[mm]	50	37.13
Side-spacing	110	[mm]	40	34.37
Charge type	20	[g/m]	31.5	31.75
Planned delay	0	[µs]	25	27.49
			20	23.72
			14	19.60
			12.5	18.48
			10	15.98
			6.3	12.11
			4	8.59
			2	6.13
			1	4.41
			0.5	3.00
			< 0.5	0.00

Sample-ID	#0113 - CH02B01		Screen size [mm]	Mass passing [%]
Blasting date	03.07.2013		125	100.00
Blasting type	Shots in a row		100	100.00
Row-#	3		80	91.69
Blasthole diameter	10	[mm]	63	78.71
Burden	70	[mm]	50	70.66
Side-spacing	110	[mm]	40	58.59
Charge type	20	[g/m]	31.5	49.33
Planned delay	0	[µs]	25	41.61
			20	35.06
			14	27.32
			12.5	25.14
			10	22.06
			6.3	15.92
			4	11.20
			2	7.94
			1	5.74
			0.5	3.86
			< 0.5	0.00

Sample-ID	#0213 - CH02B02		Screen size [mm]	Mass passing [%]
Blasting date	17.07.2013		125	100.00
Blasting type	Shots in a row		100	86.23
Row-#	1		80	64.18
Blasthole diameter	10	[mm]	63	45.71
Burden	70	[mm]	50	35.95
Side-spacing	110	[mm]	40	29.91
Charge type	20	[g/m]	31.5	25.87
Planned delay	28	[µs]	25	23.42
			20	21.26
			14	17.12
			12.5	15.64
			10	13.69
			6.3	9.51
			4	6.27
			2	4.38
			1	3.12
			0.5	2.11
			< 0.5	0.00

Sample-ID	#0213 - CH02B02		Screen size [mm]	Mass passing [%]
Blasting date	17.07.2013		125	100.00
Blasting type	Shots in a row		100	78.68
Row-#	2		80	67.95
Blasthole diameter	10	[mm]	63	49.77
Burden	70	[mm]	50	42.39
Side-spacing	110	[mm]	40	39.12
Charge type	20	[g/m]	31.5	34.40
Planned delay	28	[µs]	25	30.52
			20	26.34
			14	21.10
			12.5	19.79
			10	16.50
			6.3	11.64
			4	7.40
			2	5.00
			1	3.45
			0.5	2.21
			< 0.5	0.00

Sample-ID	#0213 - CH02B02		Screen size [mm]	Mass passing [%]
Blasting date	17.07.2013		125	100.00
Blasting type	Shots in a row		100	100.00
Row-#	3		80	86.80
Blasthole diameter	10	[mm]	63	67.11
Burden	70	[mm]	50	54.54
Side-spacing	110	[mm]	40	47.55
Charge type	20	[g/m]	31.5	41.43
Planned delay	28	[µs]	25	34.05
			20	30.08
			14	22.69
			12.5	21.08
			10	17.75
			6.3	11.96
			4	7.79
			2	5.20
			1	3.55
			0.5	2.32
			< 0.5	0.00

Sample-ID	#0313 - CH02B03		Screen size [mm]	Mass passing [%]
Blasting date	17.07.2013		125	100.00
Blasting type	Shots in a row		100	94.94
Row-#	1		80	80.23
Blasthole diameter	10	[mm]	63	62.74
Burden	70	[mm]	50	56.98
Side-spacing	110	[mm]	40	49.78
Charge type	20	[g/m]	31.5	41.57
Planned delay	140	[µs]	25	35.93
			20	29.17
			14	21.35
			12.5	19.04
			10	15.70
			6.3	9.89
			4	6.19
			2	4.13
			1	2.84
			0.5	1.90
			< 0.5	0.00

Sample-ID	#0313 - CH02B03		Screen size [mm]	Mass passing [%]
Blasting date	17.07.2013		125	100.00
Blasting type	Shots in a row		100	92.39
Row-#	2		80	88.23
Blasthole diameter	10	[mm]	63	73.92
Burden	70	[mm]	50	61.25
Side-spacing	110	[mm]	40	52.43
Charge type	20	[g/m]	31.5	46.09
Planned delay	0	[µs]	25	40.48
			20	35.35
			14	27.46
			12.5	24.91
			10	21.18
			6.3	14.17
			4	8.64
			2	6.01
			1	4.23
			0.5	2.69
			< 0.5	0.00

Sample-ID	#0313 - CH02B03		Screen size [mm]	Mass passing [%]
Blasting date	17.07.2013		125	100.00
Blasting type	Shots in a row		100	100.00
Row-#	3		80	93.51
Blasthole diameter	10	[mm]	63	77.50
Burden	70	[mm]	50	67.08
Side-spacing	110	[mm]	40	54.85
Charge type	20	[g/m]	31.5	44.19
Planned delay	0	[µs]	25	38.46
			20	32.19
			14	24.84
			12.5	22.47
			10	18.97
			6.3	13.00
			4	8.46
			2	5.80
			1	4.01
			0.5	2.57
			< 0.5	0.00

Sample-ID	#0413 - CH02B04		Screen size [mm]	Mass passing [%]
Blasting date	30.08.2013		125	100.00
Blasting type	Shots in a row		100	82.96
Row-#	1		80	79.10
Blasthole diameter	10	[mm]	63	61.33
Burden	70	[mm]	50	54.45
Side-spacing	110	[mm]	40	45.50
Charge type	20	[g/m]	31.5	38.11
Planned delay	73	[µs]	25	32.18
			20	26.04
			14	18.79
			12.5	17.40
			10	13.18
			6.3	9.23
			4	5.68
			2	3.99
			1	2.70
			0.5	1.74
			< 0.5	0.00

Sample-ID	#0413 - CH02B04		Screen size [mm]	Mass passing [%]
Blasting date	30.08.2013		125	100.00
Blasting type	Shots in a row		100	100.00
Row-#	2		80	95.15
Blasthole diameter	10	[mm]	63	81.03
Burden	70	[mm]	50	72.93
Side-spacing	110	[mm]	40	65.71
Charge type	20	[g/m]	31.5	55.08
Planned delay	73	[µs]	25	47.36
			20	40.28
			14	30.12
			12.5	27.90
			10	22.95
			6.3	13.72
			4	8.83
			2	5.76
			1	3.87
			0.5	2.48
			< 0.5	0.00

Sample-ID	#0413 - CH02B04		Screen size [mm]	Mass passing [%]
Blasting date	30.08.2013		125	100.00
Blasting type	Shots in a row		100	91.78
Row-#	3		80	89.49
Blasthole diameter	10	[mm]	63	88.42
Burden	70	[mm]	50	82.93
Side-spacing	110	[mm]	40	70.25
Charge type	20	[g/m]	31.5	63.13
Planned delay	73	[µs]	25	52.20
			20	43.25
			14	32.39
			12.5	29.38
			10	24.08
			6.3	15.69
			4	10.25
			2	6.80
			1	4.67
			0.5	3.05
			< 0.5	0.00

Sample-ID	#0513 - CH02B05		Screen size [mm]	Mass passing [%]
Blasting date	24.09.2013		125	100.00
Blasting type	Shots in a row		100	83.60
Row-#	1		80	65.11
Blasthole diameter	10	[mm]	63	46.97
Burden	70	[mm]	50	42.85
Side-spacing	110	[mm]	40	37.02
Charge type	20	[g/m]	31.5	32.15
Planned delay	28	[µs]	25	27.11
			20	22.84
			14	17.55
			12.5	16.17
			10	13.46
			6.3	9.54
			4	6.44
			2	4.60
			1	3.40
			0.5	2.39
			< 0.5	0.00

Sample-ID	#0613 - CH03B05		Screen size [mm]	Mass passing [%]
Blasting date	08.10.2013		125	100.00
Blasting type	Shots in a row		100	79.57
Row-#	1		80	52.83
Blasthole diameter	10	[mm]	63	38.11
Burden	70	[mm]	50	33.34
Side-spacing	110	[mm]	40	29.77
Charge type	20	[g/m]	31.5	25.83
Planned delay	28	[µs]	25	23.02
			20	20.09
			14	14.94
			12.5	13.58
			10	11.91
			6.3	8.54
			4	5.47
			2	3.76
			1	2.55
			0.5	1.79
			< 0.5	0.00

Sample-ID	#0613 - CH03B05		Screen size [mm]	Mass passing [%]
Blasting date	08.10.2013		125	100.00
Blasting type	Shots in a row		100	93.91
Row-#	2		80	80.64
Blasthole diameter	10	[mm]	63	67.27
Burden	70	[mm]	50	54.09
Side-spacing	110	[mm]	40	45.19
Charge type	20	[g/m]	31.5	40.02
Planned delay	0	[µs]	25	34.03
			20	29.34
			14	22.34
			12.5	20.86
			10	17.57
			6.3	12.34
			4	7.68
			2	5.16
			1	3.35
			0.5	2.10
			< 0.5	0.00

Sample-ID	#0613 - CH03B05		Screen size [mm]	Mass passing [%]
Blasting date	08.10.2013		125	100.00
Blasting type	Shots in a row		100	92.14
Row-#	3		80	87.91
Blasthole diameter	10	[mm]	63	67.90
Burden	70	[mm]	50	62.13
Side-spacing	110	[mm]	40	52.90
Charge type	20	[g/m]	31.5	45.44
Planned delay	0	[µs]	25	39.54
			20	33.76
			14	25.80
			12.5	23.89
			10	20.29
			6.3	14.00
			4	8.59
			2	5.56
			1	3.67
			0.5	2.34
			< 0.5	0.00

Sample-ID	#0713 - CH03B04		Screen size [mm]	Mass passing [%]
Blasting date	14.10.2013		125	100.00
Blasting type	Shots in a row		100	83.98
Row-#	1		80	51.69
Blasthole diameter	10	[mm]	63	40.38
Burden	70	[mm]	50	34.09
Side-spacing	110	[mm]	40	29.86
Charge type	20	[g/m]	31.5	28.10
Planned delay	28	[µs]	25	23.67
			20	20.90
			14	15.92
			12.5	14.36
			10	12.13
			6.3	8.65
			4	5.31
			2	3.57
			1	2.37
			0.5	1.54
			< 0.5	0.00

Sample-ID	#0713 - CH03B04		Screen size [mm]	Mass passing [%]
Blasting date	14.10.2013		125	100.00
Blasting type	Shots in a row		100	89.00
Row-#	2		80	83.94
Blasthole diameter	10	[mm]	63	72.76
Burden	70	[mm]	50	60.91
Side-spacing	110	[mm]	40	55.28
Charge type	20	[g/m]	31.5	48.97
Planned delay	73	[µs]	25	43.09
			20	36.66
			14	26.75
			12.5	24.70
			10	20.45
			6.3	13.61
			4	7.97
			2	5.30
			1	3.43
			0.5	2.18
			< 0.5	0.00

Sample-ID	#0713 - CH03B04		Screen size [mm]	Mass passing [%]
Blasting date	14.10.2013		125	100.00
Blasting type	Shots in a row		100	100.00
Row-#	3		80	100.00
Blasthole diameter	10	[mm]	63	92.58
Burden	70	[mm]	50	81.72
Side-spacing	110	[mm]	40	72.69
Charge type	20	[g/m]	31.5	61.84
Planned delay	73	[µs]	25	54.95
			20	46.41
			14	33.58
			12.5	31.26
			10	25.59
			6.3	16.89
			4	10.28
			2	6.93
			1	4.57
			0.5	2.95
			< 0.5	0.00

Appendix 17 – Sieving Data Stage 3

Sample-ID	#0114 - BG01		Screen size [mm]	Mass passing [%]
Blasting date	20.05.2014		125	100.00
Blasting type	Shots in a row		100	74.11
Row-#	1		80	59.17
Blasthole diameter	10	[mm]	63	39.78
Burden	70	[mm]	50	33.22
Side-spacing	110	[mm]	40	31.06
Charge type	20	[g/m]	31.5	28.74
Planned delay	28	[µs]	25	27.27
			20	24.28
			14	19.88
			12.5	18.58
			10	16.06
			6.3	12.12
			4	8.59
			2	6.29
			1	4.74
			0.5	3.65
			< 0.5	0.00

Sample-ID	#0114 - BG01		Screen size [mm]	Mass passing [%]
Blasting date	20.05.2014		125	100.00
Blasting type	Shots in a row		100	81.11
Row-#	2		80	73.67
Blasthole diameter	10	[mm]	63	64.10
Burden	70	[mm]	50	58.13
Side-spacing	110	[mm]	40	49.35
Charge type	20	[g/m]	31.5	46.03
Planned delay	28	[µs]	25	39.59
			20	35.20
			14	28.19
			12.5	25.84
			10	22.44
			6.3	16.15
			4	10.70
			2	7.70
			1	5.66
			0.5	4.21
			< 0.5	0.00

Sample-ID	#0114 - BG01		Screen size [mm]	Mass passing [%]
Blasting date	20.05.2014		125	100.00
Blasting type	Shots in a row		100	100.00
Row-#	3		80	93.03
Blasthole diameter	10	[mm]	63	88.87
Burden	70	[mm]	50	78.84
Side-spacing	110	[mm]	40	68.29
Charge type	20	[g/m]	31.5	58.71
Planned delay	28	[µs]	25	51.93
			20	45.18
			14	35.82
			12.5	33.27
			10	27.83
			6.3	20.01
			4	13.34
			2	9.30
			1	6.77
			0.5	5.00
			< 0.5	0.00

Sample-ID	#0214 - BG02		Screen size [mm]	Mass passing [%]
Blasting date	06.06.2014		125	100.00
Blasting type	Shots in a row		100	69.59
Row-#	1		80	45.14
Blasthole diameter	10	[mm]	63	35.31
Burden	70	[mm]	50	28.05
Side-spacing	110	[mm]	40	24.41
Charge type	20	[g/m]	31.5	20.64
Planned delay	28	[µs]	25	18.73
			20	16.59
			14	13.79
			12.5	12.76
			10	10.97
			6.3	7.76
			4	5.02
			2	3.48
			1	2.46
			0.5	1.82
			< 0.5	0.00

Sample-ID	#0214 - BG02		Screen size [mm]	Mass passing [%]
Blasting date	06.06.2014		125	89.60
Blasting type	Shots in a row		100	71.67
Row-#	2		80	62.01
Blasthole diameter	10	[mm]	63	52.58
Burden	70	[mm]	50	39.84
Side-spacing	110	[mm]	40	37.21
Charge type	20	[g/m]	31.5	33.03
Planned delay	28	[µs]	25	28.32
			20	25.02
			14	19.87
			12.5	18.47
			10	15.71
			6.3	10.82
			4	7.03
			2	4.65
			1	3.27
			0.5	2.40
			< 0.5	0.00

Sample-ID	#0214 - BG02		Screen size [mm]	Mass passing [%]
Blasting date	06.06.2014		125	100.00
Blasting type	Shots in a row		100	94.12
Row-#	3		80	86.43
Blasthole diameter	10	[mm]	63	77.58
Burden	70	[mm]	50	64.82
Side-spacing	110	[mm]	40	57.36
Charge type	20	[g/m]	31.5	49.32
Planned delay	28	[µs]	25	42.08
			20	35.65
			14	25.47
			12.5	23.14
			10	18.88
			6.3	12.54
			4	8.05
			2	5.06
			1	3.43
			0.5	2.41
			< 0.5	0.00

Sample-ID	#0314 - BG03		Screen size [mm]	Mass passing [%]
Blasting date	16.06.2014		125	100.00
Blasting type	Shots in a row		100	60.63
Row-#	1		80	57.44
Blasthole diameter	10	[mm]	63	43.33
Burden	70	[mm]	50	33.99
Side-spacing	110	[mm]	40	30.66
Charge type	20	[g/m]	31.5	27.81
Planned delay	28	[µs]	25	25.91
			20	22.88
			14	18.62
			12.5	17.11
			10	14.08
			6.3	9.77
			4	6.55
			2	4.14
			1	2.77
			0.5	1.92
			< 0.5	0.00

Sample-ID	#0314 - BG03		Screen size [mm]	Mass passing [%]
Blasting date	16.06.2014		125	100.00
Blasting type	Shots in a row		100	82.82
Row-#	2		80	75.10
Blasthole diameter	10	[mm]	63	63.49
Burden	70	[mm]	50	54.80
Side-spacing	110	[mm]	40	47.00
Charge type	20	[g/m]	31.5	42.05
Planned delay	28	[µs]	25	35.84
			20	31.68
			14	25.05
			12.5	23.01
			10	19.61
			6.3	13.70
			4	9.30
			2	5.96
			1	3.99
			0.5	2.78
			< 0.5	0.00

Sample-ID	#0314 - BG03		Screen size [mm]	Mass passing [%]
Blasting date	16.06.2014		125	100.00
Blasting type	Shots in a row		100	94.89
Row-#	3		80	92.22
Blasthole diameter	10	[mm]	63	82.11
Burden	70	[mm]	50	63.32
Side-spacing	110	[mm]	40	53.42
Charge type	20	[g/m]	31.5	44.76
Planned delay	28	[µs]	25	38.61
			20	33.92
			14	26.76
			12.5	24.20
			10	20.77
			6.3	14.69
			4	9.79
			2	6.31
			1	4.32
			0.5	3.08
			< 0.5	0.00

Sample-ID	#0314 - BG03		Screen size [mm]	Mass passing [%]
Blasting date	16.06.2014		125	100.00
Blasting type	Shots in a row		100	100.00
Row-#	4		80	100.00
Blasthole diameter	10	[mm]	63	77.70
Burden	70	[mm]	50	59.51
Side-spacing	110	[mm]	40	52.95
Charge type	20	[g/m]	31.5	44.55
Planned delay	28	[µs]	25	40.41
			20	34.91
			14	27.54
			12.5	25.18
			10	21.70
			6.3	15.36
			4	10.55
			2	6.80
			1	4.59
			0.5	3.19
			< 0.5	0.00

Sample-ID	#0414 - BG04		Screen size [mm]	Mass passing [%]
Blasting date	01.07.2014		125	100.00
Blasting type	Shots in a row		100	76.36
Row-#	1		80	55.20
Blasthole diameter	10	[mm]	63	44.92
Burden	70	[mm]	50	40.34
Side-spacing	110	[mm]	40	37.64
Charge type	20	[g/m]	31.5	33.91
Planned delay	28	[µs]	25	29.99
			20	26.01
			14	21.28
			12.5	19.60
			10	16.73
			6.3	11.94
			4	8.15
			2	5.61
			1	3.97
			0.5	2.86
			< 0.5	0.00

Sample-ID	#0414 - BG04		Screen size [mm]	Mass passing [%]
Blasting date	01.07.2014		125	89.84
Blasting type	Shots in a row		100	89.84
Row-#	2		80	87.30
Blasthole diameter	10	[mm]	63	74.10
Burden	70	[mm]	50	65.28
Side-spacing	110	[mm]	40	58.34
Charge type	20	[g/m]	31.5	51.66
Planned delay	28	[µs]	25	46.14
			20	39.94
			14	31.28
			12.5	28.41
			10	24.40
			6.3	17.14
			4	11.31
			2	7.86
			1	5.61
			0.5	4.06
			< 0.5	0.00

Sample-ID	#0414 - BG04		Screen size [mm]	Mass passing [%]
Blasting date	01.07.2014		125	100.00
Blasting type	Shots in a row		100	94.05
Row-#	3		80	94.05
Blasthole diameter	10	[mm]	63	83.82
Burden	70	[mm]	50	72.13
Side-spacing	110	[mm]	40	61.39
Charge type	20	[g/m]	31.5	53.11
Planned delay	28	[µs]	25	46.54
			20	41.58
			14	32.08
			12.5	29.78
			10	25.23
			6.3	17.63
			4	11.79
			2	8.13
			1	5.77
			0.5	4.28
			< 0.5	0.00

Sample-ID	#0414 - BG04		Screen size [mm]	Mass passing [%]
Blasting date	01.07.2014		125	100.00
Blasting type	Shots in a row		100	90.07
Row-#	4		80	90.07
Blasthole diameter	10	[mm]	63	82.59
Burden	70	[mm]	50	71.15
Side-spacing	110	[mm]	40	64.38
Charge type	20	[g/m]	31.5	58.01
Planned delay	28	[µs]	25	51.38
			20	44.64
			14	35.23
			12.5	32.51
			10	27.49
			6.3	19.25
			4	13.34
			2	9.13
			1	6.61
			0.5	4.83
			< 0.5	0.00

Appendix 18 – Swebrec-Fits Preliminary Tests

#0111

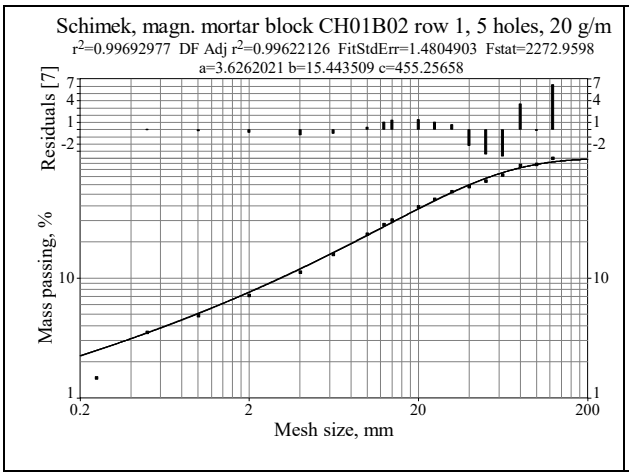

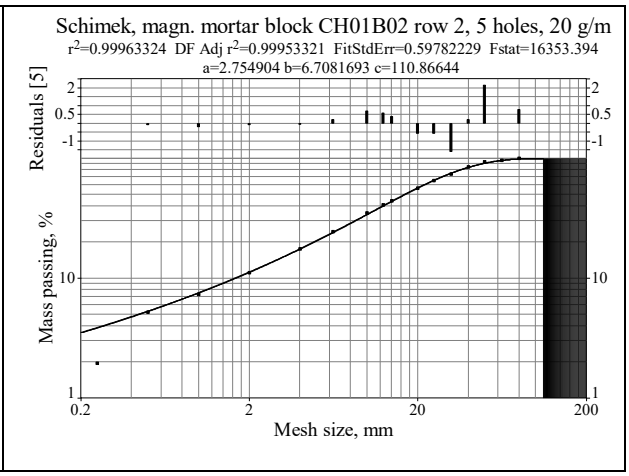

#0211

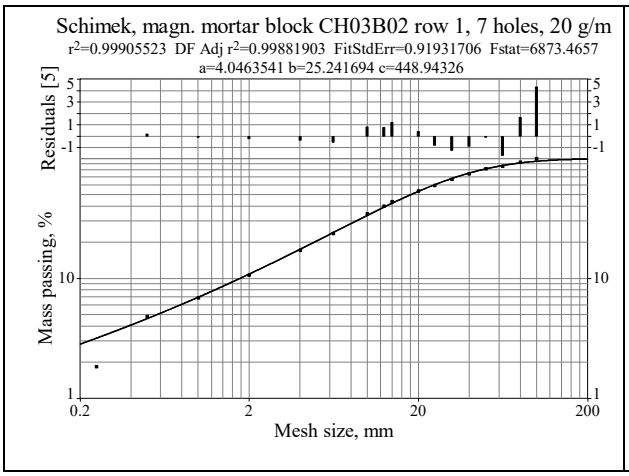

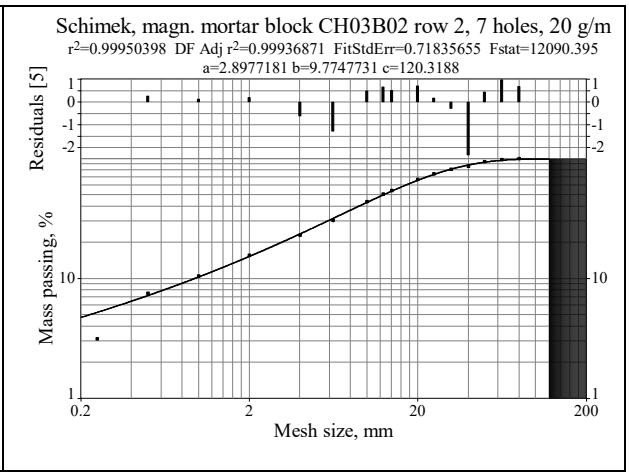

#0411

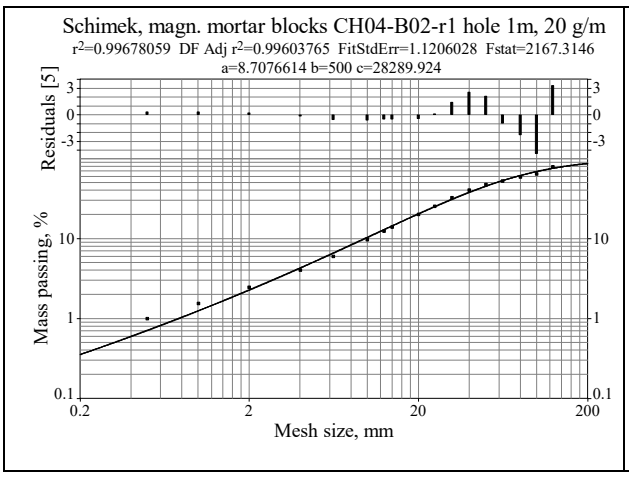

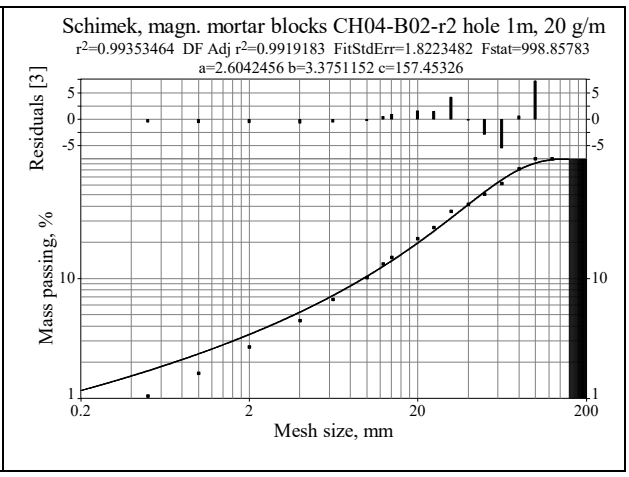

#0511

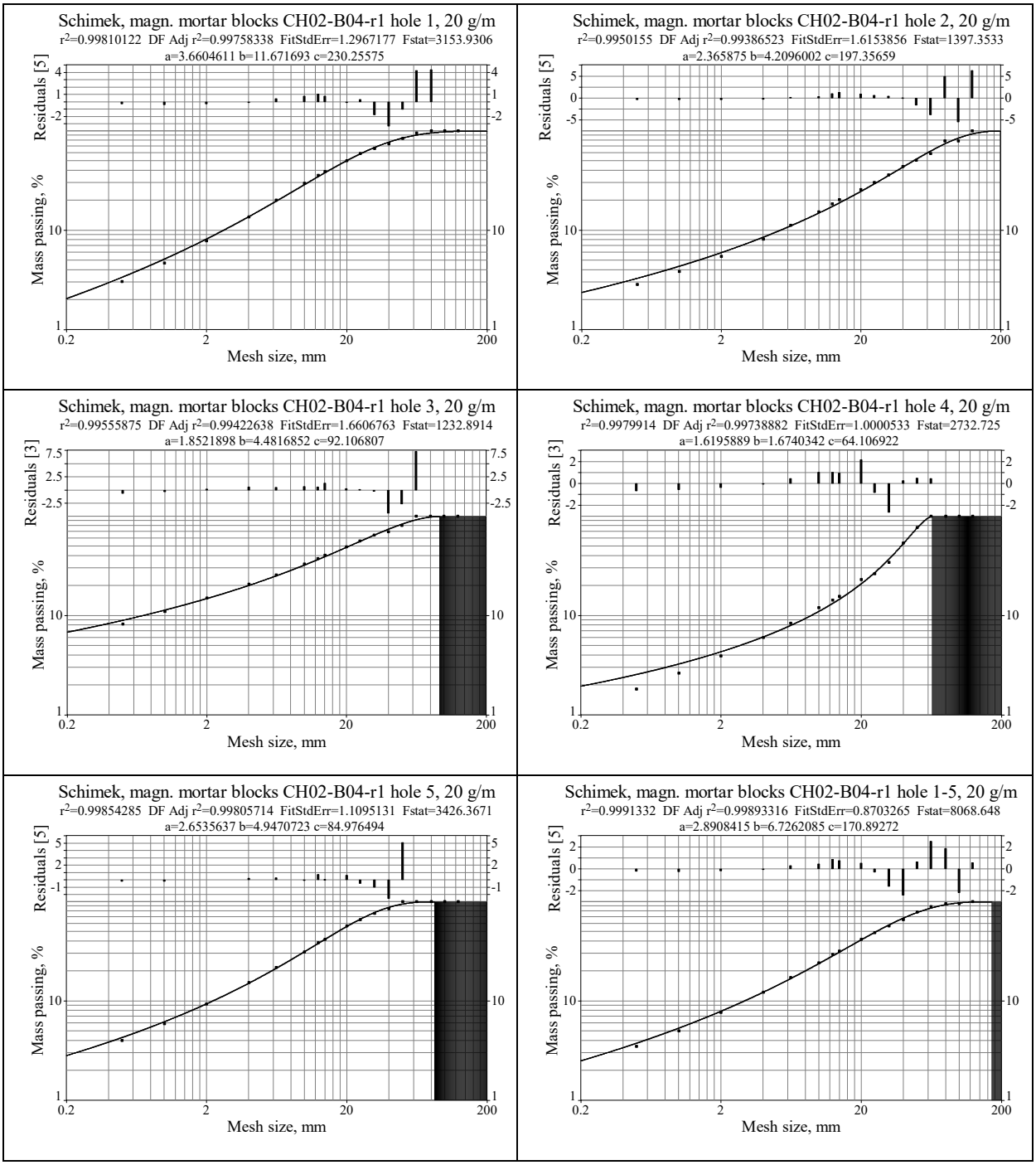
Schimek, magn. mortar blocks CH02-B04-r1 hole 1, 20 g/m
r²=0.99810122 DF Adj r²=0.99758338 FitStdErr=1.2967177 Fstat=3153.9306
a=3.6604611 b=11.671693 c=230.25575
Residuals [5]
Mass passing, %
Mesh size, mm
Schimek, magn. mortar blocks CH02-B04-r1 hole 2, 20 g/m
r²=0.9950155 DF Adj r²=0.99386523 FitStdErr=1.6153856 Fstat=1397.3533
a=2.365875 b=4.2096002 c=197.35659
Residuals [5]
Mass passing, %
Mesh size, mm
Schimek, magn. mortar blocks CH02-B04-r1 hole 3, 20 g/m
r²=0.99555875 DF Adj r²=0.99422638 FitStdErr=1.6606763 Fstat=1232.8914
a=1.8521898 b=4.4816852 c=92.106807
Residuals [3]
Mass passing, %
Mesh size, mm
Schimek, magn. mortar blocks CH02-B04-r1 hole 4, 20 g/m
r²=0.9979914 DF Adj r²=0.99738882 FitStdErr=1.0000533 Fstat=2732.725
a=1.6195889 b=1.6740342 c=64.106922
Residuals [3]
Mass passing, %
Mesh size, mm
Schimek, magn. mortar blocks CH02-B04-r1 hole 5, 20 g/m
r²=0.99854285 DF Adj r²=0.99805714 FitStdErr=1.1095131 Fstat=3426.3671
a=2.6535637 b=4.9470723 c=84.976494
Residuals [5]
Mass passing, %
Mesh size, mm
Schimek, magn. mortar blocks CH02-B04-r1 hole 1-5, 20 g/m
r²=0.9991332 DF Adj r²=0.99893316 FitStdErr=0.8703265 Fstat=8068.648
a=2.8908415 b=6.7262085 c=170.89272
Residuals [5]
Mass passing, %
Mesh size, mm

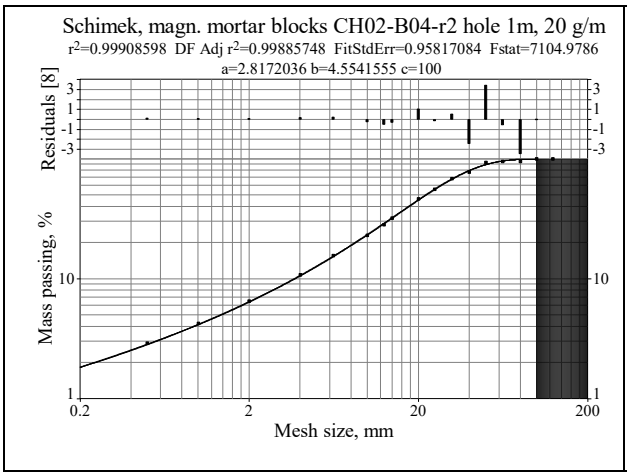
Schimek, magn. mortar blocks CH02-B04-r2 hole 1m, 20 g/m
r²=0.99908598 DF Adj r²=0.99885748 FitStdErr=0.95817084 Fstat=7104.9786
a=2.8172036 b=4.5541555 c=100
Residuals [8]
Mass passing, %
Mesh size, mm

#0611

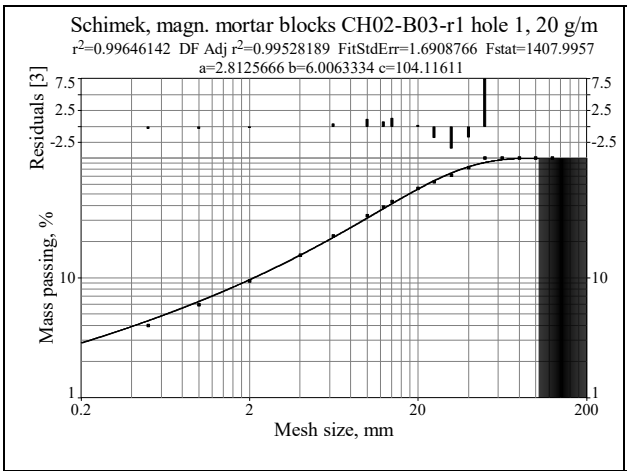
Schimek, magn. mortar blocks CH02-B03-r1 hole 1, 20 g/m
r²=0.99646142 DF Adj r²=0.99528189 FitStdErr=1.6908766 Fstat=1407.9957
a=2.8125666 b=6.0063334 c=104.11611
Residuals [3]
Mass passing, %
Mesh size, mm

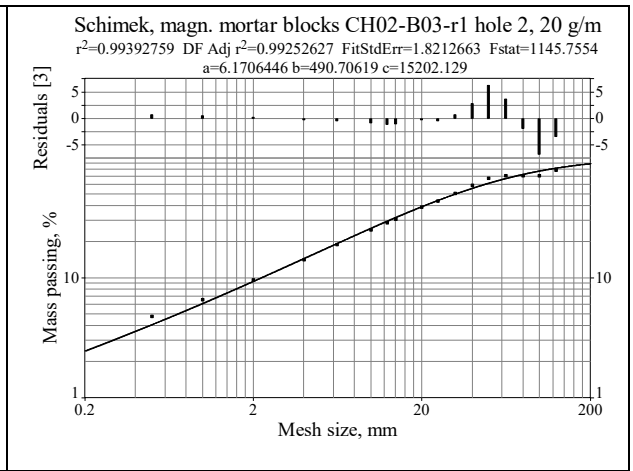
Schimek, magn. mortar blocks CH02-B03-r1 hole 2, 20 g/m
r²=0.99392759 DF Adj r²=0.99252627 FitStdErr=1.8212663 Fstat=1145.7554
a=6.1706446 b=490.70619 c=15202.129
Residuals [3]
Mass passing, %
Mesh size, mm

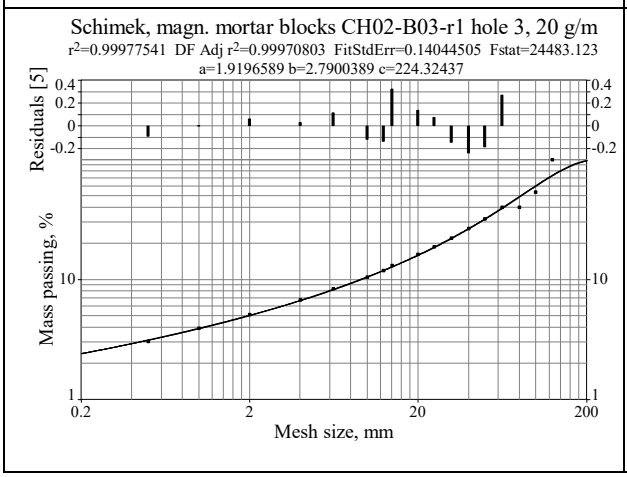
Schimek, magn. mortar blocks CH02-B03-r1 hole 3, 20 g/m
r²=0.99977541 DF Adj r²=0.99970803 FitStdErr=0.14044505 Fstat=24483.123
a=1.9196589 b=2.7900389 c=224.32437
Residuals [5]
Mass passing, %
Mesh size, mm

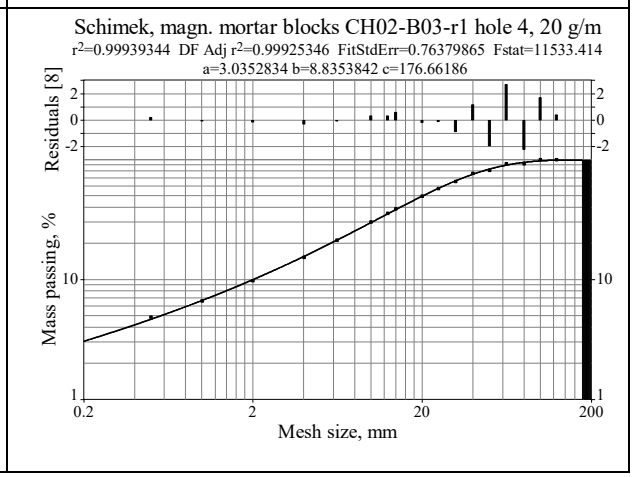
Schimek, magn. mortar blocks CH02-B03-r1 hole 4, 20 g/m
r²=0.99939344 DF Adj r²=0.99925346 FitStdErr=0.76379865 Fstat=11533.414
a=3.0352834 b=8.8353842 c=176.66186
Residuals [8]
Mass passing, %
Mesh size, mm

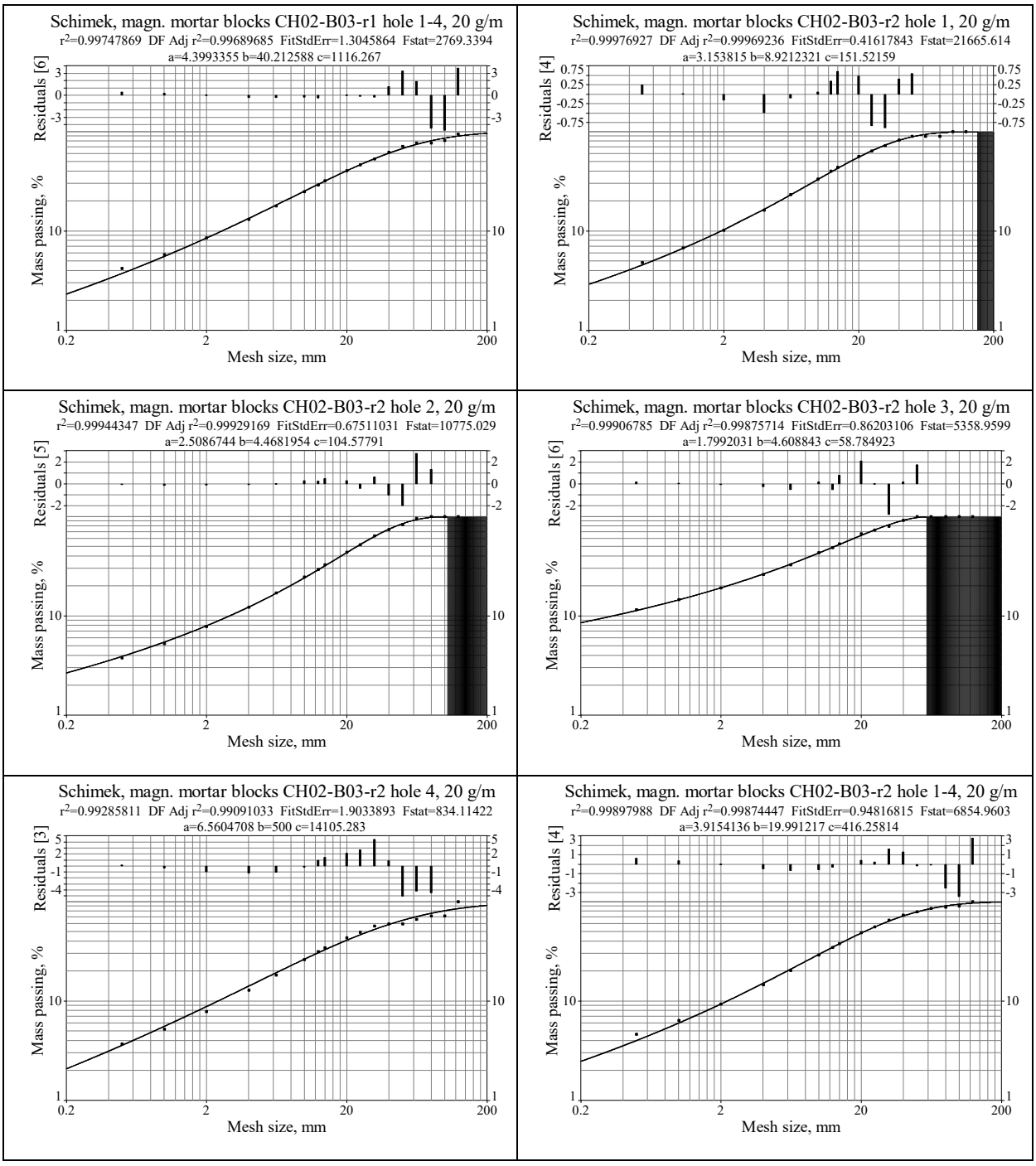
Schimek, magn. mortar blocks CH02-B03-r1 hole 1-4, 20 g/m
r²=0.99747869 DF Adj r²=0.99689685 FitStdErr=1.3045864 Fstat=2769.3394
a=4.3993355 b=40.212588 c=1116.267
Residuals [6]
Mass passing, %
Mesh size, mm
Schimek, magn. mortar blocks CH02-B03-r2 hole 1, 20 g/m
r²=0.99976927 DF Adj r²=0.99969236 FitStdErr=0.41617843 Fstat=21665.614
a=3.153815 b=8.9212321 c=151.52159
Residuals [4]
Mass passing, %
Mesh size, mm
Schimek, magn. mortar blocks CH02-B03-r2 hole 2, 20 g/m
r²=0.99944347 DF Adj r²=0.99929169 FitStdErr=0.67511031 Fstat=10775.029
a=2.5086744 b=4.4681954 c=104.57791
Residuals [5]
Mass passing, %
Mesh size, mm
Schimek, magn. mortar blocks CH02-B03-r2 hole 3, 20 g/m
r²=0.99906785 DF Adj r²=0.99875714 FitStdErr=0.86203106 Fstat=5358.9599
a=1.7992031 b=4.608843 c=58.784923
Residuals [6]
Mass passing, %
Mesh size, mm
Schimek, magn. mortar blocks CH02-B03-r2 hole 4, 20 g/m
r²=0.99285811 DF Adj r²=0.99091033 FitStdErr=1.9033893 Fstat=834.11422
a=6.5604708 b=500 c=14105.283
Residuals [3]
Mass passing, %
Mesh size, mm
Schimek, magn. mortar blocks CH02-B03-r2 hole 1-4, 20 g/m
r²=0.99897988 DF Adj r²=0.99874447 FitStdErr=0.94816815 Fstat=6854.9603
a=3.9154136 b=19.991217 c=416.25814
Residuals [4]
Mass passing, %
Mesh size, mm

Appendix 19 – Swebrec-Fits Stage 1

#0212

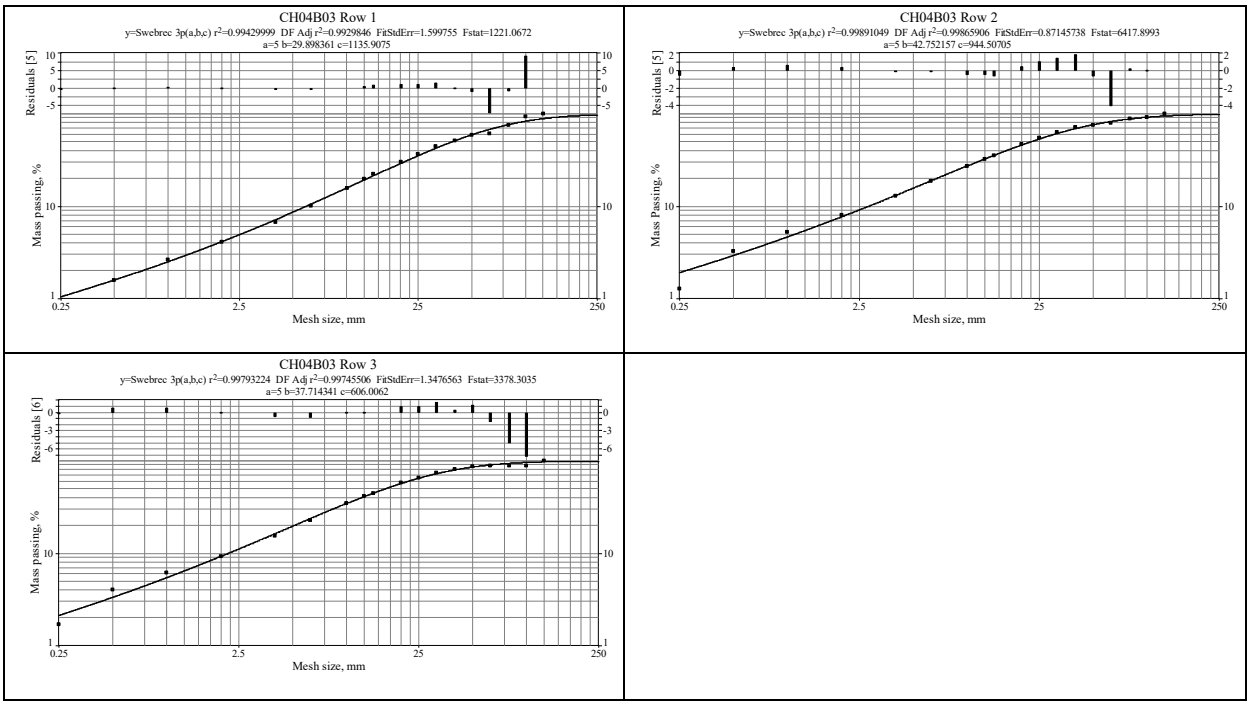

#0312

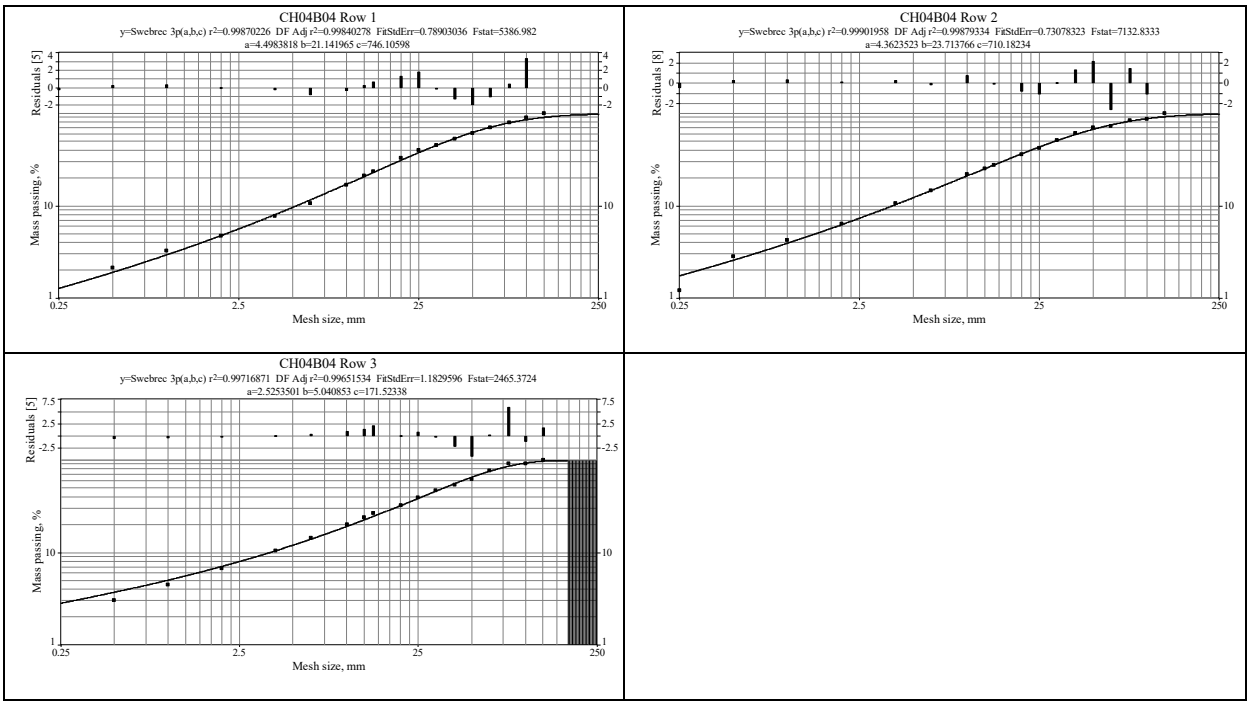

#0412

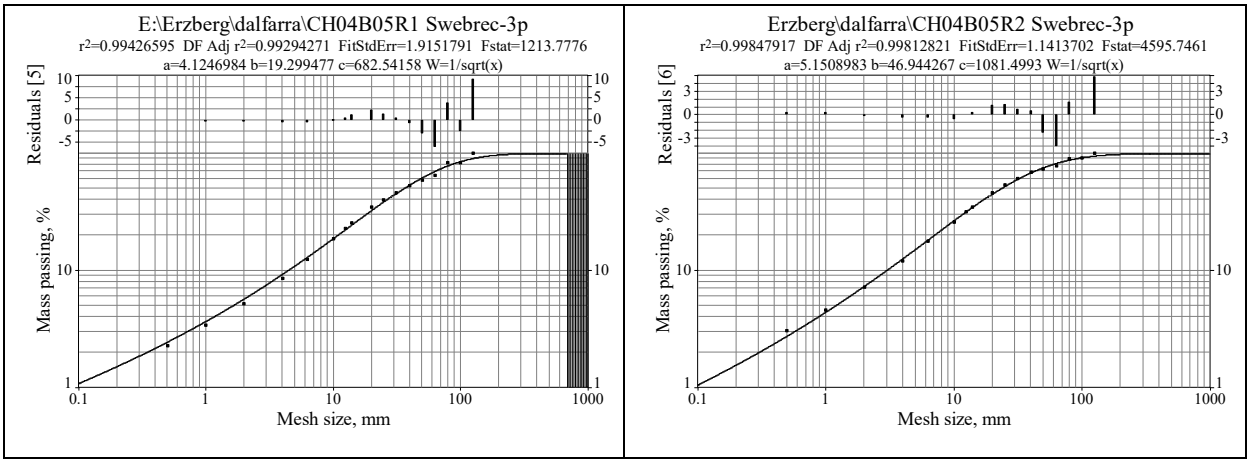

#0512

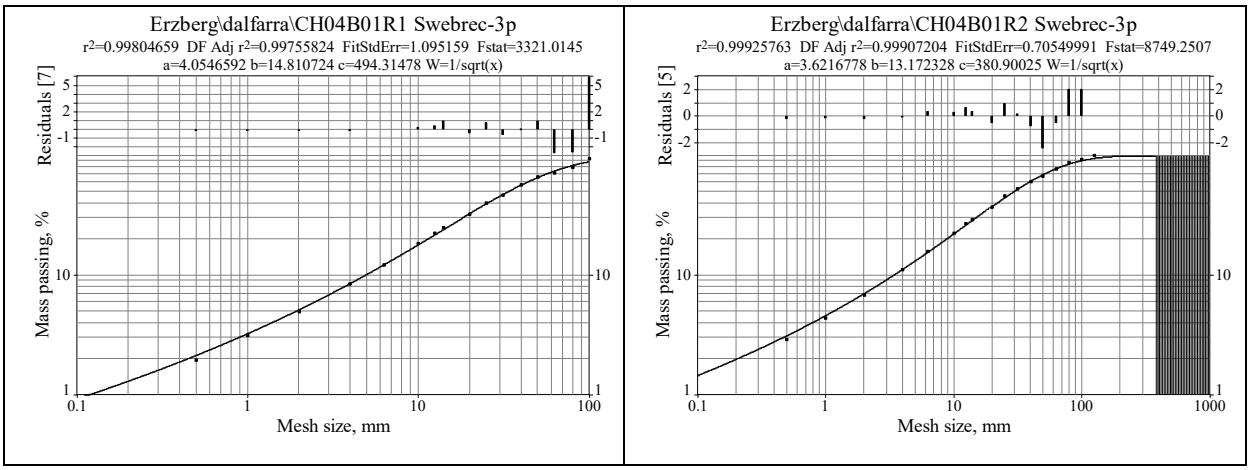

#0612

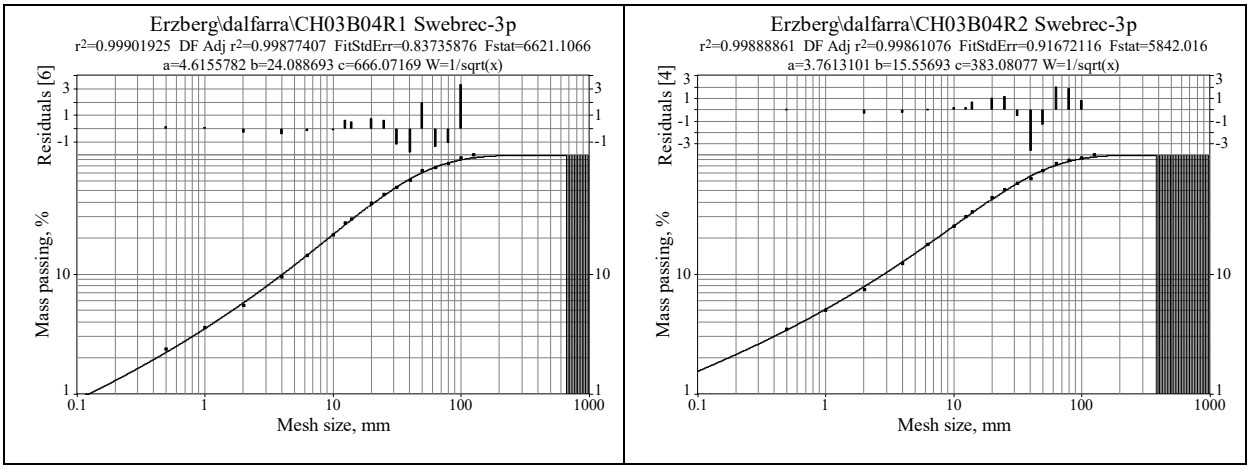

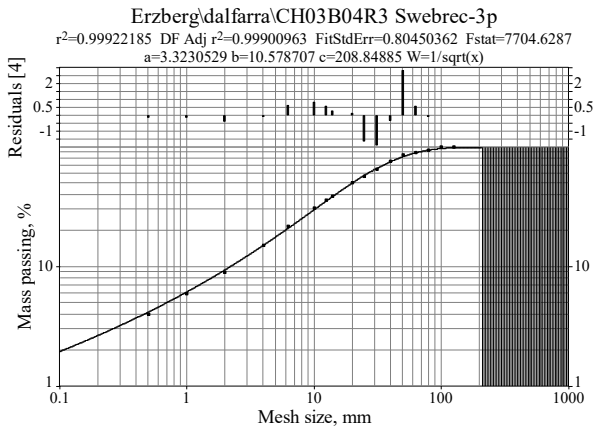
Erzberg\dalfarra\CH03B04R3 Swebrec-3p
r²=0.99922185 DF Adj r²=0.99900963 FitStdErr=0.80450362 Fstat=7704.6287
a=3.3230529 b=10.578707 c=208.84885 W=1/sqrt(x)
Residuals [4]
Mass passing, %
Mesh size, mm

#0712

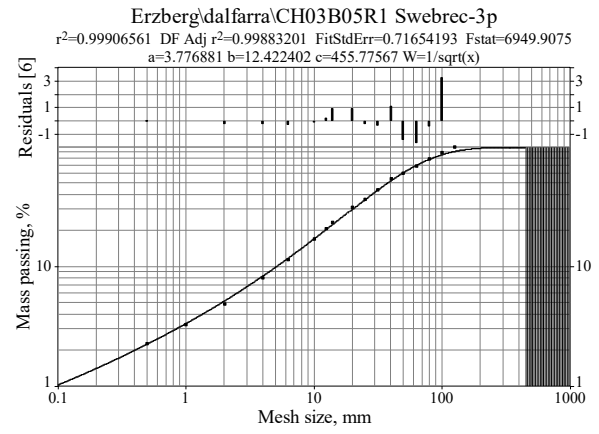
Erzberg\dalfarra\CH03B05R1 Swebrec-3p
r²=0.99906561 DF Adj r²=0.99883201 FitStdErr=0.71654193 Fstat=6949.9075
a=3.776881 b=12.422402 c=455.77567 W=1/sqrt(x)
Residuals [6]
Mass passing, %
Mesh size, mm

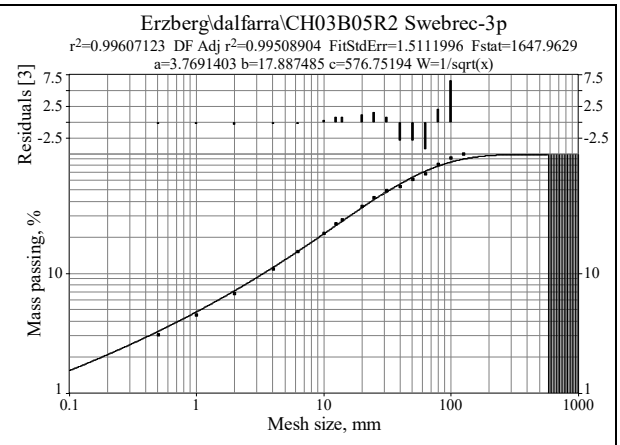
Erzberg\dalfarra\CH03B05R2 Swebrec-3p
r²=0.99607123 DF Adj r²=0.99508904 FitStdErr=1.5111996 Fstat=1647.9629
a=3.7691403 b=17.887485 c=576.75194 W=1/sqrt(x)
Residuals [3]
Mass passing, %
Mesh size, mm

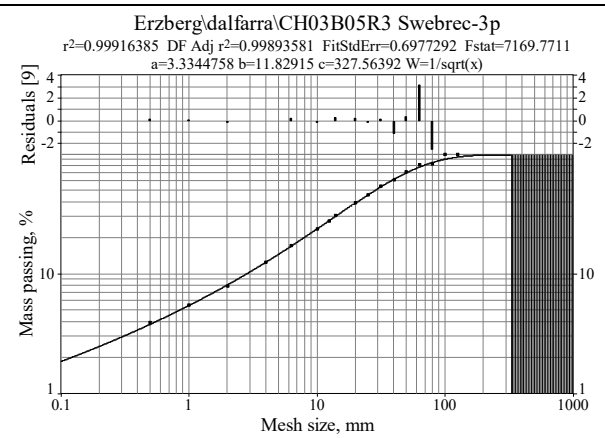
Erzberg\dalfarra\CH03B05R3 Swebrec-3p
r²=0.99916385 DF Adj r²=0.99893581 FitStdErr=0.6977292 Fstat=7169.7711
a=3.3344758 b=11.82915 c=327.56392 W=1/sqrt(x)
Residuals [9]
Mass passing, %
Mesh size, mm

#0812

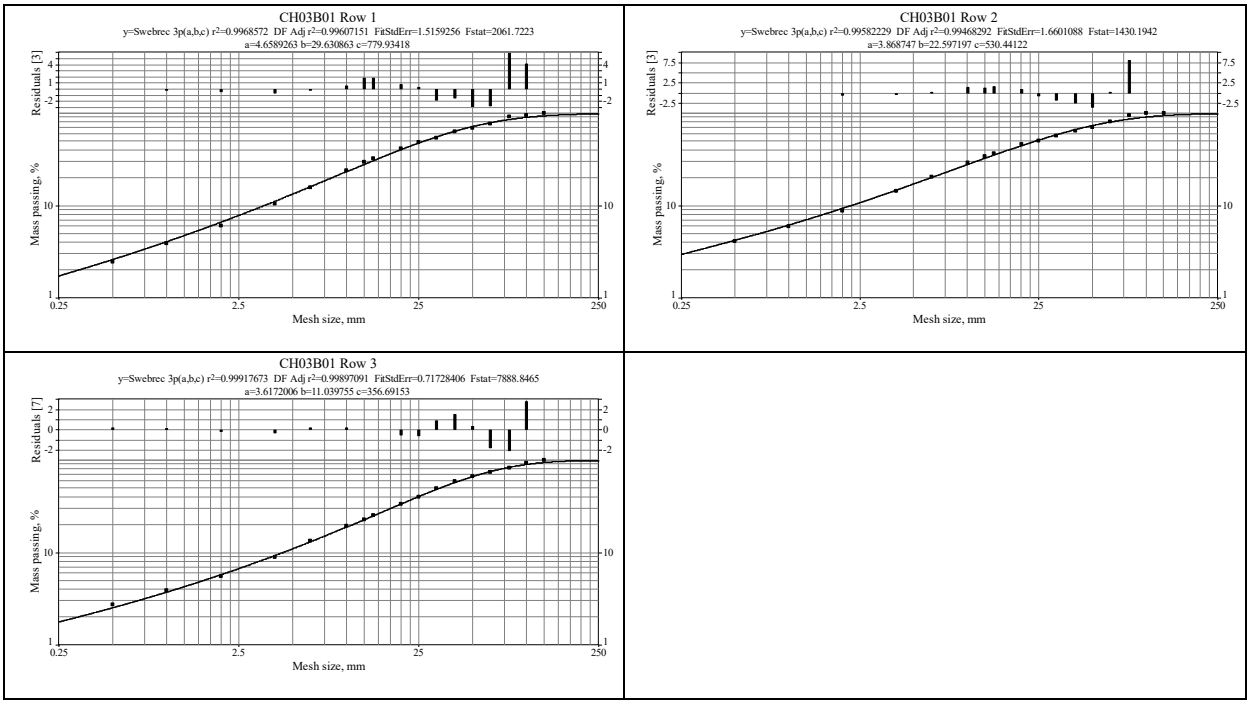
CH03B01 Row 1
y=Swebrec 3p(a,b,c) r²=0.9968572 DF Adj r²=0.99607151 FitStdErr=1.5159256 Fstat=2061.7223
a=4.6589263 b=29.630863 c=779.93418
Residuals [3]
Mass passing, %
Mesh size, mm
CH03B01 Row 2
y=Swebrec 3p(a,b,c) r²=0.99582229 DF Adj r²=0.99468292 FitStdErr=1.6601088 Fstat=1430.1942
a=3.868747 b=22.597197 c=530.44122
Residuals [3]
Mass passing, %
Mesh size, mm
CH03B01 Row 3
y=Swebrec 3p(a,b,c) r²=0.99917673 DF Adj r²=0.99897091 FitStdErr=0.71728406 Fstat=7888.8465
a=3.6172006 b=11.039755 c=356.69153
Residuals [7]
Mass passing, %
Mesh size, mm

#0912

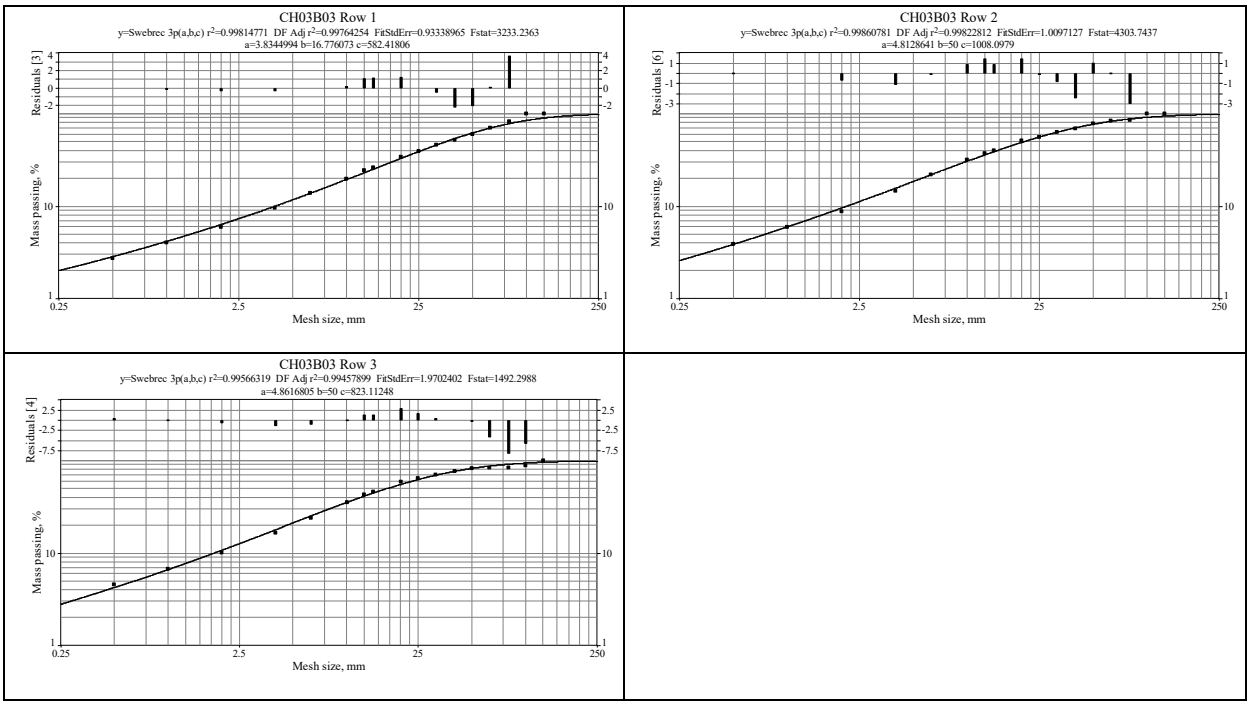
CH03B03 Row 1
y=Swebrec 3p(a,b,c) r²=0.99814771 DF Adj r²=0.99764254 FitStdErr=0.93338965 Fstat=3233.2363
a=3.8344994 b=16.776073 c=582.41806
Residuals [3]
Mass passing, %
Mesh size, mm
CH03B03 Row 2
y=Swebrec 3p(a,b,c) r²=0.99860781 DF Adj r²=0.99822812 FitStdErr=1.0097127 Fstat=4303.7437
a=4.8128641 b=50 c=1008.0979
Residuals [6]
Mass passing, %
Mesh size, mm
CH03B03 Row 3
y=Swebrec 3p(a,b,c) r²=0.99566319 DF Adj r²=0.99457899 FitStdErr=1.9702402 Fstat=1492.2988
a=4.8616805 b=50 c=823.11248
Residuals [4]
Mass passing, %
Mesh size, mm

Appendix 20 – Swebrec-Fits Stage 2

#0113

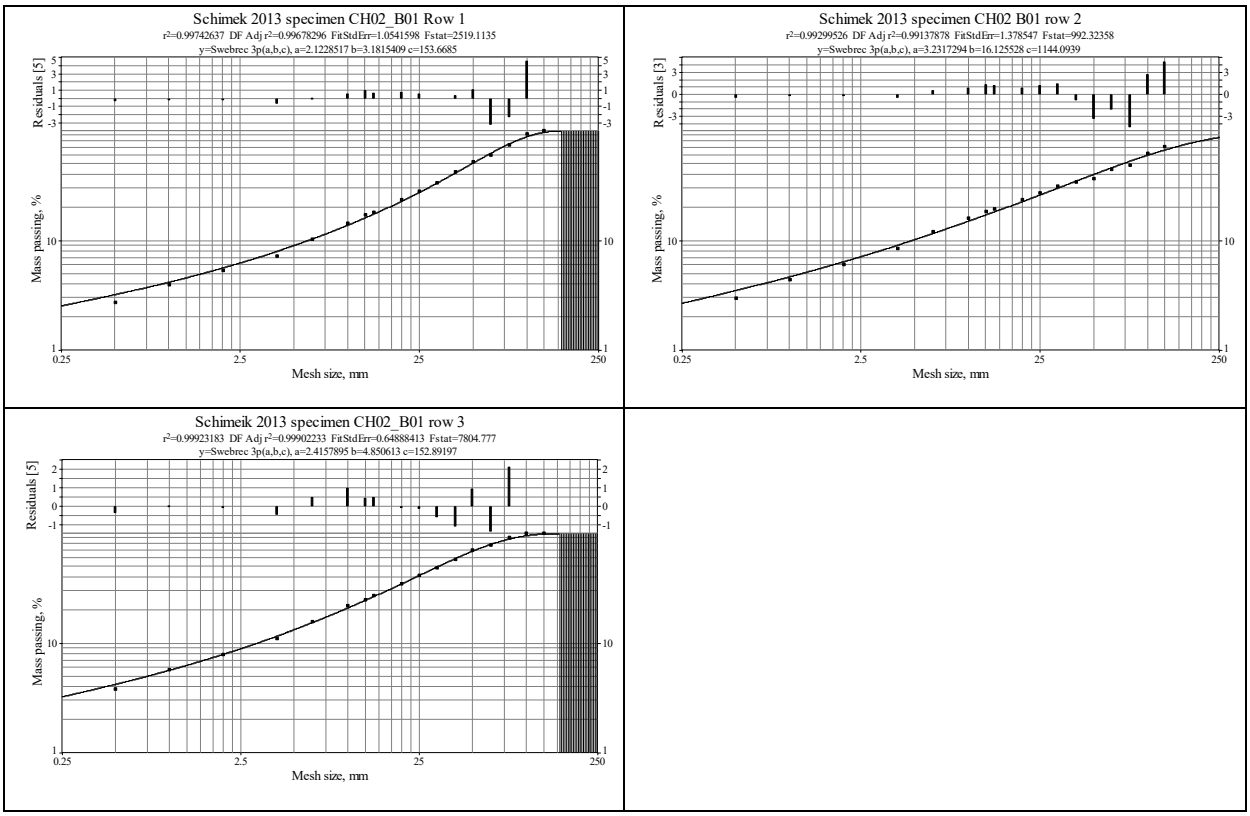

#0213

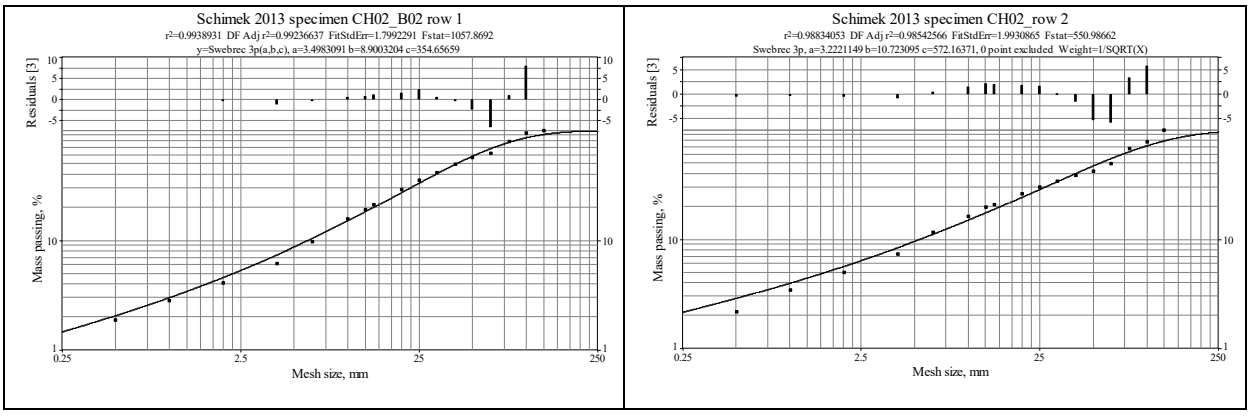

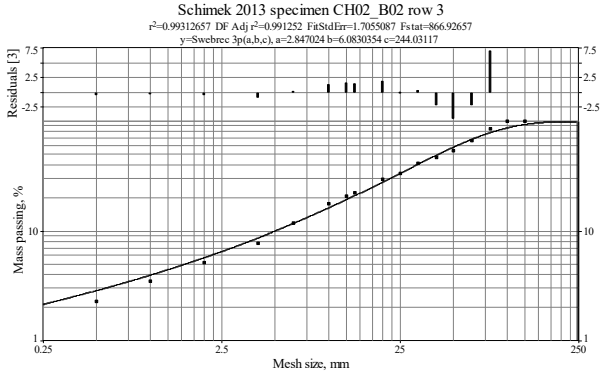
Schimek 2013 specimen CH02_B02 row 3
r²=0.99312657 DF Adj r²=0.991252 FitStdErr=1.7055087 Fstat=866.92657
y=Swebrec 3p(a,b,c), a=2.847024 b=6.0830354 c=244.03117
Residuals [3]
Mass passing, %
Mesh size, mm

#0313

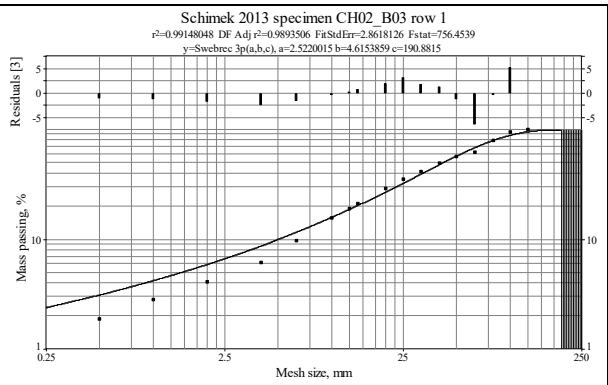
Schimek 2013 specimen CH02_B03 row 1
r²=0.99148048 DF Adj r²=0.9893506 FitStdErr=2.8618126 Fstat=756.4539
y=Swebrec 3p(a,b,c), a=2.5220015 b=4.6153859 c=190.8815
Residuals [3]
Mass passing, %
Mesh size, mm

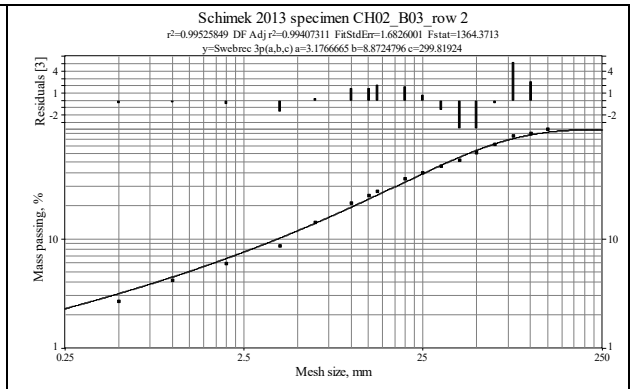
Schimek 2013 specimen CH02_B03_row 2
r²=0.99525849 DF Adj r²=0.99407311 FitStdErr=1.6826001 Fstat=1364.3713
y=Swebrec 3p(a,b,c) a=3.1766665 b=8.8724796 c=299.81924
Residuals [3]
Mass passing, %
Mesh size, mm

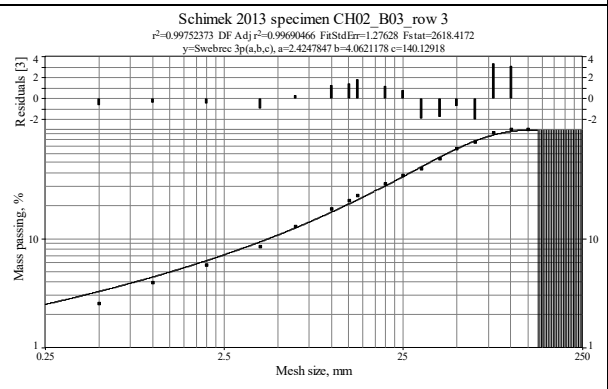
Schimek 2013 specimen CH02_B03_row 3
r²=0.99752373 DF Adj r²=0.99690466 FitStdErr=1.27628 Fstat=2618.4172
y=Swebrec 3p(a,b,c), a=2.4247847 b=4.0621178 c=140.12918
Residuals [3]
Mass passing, %
Mesh size, mm

#0413

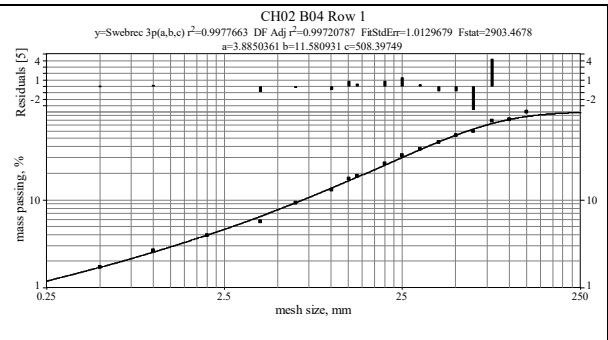
CH02 B04 Row 1
y=Swebrec 3p(a,b,c) r²=0.9977663 DF Adj r²=0.99720787 FitStdErr=1.0129679 Fstat=2903.4678
a=3.8850361 b=11.580931 c=508.39749
Residuals [5]
mass passing, %
mesh size, mm

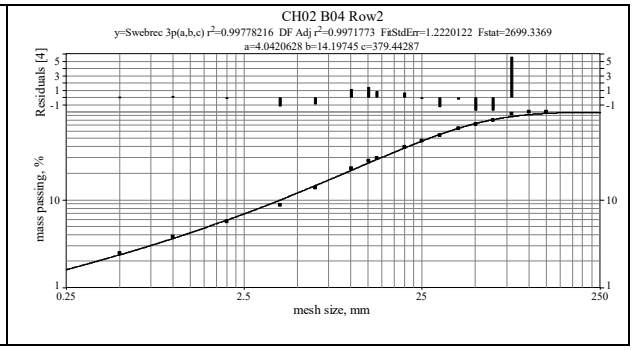
CH02 B04 Row2
y=Swebrec 3p(a,b,c) r²=0.99778216 DF Adj r²=0.9971773 FitStdErr=1.2220122 Fstat=2699.3369
a=4.0420628 b=14.19745 c=379.44287
Residuals [4]
mass passing, %
mesh size, mm

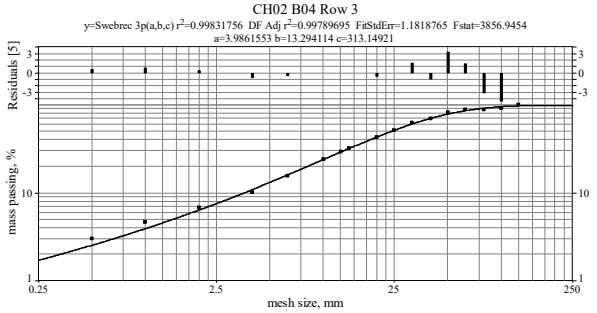
CH02 B04 Row 3
y=Swebrec 3p(a,b,c) r²=0.99831756 DF Adj r²=0.99789695 FitStdErr=1.1818765 Fstat=3856.9454
a=3.9861553 b=13.294114 c=313.14921
Residuals [5]
mass passing, %
mesh size, mm

#0513

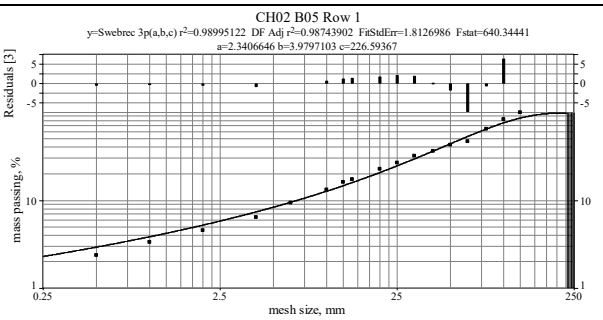
CH02 B05 Row 1
y=Swebrec 3p(a,b,c) r²=0.98995122 DF Adj r²=0.98743902 FitStdErr=1.8126986 Fstat=640.34441
a=2.3406646 b=3.9797103 c=226.59367
Residuals [3]
mass passing, %
mesh size, mm

#0613

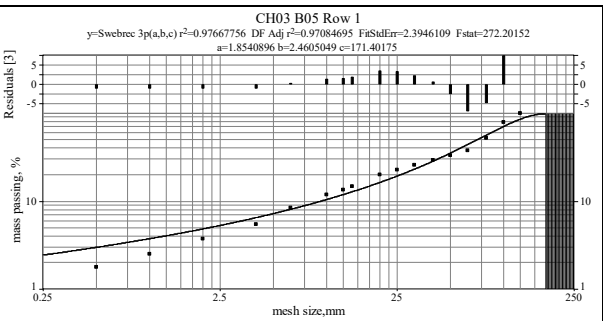
CH03 B05 Row 1
y=Swebrec 3p(a,b,c) r²=0.97667756 DF Adj r²=0.97084695 FitStdErr=2.3946109 Fstat=272.20152
a=1.8540896 b=2.4605049 c=171.40175
Residuals [3]
mass passing, %
mesh size,mm

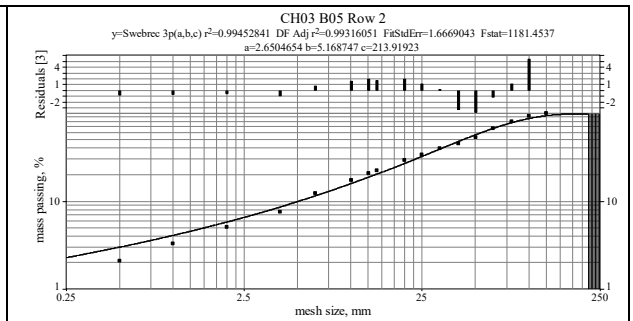
CH03 B05 Row 2
y=Swebrec 3p(a,b,c) r²=0.99452841 DF Adj r²=0.99316051 FitStdErr=1.6669043 Fstat=1181.4537
a=2.6504654 b=5.168747 c=213.91923
Residuals [3]
mass passing, %
mesh size, mm

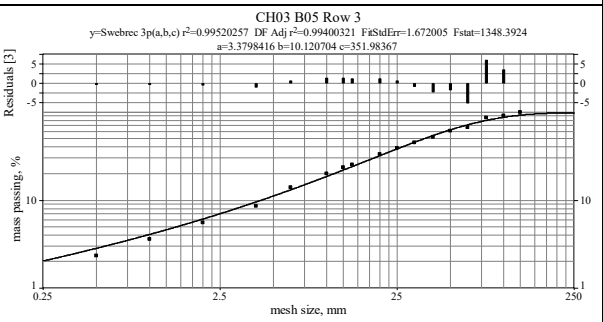
CH03 B05 Row 3
y=Swebrec 3p(a,b,c) r²=0.99520257 DF Adj r²=0.99400321 FitStdErr=1.672005 Fstat=1348.3924
a=3.3798416 b=10.120704 c=351.98367
Residuals [3]
mass passing, %
mesh size, mm

#0713

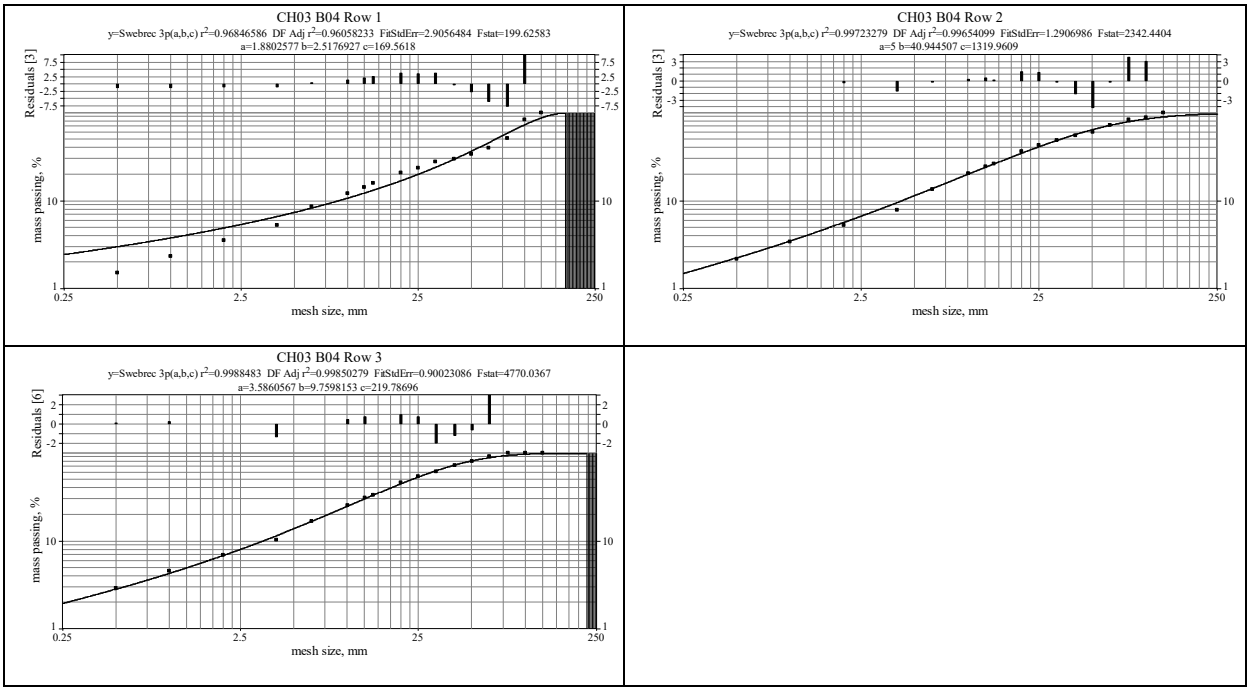
CH03 B04 Row 1
y=Swebrec 3p(a,b,c) r²=0.96846586 DF Adj r²=0.96058233 FitStdErr=2.9056484 Fstat=199.62583
a=1.8802577 b=2.5176927 c=169.5618
Residuals [3]
mass passing, %
mesh size, mm
CH03 B04 Row 2
y=Swebrec 3p(a,b,c) r²=0.99723279 DF Adj r²=0.99654099 FitStdErr=1.2906986 Fstat=2342.4404
a=5 b=40.944507 c=1319.9609
Residuals [3]
mass passing, %
mesh size, mm
CH03 B04 Row 3
y=Swebrec 3p(a,b,c) r²=0.9988483 DF Adj r²=0.99850279 FitStdErr=0.90023086 Fstat=4770.0367
a=3.5860567 b=9.7598153 c=219.78696
Residuals [6]
mass passing, %
mesh size, mm

Appendix 21 – Swebrec-Fits Stage 3

#0114

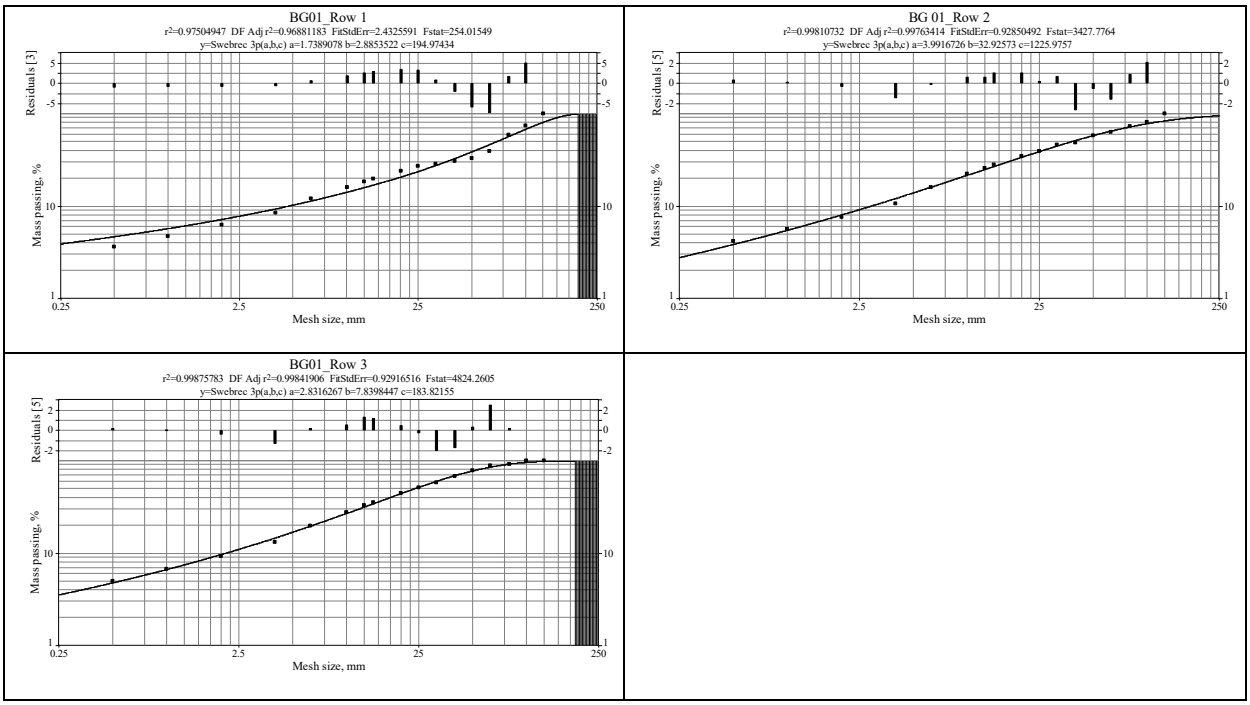

#0214

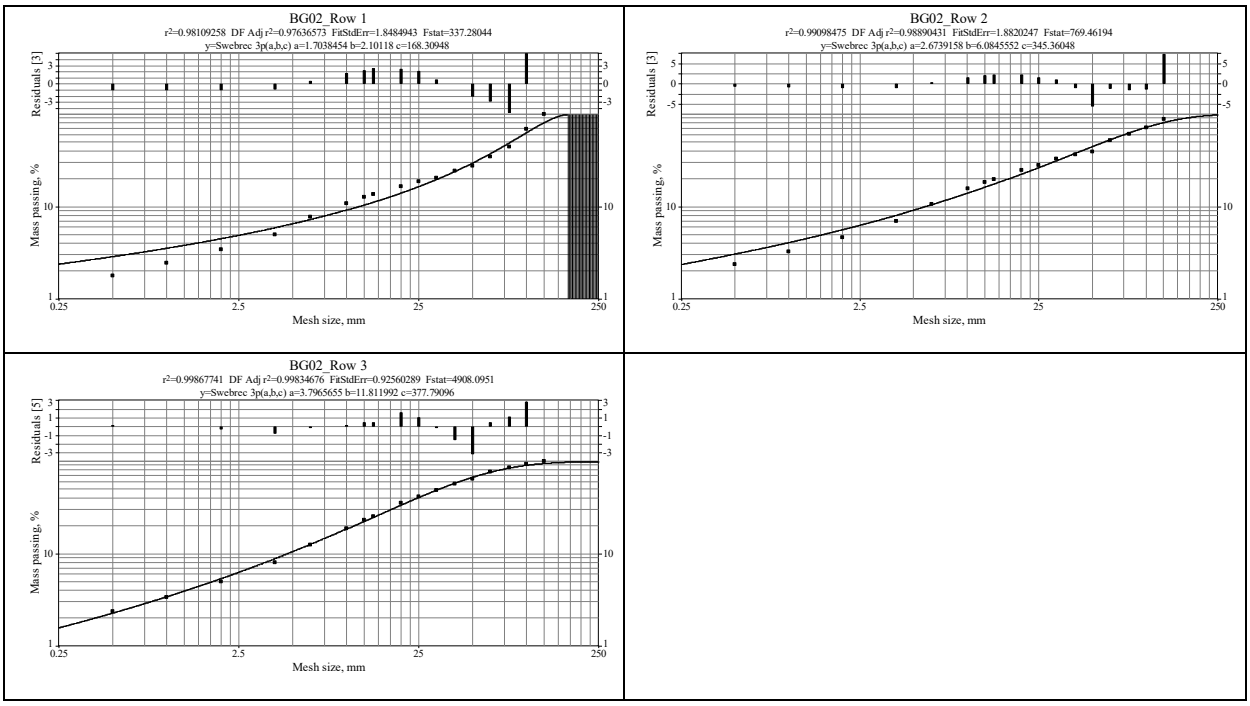

#0314

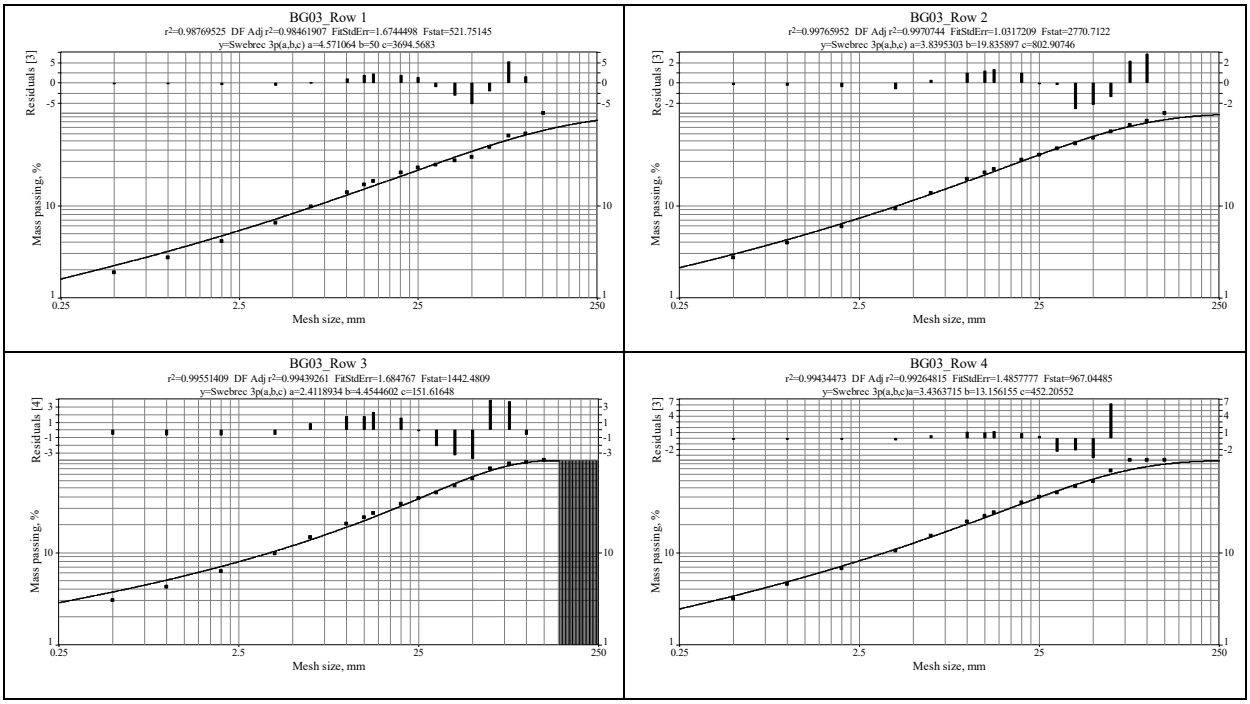
BG03_Row 1
r²=0.98769525 DF Adj r²=0.98461907 FitStdErr=1.6744498 Fstat=521.75145
y=Swebrec 3p(a,b,c) a=4.571064 b=50 c=3694.5683
BG03_Row 2
r²=0.99765952 DF Adj r²=0.9970744 FitStdErr=1.0317209 Fstat=2770.7122
y=Swebrec 3p(a,b,c) a=3.8395303 b=19.835897 c=802.90746
BG03_Row 3
r²=0.99551409 DF Adj r²=0.99439261 FitStdErr=1.684767 Fstat=1442.4809
y=Swebrec 3p(a,b,c) a=2.4118934 b=4.4544602 c=151.61648
BG03_Row 4
r²=0.99434473 DF Adj r²=0.99264815 FitStdErr=1.4857777 Fstat=967.04485
y=Swebrec 3p(a,b,c)a=3.4363715 b=13.156155 c=452.20552
Residuals [3]
Residuals [4]
Mass passing, %
Mesh size, mm
0.25
2.5
25
250

#0414

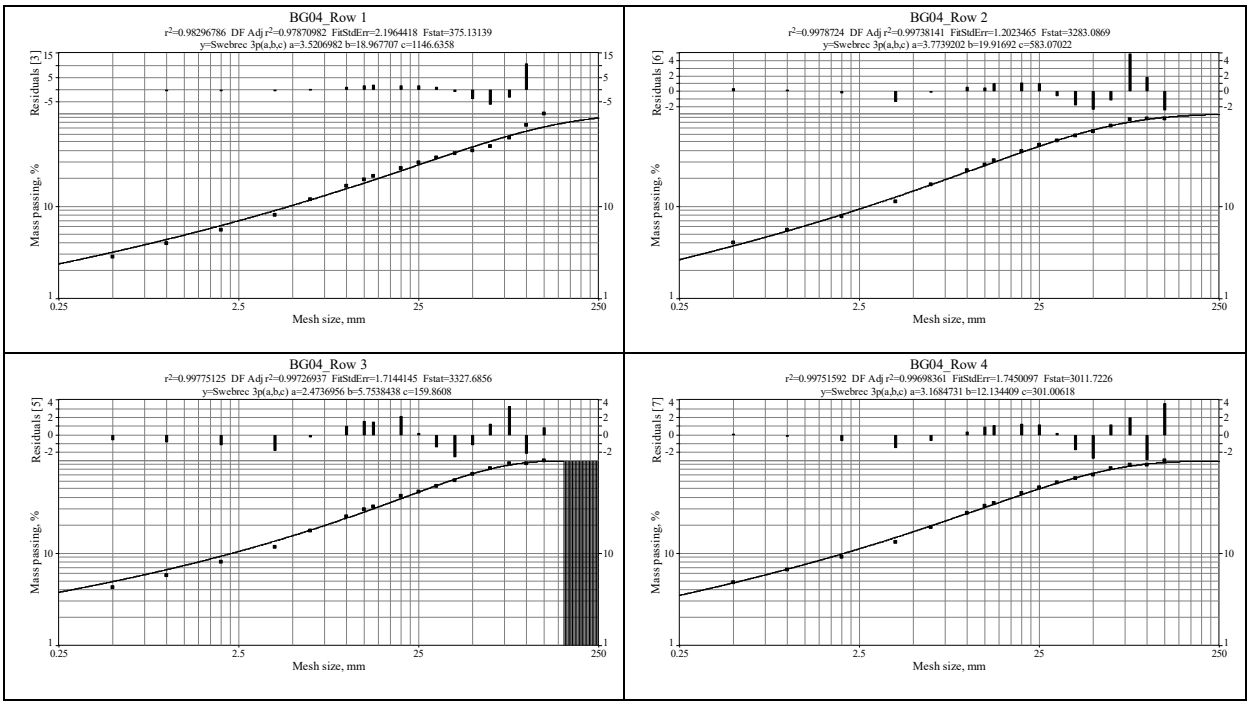
BG04_Row 1
r²=0.98296786 DF Adj r²=0.97870982 FitStdErr=2.1964418 Fstat=375.13139
y=Swebrec 3p(a,b,c) a=3.5206982 b=18.967707 c=1146.6358
BG04_Row 2
r²=0.9978724 DF Adj r²=0.99738141 FitStdErr=1.2023465 Fstat=3283.0869
y=Swebrec 3p(a,b,c) a=3.7739202 b=19.91692 c=583.07022
BG04_Row 3
r²=0.99775125 DF Adj r²=0.99726937 FitStdErr=1.7144145 Fstat=3327.6856
y=Swebrec 3p(a,b,c) a=2.4736956 b=5.7538438 c=159.8608
BG04_Row 4
r²=0.99751592 DF Adj r²=0.99698361 FitStdErr=1.7450097 Fstat=3011.7226
y=Swebrec 3p(a,b,c) a=3.1684731 b=12.134409 c=301.00618
Residuals [3]
Residuals [5]
Residuals [6]
Residuals [7]
Mass passing, %
Mesh size, mm
0.25
2.5
25
250